GDANSK UNIVERSITY OF TECHNOLOGY
FACULTY OF OCEAN ENGINEERING AND SHIP TECHNOLOGY
SECTION OF TRANSPORT TECHNICAL MEANS
OF TRANSPORT COMMITEE OF POLISH ACADEMY OF SCIENCES
UTILITY FOUNDATIONS SECTION
OF MECHANICAL ENGINEERING COMMITTEE OF POLISH ACADEMY OF SCIENCE

ISSN 1231 – 3998
ISBN 83 – 900666 – 2 – 9

Journal of

POLISH CIMAC

ENERGETIC ASPECTS

Vol. 4 **No. 1**

Gdansk, 2009

Science publication of Editorial Advisory Board of POLISH CIMAC

Editor in Chief: Jerzy Girtler Editorial Office Secretary: Jacek Rudnicki

Editorial Advisory Board

J. Girtler (President) - *Gdansk University of Technology*
L. Piaseczny (Vice President) - *Naval Academy of Gdynia*
A. Adamkiewicz - *Maritime Academy of Szczecin*
J. Adamczyk - *University of Mining and Metallurgy of Krakow*
J. Błachnio - *Air Force Institute of Technology*
L. Będkowski - *WAT Military University of Technology*
C. Behrendt - *Maritime Academy of Szczecin*
P. Bielawski - *Maritime Academy of Szczecin*
J. Borgoń - *Warsaw University of Technology*
T. Chmielniak - *Silesian Technical University*
R. Cwilewicz - *Maritime Academy of Gdynia*
T. Dąbrowski - *WAT Military University of Technology*
Z. Domachowski - *Gdansk University of Technology*
C. Dymarski - *Gdansk University of Technology*
M. Dzida - *Gdansk University of Technology*
J. Gronowicz - *Maritime University of Szczecin*
V. Hlavna - *University of Žilina, Slovak Republic*
M. Idzior – *Poznan University of Technology*
A. Iskra - *Poznan University of Technology*
A. Jankowski – *President of KONES*
J. Jaźwiński - *Air Force Institute of Technology*
R. Jedliński - *Bydgoszcz University of Technology and Agriculture*
J. Kiciński - *President of SEF MEC PAS, member of MEC*
O. Klyus - *Maritime Academy of Szczecin*
Z. Korczewski - *Naval Academy of Gdynia*
K. Kosowski - *Gdansk University of Technology*
L. Ignatiewicz Kowalczuk - *Baltic State Maritime Academy in Kaliningrad*
J. Lewitowicz - *Air Force Institute of Technology*
K. Lejda - *Rzeszow University of Technology*
J. Macek - *Czech Technical University in Prague*
Z. Matuszak - *Maritime Academy of Szczecin*
J. Merkisz – *Poznan Unversity of Technology*
R. Michalski - *Olsztyn Warmia-Mazurian University*
A. Niewczas - *Lublin University of Technology*
Y. Ohta - *Nagoya Institute of Technology*
M. Orkisz - *Rzeszow University of Technology*
S. Radkowski - *President of the Board of PTDT*
Y. Sato - *National Traffic Safety and Environment Laboratory, Japan*
M. Sobieszczański - *Bielsko-Biala Technology-Humanistic Academy*
A. Soudarev - *Russian Academy of Engineering Sciences*
Z. Stelmasiak - *Bielsko-Biala Technology-Humanistic Academy*
M. Ślęzak - *Ministry of Scientific Research and Information Technology*
W. Tarełko - *Maritime Academy of Gdynia*
W. Wasilewicz Szczagin - *Kaliningrad State Technology Institute*
F. Tomaszewski - *Poznan University of Technology*
J. Wajand – *Lodz University of Technology*
W. Wawrzyński - *Warsaw University of Technology*
E. Wiederuh - *Fachhochschule Giessen Friedberg*
B. Wojciechowicz - *Honorary President of SEF MEC PAS*
M. Wyszyński - *The University of Birmingham, United Kingdom*
M. Zabłocki – *V-ce President of KONES*
S. Żmudzki - *Szczecin University of Technology*
B. Żółtowski - *Bydgoszcz University of Technology and Life Sciences*
J. Żurek - *Air Force Institute of Technology*

Editorial Office:

GDANSK UNIVERSITY OF TECHNOLOGY
Faculty of Ocean Engineering and Ship Technology
Department of Ship Power Plants
G. Narutowicza 11/12 80-233 GDANSK POLAND
tel. +48 58 347 29 73, e – mail: sek4oce@pg.gda.pl

www.polishcimac.pl

This journal is devoted to designing of diesel engines, gas turbines and ships' power transmission systems containing these engines and also machines and other appliances necessary to keep these engines in movement with special regard to their energetic and pro-ecological properties and also their durability, reliability, diagnostics and safety of their work and operation of diesel engines, gas turbines and also machines and other appliances necessary to keep these engines in movement with special regard to their energetic and pro-ecological properties, their durability, reliability, diagnostics and safety of their work, and, above all, rational (and optimal) control of the processes of their operation and specially rational service works (including control and diagnosing systems), analysing of properties and treatment of liquid fuels and lubricating oils, etc.

All papers have been reviewed
@Copyright by Faculty of Ocean Engineering and Ship Technology Gdansk University of Technology
All rights reserved
ISSN 1231 – 3998
ISBN 83 – 900666 – 2 – 9

Printed in Poland

CONTENTS

Journal of POLISH CIMAC
Faculty of Ocean Engineering & Ship Technology
GDAŃSK UNIVERSITY OF TECHNOLOGY

MARINE TURBINE APPLICATION IN WASTE HEAT RECOVERY SYSTEMS

Andrzej Adamkiewicz*, Bartłomiej Wietrzyk**

Maritime University of Szczecin
Faculty of Mechanical Engineering, Institute of Ship Power Plant Operation
Wały Chrobrego 1-2, 70-500 Szczecin, Poland
**e-mail: andrzej.adamkiewicz@am.szczecin.pl*
***e-mail: w.bartek@wp.pl*

Abstract

This study shows an analysis of a ship power plant with waste heat recovery systems – Thermo Efficiency System (TES) with main engine exhaust gases utilization and exhaust power gas and steam turbines application. The systems were compared each other. The energetic efficiency in chosen waste heat recovery systems was compared. The advantages and disadvantages of turbines application in waste heat recovery systems were listed in a summary.

Keywords: *turbine, engine, waste heat energy, recovery, ship, power plant,*

1. Introduction

Ship's engine room efficiency determines the stage of the heat, which is received by fuel oil combustion in the main components of her power plants. Modern solutions of ship's power plants ensure the biggest possible efficiencies of converting fuel oil chemical energy for other aspects. One of the methods increasing efficiency of the power plant is recovering the heat which is lost with exhaust gases, main engine cooling water and charging air [2, 3, 4, 5]. Solution of this problem is possible through maximization of waste heat recovery generated by marine diesel engines and applying it in other installations to produce heat, electric and mechanical or combination of these energies. As a consequence of increasing main propulsion unit power of modern ships (increasing its deadweight), is forming a surplus energy which is produced in exhaust gas boilers as heating steam. In these circumstances, applying the combined waste heat recovery systems with exhaust gas and steam turbo generators is rational. There are a lot of waste heat recovery systems possible to apply on the motor ships. Their configuration depends on type of the vessel, her capacities, operating speeds and the output values implemented by the main propulsion plant [2]. Selection of the system solution on the specific ship should be result of widely comprehended, penetrating technical-economical analysis, based on solid mounts of thermodynamic and reliability analysis – methods keeping the engine room mobility.

2. Waste heat energy availability

Main and auxiliary engines are sources of waste heat energy in ship's propulsion plant. Quantity of these streams are diversified, energy included inside is not utilized fully. Waste heat energy losses size depend on main propulsion plant which has been used (diesel engine

or/and gas turbine). Low speed diesel engines have the highest thermal efficiency which is formed in range between 45÷55% (for comparison the turbine engines have lower thermal efficiency even 20%) [3, 4, 7]. Waste heat energy include heat losses of an exhaust gases, scavenging air and cooling water streams.

Increasing ship's energetic power plant efficiency is lashed with taking off assist of huge, available waste heat energy streams coming from main components of the system. On the pictures no. 1, 2 there are adequately heat balance diagrams of marine low speed diesel engines without and with recovery of energy, 12RT-flex96C type [9] and 12K98ME/MC type [8] on Fig. 3 and 4. Both of the engines evolve the 68640 kW output power which is realized with 94 rev/min.

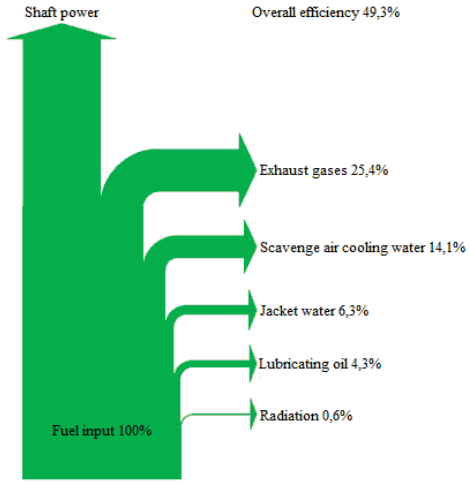

Fig.1 Heat balance diagram of marine low speed diesel engine 12RT-flex96C type [9]

In WARTSILA solution, both waste heat recovery system uses exhaust gas stream generated by main propulsion plant and scavenging air and cooling water streams. The biggest, possible waste heat recovery stream is carried by exhaust gases leaving the main engine. The lesser are: scavenge air, cooling water and lubricating oil streams. Systems offered by MAN B&W utilize only the exhaust gas stream. Overall efficiency of these engines without recovery is equal in total 49,3%.

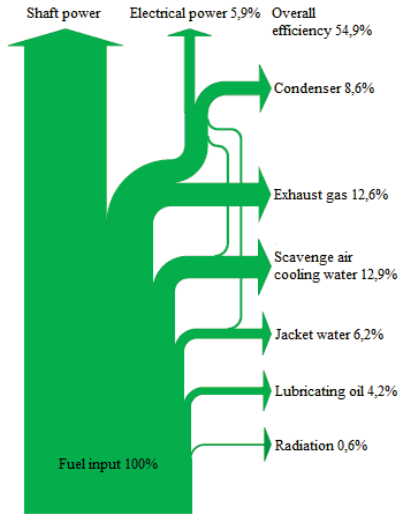

Fig. 2 Heat balance diagram of marine low speed diesel engine 12RT-flex96C type cooperating with waste heat recovery system [9]

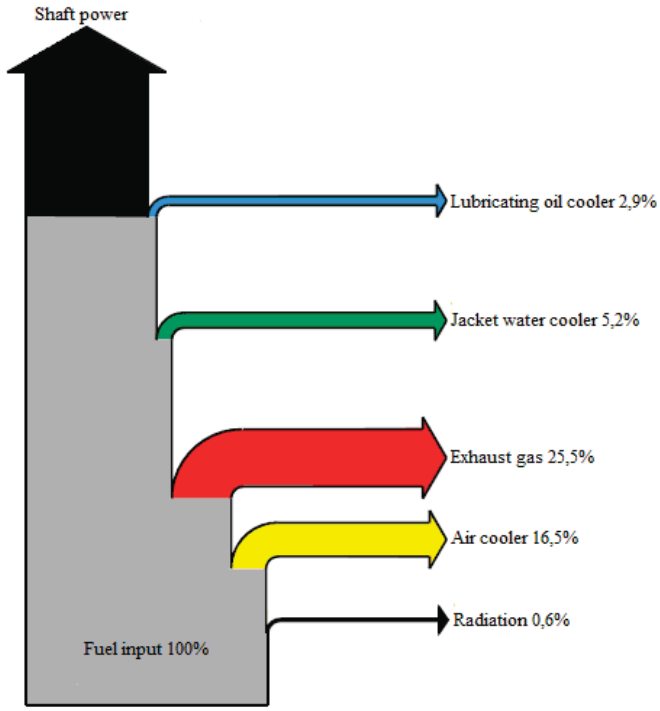

Fig. 3 Heat balance diagram of marine low speed diesel engine 12K98ME/MC type [8]

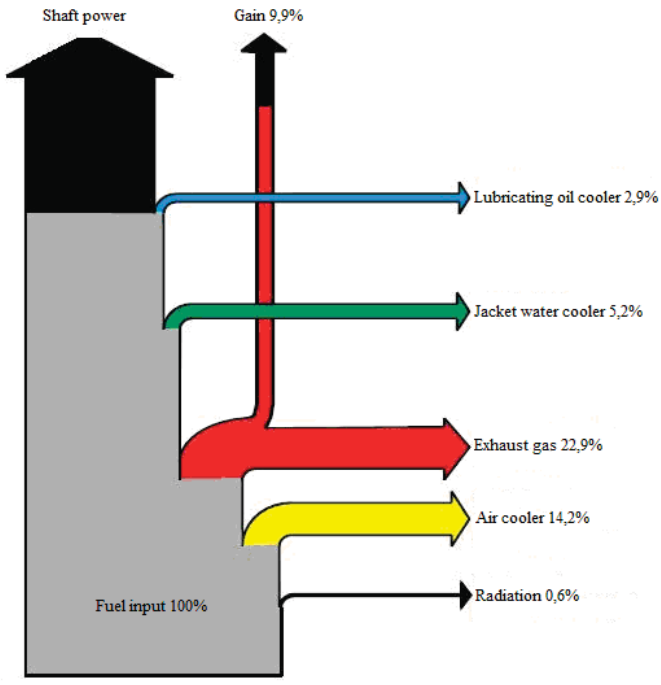

Fig. 4 Heat balance diagram of marine low speed diesel engine 12K98ME/MC type cooperating with waste heat recovery system [8]

3. Waste heat recovery systems

There are a lot of waste heat recovery systems with exhaust and steam turbines [7, 8, 9]. They are representing various energetic efficiency.

In this study, the standard, referencing solution of waste heat recovery system is system with exhaust power gas turbine, working according to the scheme shown on Fig. 8. The basic waste heat recovery system consists of a main engine with high efficiency turbochargers, exhaust power gas turbine via reduction gear and clutch driven AC generator. The energy of exhaust gases, leaving the main engine, is partly recovered in a turbochargers to compress, charge air or supply the exhaust power gas turbine driving the generator. About 10% of exhaust gas leaving the main engine is used to drive the generator [8]. The exhaust gases are being carried off through the cumulative manifold to the funnel in which there dampers installed and then to the atmosphere.

This solution is an alternative source of producing an electric power and now it is being introduced to the new building ships.

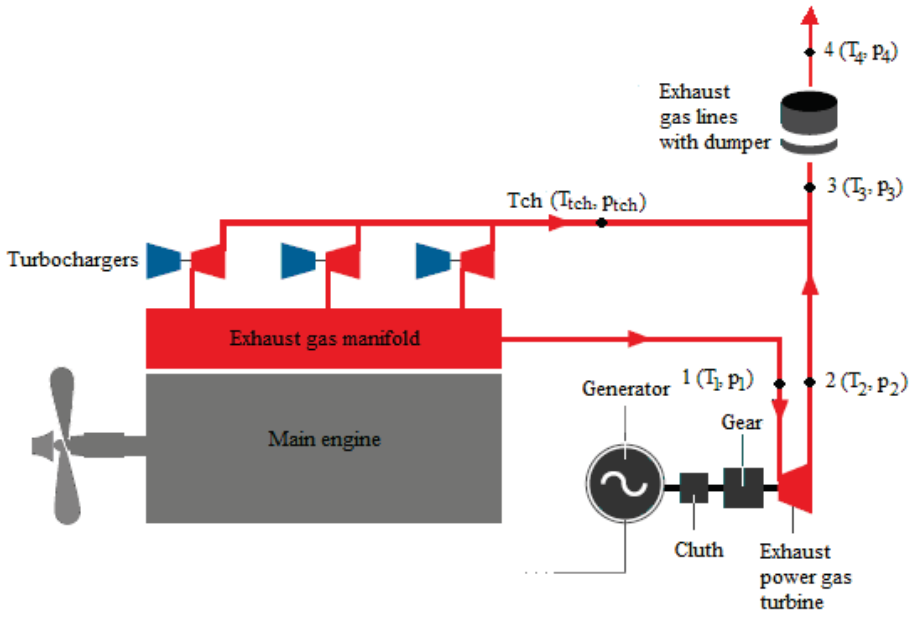

Fig. 5 Waste heat recovery system with exhaust power gas turbine [8]

Engine working waste heat recovery system (Fig. 8) is equipped with an air waste gate, stifle valve aim at keeping the normal cylinder pressure without the other restrictions at the very low intake air temperatures. At present, the propulsion plant cooperating with waste heat recovery systems can work at the intake air temperatures maintaining at the level of –5 to 35 centigrade. After exceeding the maximal pressure in a cylinder, the flow rate of exhaust gases feeding the exhaust power gas turbine, turbine and generator rotor speed would increase. It will cause the generator load disturbance.

Adopting the main engine to work at lower intake air temperatures involves the costs of fuel oil consumption, however the rate of recovered energy compensates this disadvantage.

Exhaust power turbine is working in the range 55÷100% of main engine load. Exhaust gas outflow is controlled by orifice on the outlet of the exhaust gas receiver, keeping the constant value of exhaust gas flow rate feeding the power turbine. In this way, the constant turbine load rate is being kept. With the main engine output lower than 55%, the exhaust gases feeding the turbine are being cut off. The air flow which is given by turbochargers is too low to generate properly large exhaust gas flow rate to ensure stabilized turbine load rate. Expand stage and

exhaust gas flow rate value are compared with suitable turbochargers parameters. Turbine outlet exhaust gases temperature is close to the temperature after the turbocharger.

Basic waste heat recovery system (Fig. 5) is often compared to the system with the exhaust gas boiler and steam turbine driving the generator. These systems are different in respect to the configuration and outputs. On the picture 6 there is waste heat recovery system with steam turbine feeding the steam from exhaust gas boiler [9].

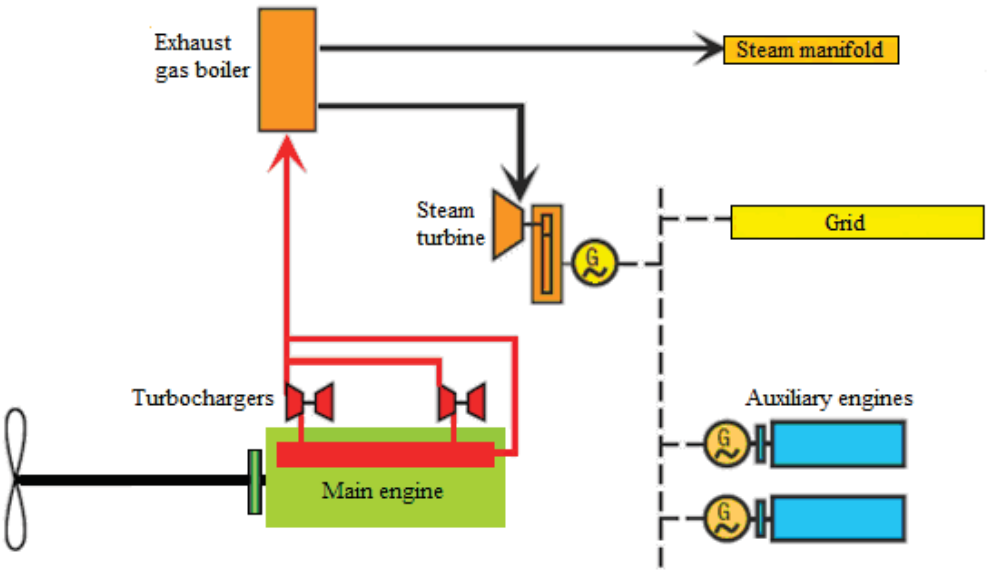

Fig. 6 Waste heat recovery system with an exhaust gas boiler and steam turbine [9]

On the Fig. 7 there is waste heat recovery system with an exhaust gas boiler exhaust power gas turbine and shaft generator. This system consists of main engine, turbochargers, exhaust gas turbine mechanically connected with the generator, exhaust gas boiler, shaft generator and self-contained auxiliary engines feeding the common board grid Described system differs from above one in relation to waste heat energy division between turbines.

Main exhaust gas energy stream: carrying by exhaust gases, after energy conversion in turbochargers is divided in two: exhaust gas stream heating the exhaust gas boiler and exhaust gas stream feeding the power turbine. During main engine working one part of exhaust energy stream is used to produce heating steam in exhaust gas boiler. Second part of this exhaust gas stream is converted by power turbine set mechanically connected with the generator to electric energy for the board grid. Controlling of the exhaust gas amount feeding the power turbine is realized in relation of main engine load through an orifice. About 10% of exhaust gases energy are used in this waste heat recovery system in power turbine.

Exhaust gases leaving the exhaust power gas turbine are guided to exhaust gas boiler too.

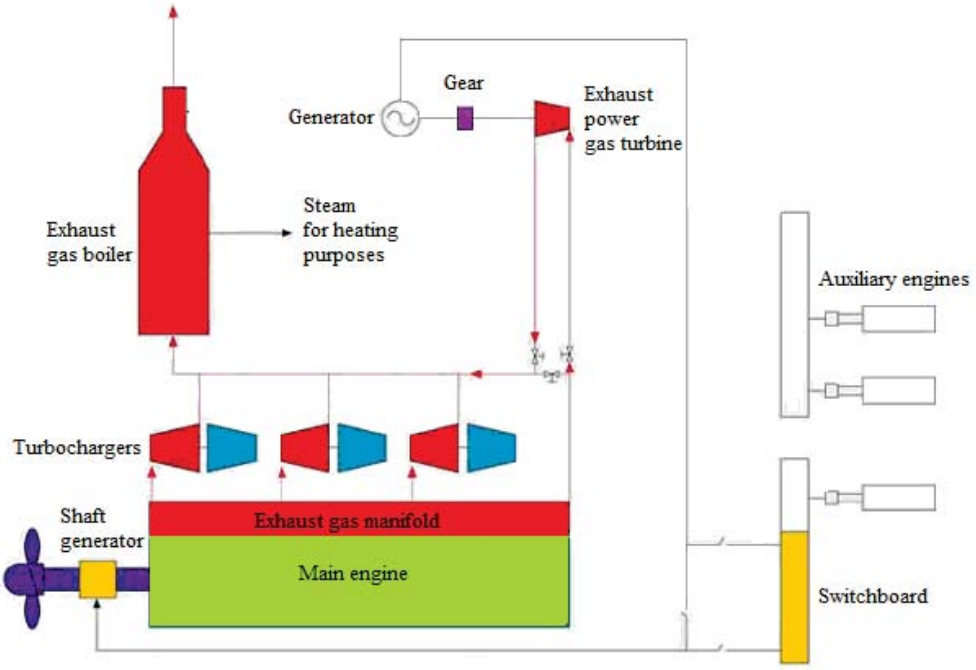

Fig. 7 Waste heat recovery system with an exhaust gas boiler, power turbine and shaft generator [8]

The efficiency of whole system is increased by a shaft generator application. This generator can work in a two variants. It can taking off the energy to the board grid or taking in assist the main propulsion plant. Engine running variant can be used for reduce fuel oil consumption amount with the reduced main engine output. The second variant is electric energy production for ship requirements, while the waste heat recovery system is stopped.

Beyond supplying the electric power, this system, allows to save the fuel oil (even to 5% per year) and essentially reduces the emission of toxic combustion substances.

Advanced waste heat recovery system, shown on Fig. 8 consists of an exhaust gas boiler, steam turbine, exhaust power turbine, synchronous generator driven by these turbines and shaft generator working for the board grid. Exhaust power gas turbine impeller connected with steam turbine impeller via power transferring system (reduction gear and clutch) drives the AC generator. Steam turbine is fed by superheated steam from the exhaust gas boiler. Shaft generator application increases whole efficiency of the system. This solution has been used for a first time on m/v Gudrun Maersk containership [9].

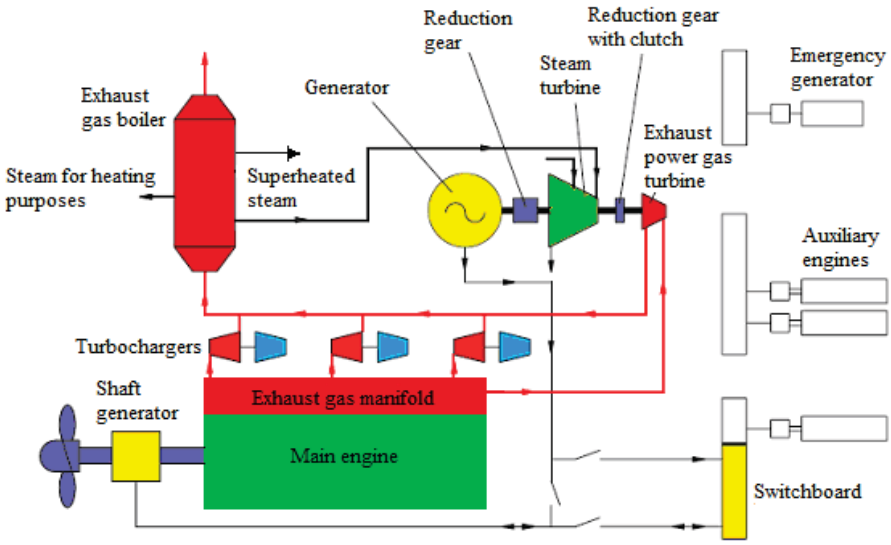

Fig. 8 Advanced waste heat recovery system with an exhaust power turbine, steam turbine and shaft generator [9]

Combined system application with en exhaust and steam turbine considerably increases its efficiency and reliability. Due to increase of an electric energy production at main engine loads above 50%, system efficiency grows even to 10% (see Fig. 9).

One possibility to improve the efficiency of the recovery of more heat without increasing the heat exchange surfaces can be applied fluidized bed exhaust boiler [1].

4. Chosen aspects of turbine application advisability in waste heat recovery systems

Economical efficiency of examined waste heat recovery systems with exhaust and steam turbines can be measure of its quality solution assessment [6]. Its final measurement will always be derivative brief fore designs accepted for the specific ship, conditions of her operating and stabilized technical – economical criterion. In this study, it was restricted to some aspects of turbine applications in waste heat recovery systems [5, 6].

Profitability of use and operate turbine in waste heat recovery system is conditioned by vessel state operating (sailing speed and the power involved by the main propulsion plant)and the time of being in its, which determines the quantity of energy possible to utilize. Modern waste heat recovery systems, with gas and steam turbines or their combination, are different due to their configuration, machines property and working parameters.

With increasing the exhaust power gas turbine output, disposal waste heat recovery streams increases in waste heat recovery system. The power turbine output increases and as a consequence the amount of the saved fuel combusted by propulsion plant increases too [9]. On Fig. 9 there are example ranges of possible output values reached by exhaust power gas turbine in relation to main engine output type 12K98ME/MC manufactured by MAN B&W [8].

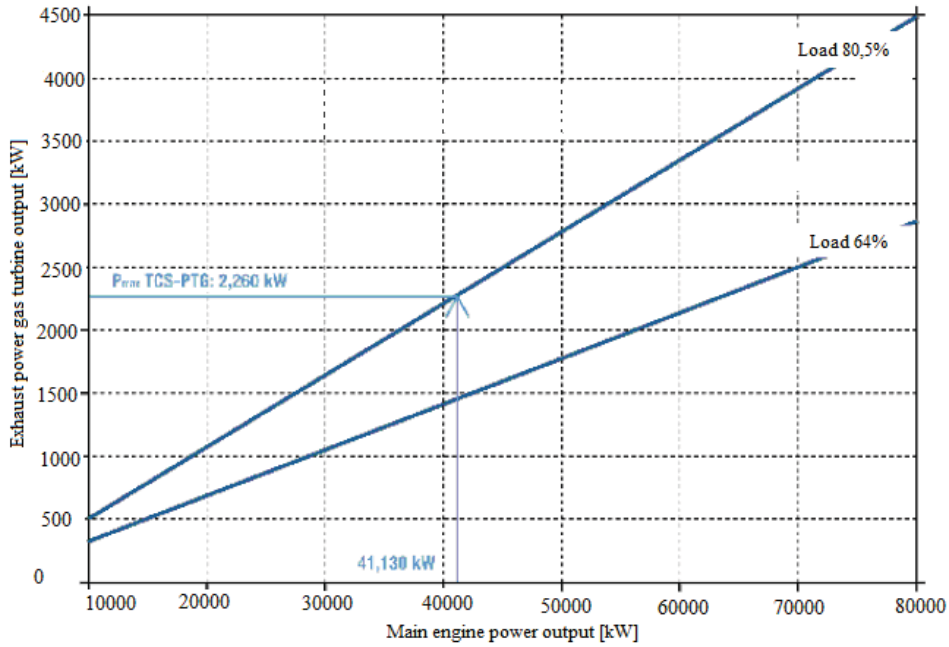

Fig. 9 Exhaust power gas turbine output waste heat recovery system in relation to main engine power [8]

With the main engine power 41130 kW exhaust power gas turbine working in TCS – PTG system evolves repayable power 2260 kW.
As a result of extracting specified outputs, there are fuel oil savings shown for the same engine on Fig. 10 in relation to exhaust power gas turbine output and main engine operating hours [8].

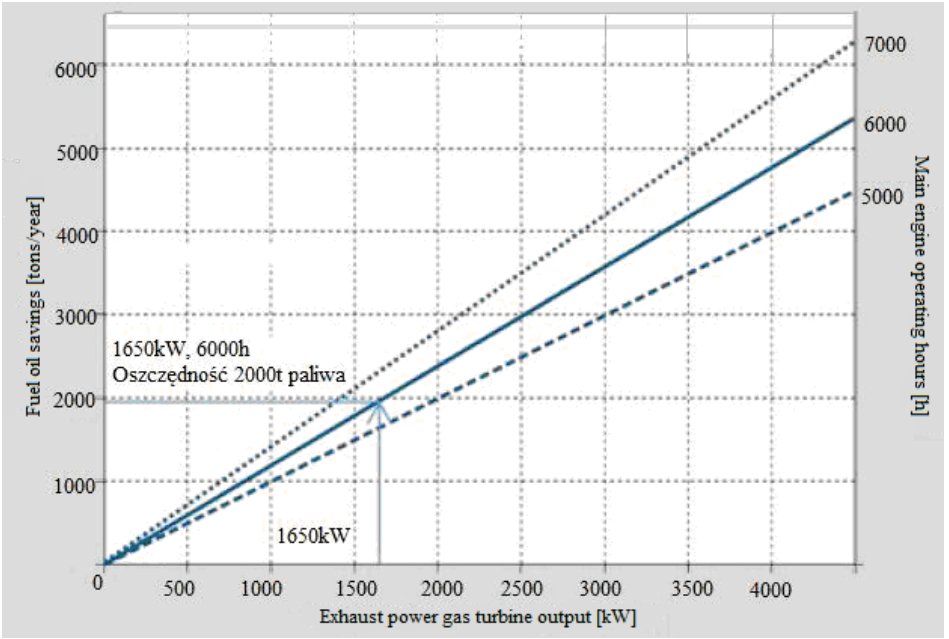

Fig. 10 Prediction fuel oil savings obtained as a result of waste heat recovery application in relation to exhaust turbine output [8]

In a case of waste heat recovery system with exhaust power gas turbine output 1650 kW, after 6000 working hours, the 2000 tons of fuel oil can be saved in a year. Such rational advantage coming from waste heat recovery system application can be gained in case of huge main propulsion plants, here exceeding 40000 kW [8].

5. Thermodynamic analysis of examined waste heat recovery system

Exhaust gases ability was analyzed to conversion part of the waste to effective electric energy with intermediate aspect reciprocating energy generated by power turbine. On the Fig. 5 there is basic waste heat recovery system with alluvial points enable the thermodynamic identification. Inlet exhaust gas parameters marked as 1, outlet parameters as 2.

Large flow rate and exhaust gases temperatures relatively keeping at the same level ensure working stability of power turbine and constant internal efficiency close to project value. On table 1 there are technical data of radial and axial power turbines applying in waste heat recovery systems manufactured by MAN B&W [8]. Expand stage turbine π_t is 3,3, exhaust gas temperature before turbine is 450^0C.

Tab. 1. Basic technical data of power turbines

Radial power turbines			
	Output [kW]	Flow rate [kg/s]	Speed [1/min]
(TCS-) PTG16	600	3.0	41,000
(TCS-) PTG18	900	4.3	34,000
(TCS-) PTG20	1,300	6.3	28,500
(TCS-) PTG22	2,300	13.0	21,500
Axial power turbines			
(TCS-) PTG55	3,400	19.0	17,000
(TCS-) PTG66	4,800	27.0	14,500

They can work in system TCS/PTG (Turbo Compound System/Power Turbine Generator) – the system taking off main engine assistance/exhaust power generator set.

For the turbines described in table 1 the disposal enthalpy drops were calculated according to the dependence [3, 4, 6]:

$$\Delta h_{sT} = \frac{P_e}{\dot{m}_{exh} \cdot \eta_{iT} \cdot \eta_{mT}} \tag{1}$$

and heat streams [4, 6]:

$$\Delta \dot{Q}_t = \dot{m}_{exh} \cdot \Delta h_{st} \tag{2}$$

The results of calculations are show in table 2. The biggest heat streams convert axial power turbines whereas disposal enthalpy drop values render that it can be even single stage turbines. Bigger disposal enthalpy drops are converted by radial power turbines, in comparison with axial they give less outputs. Higher output values gained by axial turbines are result of bigger flow rates exhaust gases conversion. Bigger turbines internal efficiencies are fostering in gaining higher axial turbine outputs, which influences on waste heat recovery system efficiency.

Tab. 2. Calculated dispose enthalpy and heat streams in turbine

Radial power turbines		
Turbine type	Δh_{sT} [kJ/kg]	$\Delta \dot{Q}_T$ [kW]
TCS – PTG 16	266,6	799,8
TCS – PTG 18	279,1	1200,13
TCS – PTG 20	275,1	1733,13
TCS – PTG 22	235,9	3066,7
Axial Power turbines		
TCS – PTG 55	210,5	3999,5
TCS – PTG 66	209,1	5645,7

5. Summary and conclusion

Heat balance diagrams analysis of marine low speed diesel engines confirms possibility and advisability use of waste heat recovery energy in marine energetic power plants. Marine engine power output, temperature of medium feeding the waste heat recovery system (exhaust gases, cooling water), pressure and flow rate factor determine the quantity of available heat in waste heat recovery system. Exhaust gas and steam turbine application takes effect in additional electric energy production, fuel oil savings and limitation of emission toxic substances to the atmosphere [8]. Exhaust gas and steam turbine cooperating increases systems efficiency especially in direction to enlarge of electric energy production. Use character of waste heat recovery system with power turbine is conditioned by continuity of steady turbine work at main engines load ranges above 50% rated power ensuring adequately large waste heat streams carrying by exhaust gases. Quantity of saved energy can be estimated after penetrating analysis of each other of waste heat recovery systems.

Literature

[1] Adamkiewicz A., Zeńczak W., *Model Testing of Fluidized Bed Boiler for Sea-Going Ships,* Marine Technology Transactions, Vol.17 , Gdańsk 2006, pp. 23-35.

[2] Behrendt C., Adamkiewicz A., Krause P., *Dostępność energii odpadowej w układach energetycznych statków morskich z utylizacyjnymi kotłami parowymi,* Prace Naukowe. Monografie. Konferencje, Zeszyt 16. Politechnika Śląska, Instytut Maszyn i Urządzeń Energetycznych. Gliwice 2006, s. 29 – 48.

[3] Chmielniak T.J., Rusin A., Czwiertnia K., *Turbiny gazowe*. Ossolineum, Wydawnictwo IMP PAN, w serii Maszyny Przepływowe Tom 25, Gdańsk 2001.

[4] Kowalski A., Krzyżanowski J., *Okrętowe siłownie parowe*. Wydawnictwo Uczelniane WSM Gdynia 1995.

[5] Michalski R., *Ocena termodynamiczna okretowych systemów utylizacji energii odpadowej spalin.* Zeszyty naukowe Nr 66, Wyższa Szkoła Morska w Szczecinie, Szczecin 2002.

[6] Perycz S., *Turbiny parowe i gazowe.* Ossolineum, IMP PAN, w serii Maszyny Przepływowe Tom 25, Gdańsk 1995 lub Wydawnictwo Politechniki Gdańskiej, Gdańsk 1986.

[7] www.abb.com

[8] www.manbw.com

[9] www.wartsila.com

Praca naukowa finansowana ze środków na naukę w latach 2009-2012 jako projekt badawczy własny nr N N509 404536.

Journal of POLISH CIMAC
Faculty of Ocean Engineering & Ship Technology
GDAŃSK UNIVERSITY OF TECHNOLOGY

DETERMINATION OF OPERATIONAL LOAD PARAMETERS OF DREDGE PUMPS UNDER DREDGING OPERATIONS

Damian Bocheński

Gdansk University of Technology
Faculty of Ocean Engineering & Ship Technology
Department of Ship Power Plants
tel. (+48 58) 347-24-30; fax (+48 58) 347-19-81
e-mail: daboch@pg.gda.pl

Abstract

This paper presents proposal of a method for determining operational load parameters of dredge pumps, one of the crucial mechanical energy consumers on dredgers. The method based on results of the author's operational investigations, deals with two main service states of dredge pumps on dredgers, namely: the state of loading the solid into soil hold (of dredger or hopper barge) and the state of pumping ashore.

Keywords*: dredgers, dredge pumps, ship power systems.*

1. Introduction

Dredge pumps belong to the most important consumers of mechanical energy on dredgers. Their function is to hydraulically transport loosened soil from the sea bed into soil hold of the dredger or hopper barge (a service state called loading the spoil) as well as from the hold (sometimes directly from the sea bed) through long transfer piping to a dump on shore (a service state called transferring the spoil ashore). The states occur always on suction dredgers (e.g. trailing suction hopper dredgers, cutter suction dredgers, barge unloading dredgers), sometimes also on dredgers with mechanical dredging systems (e.g. bucket ladder dredgers) [8]. Power demand of dredge pumps depends on their use and design assumptions as well as on size of dredger. It is contained in a broad interval ranging from several hundreds kW to even a dozen or so thousands kW [7,8].

Irrespective of a type of dredger the dredge pumps can operate in two basic service states [3,4,6,7,8]:

- the loading of the spoil into the hopper (soil hold) on the dredger or assisting hopper barge; operational conditions of the pump system are characterized by the following features: the static lifting height of the system is as a rule greater than the dynamic one ($H_{st} \geq H_{dyn}$), similar values of flow drag of water-soil mixture on suction and pressure side of pump ($\Delta h_s \approx \Delta h_p$);
- the hydraulic emptying of the soil hold or transferring the spoil directly to a dump on shore (the pumping the spoil ashore); in this case operational conditions of the pump system are characterized by a much greater dynamic lifting height than the static one

($H_{st} << H_{dyn}$) and much greater values of flow drag on the pump pressure side than on its suction side ($\Delta h_s << \Delta h_p$).

The state called loading the spoil into the hold always occurs on trailing suction hopper dredgers (it concerns their own holds) , and may also occur on cutter suction dredgers (in this case it concerns hopper barge holds). The pumping-away the spoil occurs on trailing suction hopper dredgers and cutter suction dredgers, sometimes also on bucket ladder ones. Great differences in the parameters which characterize the pump systems operating in the above mentioned service states must result in great differences in the loads applied upon dredge pumps during loading and pumping-away the spoil. On the trailing suction hopper dredgers the using of the same pumps both for the loading and pumping-away the spoil is common. Then their driving systems are fitted with multi-speed gear transmission devices.

This paper presents a proposal of determining the distribution parameters of operational loads of dredge pumps installed on various types of dredgers, depending on their service states. For the determining of the distribution parameters of pump loads the use of linear form of dependence of mean driving loads of dredge pumps on their rated power outputs, is proposed [1,2]. Standard deviations are proposed to be determined by means of the data concerning the load distribution variability coefficient of dredge pumps, obtained on the basis of operational investigations.

2. Investigations of relations between mean operational loads of dredge pumps and their rated power outputs

Investigations of relations between the mean operational loads of main power consumers N_{MC}^{av} , and their rated power outputs $(N_{MC}^{eff})^{nom}$ are important in view of possible making use of their results further in preliminary design stages of ship power plants.

As far as the main consumers are concerned, it can be considered effective energy flow (i.e. power output or effective power) associated with them, each case expressed by the product of the so called „ generalized potential" and the „ generalized flow" [1].

The investigations of relations between the mean operational loads of main power consumers and their rated power outputs were already performed for fish factory trawlers as well as certain main consumers on dredgers [1,2].

The performed investigations show that for all main power consumers on the investigated ships the following linear relation takes place [1,2]:

$$N_{MC}^{eff} = a + b\,(N_{MC}^{eff})^{nom} \tag{1}$$

where: a, b - constants

The statement on validity of the linear relation (1) as well as on possibility of determining the constants a, b, is very important as the relation can be used for determining the power demand of main engines for ships of the considered types in the stage of offer or preliminary design [1,2,3].

The dredge pump power output N_{DP}^{eff} is determined by the relation:

$$N_{DP}^{eff} = H_{DP}^{w} \cdot Q_{DP}^{w} \tag{2}$$

where: H_{DP}^{w} - the dredge pump lifting height determined for water ,

Q_{DP}^{w} - the dredge pump volumetric rate of delivery determined for water.

It is important that producers of dredge pumps usually provide nominal (rated) parameters and characteristics of the pumps valid for the conditions of water pumping but not water-soil mixture pumping. Change of characteristics of dredge pump handling water-soil mixture, as well as change of pipeline characteristics is most influenced by density of the mixture and soil graining (a.o. mean grain diameter, grain-size distribution, grain shape) [7,8]. High variability of the parameters causes that the providing of the parameters of dredge pumps for the conditions of water-soil mixture pumping would be unjustifiable.

In Tab. 1 and 2 are given the rated parameters of the dredge pumps on the investigated dredgers as well as the distribution parameters of operational loads of the pumps during operation in two basic stages of their service (loading the spoil to hopper and pumping the spoil ashore) [6]. The distribution parameters of operational loads of dredge pumps have been obtained as a result of long-lasting operational investigations carried out by this author on a dozen or so dredgers of various types. The problem of operational loads of dredge pumps, which covers measurement methods, measurement system characteristics, distributions of pump loads, has been presented more thoroughly in a few publications of this author [3,4,5,6].

Tab.1. Rated parameters of dredge pumps and characteristics of their operational loads during loading the spoil to hopper, for 8 investigated dredgers

Dredger	Number pumps	Rated parameters of dredge pumps (pumping water)			Characteristics of load distributions of dredge pumps		
		H_{DP}^{w}	Q_{DP}^{w}	N_{DP}^{eff}	N_{DP}^{av}	σ_{DP}	ν_{DP}
		kPa	m^3/s	kW	kW	kW	-
Kostera	1	105	0,65	68,2	82,1	6,9	0,084
Kronos	1	140	0,65	91	95,1	7,8	0,082
Łęgowski	2	175	1,8	2×315	774,9	62,3	0,08
Bukowski	2	175	1,8	2×315	786,4	54,5	0,069
Nautilus	1	210	2,5	525	706,8	26,2	0,037
Gogland	2	220	3,2	2×704	1787,1	61,2	0,034
Geopotes 15	2	265	3,4	2×901	1987,7	71,9	0,036
Lange Wapper	1	395	4,6	1817	2482,6		

Tab.2. Rated parameters of dredge pumps and characteristics of their operational loads during pumping the spoil ashore, for 13 investigated dredgers

Dredger	Number pumps	Rated parameters of dredge pumps (pumping water)			Characteristics of load distributions of dredge pumps		
		H_{DP}^{w}	Q_{DP}^{w}	N_{DP}^{eff}	N_{DP}^{av}	σ_{DP}	ν_{DP}
		kPa	m^3/s	kW	kW	kW	-
Kostera	1	370	0,55	203,5	216,5	29,6	0,137
Kronos	1	490	0,5	245	189,4	20,6	0,109
Łęgowski	2	385	1,6	616	832,9	101,4	0,122
Bukowski	2	385	1,6	616	835,7	52,8	0,064
Gogland	2	430	3,0	1290	1815,9	178,4	0,098
Geopotes 15	2	560	3,0	1680	2211,1	239,9	0,109

Lange Wapper	2	1240	4,1	5084	3861,9		
Trojan	1	600	1,0	600	536,7	122,9	0,229
Toruń	1	530	0,95	503,5	431,5	52,3	0,121
Scorpio	1	610	2,05	1250,5	1667,5	278,6	0,167
Rozkolec	2	1160	1,75	2030	1188,1	334,8	0,282
Raja	1	440	0,7	308	240,5	32,3	0,134
Małż II	1	410	0,4	164	158,26	30,78	0,194

Tab.3. Linear regression equations which determine mean loads of dredge pumps during two basic states of their service

States of dredge pumps	Postać zależności	Statistical evaluation				
		R	σ	F	F_{kr}	m
loading of the spoil to hopper	$(N_{DP}^{av})^{ls} = 1{,}242 \cdot (N_{DP}^{eff})^{ls} + 5{,}745$	0,988	81,4	276,6	5,99	8
pumping the spoil ashore	$(N_{DP}^{av})^{sp} = 0{,}755 \cdot (N_{DP}^{eff})^{sp} + 244{,}43$	0,934	147,4	75,8	4,84	13

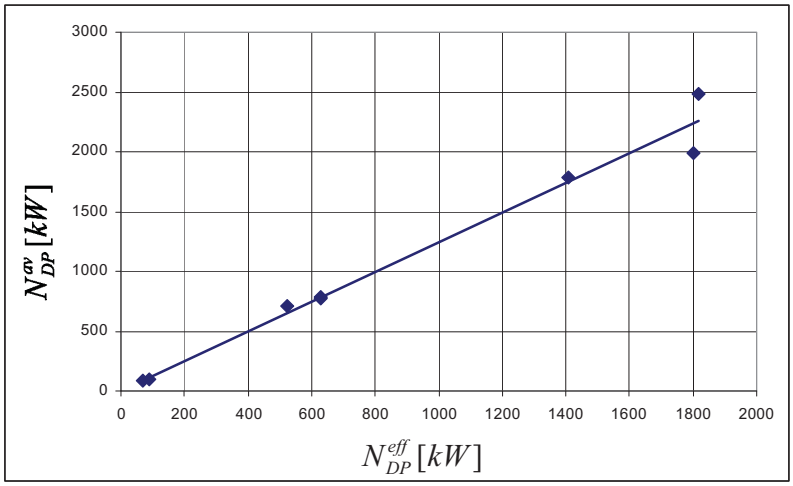

Fig. 1a. The relations $N_{DP}^{av} = f(N_{DP}^{eff})$ for dredge pumps in state of loading the spoil to hopper

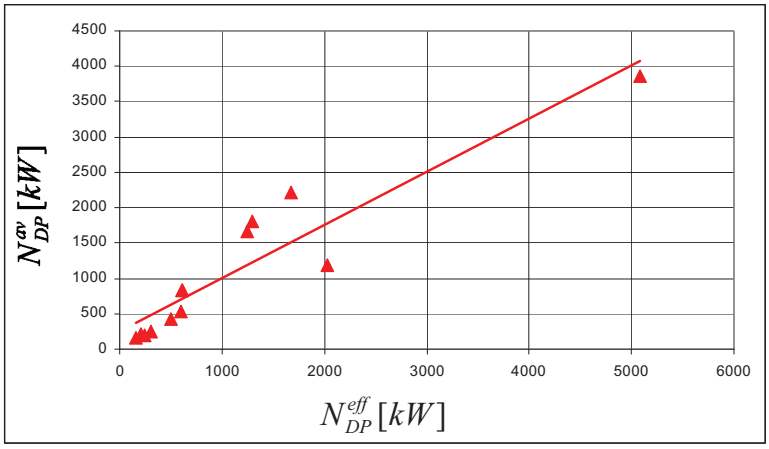

Fig. 1b. The relations $N_{DP}^{av} = f(N_{DP}^{eff})$ *for dredge pump in state of pumping ashore*

If rated parameters of dredge pump (-s) are known it is possible - by making use of the relations given in Tab.3 - to predict its (their) mean load during a considered service state.

3. Standard deviations of operational load distributions of dredge pumps, working time fractions of the pumps in a given service state

Value of the standard deviation σ_{DP} can be determined by using data which deal with the variability coefficient $\nu_{DP} = \sigma_{DP} / N_{DP}^{av}$ (Tab.1 and 2). Values of the variability coefficients of load distributions of dredge pumps during loading the winning are contained within the interval of $0{,}034 \div 0{,}084$ at the mean value of ν_{DP} equal to 0,06 (Tab.1). In the case of the service state of transferring the winning values of the variability coefficients of load distributions of dredge pumps are contained within the interval of $0{,}064 \div 0{,}229$ at the mean value of ν_{DP} equal to 0,146 (Tab.2).

The analyzed loads of dredge pumps concern duration time of loading the spoil to the hold (of the dredger or hopper barge) or hydraulic unloading the spoil from the hold (of the dredger or hopper barge), that is determined by values of the usage time coefficients λ_{DP}^{ls}, λ_{DP}^{sp} (Tab.1 and 2 given in [6]).Values of the coefficient λ_{DP}^{ls} are contained in the interval of 0,95÷0,98, at its mean value equal to 0,972. Values of the coefficient λ_{DP}^{sp} are close to the λ_{DP}^{ls} values and are contained in the interval of 0,96÷0,99 , at its mean value of 0,978.

If the relation of the duration time of „dredging operations" has to be determined the coefficient λ_{ls}^{do} or λ_{sp}^{do} is to be additionally taken into account. Values of the coefficients depend on a type of dredger and its design solution.

In addition the case of cutter suction dredger with underwater pump should be highlighted. The so applied pumps operate both during loading the winning into hopper barge (dredging to hopper barges) and during dredging with simultaneous pumping ashore with the use of dredge pump (pumps) installed onboard. For both the situations working conditions of the underwater pump can be assumed the same and corresponding with the conditions of loading the spoil. Of course, the dredge pump installed onboard operates only during pumping the spoil ashore.

4. Summary

All the calculation results which concern load characteristics of dredge pumps, presented in this paper, reflect operational reality of the pumps on dredgers. The results can be deemed representative for the whole population of dredge pumps used on dredgers, in view of the large number of the investigated dredgers and wide range of their size.

The presented results may be useful in predicting operational loads of dredge pumps, depending on their service states typical on various types of dredgers. That will make it possible – in association with knowledge of loads of other main consumers and efficiency characteristics of power transmission systems of particular consumers - to determine characteristics of operational loads of main engines on dredgers. It is especially important in preliminary design stages of power systems for dredgers.

Bibliography

[1] Balcerski A., *Modele probabilistyczne w teorii projektowania i eksploatacji spalinowych siłowni okrętowych*. Fundacja Promocji Przemysłu Okrętowego i Gospodarki Morskiej, Gdańsk 2007

[2] Balcerski A., Bocheński D., *Badania zależności średnich obciążeń napędu odbiorników technologicznych na jednostkach technologicznych od ich nominalnych mocy użytecznych*. Zeszyty Naukowe Wyższej Szkoły Morskiej w Szczecinie nr 71, Szczecin 2003

[3] Bocheński D., Kubiak A., *Wybrane problemy eksploatacji pomp gruntowych na pogłębiarkach*. /Materiały/ XXI Sympozjum Siłowni Okrętowych SymSO 2000', Gdańsk 2000

[4] Bocheński D., Kubiak A., *Analiza i ocena warunków pracy pomp gruntowych na pogłębiarkach ssących nasiębiernych*. Międzynarodowa XIX Sesja Naukowa Okrętowców NT. TECHNIKA MORSKA NA PROGU XXI WIEKU. Materiały konferencyjne, vol.2, Szczecin-Dziwnówek 4-6.V.2000r, 35-43

[5] Bocheński D. (Kierownik projektu) i in., *Badania identyfikacyjne energochłonności i parametrów urabiania oraz transportu urobku na wybranych pogłębiarek i refulerów*. Raport końcowy projektu badawczego KBN nr 9T12C01718. Prace badawcze WOiO PG nr 8/2002/PB, Gdańsk 2002

[6] Bocheński D., *Operational loads of dredge pumps in their basic service on selected types of dredgers*. Journal of Polish CIMAC, Energetic aspects vol. 2, no 2, Gdańsk 2008

[7] Vlasblom J. W., *Dredger pumps*. Lecture notes, TUDelft 2002

[8] Vlasblom J. W., *Designing dredging equipment*. Lecture notes, TUDelft 2003-05

Journal of POLISH CIMAC

Faculty of Ocean Engineering & Ship Technology
GDAŃSK UNIVERSITY OF TECHNOLOGY

ANALYSIS OF TRENDS IN ENERGY DEMAND FOR MAIN PROPULSION, ELECTRIC POWER AND AUXILIARY BOILERS CAPACITY OF GENERAL CARGO AND CONTAINER SHIPS

Zygmunt Górski, Mariusz Giernalczyk

Gdynia Maritime University
83 Morska Street, 81-225 Gdynia, Poland
tel.: +48 58 6901307, +48 58 6901324
e-mail: magier@am.gdynia.pl, zyga@am.gdynia.pl

Abstract

The paper deals with the problem of energy demand for the main propulsion as a function of deadweight and speed for general cargo vessels built in the 60-ties, multi-purpose general cargo vessels built In the 80-ties as well as recently built container vessels. Changes in power of the main propulsion and trends observed in the matter are defined. In the same way the analysies of electric power and boilers capacity are carried out. In the summary conclusions and prognosis concerning energetic plants of general cargo and container vessels are expressed.

Keywords: *cargo ship, container ship, main propulsion power, electrical power, auxiliary steam delivery, statistics*

1. Introduction

General cargo vessels built in the 60-ties were designed for carriage of general cargo i.e. industrial goods counted in number and packed in boxes, drums, bales, bags or other similar packages. Such vessels were usually provided with cargo handling equipment (deck cranes, cargo booms) to make possible cargo operation without aid of harbour cargo facilities. Cargo space of the vessel was divided by bulkheads and twin decks to optimise the space utilisation and to separate different kinds of cargo as well as to separate cargo of different destinations. The speed of these vessels was 16 ÷17 knots. At the turn of the 60-ties and the 70-ties a new kind of general cargo vessels fitted for container carrying named **universal** or **multi purpose general cargo vessels** were built. They achieved service speed of 18÷20 knots. In the mid of 70-ties traditional general cargo as well as multi purpose general cargo vessels were almost entirely replaced by containerised cargo and ships named **container vessels.**

Container vessels are the ships equipped with special guides to freight vertically loaded and unloaded containers. The first ship adapted in 1956 from tanker for container transport was *Ideal-X*. Nowadays, the biggest container vessels can carry above 10,000 TEU and can hardly be situated in panamax class dimensions. The number of those ships is bigger than panamax class and they are used on routes excluding Panama Canal passing e.g. China – USA West Coast. Today the biggest container vessel is MS EMMA MAERSK with carrying capacity of 11,500 TEU shown in fig. 1.To ensure quick transport of containers all around the world and to minimise transport expenses large container vessels travel overseas calling at a

number of big ports called *hubs*. Containers are delivered from smaller ports to *hubs* by small container vessels (200-500 TEU) named *feeders*. A number of small container vessels (below 3000 TEU) is equipped with cargo handling facilities (deck cranes or bridge cranes), so they are able to call at ports not equipped with cargo facilities. Bigger container vessels have to use harbour equipment. Regarding vessel dimensions and weight of containers a special goliath gantry cranes are used. Container vessels are the quickest freighters. They achieve service speed of 24-26 knots.

Fig.1. M/S EMMA MAERSK at sea

An initial analysis shows as follow:

- the main propulsion is executed by low speed diesel engines; in case of modern container vessels steaming with high speed very large and powerful diesel engines of 100,000 HP and bigger shaft power are used,
- three diesel generators create onboard power station on general cargo vessels; sometimes an additional shaft generator is used; in case of container vessels the onboard power station is considerably bigger due to the necessity of bow thrusters and refrigerated containers supply,
- a boiler room usually consists of two auxiliary steam boilers one fuel fired and the second one heated by main engine exhaust gases; capacity of boilers 2000-3000 kg/h and considerably higher on big container vessel.

The aim of this paper is an analysis of the trends in development of main propulsion power, electric power and auxiliary boiler capacity on general cargo and container vessels by means of statistics.

2. Analysis of main propulsion plants development

To determine main propulsion power of general cargo vessels built in the 60-ties the data of 287 such ships was taken to considerations [3]. The result of statistic calculations is the formula (1) [3] [5] which shows the dependency of main propulsion power on deadweight and ship service speed:

$$\mathbf{N_n = 0{,}039 \cdot D^{0{,}435} \cdot v^{2{,}918}\ [kW],} \qquad (1)$$

where: N_n [kW] – shaft power of the main engine,
D [tons] – deadweight,

v [knots] – ship service speed.

Statistic researches of container vessels built in the last years gave formula (2) [2]:

$$N_n = (0{,}99179 + 0{,}00003412 \cdot D) \cdot v^3 \quad [kW], \tag{2}$$

On the basis of formulas (1) and (2) the dependency of main propulsion power on deadweight and different service speed for general cargo vessels is shown in figure 2 and the same for container vessels is shown in figure 3. To enable the comparison of main propulsion plants development in last years for both cases, the approximation of both formulas was done by means of linear functions. An example of the final analysis concerning main propulsion power of both types of vessels for given speed v=18 knots is shown in figure 4.

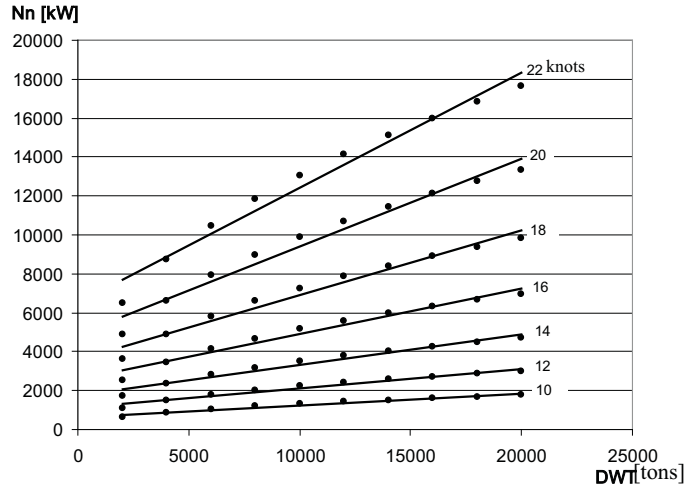

Fig. 2. Dependency of general cargo vessels main propulsion power on deadweight for different speed

$N_n = 0{,}0287 * D^{0{,}435} * v^{2{,}918}$ [kW] DWT [tons], v [knots]

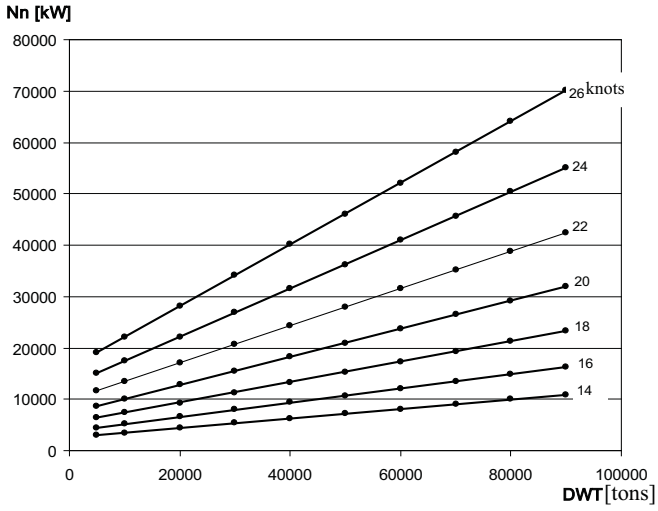

Fig. 3. Dependency of general container vessels main propulsion power on deadweight for different speed

$N_n = (0{,}9179 + 0{,}00003412 * D) * v^3$ [kW] DWT [tons], v [knots]

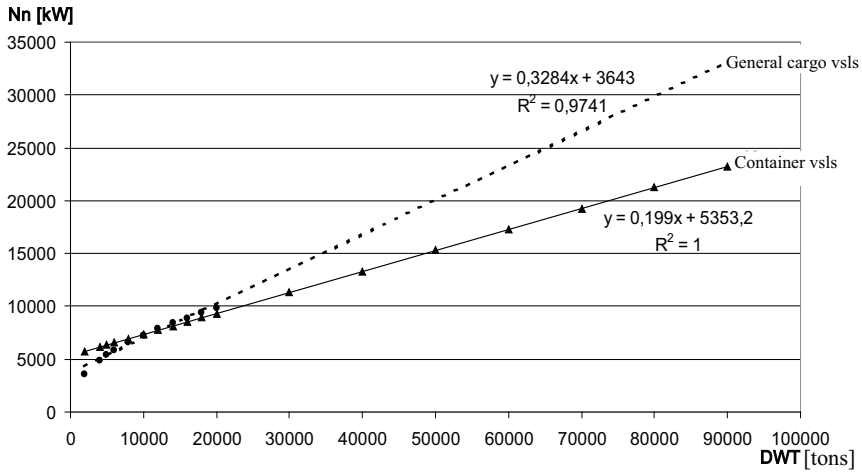

Fig. 4. Comparison of main propulsion power of general cargo vessels and container vessels at service speed 18 knots

As the largest built general cargo vessels achieved deadweight of about 20,000 tons to make it possible to compare with container vessels an extrapolation of power describing function was executed as a prognosis. The result of comparison (fig. 4) shows that for vessels larger than about 15,000 tons the main propulsion energy demand of general cargo vessels is much bigger than the same of contemporary built container vessels. It is probably possible due to the improvement in hull construction. General cargo vessels built in the 60-ties and the 70-ties did not have bow bulb and modern stern construction thus the resistance of ship hull in motion was higher and the same for main propulsion power demand. On the other hand, a high main propulsion power of container vessels is the result of high service speed because container vessels are the fastest merchant vessels.

3. Analysis of onboard power station development

The total electric power of general cargo vessels onboard power station can be approximately estimated from formula (3) elaborated by Centrum Techniki Okrętowej in Gdańsk [4]:

$$\mathbf{\Sigma N_{el} = 23 + 0{,}1088\, N_n}\ [\mathrm{kW}], \tag{3}$$

where: ΣN_{el} [kW] – total electric power,
N_n [kW] – main propulsion power (main engine shaft power).

Next, the total electric power of container vessels power station is given in formula (4) described in method [1]:

$$\mathbf{\Sigma N_{el} = 1077 + 0{,}1580\, N_n}\ [\mathrm{kW}], \tag{4}$$

The dependencies of total electric power on main propulsion shaft power for general cargo vessels and container vessels from formulas (3) and (4) are compared in figure 5. It is possible to observe much bigger demand of electric power for container vessels than for general cargo vessels. However some general cargo vessels were equipped with cargo handling facilities which increase electric power demand, container vessels have bigger electric power demand due to installation of bow thrusters and the necessity of power supply for a big number of refrigerated containers.

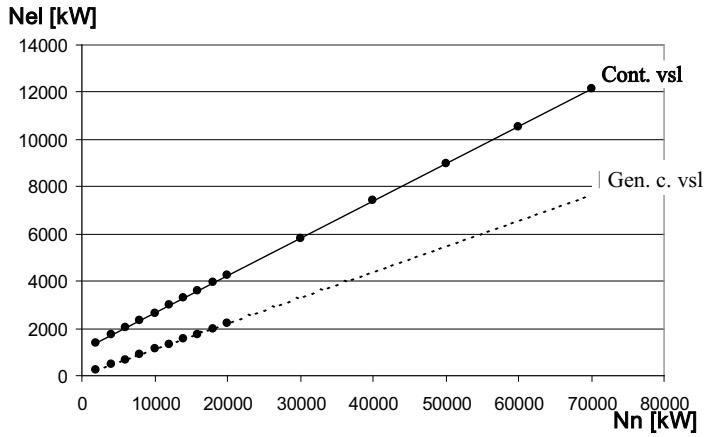

Fig. 5. Comparison of total electric power installed on general cargo vessels and container vessel as a function of main propulsion power

4. Analysis of auxiliary steam boilers development

To determine total auxiliary boilers capacity on general cargo vessels formula (5) given in [2] was used:

$$\mathbf{D_k = 0{,}075045\ N_n + 1054{,}5\ [kg/h],} \quad (5)$$

where: D_k [kg/h] – total boilers capacity,
N_n [kW] – main propulsion power (main engine shaft power).

In turn total auxiliary boilers capacity on container vessels is given in formula (6) described in [1]:

$$\mathbf{D_k = 0{,}0657\ N_n + 2536{,}6\ \ [kg/h],} \quad (6)$$

Dependency of total boilers capacity on main propulsion power for general cargo vessels and container vessels calculated according to formulas (5) and (6) is compared in figure 6.

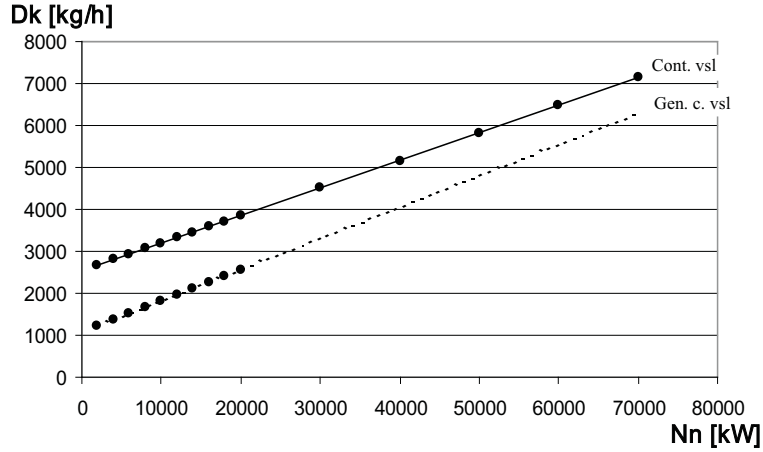

Fig. 6. Comparison of total boilers capacity on general cargo vessels and container vessel as a function of main propulsion power

Much bigger heat energy consumption on container vessels (fig. 6) is the result of a considerably higher heavy fuel oil consumption. Heavy fuel oil system is the biggest heat energy consumer on board up to 70% of produced energy. On the other hand powerful engines of container vessels produce more exhaust gases which are used in gas heat boilers.

5. Summary

Obviously contemporary container vessels belong to ships with the biggest energetic plants i.e. main propulsion plant, electric power station and steam boilers. An example of these is the biggest container vessel in the world MS EMMA MAERSK built in 2006 with loading capacity 11,500 TEU and service speed 25 knots (fig.1). The main propulsion of the vessel is low speed diesel engine Wartsila Sulzer 14RT-flex 96C nominal shaft power 80,080 kW. Onboard power station consists of 5 diesel generators of total power 20,700 kW and additional 8,500 kW steam turbo alternator using steam from main engine exhaust gases heat auxiliary boiler. Thanks to high waste heat utilisation the energetic efficiency of engine room achieves 70% during sea passage. Economic analysis show that even bigger container vessels are expected. However there is a limitation in the maximum power of the main engine. The main engine mounted on MS EMMA MAERSK is the biggest diesel engine offered up till now by diesel engine producers. Today, the only alternative is double engine propulsion the same as used on modern biggest liquefied gas tankers. Other possibilities are turbine propulsion, COGES propulsion system and V-type slow speed diesel engines which have not been constructed yet.

References

[1] Giernalczyk, M., Górski, Z., *Method for determination of energy demand for main propulsion, electric power production and heating purposes for modern container vessels by means of statistics.* Marine Technology Transactions. Marine Technology Commity of the Polish Academy of Sciences. Gdańsk 2004

[2] Michalski, R., *Ship propulsion plants. Preliminary calculations.* Szczecin Technical University. Szczecin (1997).

[3] Nowakowski, L., *Obliczenie przybliżonej mocy napędu drobnicowców w zależności od nośnosci i prędkości (Calculation of approximate proulsion power of general cargo ships relation of deadweight capacity and speed).* Budownictwo Okrętowe IX/1970,

[4] *Unification of ship engine room. Part V. Ship power plant.* Study of Ship Techniques Centre (CTO). Gdańsk 1978.

[5] Urbański, P., *Gospodarka energetyczna na statkach.* Wydawnictwo Morskie. Gdańsk 1978.

Journal of POLISH CIMAC
Faculty of Ocean Engineering & Ship Technology
GDAŃSK UNIVERSITY OF TECHNOLOGY

POSSIBILITY OF VALUATION OF OPERATION OF MARINE DIESEL ENGINES

Jerzy Girtler

Gdansk University of Technology
Faculty of Ocean Engineering & Ship Technology
Department of Ship Power Plants
tel. (+48 58) 347-24-30; fax (+48 58) 347-19-81
e-mail: jgirtl@pg.gda.pl

Abstract

The paper provides a proposal of a quantitative interpretation of operation which (as the operation of Hamilton and Maupertius presented in the classical mechanics and the operation after change of the body momentum) is considered as a physical quantity with the measurement unit called a joule-second [joule×second]. An original method for analyzing and estimating the engine operation has been demonstrated in energetic aspect for operational needs. Herein it has been shown that the operation of this kind of engines considered in the proposed aspect enables obtaining essential information about energetic properties of the engines, that completes the information regarding energy conversion in the form of work and heat. Possibilities of analyzing the diesel engine operation have been demonstrated in deterministic and probabilistic aspects. Basing on deterministic aspect of operation of this kind of engines there have been presented possibilities of determining the operational usability of the engines through determining the possible operation and demanded operation to perform a task.

Keywords*: operation, energy, technical state, diesel engine, Poisson process, semi-Markov process*

1. Introduction

During operation of diesel engines we need to identify not only their technical states but also their energetic properties [5, 7, 8, 12, 13, 15]. The properties characterize the medium torque (M_o) and rotational speed of a crankshaft (n) of this type of engines. The torque M_o and rotational speed n (as measurable values) enable to define a useful power (N_e) [12, 13, 15]. The useful power (N_e) is a quantity that characterizes the stream of energy converted in a form of useful work (L_e) at a defined time (t). From this reason the work L_e can be interpreted as the output of the delivered power $N_e = \dot{L}_e$ at time t and therefore expressed with the formula:

$$L_e = N_e t \,. \tag{1}$$

From the formula (1) results that the power N_e is a quantity containing information how quickly the work L_e has been (or can be) performed by a combustion engine.

However in practice also a quantity is significant that provides information how long the work L_e must be delivered by engine to a receiver (screw propeller of a ship, generator,

compressor) in order the given task could be performed. This quantity can be called operation [5, 6, 7]. Because each type of work being performed by engine (ex. useful work, compression, expansion, etc.) is a form of energy conversion, thus just understood operation (D) is a quantity expressing the energy (E) released over the time (t), and that is the reason it can be defined (when E=idem can be accepted) with the formula:

$$D = Et. \tag{2}$$

The operation (2) determines thus the energy released over the time during which this energy has been consumed. When the engine wear is considered, the operation equals to the energy drop (decrease) at time at which it proceeded [4, 8, 11]. The energy can reveal only when converted into form of work or heat [2, 6, 8, 13, 14].

In case of any diesel engine the useful energy (E_e) generated by the engine with a defined useful power (N_e), in strictly determined conditions, can be considered as a measure of its ability to perform the work L_e at a defined time t. Therefore the work as a form of energy conversion, generated by the engine, can be defined from the formula [13]

$$L_e = 2\pi n M_o t\,, \tag{3}$$

in the case when: M_o = idem and n = idem.

When $M_o \neq$ idem and $n \neq$ idem the work performed in the time interval [t_1, t_2] can be presented in the form of dependences:

$$L_e = 2\pi \int_{t_1}^{t_2} n(\tau) M_o(\tau) \mathrm{d}\tau\,. \tag{4}$$

In the operating practice of diesel engines (main engines) being applied to marine propulsion systems it is extremely important how long the work L_e can be released for the needs of the propulsion system of the given ship. This refers especially to the ships of which propulsion systems are equipped with such engines. In the case when due to the wear, the main engine cannot be loaded with the demanded useful power (N_e) at time t, it is not able to perform in this time the demanded work L_e needed to ensure generation of the demanded pressure force (T) by the screw propeller of the ship. In consequence the ship is not able to perform the transportation task. Moreover, when the cruise runs in storm conditions, it can lead to a catastrophe [9].

From the above considerations follows that it is reasonable to analyze not only the power N_e released in diesel engine's workspaces, and simultaneously the work L_e, but also the operation (D) of this type of engines, understood in this case as energy conversion in these workspaces that leads to obtaining the demanded useful work (L_e) at a defined time (t). This will enable to fix whether the possible engine operation (D_M) for the given conditions is at least equal to the demanded operation (D_W) being indispensable to perform a defined task Z.

2. Diesel engine operation as energy conversion in the form of heat and work

Operation of engines consists in converting and transferring the supplied energy. In case of diesel engines, first the chemical energy contained in fuel-air mixture, generated in

workspaces, is converted into thermal energy and then the thermal energy – into mechanical energy [2, 5, 12, 13, 14].

It is obvious that the energy conversion in the form of heat in workspaces of each diesel engine can proceed at a different time. In practice it is essential to make the performance of the work as greatest as possible or as quickly as possible at a defined time. If it is not possible to obtain such energy conversion which is favorable the engine is considered to work incorrectly and to be in the state of partial usability [7, 12, 14].

In case of diesel engines, conversion of chemical energy into thermal energy and then into mechanical energy, enables creation of a torque (M_o) of a crankshaft at a defined rotational speed (n) of each engine [12, 13]. Thus, the operation of engine, interpreted as energy conversion in form of useful work L_e expressed with the formula (4) can be defined by the equation as follows

$$D_{L_e} = \int_{t_1}^{t_2} L_e(\tau)\mathrm{d}\tau = 2\pi \int_{t_1}^{t} n(\tau) M_o(\tau)\pi \mathrm{d}\tau \tag{5}$$

Engine operation connected with energy conversion in the form of work like compression of fresh charge, expansion of combustion gases in a cylinder, etc. can be considered in a similar way.

Determination of engine operation consisting in conversion of chemical energy (E_{ch}) contained in fuel-air mixture generated in engine combustion chambers into thermal energy (E_c) is equally important. Such operation (Fig. 1) when conversion of this kind of energy proceeds in the form of heat (Q) can be defined by the formula:

$$D_Q = \int_{t_1}^{t_2} Q(\tau)\mathrm{d}\tau \tag{6}$$

Because the operation of this kind of engines consists in converting the energy E in the form of work and heat, can be generally interpreted as follows

$$D = \int_{t_1}^{t_2} E(\tau)\mathrm{d}\tau \tag{7}$$

where:

D –engine operation, E – converted (obtained) energy enabling realization of a task Z,

t –time of E energy conversion (consumption).

Usability of particular combustion engines can be inferred after making value calculations of their operations (7) which are. in the interpretation proposed herein, equaled to physical quantities with the measurement unit: „joule-second". Apparently, the functional dependence of energy from time, so $E = f(t)$ must be known in order to determine the field of operation (D). Because $D = f(E, t)$ the operation of machines can be presented in the coordinate system „D–E–t" [5, 6, 7].

Such understood operation defined by the formula (7) can be presented in the coordinate system „E–t" so in the form of graph which I propose to call *operation graph*. An example of such an operation graph for the range of the energy transformation from E_1 into E_2 for any selected time $t_0 = 0$ and t is presented in Fig. 1.

From the formulas (2) and (7) follows that the functional dependence of energy (E) from time (t) must be known in order to determine the operation field (D). Because $D = f(E, t)$, the machine operation can be displayed in the co-ordinate system „D, E, t".

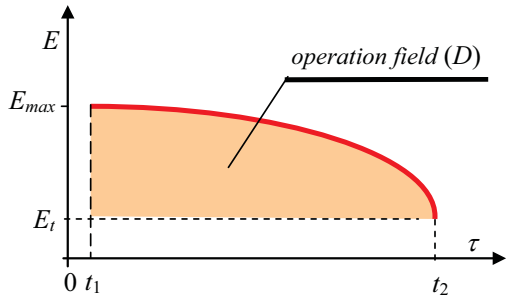

Fig. 1. An exemplary graph of engine operation: E – energy, E_{max} – maximum energy, E_t – energy in the moment t, τ – time

Diesel engine operation can be and sometimes must be considered as a stochastic process [1, 3. 6, 7]. Such operation can be then displayed in a form of stochastic process realization as the dependence $\{E(t); t \geq 0]$, where energy E is a random value. The process is characterized by the expected value $E[E(t)]$ and the standard deviation $\sigma[E(t)]$ of energy E. Such approach follows from that the analysis and the resulted estimation of the operation of diesel engines can be presented in a probabilistic aspect by applying the theory of the stochastic processes. An exemplary graph of such engine operation is show in Fig. 2.

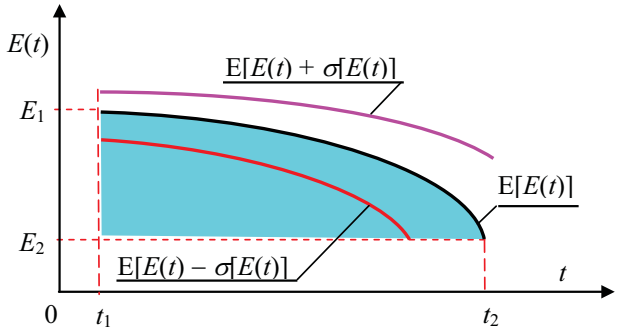

Fig. 2 . An example of a stochastic process showing the dependence E(t), where E is a random value: E – energy, E_1 – energy assigned to time t_1, E_2 – energy assigned to time t_2, t – time being a parameter of the process, E[E(t)] – expected value E, σ[E(t)] – standard deviation of E

A stochastic process is a random function of which the parameter is the time t. The time is not a random variable [1, 3]. This approach towards the issue of expressing the diesel engine operation as a value, results from the necessity of getting information what the operation can be in the interval defined by two arbitrary moments, ex. in the interval $[t_0, t_n]$. In this case, analyzing operation of each combustion engine, each time t from the considered time interval $[t_0, t_n)]$ can be assigned by a state called momentary state of the process, which is a random variable X_t with the excepted value $E(X_t)$ and variation $D^2(X_t)$ dependent from the t value. For the considerations the variable can be energy (E) or forms of its conversion, so

work (L_e) or heat (Q). Thus the stochastic process (a random function) is a set of random variables X_t for $t \in [t_0, t_n]$, so for $t_0 \le t \le t_n$. The function's expected value $E[X(t)]$ and variation $D^2[X(t)]$ are defined by the sets of expected values $E(X_t)$ and variations $D^2(X_t)$ for $t_0 \le t \le t_n$. It should be pointed here that the expected value $E(X_t)$ and the variation $D^2(X_t)$ of the random function $\{X(t): t \ge 0\}$ depend on time t because the values $E(X_t)$ and $D^2(X_t)$ can be different for different t values. They are not, however, random functions X(t) because $E(X_t)$ and $D^2(X_t)$ are not random variables but the constants for the given t value and the given set of realizations of the random variable X_t [3].

An example of dependences of $E(X_t)$ and $D^2(X_t)$ from time t is shown in Fig. 2, at the assumption that the random variable X is the energy E supplied by a combustion engine to a receiver of the energy. In this Fig. the $\sigma[E(t)]$ quantity is a standard deviation of the random variable E. This quantity is a square root of the variation $D^2(E_t)$.

In this case to define the operation D from the formula (7) the integral calculus can be applied because the integral defined by the formula is a definite Riemann integral with the integration range $[0, t]$ and the integrand $E(\tau)$. Because the function $E(\tau)$ is continuous for the examined exemplary range $[0, t]$, it can be stated in compliance with the second fundamental theorem of integral calculus (Newton-Leibniz Theorem) that [16]

$$\int_{t_1}^{t_2} E(\tau)\mathrm{d}\tau = D(\tau)\Big|_{t_1}^{t_2} \tag{8}$$

whereas:

$$D(\tau)\Big|_0^t = D(t) - D(0)$$

Estimation of the expected value $E(E_t)$ for each value of time t requires application of statistical inference, so point or interval estimation [1, 3].

From the presented interpretation of combustion engine operation follows that the operation consists in converting and transferring the released energy in the form of work (L) and heat (Q), whereas both of the forms of energy conversion can be presented as the fields [13, 14]:

- in the Clapeyron diagram (diagram of work) when analyzing the work L (Fig. 3 and 4),
- in the Belpaire diagram (diagram of heat) when analyzing the heat Q (Fig. 5).

For instance, in case of a piston engine the absolute work (L_a) of exhaust decompression (i.e. work determined in relation to the ambient pressure $p_0 = 0$), of which the field is displayed in Fig. 3a in the p-V co-ordinate system, called the Clapeyron diagram, can be calculated from the formula

$$L_a = \int_{V_1}^{V_2} p(V)dV \tag{9}$$

where: p – pressure, V – volume.

That means that the integral (9) can be determined when the functional dependence $p = f(V)$ is known. The technical work of exhaust decompression (L_t), of which the field is displayed in Fig. 3b can be determined from the formula

$$L_t = -\int_{p_1}^{p_2} V(p)dp \tag{10}$$

Also in this case the integral (10) can be determined when the functional dependence $V = f(p)$ is known. The technical work of exhaust decompression can be however determined also by employing the definition of absolute work. Then the following formula is of application (Fig. 3)

$$L_t = p_1 V_1 - p_2 V_2 - \int_{p_1}^{p_2} V(p)dp \tag{11}$$

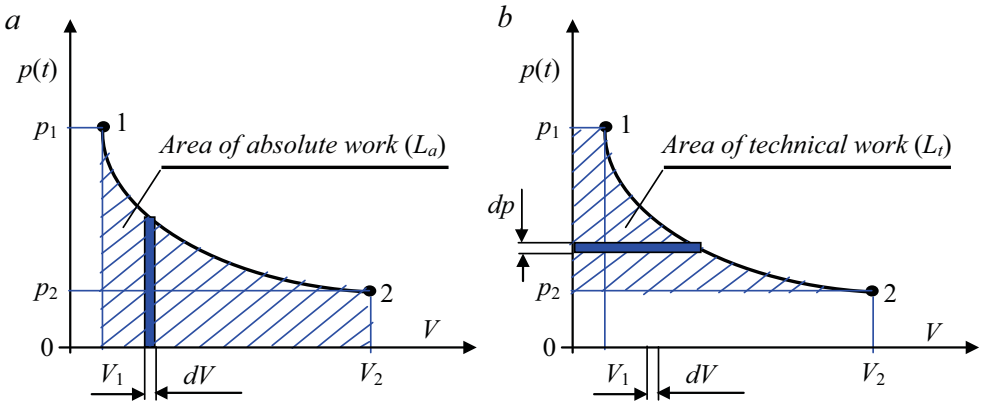

Fig. 3. Graphical examples of work: a) absolute, b) technical: p – pressure, V – volume

Taking into account that the work of exhaust decompression in the piston engine space is performed till the moment of opening the exhaust valve, when the exhaust gases are removed outside to the environment with the pressure $p_o = p_b$, the useful work can be then considered (Fig. 4).

The mentioned useful work (L_u) can be defined (Fig. 4) from the formula

$$L_u = \int_{V_1}^{V_2} p(V)dV - p_b(V_2 - V_1) \tag{12}$$

where: p – pressure, V – volume, p_b – barometric pressure (ambient pressure).

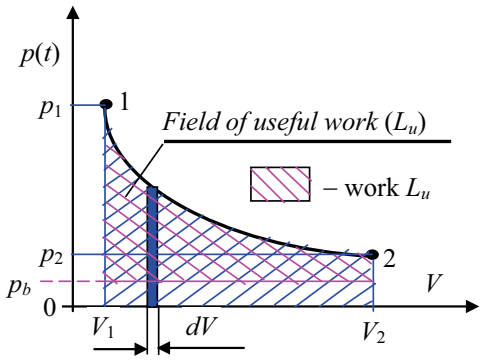

Fig. 4. An exemplary graph of useful work: p – pressure, V – volume, p_b – barometric pressure

A field of any other work (e.g. air compression in a cylinder, indicated work, useful work, etc.) can be presented in a similar way.

The carried away heat can be shown (Fig. 5) in the form of a graph by using the „$T - S$" co-ordinate system (in the Belpaire diagram). The mentioned heat (Q) can be determined (Fig. 5) from the formula:

$$Q = \int_{S_1}^{S_2} T(S)dS \tag{13}$$

where: T – absolute temperature, S – entropy.

The following restrictions must be taken into account for the formula (13):

$$S_1 \le S \le S_2 ; \quad T_2 \le T \le f(S)$$

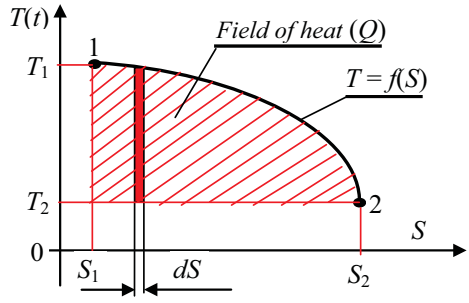

Fig. 5. An exemplary graph of heat: T – absolute temperature, S – entropy

In the paper's introduction it has been signaled that the operation in the interpretation presented herein will enable to determine if the possible engine operation (D_M) for the given conditions is at least equal to the demanded operation (D_W) being indispensable to perform the task (Z). That means the operation in the presented interpretation is of essential practical significance.

3. Practical significance of engine operation with value interpretation

Task for which a combustion engine has been designed and manufactured can be performed only when the following inequality is satisfied

$$D_M \ge D_W, \tag{14}$$

so when:

$$t_M \ge t_W, \text{ when at the same time } E_M \ge E_W.$$

where: t_M – possible operating time, t_W – demanded operating time, E_M – energy that can be converted by engine, E_W – demanded (desired) energy to perform the task Z (energy that must be converted to enable performance of the task).

That means that when analyzing the energetic properties of combustion engines (not only diesel ones) ability of this type of engines (as well as other energetic systems) to work can be considered in the following alternatives:

$$\left.\begin{array}{l} t_M = t_W, \text{ when simultameously } E_M = E_W, \\ t_M = t_W, \text{ when simultameously } E_M > E_W, \\ t_M > t_W, \text{ when simultameously } E_M = E_W, \\ t_M > t_W, \text{ when simultameously } E_M > E_W. \end{array}\right\} \quad (15)$$

In case when the inequality emerges:

$$D_M < DW, \quad (16)$$

the engine is damaged and is not able to perform the task *Z*.

The inequalities (14), (15) and (16) are also true when dissipation of energy converted in the form of heat is considered. In such a case the heat is carried away from the engine and therefore (in accordance with the interpretation used by thermodynamics) gets a negative value.

Fig. 6. presents a case when the possible operation of engine $D_M = E_1 (t_2 - t_1)$ which while working can supply the energy $E_1 = idem$ being indispensable to perform a defined task at time t_1. In this case however, in order to perform the task the demanded operation is required to be greater than the possible one, so $D_M < D_W$, where $D_W = E_1 (t_3 - t_1)$. That means that the possible operation (D_M) of engine will not ensure the task performance and that is why before starting the task realization the engine should be submitted to reconditioning through performing the adequate preventive service work.

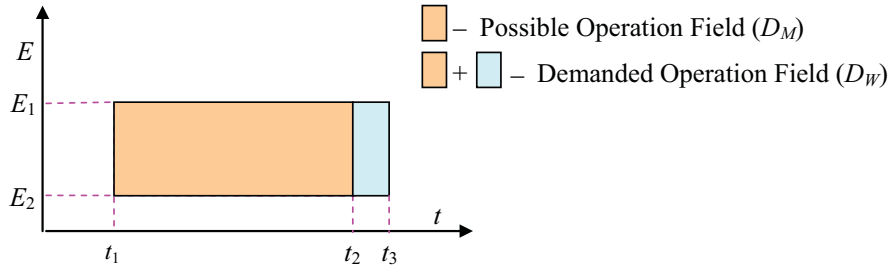

Fig. 6. An exemplary graph of possible operation (D_M) and demanded operation (D_W): E – energy, E_1 – energy assigned to time t_1, E_2 – energy assigned to time t_2, t –time

When no preventive service is carried out and any refurbishment on the machine is not done the performance of its operation can be presented in the form of a field provided in Fig. 7.

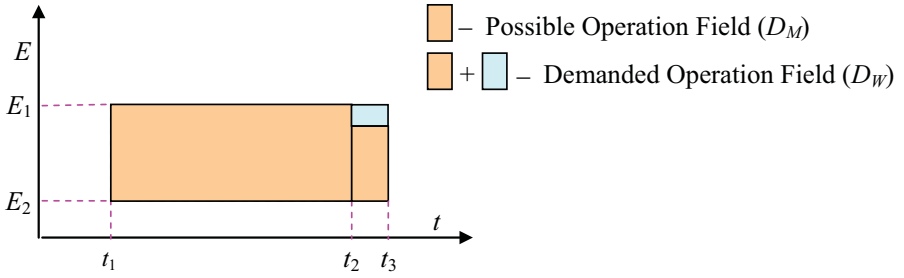

Fig. 7. An exemplary graph of possible operation (D_M) and demanded operation (D_W): E – energy, E_1 – energy assigned to time t_1, E_2 – energy assigned to time t_2, t –time

When diesel engine energy transmitted to a receiver is constant (E = idem) in the time interval [t_1, t_2], the operation follows in accordance with the formula (7)

$$D = \int_{t_1}^{t_2} E(t)dt = E\int_{t_1}^{t_2} dt = Et\Big|_{t_1}^{t_2} = E(t_2 - t_1) \tag{17}$$

Taking into account the ways of energy E conversion (7) in energetic machines, work (L) and heat (Q), their operation can be determined by using the formulas (5) and (6), as follows:

$$D_L = \int_{t_1}^{t_2} Ldt = L(t_2 - t_1); \qquad D_Q = \int_{t_1}^{t_2} Qdt = Q(t_2 - t_1) \tag{18}$$

Dependences (17) and (18) own interesting cognitive attributes, but may be also of utility significance. Applying them it is very easy to determine the demanded operation (D_W) as well as the possible operation (D_M) for each energetic machine and to obtain preliminary information on its usefulness (operational) to perform a defined task. Moreover, the formulas enable making simple graphs of demanded operation (D_W) and possible operation (D_M), which are presented in Fig. 6.

The characterized operation of diesel engines and the examples of its demonstration in the form of operation fields refer to the case when important is to determine energy or its possible conversions in forms of work and/or heat being indispensable to ensure performance of the given task. However, each operation of an energetic system at determined time is followed by energy dissipation in accordance with the second law of thermodynamics. In case of diesel engines, a part of the produced energy is used to overcome their mechanical resistances. From this reason for the piston diesel engines we distinguish indicated work (L_i) and connected with it indicated power (N_i) and useful work (L_e) and connected with it effective power (N_e). The indicated work of engine is a power being produced by the engine in its working spaces (in cylinders), without regard to its own mechanical resistances. The effective power, however, is a power which can be delivered to a power receiver in any conditions of engine operation. The difference between the two powers is the power (N_m) lost for overcoming the mechanical resistances of the engine. Taking this power into account, the energy or forms of its conversion, which are work and heat, can be considered from the conventional zero level. Then, the operation of a diesel engine can be presented with the same formulas but in the form of a field determined by the function $E(t)$ or $L(t)$ or $Q(t)$ and the time axis (t), what is displayed in Fig. 8. for the case when change in energy at time t is considered.

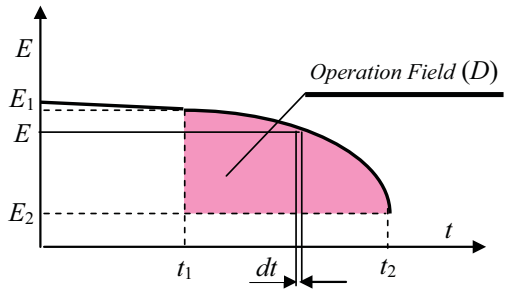

Fig. 8. An exemplary graph of operation for the case when E = f(t): E – energy, E_1 – energy assigned to time t_1, E_2 – energy assigned to time t_2, t –time

In case, when the energy average value is considered, so when it can be accepted that E = idem in the time interval $[t_1, t_2]$, the operation field can be presented as in Fig. 9.

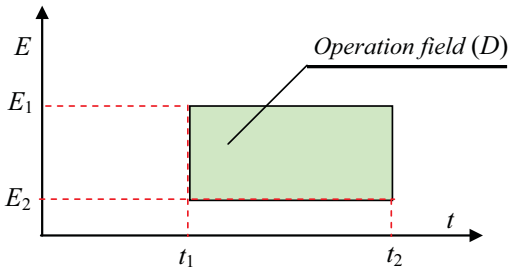

Fig. 9. An exemplary graph of operation for the case when E = idem: E – energy, E_1 – energy assigned to time t_1, E_2 – energy assigned to time t_2, t –time

Dependences (17) and (18) follow from that the integral expressed with the formula (7) or (5) or (6) is the Riemman integral with the interval $[t_1, t_2]$ in this case and the sub-interval function $E(\tau) = E$. This function is integrable in terms of Riemman in the mentioned time interval according to the formula:

$$\int_{t_1}^{t_2} E dt = E(t_2 - t_1) = (E_1 - E_2)(t_2 - t_1) \tag{19}$$

However, in practice it is not always possible to accept that energy supplied by an energetic machine to a receiver is constant [8, 12, 17, 18, 19]. Then we need to define the functional dependence of energy (E) from the time (t) of machine operation, so the dependence $E = f(t)$. In case when this is possible because the function $E = f(t)$ is continuous in the considered exemplary interval $[t_1, t_2]$, following the second fundamental theorem of calculus (theorem by Newton and Leibniz) we can write in accordance with the formula (8) that (Fig. 8).

$$\int_{t_1}^{t_2} E(t) dt = D(t_2) - D(t_1) \tag{20}$$

Application of the theorem by Newton and Leibniz is here necessary because it enables effective determination of the definite integral of the continuous functions if determination of any primitive for the functions is possible.

Generally, the functional dependence $E = f(t)$ is composite. In case, when for such a function the internal function derivative is a constant function, the definite integral of the function $f(t)$ can be determined by application of integration consisting in substitution [22].

Not always however the elementary function describing the dependence of energy from time is possible to be defined with elementary functions. Then determination of the definite integral from the Newton-Leibniz formula is troublesome, and sometimes even impossible. The trouble is that determination of a primitive is connected then with necessity of making difficult transformations. In such cases, just like when sub-integral function is determined in a table form, we can calculate an approximate value of the operation of an energetic machine, being the definite integral value, applying the method of trapezoids or the Simpson method. The attention must be paid that at a fixed n the Simpson method enables obtaining more accurate results in integration than the method of trapezoids.

9. Conclusion

Operation of combustion engines is understood as generating the energy E by them at a defined time t. It has been equated to a physical quantity which can be expressed with a numerical value and the measurement unit called *joule-second* [joule×second]. Such understood operation gets worse with the growing wear of this type of engines. This means that the operation value at a defined time decreases in the result of decreasing energy generated by the engines. It has been signaled herein that in case of application of the theory of stochastic processes to the analysis of changes of such understood operation the integral calculus can be applied. Two stochastic models of decreasing useful energy generated by the engines have been proposed for defining the range of worsening operation. The first model has been presented in the form of a homogenous Poisson process and the second – in the form of a discrete-state, continuous-time semi-Markov process.

Operation in such interpretation depends on the technical state of the engines and is characterized simultaneously by the energy converted by the engines and the energy generation time.

The advantage of the engine operation in the presented interpretation is that it can be tested through doing precise measurements and then expressed in the form of:

– a number with the measurement unit called *joule-second* [joule×second] (formulas 5, 6 and 7);

– a graph, as a field of operation (Fig. 2, 3 and 4).

Operation in the presented interpretation, although formulated for diesel engines, refers also to spark-ignition engines. Similar interpretation of operation can be provided for turbine combustion engines and other energetic machines.

References

[1] Benjamin J. R., Cornell C. A., *Probability, Statistics, and Decision for Civil Engineers*. Copyright 1970 by McGraw-Hill, Inc. Wyd. polskie, Rachunek prawdopodobieństwa, statystyka matematyczna i teoria decyzji dla inżynierów. WNT, Warszawa 1977.

[2] Chmielniak T.J., Rusin A., Czwiertnia K., *Turbiny gazowe*. Maszyny Przepływowe Tom 15. Polska Akademia Nauk. Instytut Maszyn Przepływowych. Zakład Narodowy im. Ossolińskich. Wyd. PAN, Wrocław- Warszawa-Kraków 2001.

[3] Firkowicz S., *Statystyczna ocena jakości i niezawodności lamp elektronowych*. WNT, Warszawa 1963.

[4] Gercbach I. B., Kordonski Ch. B., *Модели отказов*. Изд. Советское Радио, Москва 1966. Wyd. polskie, *Modele niezawodnościowe obiektów technicznych*. WNT, Warszawa 1968.

[5] Girtler J., *Work of a compression-ignition engine as the index of its reliability and safety*. II International Scientifically-Technical Conference *EXPLO-DIESEL & GAS* TURBINE"01. Conference Procedings. Gdansk-Miedzyzdroje-Copenhagen, 2001, pp.79-86.

[6] Girtler J., *Conception of valuation of combustion engine operation*. Journal of KONES. Powertrain and Transport. Editorial Office Institute of Aeronautics BK, Warsaw 2008, pp. 89-96.

[7] Girtler J., *Energetyczny aspekt diagnostyki maszyn*. Diagnostyka Nr 1(45)/2008. Wyd. Polskie Towarzystwo Diagnostyki Technicznej, Warszawa 2008, s. 149-156.

[8] Girtler J., *Diagnostyka jako warunek sterowania eksploatacją okrętowych silników spalinowych*. Studia Nr 28. WSM, Szczecin 1997.

[9] Girtler J., *Semi-Markov model of changes of sea-ships' and aircrafts' moving*. Archives of Transport, vol. 11, iss.1-2/99 pp.
[10] Grabski F., *Teoria semimarkowskich procesów eksploatacji obiektów technicznych*. Zeszyty Naukowe WSMW, Nr 75A, Gdynia 1982.
[11] Niewczas A., *Podstawy stochastycznego modelu zużywania poprzez tarcie w zagadnieniach trwałości elementów maszyn*. Zeszyty naukowe WSI w Radomiu, Radom 1989.
[12] Piotrowski I., Witkowski K., *Eksploatacja okrętowych silników spalinowych*. AM, Gdynia 2002.
[13] Wajand J.A., *Silniki o zapłonie samoczynnym*. WNT, Warszaw 1988.
[14] Wiśniewski S., *Termodynamika techniczna*. WNT, Warszawa 1 995.
[15] Włodarski J.K., *Tłokowe silniki spalinowe. Procesy trybologiczne*. WKiŁ, Warszawa Instytut Technologii Eksploatacji, Radom 2000.
[16] *Matematyka. Kompendium*. Praca zbiorowa. Świat Książki, Warszawa 2005.

Journal of POLISH CIMAC
Faculty of Ocean Engineering & Ship Technology
GDAŃSK UNIVERSITY OF TECHNOLOGY

DYNAMIC ANALYSIS OF HIGH POWER VERTICAL MIXED FLOW PUMP

Henryk Holka,Tomasz Jarzyna

University of Technology and Life
al. Prof. S. Kaliskiego 7, 85-789 Bydgoszcz, Poland
tel.: +48 52 373-02-80, fax:+48 52 374-93-27
e-mail: holka@utp.edu.pl, tomasz_jarzyna@o2.pl

Abstract

In this article the vertical mixed flow pumps and problems accompanying during working of the devices vere presented. At the begining few issues which are consider in this type of machines were mentioned. The results of measurements a velocity of vibrations on the pump were presented in next point of the paper and compared with norm. Important issue in the article is modeling, therefore 3D model, discreet model of the rotor, numerical analysis of the rotor, four-masses discreet model and equations of the free motion of the rotor were presented. For finding stiffness and suppression parameters of bearings the special research stand were built and shown in the article. Range of future works was also described.

Keywords: *vibrations, dynamic analysis, impeller pump, mixed flow pump, structural model*

1. Introduction

The object considered in this work is mixed flow pump with two impellers, which works in company from Włocławek. Large dimensions, complicated structure and mechanical processes which accompany during working of the device provide too difficult dynamic analysis of the machine. Additionaly is not possible to measure vibrations on part of the device which is plunged in the water. Rotary motion of the mojor shaft with two impellers is a basic motion in the pump. In these devices, a special attention is directed on:
- stability of rotor and critical rotations,
- unbalancing of blades and the rotor,
-defining the level of dynamic loading of bearings and the support structure,
- identyfication loads generated during working of the machine [2].

2. Specifity of research object

High power - 1250kW and efficiency - 5000 m^3/h are characteristic for the device.
These parameters have influence on the way of supporting the pump, the device is spupported on two foundations. Basic parts of the machine: electrical motor which is based on upper foundation (fig. 1.) and pump – supported by bottom foundation (fig. 2.).

Fig.1. Electrical motor of mixed flow pump

Fig.2. Part of machine to escape the water

In one hall were installed 8 same pumps, because demand of water is different. The measure of vibrations is difficult when few devices are working together. Ratory speed of the pump is established on 740 rpm.

3. Results of measures

Measures of vibrations were based on norm PN – ISO 10816-1:1998, which describe border levels of intensity of vibrations for classified devices (tab. 1). The considered pump is classified as III class, but intesity of vibrations in B zone (for devices admitted to long exploitation).

Tab. 1. Border values of intensity of vibrations according to PN-ISO 10816-1:1998

Velocity of vibrations RMS in mm/s	Class I	Class II	Class III	Class IV
0,28	A	A	A	A
0,45				
0,71				
1,12	B	B	B	B
1,8				
2,8	C	C	C	C
4,5				
7,1	D	D	D	D
11,2				
18				
28				
45				

Measure points of vibrations are shown on figure 3, results of measures in table 2.

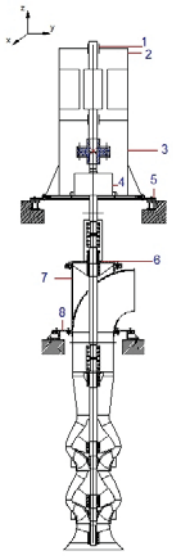

Fig. 3. Measure pionts of vibrations

Tab. 2. Results of measures

Measure point	Direction of measures vibrations					
	x		y		z	
	Veloc. [mm/s]	Accel. [m/s^2]	Veloc. [mm/s]	Accel. [m/s^2]	Veloc. [mm/s]	Accel. [m/s^2]
1	4,0108	1,2332	5,5884	1,8884	-	-
2	5,0412	1,3568	5,158	1,6092	-	-
3	1,394	1,2896	1,5112	1,7412	-	-
4	1,276	0,61	1,1312	0,7532	-	-
5	-	-	-	-	2,2176	0,7012
6	0,6392	0,7288	1,3912	0,6996	-	-
7	1,1968	0,4456	0,7972	0,7984	-	-
8	-	-	-	-	0,4552	0,5628

4. Modelling

For creating spatial model (fig. 4.) of the pump, documentation 2D were used. The model was useful to numerical analysis and wizualization how the device works. Additionally, the model is used to fast estimate physical properties of elements like for example: moments of inetria or centers of masses.

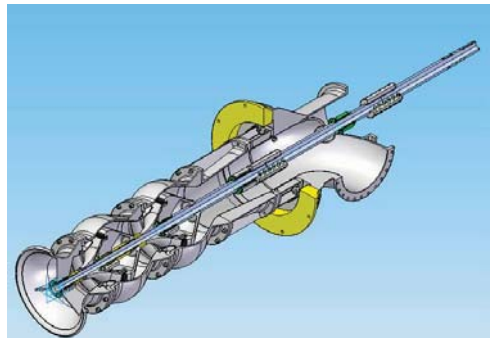

Fig.4. Cutting view of vertical mixed flow pump

Basic part of the pump is consisting from three rotors, which are connected by stiff clutches and two impellers. Whole part was numerical analyzed in MSC.ADAMS program. Parameters of stiffness and suppression were taken from literature: $k=1\cdot10^5$ N/mm, c=1Ns/mm. Results of the analysis are shown on figure 5.

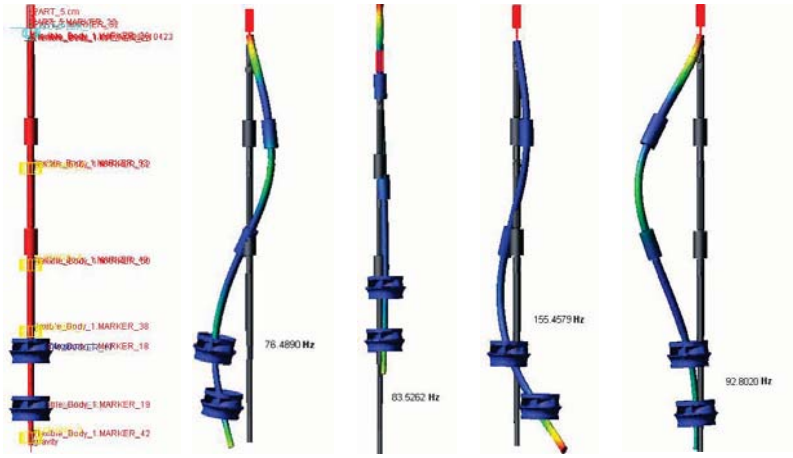

Rys. 5. Numerical analysis in MSC.ADAMS program

Results of the numerical analysis and energetical Rayleigh's method were used to creation four-masses discreet model of rotor stiffness supported (fig. 6.).

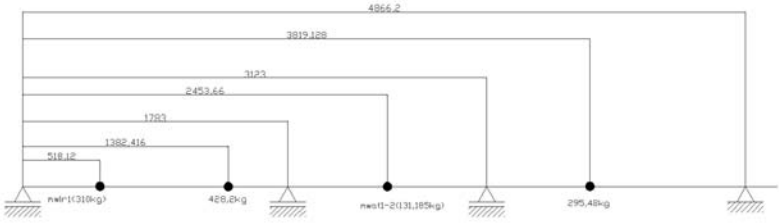

Fig. 6. Discreet model of rotor

For the model equations of the free motion were written (1):

$$\begin{aligned}
\delta_{11}m_1\ddot{y}_1+\delta_{12}m_2\ddot{y}_2+\delta_{13}m_3\ddot{y}_3+\delta_{14}m_4\ddot{y}_4+y_1=0\\
\delta_{21}m_1\ddot{y}_1+\delta_{22}m_2\ddot{y}_2+\delta_{33}m_3\ddot{y}_3+\delta_{24}m_4\ddot{y}_4+y_2=0\\
\delta_{31}m_1\ddot{y}_1+\delta_{32}m_2\ddot{y}_2+\delta_{33}m_3\ddot{y}_3+\delta_{34}m_4\ddot{y}_4+y_3=0\\
\delta_{41}m_1\ddot{y}_1+\delta_{42}m_2\ddot{y}_2+\delta_{43}m_3\ddot{y}_3+\delta_{44}m_4\ddot{y}_4+y_4=0
\end{aligned} \tag{1}$$

where:
δ_{ij} – Maxwell's coefficients,
m_i – discreet masses,
y_i – statical deformation of rotor,

and solved. At present the model is werryfied.

The discreet model is simply in relation with real object. Therefore, in next step the parameters of stiffness and suppression of supports will be regarded. Parameters of k and c were taken from literature. Verification of the parameters will be done in experiments. Price of real bearings in high, therefore research stand for bearing with different diameter, clearance between toe and bearing, pressure of reinforced water, rotary speed of rotor was built (fig. 7.).

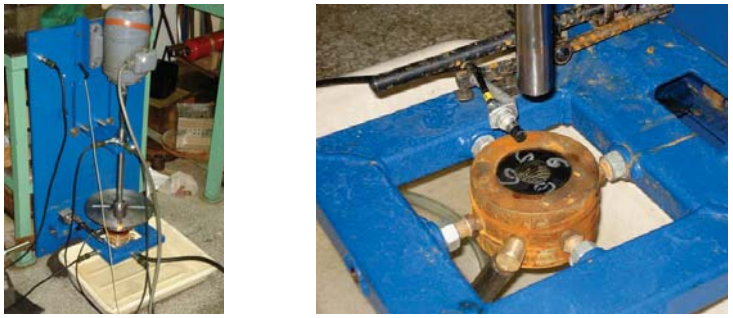

Fig. 6. Research stand

For different diameters of bearings, it is planed to find formula which will be use for finding k and c parameters.

5. Range of future works

Next works will concern the following topisc:
- creation of mathematical model which will nclude stiffness and suppression parameters,
- identyfication of bearings parameters,
- identyfication loads generated during working of the machine,
- reserching of stability of rotor and critical rotations,
- reserching of inluences between different places of supports and durability of plugging and bearing,
- reserching of inluences kinematical random impacts from trunk and rotor's vibrations,
- describing guidelines for construction changing.

6. Conclusions

1. Problems with veryfication of ceated model exist, because is not possible to measure vibrations on all parts of the object.
2. Measures of velocity of vibrations showed that them (these, their?) values are higher than those described in norm.
3. Created discreet model will be developed by consider parameters based on reserches.
4. Beginning calculations showed that torsional vibrations can be skipped.

References

[1] Borkowski, W., Konopna, S., Grochowski, L.: *Dynamika maszyn roboczych*. Wydawnictwa Naukowo – Techniczne. Warszawa, 1996.
[2] Gryboś, R.: *Drgania maszyn*. Skrypty Uczelniane Nr 1927, Wydawnictwo Politechniki Śląskiej, Gliwice 1994.
[3] Jędral, W.: *Pompy wirowe*. Wydawnictwo Naukowe PWN S A, Warszawa 2001.
[4] Kiciński, J.: Modelowanie *i diagnostyka oddziaływań mechanicznych, aerodynamicznych i magnetycznych w turbozespołach energetycznych*. Wyd. Instytutu Maszyn Przepływowych PAN, Gdańsk 2005.
[5] Muszyńska, A. *Rotordynamics*, CRC Press Taylor & Francis Group Work V. Machinery Vibration, McGraw-Hill, 2005.

[6] Tomski, L.: *Drgania i stateczność układów dyskretnych*. Wydawnictwo Politechniki Częstochowskiej, Częstochowa 2006.
[7] Kazimierczak, G., Pacula, B., Budzyński, A.: *Solid Edge – komputerowe wspomaganie projektowania*. Wydawnictwo HELION. Gliwice 2004.

Journal of POLISH CIMAC
Faculty of Ocean Engineering & Ship Technology
GDAŃSK UNIVERSITY OF TECHNOLOGY

PROBLEMS WITH REPRESENTATION OF THE OIL FILM GENERATING CONDITIONS ON THE WANKEL ENGINE CYLINDER SLIDING SURFACE

Antoni Iskra

Poznan University of Technology
ul Piotrowo 3, 60-965 Poznan, Poland
tel.:+48 61 6652511, fax: +48 61 6652514
e-mail: antoni.iskra@put.poznan.pl

Maciej Babiak

Poznan University of Technology
ul Piotrowo 3, 60-965 Poznan, Poland
tel.:+48 61 6652049, fax: +48 61 6652514
e-mail: maciej.babiak@interia.pl

Abstract

The fundamental problem with wide application of the Wankel engine is to assure oil film continuity on trochoidal cylinder bearing surface. For the sake of considerable difference between curvature radius of the apex seal sliding surface and the trochoidal cylinder the oil film can be generated on the short fragment of the apex seal. However there is certain field of maneuver in the apex seal shape determination which allows to approach close radiuses of curvature of both elements in the areas where the highest gas forces load is occurred. In the paper simulation of the revised apex seal oil film parameters are presented. Author described also the test stand which is going to be used for experimental verification of the simulation results. Conclusions refer to possibility of replacement the constant radius shape of the apex seal sliding surface with shape that consist of two different curvatures.

Keywords*: the Wankel engine, oil film parameters*

1. Introduction

Problems with the apex seal of the Wankel engine has been known since the first engine of that type was designed. The first apex seal designs where just to make start of the engine possible, but in the later engine development apex seal was limiting the proper working time of the engine. In early prototypes usually after just few hour of working the blow-by between adjacent working chambers were enough to stop the engine. Later rotary engine constructions which were applied in serial produced NSU Ro80 cars or even the Mazda Renesis engine apex seal was not the main

disadvantage but still it is less effective, less durable and generates more friction losses than modern piston rings in conventional reciprocating engines. Previously described difficulties can be easily explained if the apex seal angle of attack is taken into consideration. The angle between the apex seal axis and the normal to the trochoidal cylinder liner varies within limit of one radian while in conventional piston engine analogous angle do not exceed 0,001 rad. As a consequence in conventional engine the maximum gap thickness between piston ring and cylinder liner do not cut across few micrometers whereas in the Wankel engine gap reach size of several hundred micrometers. There is a question if the apex seal sections with circular or parabolic profile, that are being used nowadays, provide the best results both of the oil film thickness and friction losses caused by apex seal sliding on the trochoidal cylinder surface. As it is pointed out in present elaboration it is possible to propose the apex seal sliding surface shapes which guarantee acceptable oil film parameters when the apex seal is situated perpendicularly to the trochoid surface. What is more the oil film parameters can not get extremely worsen during inclination of the apex seal, mainly in areas where the long and short axis of the trochoid are evenly distant. When looking for analogy in functions of the apex seal and the piston ring it can be assumed that in the reciprocating engine the piston ring could cooperate with cylinder liner in similarly hard conditions as apex seal of the Wankel engine if the cylinder liner would change its diameter by few millimeter. The generating line of this cylinder liner would be sinusoidal shaped with amplitude of few millimeters and period comparable to piston stroke. This kind of model was engaged in computer simulations during the new profile of the apex seal examinations.

2. Parameters of traditional cylinder liner that creates conditions of the apex seal [1]

On the figure 1 changes course of the angle between tangent to the piston ring and tangent to the cylinder liner which is deformed in such manner that generating line of the cylinder liner has sinusoidal shape with amplitude of 1,6mm and period of 160mm.

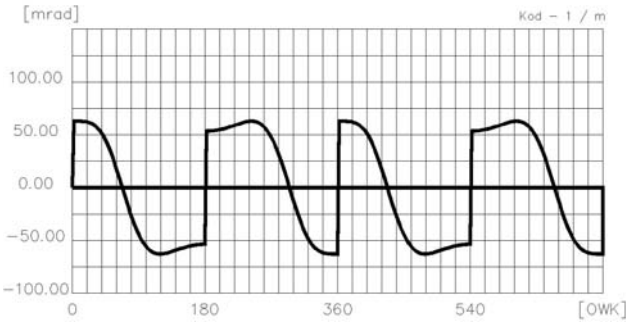

Fig. 1. The angle course changes of tangent to the cylinder liner generating line, the amplitude is 1,6mm and the period is 160mm

The tangent line to the sliding surface of the classical piston ring forms with piston axis lesser angle than angles shown on fig. 1. As a consequence the piston ring contacts with cylinder liner in predominant part of the working cycle alternately with its upper and lower edge and there is no possibility to generate continuous oil film between the piston ring and the cylinder liner. This situation is very similar to that one which occurs in the Wankel engine, where the apex seal also at considerable part of its path works with its edge. In apex seal that have been used so far the sliding surface was a parabolic shape. With the purpose of improving the oil film parameters the apex seal shape that consist of two parabolas was considered. 50% of the profile keep normal shape and the other part, closer to the edges, is multiplied. As a result the apex seal shape looks as it is shown on upper right corner of fig. 2.

When the corrected sliding surface was used oil film parameters presented on fig. 2 it the part signed as “Pier. Zg.” were obtained. If the next apex seal would not be corrected, so its profile is formed by one parabola, the oil film on the most part of apex seal path does not exist. It can be observed on fig. 2 part that is signed as “ Piersc. 2”. The not corrected profile shape is also presented in the middle part of fig. 2 above the diagrams.

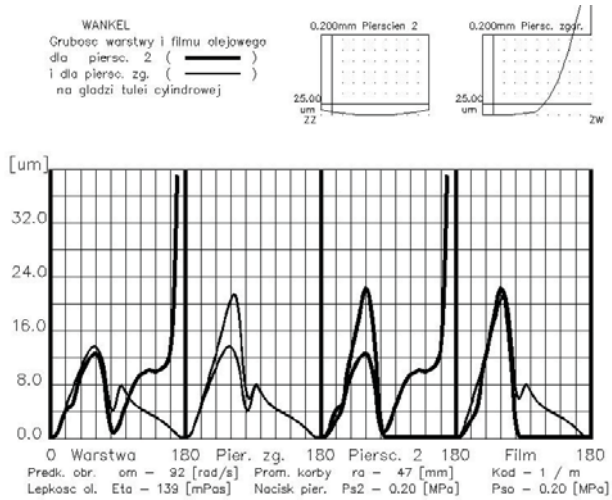

Fig. 2. Comparison of the oil layer thickness course that is left on the cylinder liner surface by two profiles of the apex seal – first part of the diagram; oil film thickness and layer thickness for double parabolic profile – second part of the diagram; oil film thickness course and layer thickness course for the parabolic profile with very high curvature radius – third part of the diagram; comparison of the oil film thickness that was generated by the one and double parabolic profiles – fourth part of the diagram

The sliding surface correction of the apex seal has to be done very carefully because improving oil film parameters in the key areas leads to deterioration of this parameters in other areas. On fig. 3 synthetic course of the oil film parameters generated by two following apex seals of the Wankel engine.

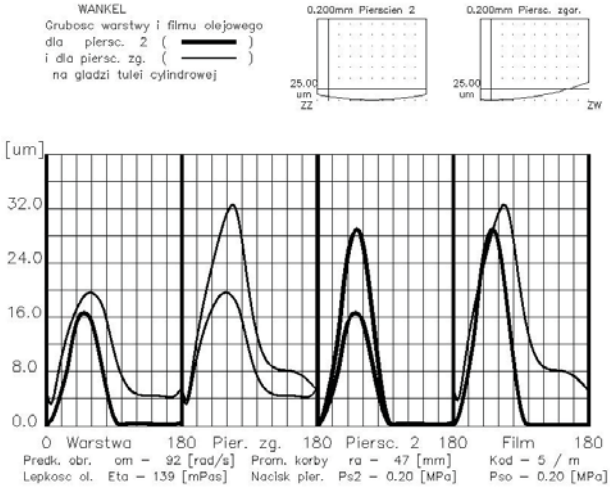

Fig. 3. Comparison of oil film thickness course which is lest on the cylinder surface by two apex seal profiles, for conventional apex seals of the Wankel engine – first part of the diagram; oil film and layer thicknesses for one parabolic profile – second part of the diagram; oil film and layer thicknesses for parabolic with very high curvature

radius – third part of the diagram; comparison of oil film thickness generated by two one parabolic apex seals – fourth part of the diagram

The results obtained from the simulations are classical course of the oil film parameters for types of apex seal that have been used so far. It can be noticed on the first part of the fig. 3 diagram that in the 90 degrees to 180 degrees area the classical one parabolic apex seal leaves no oil layer on the cylinder surface, which means that there is no oil film and intense wear of the trochoidal cylinder surface occurs. However comparing the maximum oil film thicknesses it can be observed that for classical apex seal this parameter is better because it reaches value of 33 μm fig. 3, while for the corrected two parabolic profiles only 25 μm – fig. 2.

The maximum oil film thickness areas for the classical apex seal provide to low friction forces values. It is possible that mechanical efficiency of the Wankel engine with regular apex seals is higher than with corrected two parabolic solutions. Simulations that have been used do not allow to unequivocally confirm this assumption. The partially lack of oil film on the trochoid surface needs other ways of friction losses estimation. The best way to estimate friction losses is to use one of the experimental method what is in realization phase with authors cooperation. In continuous oil film case the computer simulations allow to specify friction forces and example of its results is presented on fig. 4.

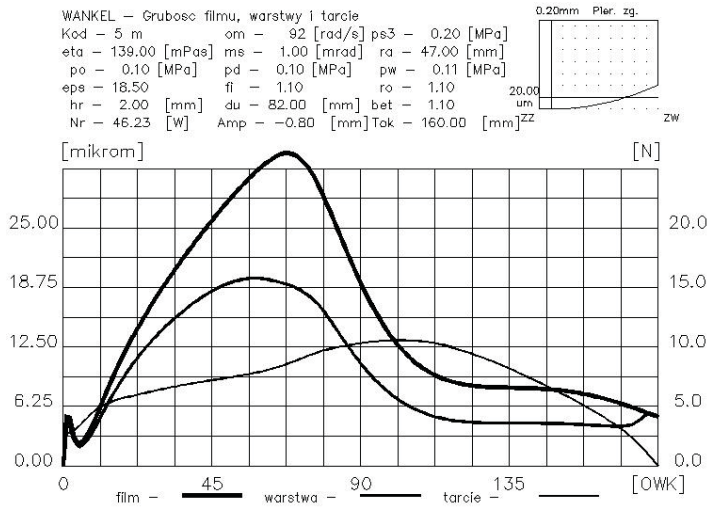

Fig. 4. The oil film and layer thicknesses for one parabolic profile and friction force course for the same apex seal profile

Very often next to basic oil film parameters which are the film thickness, layer thickness and friction force also piston profile filling by the oil film is determined. For analyzed cases profile filling by the oil film is illustrated on fig. 5 and fig. 6. In two parabolic corrected profile case the area where the oil film is generating by the parabola near the edge of slat is evident. It is area of 90 to 180 degrees range – fig. 5. For the typical apex seal with one parabolic profile filling by the oil film in 100 to 150 degrees range is lower so it is probable that the friction force is also lower – fig. 6.

In so far considerations because of its comparative nature the course of angle between tangent to the apex seal and tangent to the trochoid, which is presented on fig. 1, was taken into account. In actual conceptions of the Wankel engine the course of attack angle can be different and it depends on the Z parameter. On figure 7 the angle of attack course for greater value of the Z parameter.

In order to determine the initial oil film parameters which are obtained for matching the trochoid with two parabolic profile and for inclination angles shown on fig. 7 the suitable computer simulations were realized and it results are put together on fig. 8 and fig. 9.

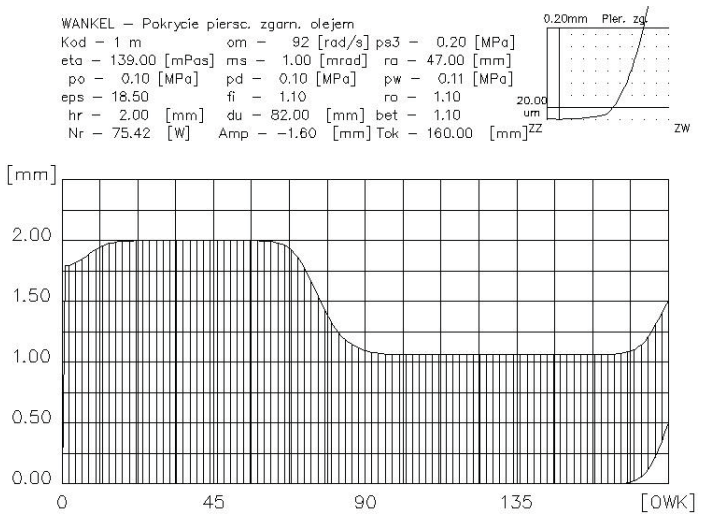

Fig. 5. Course of two parabolic profile filling by the oil film

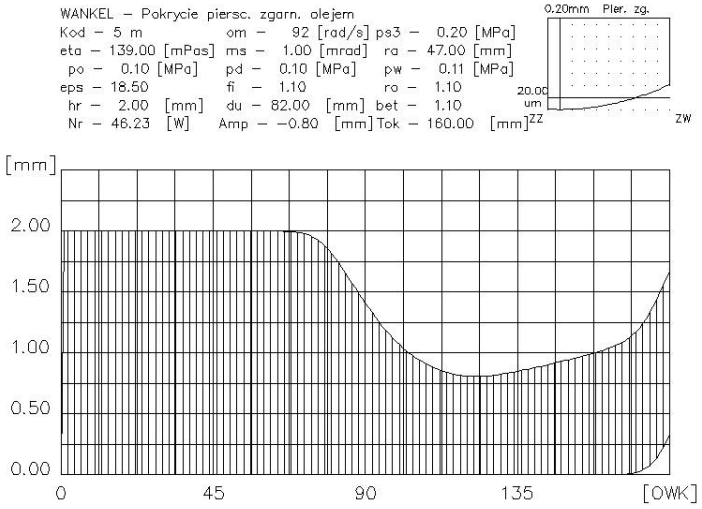

Fig. 6. Course of parabolic profile filling by the oil film, a high curvature radius profile

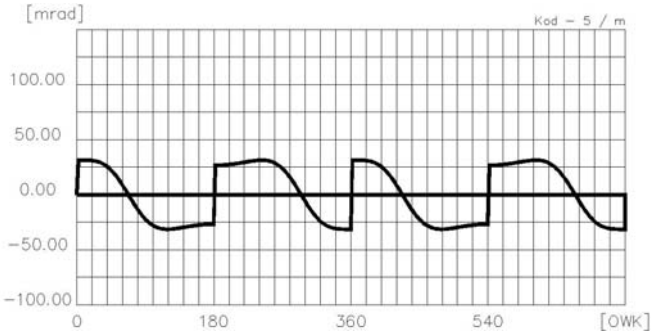

Fig. 7. The course of angle changes of tangent to the cylinder liner generating line, the cylinder liner deformation is sinusoidal with the amplitude of 0,8mm and the period of 160mm

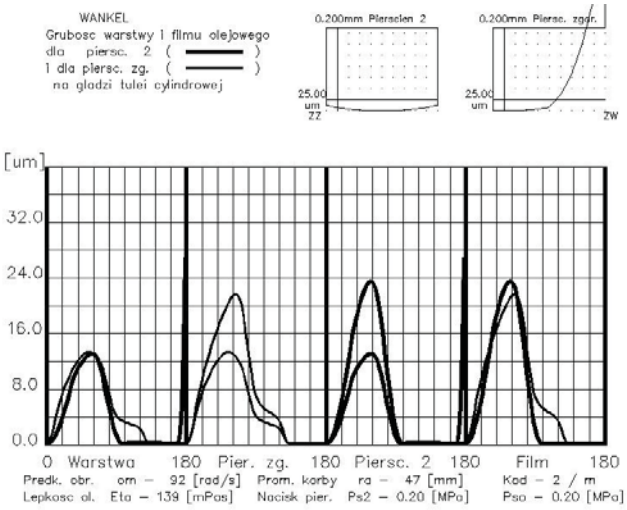

Fig. 8. Comparison of the oil layer thickness course that is left on the cylinder liner surface by two profiles of the Wankel engine apex seal with high value of the Z parameter – first part of the diagram; oil film thickness and layer thickness courses for two parabolic profile – second part of the diagram; oil film thickness course and layer thickness course for the parabolic profile with very high curvature radius – third part of the diagram; comparison of the oil film thickness that was generated by the one and two parabolic profiles – fourth part of the diagram

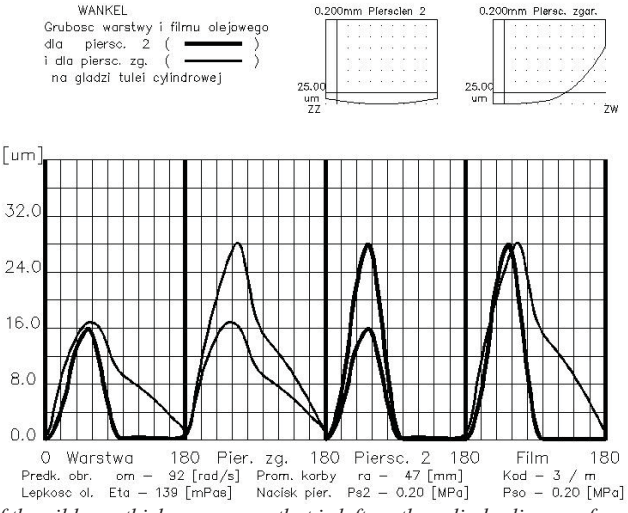

Fig. 9. Comparison of the oil layer thickness course that is left on the cylinder liner surface by two profiles of the Wankel engine apex seal with high value of the Z parameter – first part of the diagram; oil film thickness and layer thickness courses for two parabolic profile – second part of the diagram; oil film thickness course and layer thickness course for the parabolic profile with high curvature radius – third part of the diagram; comparison of the oil film thickness that was generated by the one parabolic profile and two parabolic profile which curvature radius is four times higher than on fig. 8 – fourth part of the diagram

The two parabolic profile was accepted for calculations, smaller curvature radius – fig. 8 and four times higher radius of curvature – fig. 9. It is easily to notice that in second case the results are better. The oil film in second part of the diagram demonstrated on fig. 9 is thicker and what is more important there is no break of the oil film what can be noticed on fig. 8 between 150 and 180 degrees.

3. The test stand used to verification of the computer simulations results

To the investigations authors have adopted the test stand which was formerly used for oil film investigations of piston rings of the marine two stroke engines. Scheme of the test stand is presented on fig. 10 [2].

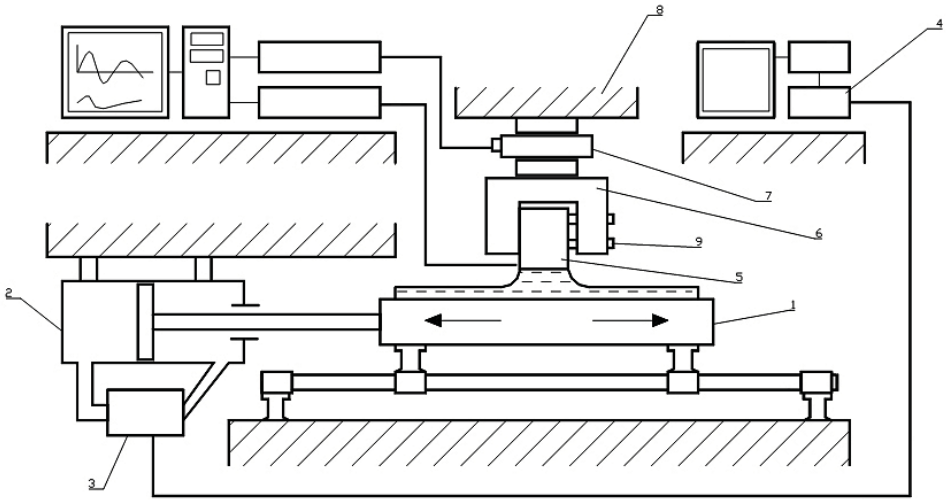

Fig. 10. Schema of construction of the research stand (description in text) [2]

On presented stand reciprocating movement is executed by cart with settled plate simulating cylinder sliding surface 1. This cart is driven by hydraulic servo-motor 2. Pressures in working chambers of servo-motor are regulated by electromagnetic valve 3 which uses the difference of voltage between signals from steering apparatus 4 and sliding resistor which is connected with piston rod. The element that simulates piston ring 5 is seated in piston block model 6 which is settled in the saddle 8 with force transducer 7.

Because in the apex seal motion there are no dead centers and the plate has finite length, the to-and-fro motion had to be substituted by a linear translational motion in the plate length limit. The next step was to reflect the apex seal kinematics was to replace analog steering method by its numerical equivalent. This allowed to specify any plate path and velocity profile, also the apex seal velocity profile. The additional advantage of numerical way of plate motion programming is that we can choose any part of apex seal track on trochoid cylinder liner to be simulated. The plate path determination consists in specifying its position for every of 4096 points. In case of reciprocating engine 4096 point mean full crankshaft turn and for the apex seal motion simulation this number is discrete division of any rotor rotation angle that has been chosen to be investigated. It was said that there are no death centers in the apex seal motion so it was important to make the acceleration and deceleration safe. Additional procedures were added to the main program which are responsible for initial and final phase realization of the plat motion. Initially authors assumed that with total plate length of 800mm only 500mm will be used to the apex seal motion simulation while 100mm will serve to acceleration and deceleration. This results from the necessity of minimization the inertia force that is generated during plate acceleration and deceleration. Actual view of the test stand is presented on fig. 11.

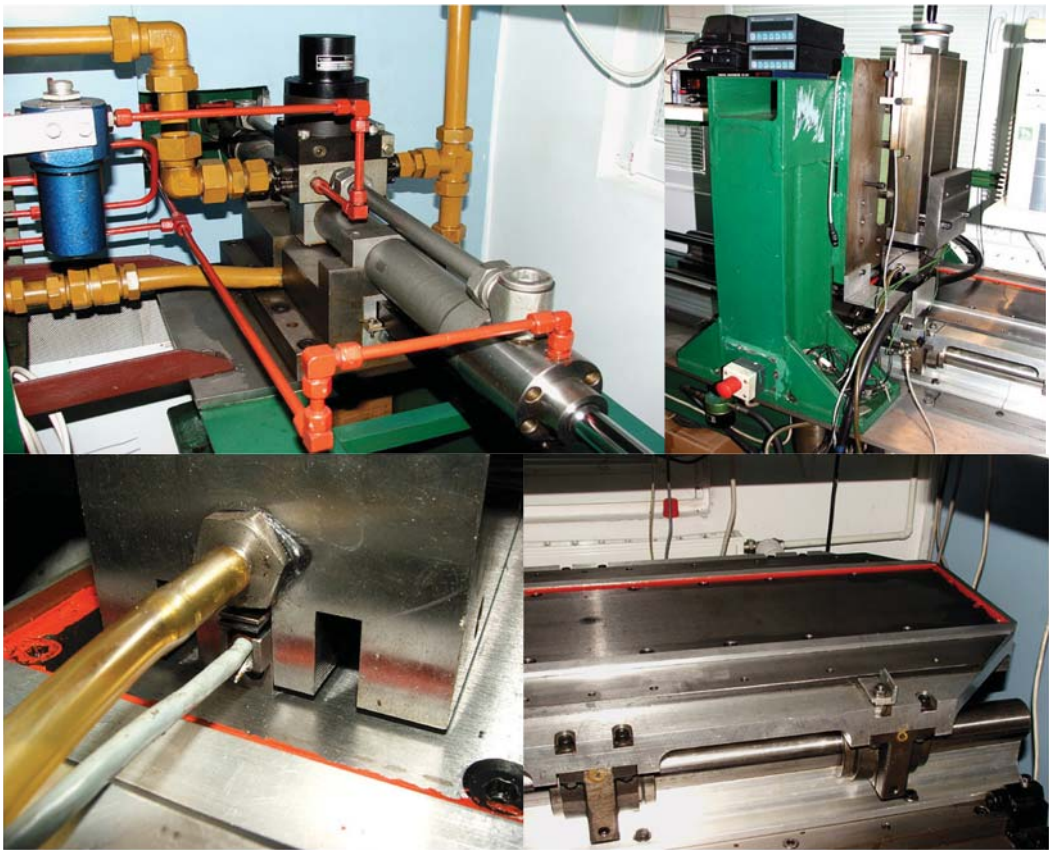

Fig. 11. View of the test stand, upper left corner – hydraulic drive, upper right corner – saddle with piston model attached, lower left corner – piston model with attached slat, lower right corner – the plate that simulates the cylinder liner surface

4. Conclusions

1. One of possible ways to improve the oil film parameters between the apex seal and trochoid sliding surface is to shape the apex seal profile as a two parabolic curve.
2. In most of the apex seal path, where the apex seal axis is perpendicular or almost perpendicular to the trochoid sliding surface, the oil film is generated by high curvature radius parabola while in the vicinity of shorter axis of trochoid the oil film is sustained by parabolic profile with lower radius of curvature.
3. The low radius of curvature profile part should be formed in such way that the convergent gap would not be less than 25% of total gap length between the apex seal and the trochoidal sliding surface.

References

[1] Iskra, A., *Studium konstrukcji i funkcjonalności pierścieni w grupie tłokowo-cylindrowej*, Wydawnictwo Politechniki Poznańskiej, Poznań 1996

[2] Iskra, A., Kałużny, J., Babiak M., *The possibilities of oil film parameters measurements for apex seal of the Wankel engine*, PTNSS Combustion Engines Nr 2007-SC1, pp. 295-301, Kraków 2007

Journal of POLISH CIMAC
Faculty of Ocean Engineering & Ship Technology
GDAŃSK UNIVERSITY OF TECHNOLOGY

PHYSICAL ASPECTS OF WEAR OF THE PISTON-RING-CYLINDER UNIT

Andrzej Kaźmierczak

Wroclaw University of Technology
Wyb. Wyspiańskiego 27, 50-370 Wroclaw, Poland
tel.: +48713477918; fax: +48713477918
e-mail: andrzej.kazmierczak@pwr.wroc.pl

Abstract

The research in presented paper has shown that the physical aspects of interfacial phenomena, described by the total value of surface free energy and the values of its components, make it possible to select more suitable materials for sliding pairs. The total value of surface free energy depends on the molecular structure and the bonds characteristic of a given material and determines its hardness. In order to reduce friction losses in a sliding pair which is being designed, it is proposed to match such materials for the pair that the surface of one of them has a high sum of surface free energy components originating from van der Waals interactions while the other material's surface has a possibly low value of the sum. Furthermore, proper values of the components of surface free energy ensure proper wettability with lubricating oil. Pursuing the practical goal of this research, a new piston packing ring/combustion engine PRC unit cylinder liner sliding pair was designed and made.

Keywords: *Surface Energy, Wear, Coatings, Nitriding, Diesel Engines*

1. Introduction

Interfacial forces produced by intermolecular interactions occur on the surfaces of sliding pair components in both rotary motion and to-and-fro motion. In solid/liquid and liquid/gas interfacial regions atoms belonging to each of the phases are subject to a different system of forces than atoms located within the phases [1]. Atoms at an interface are attracted by both their own phase atoms and the adjoining phase atoms whereby they are located in an asymmetric field of forces. When the forces of attraction towards one of the phases are greater, the atoms migrate into the phase until they reach an equilibrium through changes in the distances between the atoms located at the interface [5]. The differentiation of forces in the interfacial region is the cause of many phenomena such as: adsorption, wetting, adhesion and so on.

The state of phase boundaries can be described on the basis of thermodynamics [6]. Various thermodynamic functions such as: internal energy (U), free energy (F) and free enthalpy (G) (also called the Gibbs function) are used for this purpose. In diphase systems one can distinguish a region of pure phases, referred to as α and β, and a region of transient surface phase σ between the boundary phases [7]. Therefore free enthalpy G (at a constant temperature and pressure) or free energy F (at a constant temperature and volume) is used describe surface properties. Hence interfacial tension γ is defined as:

$$\gamma = \left(\frac{dF^s}{dA} \right)_{T,V} \quad and \quad \gamma = \left(\frac{dG^s}{dA} \right)_{T,p}, \tag{1}$$

were:

γ – surface free energy,
F – free energy,
A – surface,
G – free enthalpy.

Interfacial tension γ is also referred to as interfacial free energy or in short, interfacial energy (especially in the case of solids). When air is one of the phases or the considered phase adjoins a vacuum, then instead of the attribute 'interfacial', the attribute 'surface' is used. In his latest comprehensive study [18] H. Lyklema recommends to use the term interfacial (surface) tension for both liquids and solids. Sometimes instead of γ, symbol F_A^S, referred to as excess surface free energy, is used. In the present work, surface free energy γ and surface tension are used for respectively solids and liquids.

2. Calculation of surface free energy from surface tension of molten solid body

It is difficult to determine surface free energy for solids. According to many researchers, it is possible to calculate surface free energy from measurements of the free surface of melted solids [18]. Such problems feature prominently in metallurgy where the surface tension of fused metals is of major importance [3]. Allen [2] compared surface tension values for metals at their melting points and found a clear relationship between fusion temperature and surface tension for different metals. [5]. The relationship between surface tension and temperature is expressed by the Gibbs-Helmholtz equation:

$$\gamma_S = \gamma_m + \frac{d\gamma}{dt}(T - T_m), \tag{2}$$

where:

γ_S – surface tension of molten metal at temperature T,
γ_m – surface tension of molten metal at fusion temperature T_m,
T_m – the fusion temperature of the metal,
$\frac{d\gamma}{dT}$ – Temperature coefficient, whose value is always negative for metals, was introduced [1].

3. Calculation of surface free energy from Young's modulus and other parameters

R.J. Good [10] proposed a relationship between surface free energy and Young's modulus, assuming that the value of Young's modulus E is a consequence of intermolecular force F_r:

$$E = r_0 \left(\frac{dF_r}{dr} \right), \tag{3}$$

where:

E – Young's modulus,
r_0 – a distance between the centres of molecules being in equilibrium between attractive and repulsive forces,

F_r – the force of intermolecular interactions at distance r.

Expression (3) holds for intermolecular distance r equal to r_0 and for constant temperature. From R.J. Good's considerations [10], based on the Lennard-Jones equation [17] for the energy of a system of molecules versus the distance between them, the following expression interrelating surface free energy with Young's modulus was derived [10]:

$$E = \frac{32\gamma_S}{r_0} \quad \Rightarrow \quad \gamma_S = \frac{Er_0}{32}, \tag{4}$$

where: Young's modulus E and distance r_0 are in respectively pascals (Pa) and meters (m) and calculated surface free energy γ_S of a solid is in joules per square meter (J/m^2) or newtons per meter (N/m).

Expression (4) allows one to estimate surface free energy on the basis of Young's modulus of a solid body and the intermolecular distance at which intermolecular interactions are at equilibrium. Since the material property resulting from intermolecular interactions is taken into account through expression (4) it is possible to calculate the total surface free energy if one knows the kind and number of bonds in a given solid. Since the surface free energy calculated on the basis of Young's modulus is for a material devoid of lattice defects, it may be considerably overestimated.

It follows from the above considerations that surface free energy is a result of interactions characteristic of the molecular structure of a given phase. Another material property is hardness and similarly as surface free energy it depends on a given material's structure. Material hardness is resistance to the forcing of elastic and plastic deformations. Therefore it is associated with volume elasticity modulus K which is a measurable and, as opposed to hardness [23], well defined quantity. The hardness of selected materials versus their volume elasticity modulus K is shown in fig. 1.

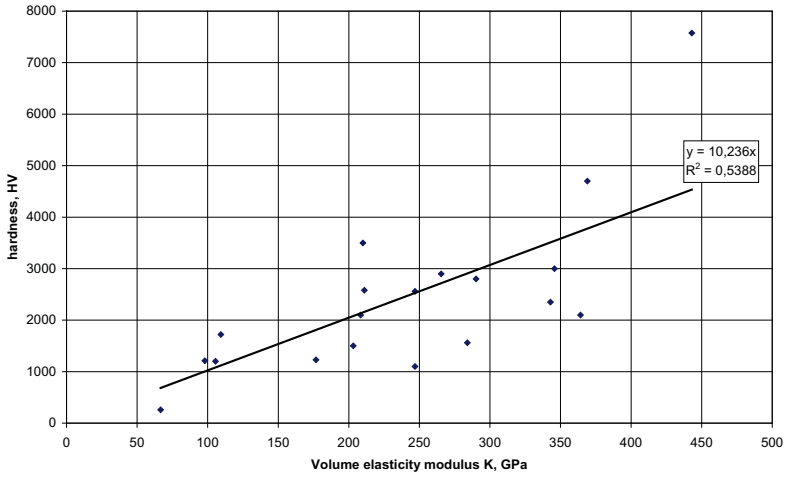

Fig.1. Hardness HV versus K for hard materials

By approximating the relation shown in fig. 1 with a linear function the following expression was obtained:

$$HV \cong a \cdot K \cong 10.236 \cdot K, \tag{16}$$

where:

HV – Vickers hardness, dimensionless quantity,
K – the modulus of volume elasticity of a perfect crystal [GPa],

a – a constant equal to 10.236 [1/GPa].

According to A. Witek [22], the value of the volume elasticity modulus is consistent with the Marvin Cohen (Berkeley University) theory proposed in 1985 and expanded in 1987. The theory allows one to calculate (with an error below 2%) the modulus of volume elasticity from this equation:

$$K = 1761 \cdot r_0^{-3.5}, \tag{6}$$

where:

K – the modulus of volume elasticity of a perfect crystal [GPa],
r_0 – an equilibrium distance between atoms or ions, i.e. the length of a chemical bond in the crystal lattice [angstroms].

According to the Cohen theory, the modulus of volume elasticity can be calculated from the bond length. Volume elasticity coefficient K is related to Young's modulus E by the following formula [24]:

$$K = \frac{E}{3(1-2\nu)}, \tag{7}$$

where:

K – a modulus of volume elasticity [Pa],
E – Young's modulus [Pa],
ν – a Poisson fraction of 0-0.5.

Young's modulus in turn is related through relations defined by R.J. Good [10] (described by formula 15) to surface free energy. Hence total surface free energy and hardness are proportionally correlated through the modulus of volume elasticity and the Poisson fraction as follows:

$$\gamma_S = \frac{Er_0}{32} = 3Kr_0 \frac{1-2\nu}{32}, \tag{8}$$

where:

the meaning and the units of all the variables are consistent with the denotations in equations (4) and (7).

Using equations (5), (6) and (8) the following expression interrelating surface free energy γ_S, hardness HV, intermolecular distance r_0 and Poisson fraction υ was obtained:

$$\gamma_S \cong 307 \cdot HV \cdot r_0 \frac{1-2\nu}{32}, \tag{9}$$

where:

γ_S – surface free energy [mN/m],
HV – Vickers hardness, dimensionless quantity,
r_0 – a mean intermolecular distance [nm],
ν – a Poisson ratio of 0-0.5.

Equations (8) and (9) were formulated for a perfect crystal free of lattice defects. Their application is, however, limited since they yield, similarly as equation (23), overestimated surface free energy values.

3. Calculation of surface free energy from its components

F.M. Fowkes [8] proposed to divide surface free energy into the following components:

$$\gamma = \gamma^d + \gamma^m + \gamma^h + \gamma^o, \tag{10}$$

where:

γ^d – a dispersion component,
γ^m – a metallic bonds component,
γ^h – a hydrogen bonds component,
γ^o – other components, e.g. an ionic component, a covalent bonds component, etc.

In a simplified formulation, the surface free energy of liquids consists of a dispersion part and a polar part. For example, the surface free energy of water is 72.8 mN/m and it consists of dispersion part γ^d = 21.8 mN/m and polar part γ^p = 51 mN/m. Water has neither a metallic component nor a covalent component.

There are several methods of determining surface free energy components, based on solid body wetting phenomena. They employ two or three calibrating liquids with known surface free energy components and assume that surface free energy has only two components: a dispersion component and a polar component [13]. The latter is composed of Keesom (permanent dipoles) and Debye interactions (inductive dipoles) of the dipole-induced dipole type, of confirmative and multipole interactions and hydrogen bonds:

$$\gamma_L = \gamma_L^d + \gamma_L^p \quad and \quad \gamma_S = \gamma_S^d + \gamma_S^p, \tag{11}$$

where:

γ_L – surface free energy as a sum of dispersion and polar interactions for the liquid,
γ_S – surface free energy as a sum of dispersion and polar interactions for the solid,
γ_L^d - the dispersion part of the liquid's surface free energy,
γ_L^p – the polar part of the liquid's surface free energy,
γ_S^d – the dispersion part of the solid's surface free energy,
γ_S^p – the polar part of the solid's surface free energy.

The above measuring methods are: the Fowkes method [8], the Owens-Wendt method [12] and the Wu method [24]. The Owens-Wendt and Wu methods are based on measurements by two calibrating liquids. The accuracy with which the methods identify dispersion and polar interactions considerably improves when a third calibrating liquid is employed. Currently the Owens-Wend and Wu methods are being replaced with the van Oss-Good acid-base method with three calibrating liquids, which is based on the Lewis theory of acids and bases [11] and Fowkes's concept of components [9]. The method is still under development and requires further theoretical-experimental research [24].

4. Taking interfacial phenomena described by surface free energy into account when matching materials for sliding pairs

Considering the above, it is proposed to match materials for friction pairs also on the basis of a quantitative description of interfacial phenomena, using calculations and measurements of the surface free energy of solid bodies [16]. In order to reduce friction losses in a sliding pair which is being designed, it is proposed to match such materials for the pair that the surface of one of them has a high sum of surface free energy components originating from van der Waals interactions while the other material's surface has a possibly low value of the sum (fig. 3).

The two surfaces should have high hardness, i.e. a high value of the total surface free energy. Thanks to the other surface's low sum of van der Waals interactions frictional resistance will be reduced due to a reduction in the work of adhesion to this surface, especially in mixed friction conditions.

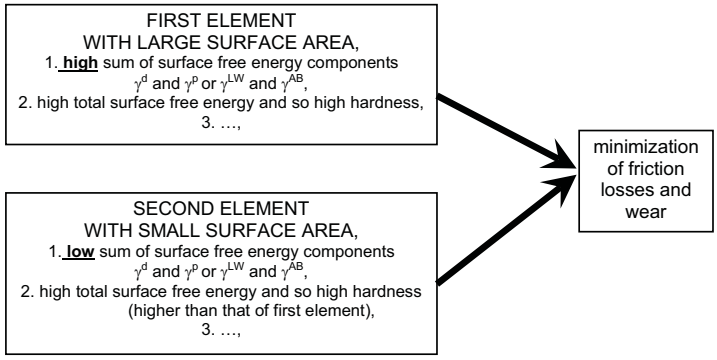

Fig.3. Scheme of matching sliding pair elements [16]

Moreover, the large difference between the sums of surface free energy components is due to the materials' insolubility in the solid state, which is pointed out by Bowle in his numerous papers. Thanks to the use of surface free energy and its components for matching sliding pair elements this process can be described quantitatively [15]. Especially in the case of the second element it is postulated that, except for the generally low value of the surface free energy component originating from dispersion forces, the dispersion component be dominant relative to the other components. If the elements are so matched, friction losses will be reduced. In mixed friction conditions, for which, in the author's opinion, the proposed solutions will be most beneficial, the features of the second element's surface will contribute to a reduction in friction losses thanks to their reduction in the boundary layer formed on the surface of this element.

5. Calculations of surface free energy of exemplary materials for sliding pairs

5.1. Calculations of surface free energy from Young's modulus and other parameters

Calculations based on Young's modulus give a full picture of surface free energy. As mentioned above, one can use equation (4) for this purpose. The calculated values of surface free energy γ for the particular materials, Young's modulus E, hardness HV, Poisson fraction υ and other are shown in table 1.

Tab. 1. Surface free energy values calculated from Young's modulus (γ_Y), hardness and Poisson fraction (γ_{HV}) and surface tension at melting point (γ_{Tt})

Material	Young's modulus *E*, GPa	Hardness *HV*	Poisson fraction *Y*	Melting point T_t, K	Temperature coefficient $d\gamma/dT$, mN/Km	γ_Y mN/m	γ_{HV} mN/m	γ_{Tt} mN/m
Cast iron EN-GJL-200	100 [20]	250**	0.25 [20]	1500 [3]	-0.49 [3]	875	342	2460
Nitrided cast iron EN-GJL-200	200 [20]	800**	0.25 [20]	1500 [3]	-0.49 [3]	1250	1093	2460
TiN	590 [4]	2100 [4] (1600)*	0.23 [20]	3223 [4]	-0.25 [3]	3503	2067 (1574)*	2734

* values for coating, ** measurement values

Similarly, surface free energy values were calculated from relation (9) for surface free energy γ_{HV} as a function of hardness *HV* and Poisson fraction υ. The values are presented in table 6 which also shows surface free energy values calculated on the basis of molten solid surface tension γ_{Tt}, using relation (2). Although the presented methods of estimating surface free energy yield different results, they are still useful considering that there are no other methods of estimating total surface free energy. In the author's opinion, the method based on hardness and the Poisson fraction is the most adequate, mainly because of the fact that hardness is resistance to the forcing of elastic and plastic deformations. The method's applicability is limited to very hard (above 200 *HV*) materials.

5.2. Measurements of surface free energy components from angle of wetting

The measurements were carried using a D2 Krüβ goniometer with the DSA (Drop Shape Sof tware). Three calibrating liquids with known surface free energy polar component γ^p and dispersion component γ^d for the Owens-Wendt, Fowkes and Kaeble methods and with known component γ^{LW} and component γ^{AB} for the van Oss-Good acidic-basic method were used for the measurements. The calibrating liquids were: water, formamide and diodomethane. The measurement results shown in table 3 confirm that after nitriding the dispersion component increases, which is accompanied by a slight increase in the sum of the components generated by van der Waals forces. Table 4 shows the results of surface free energy dispersion and polar component measurements for different coatings deposited using the PAPVD method.

Tab. 3. Measured surface free energy components of cast iron EN-GJL-200 before and after nitriding [16]

Material	Wetting angle Θ			Owen–Wendt method	Van Oss-Good acidic-basic method
	diodomethane	formamide	water		
EN-GJL-200	54.18	57.53	69.87	Sum of components: **γ =39.20**	Sum of components **γ=36.07**
				Dispersion component γ^d=29.06	Component LW γ^{LW}=31.92
				Polar component γ^p=10.14	Component AB γ^{AB}=4.15
					Acidic component=0.28
					Basic component=15.51
Nitrided EN-GJL-200 [14]	47.64	54.32	75.00	Sum of components **γ =40.41**	Sum of components **γ=39.51**
				Dispersion component γ^d=34.01	Component LW γ^{LW}=35.58
				Polar component γ^p=6.40	Component AB γ^{AB}=3.93
					Acidic component=0.47
					Basic component=8.26

Tab. 4. Sum of surface free energy components for TiN

Material	Wetting angle Θ			Surface free energy components	Calculation method	
	diodomethane	formamide	Water		Fowkes	Kaelbe
TiN [32, 33]	59.27	69.04	78.80	**Sum of components γ**	**29.44**	**29.45**
				Dispersion component γ^d	24.33	23.75
				Polar component γ^p	5.11	5.69

6. Experimental investigation of sliding pair and surface free energy of its elements

The influence of surface free energy and its components on tribological phenomena in a sliding pair was verified in a roll-block tester. Clinging to the counterface the specimen forms a distributed contact of 100 mm^2 with it. In accordance with the considerations presented in section 5, the counterspecimen was made from cast iron EN-GJL-200. Ten counterspecimens, of which five were subjected to vacuum nitriding, were prepared [19]. The specimens were made from cast iron designated in accordance with PN-EN 1560 as EN-GJL-350. As specified in section 5, their working surfaces were coated with titanium nitride, using the plasma-assisted physical vapour deposition (PAPVD) technique described in [21]. A linear speed of 1.25 m/s and a pressure of 5 MPa were used to create extremely difficult operating conditions for the sliding pairs, similar to the conditions prevailing in the first piston ring's inner dead centre area at the beginning of the internal-combustion engine's power stroke. As a result, mixed friction was obtained, as evidenced by the fact that the coefficient of friction was much above 0.01 – a value typical for fluid friction [15]. The range of tests carried out in the T05 microprocessor roller-block tribotester included measurements of friction forces and the wear and mass temperature of the specimen, which as time characteristics were archived in a computer system. After statistical handling the time characteristics were used to calculate the average friction coefficients for the sliding pairs (table 5). TiN coated specimen/cast iron counterspecimen pairs sliding in the presence of a lubricant – ELF SYNTHESE 5W50 synthetic oil (pairs: 12, 13, 15, 18). TiN coated specimen/nitrided cast iron counterspecimen pairs sliding in the presence of a lubricant – ELF SYNTHESE 5W50 synthetic oil ELF SYNTHESE 5W50 (pairs: 11, 14, 16, 17, 19).

Tab. 5. Plan of tests in tribotester T05

Specimen number	Counterspecimen	Load MPa	Speed m/s	Type of oil
11	nitrided cast iron	5	1.25	synthetic
12	cast iron	5	1.25	synthetic
13	cast iron	5	1.25	synthetic
14	nitrided cast iron	5	1.25	synthetic
15	cast iron	5	1.25	synthetic
16	nitrided cast iron	5	1.25	synthetic
17	nitrided cast iron	5	1.25	synthetic
18	cast iron	5	1.25	synthetic
19	nitrided cast iron	5	1.25	synthetic

The friction distance for one test run was set at 1350 m. The total friction distance was set at 20 runs. Once the sliding pair cooled down after each run, wear, being the sum of the wear of the specimen and that of the counterspecimen, was measured. The tests were conducted according to a static, determinate and complete test plan.

Tab. 6. Friction forces and friction and wear coefficients of sliding pairs tested for distance of 27000 m

SLIDING PAIR	Average tangent force N	Average friction coefficient	Average specimen temperature °C
TiN coated specimen Cast iron counterspecimen Synthetic oil Elf Synthese 5W50	28.1	0.044	54.5
TiN coated specimen Nitrided cast iron counterspecimen Synthetic oil Elf Synthese 5W50	8.0	0.015	40.5

Friction coefficients as a function of friction distance were calculated from friction force measurement results, as a quotient of the friction force and the pressure multiplied by the contact surface area. The graphs of the friction coefficients are shown in figs 5 and 6. Through regression analysis regression functions (in the polynomial form) were fitted to all the parameter values in the figures showing friction coefficient graphs. Through comparative studies the coefficients of friction of cast iron and nitrided cast iron counterspecimens sliding against TiN in the presence of synthetic oil were determined (tab. 6).

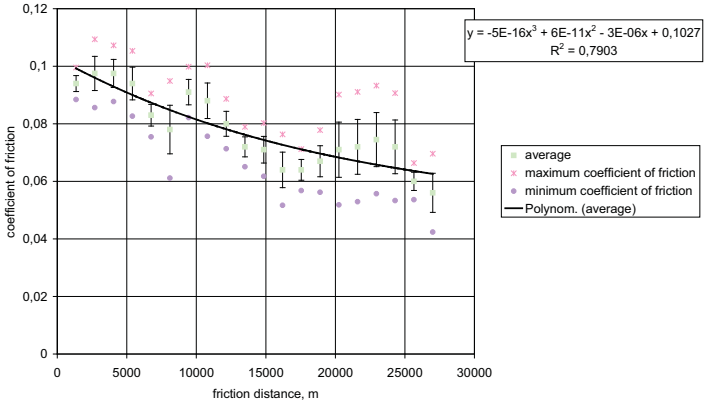

Fig.5. Coefficient of friction versus friction distance for cast iron counterface sliding against TiN coated specimen lubricated with synthetic oil

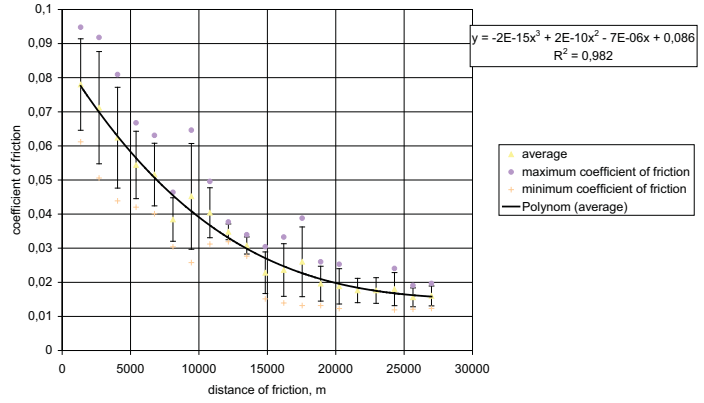

Fig. 6. Coefficient of friction versus friction distance for nitrided cast iron counterface sliding against TiN coated specimen lubricated with synthetic oil

The differences in surface free energy values between cast iron EN GJL 200 and nitrided cast iron EN GJL 200 resulted in considerable differences in the friction and wear coefficient values of the tested sliding pairs. Figures 9 show the average friction coefficients for the tested sliding pairs. The average surface free energy of the cast iron (γ=1225 mN/m) and the nitrided cast iron (γ=1600 mN/m) from which the tested counterspecimens were made, calculated from the data shown in table 4, are marked on the Y-axis. Nitriding of the cast iron resulted in an increase in total surface free energy (table 1) and consequently, in an increase in hardness. Also the dispersion component value (tables 2 and 3) of this energy increased as indicated by calculations using wetting angle measurements. High values of the surface free energy dispersion component are conducive to the formation of a uniform film of oil, which is well bounded with the base thanks to good wetting.

The causes of the lower friction coefficients are sought in the greatly reduced intensity of adhesion wear during mixed friction when microcontacts between surface irregularities occur as in the case of coatings with a lower sum of the dispersion component and the polar component of surface free energy, including the TiN coatings on the tested specimens (table 4). Also significant is the low value of the surface free energy polar component which for the TiN coating is several times lower than for the other coatings with a comparably low sum of the surface free energy dispersion and polar components (table 4). This is associated with a reduction in Keesom interactions at elevated temperatures [16].

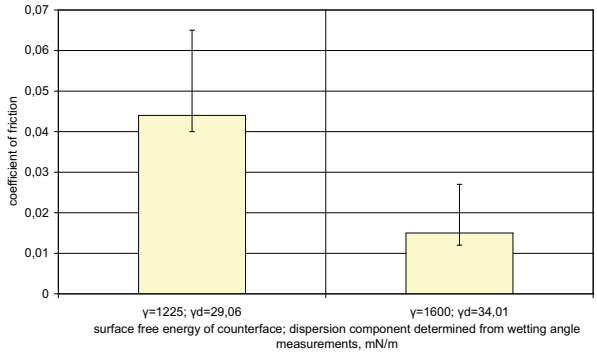

Fig. 9. Friction coefficient of sliding pair versus surface free energy of counterface

An additional factor which played a part in preventing adhesion wear was the use of synthetic oil as the lubricant. The low friction coefficients were obtained owing to the properties of the synthetic oil (mainly its ability to form an oil film already at the startup) combined with the property of the specimen's surface: low intensity of adhesion wear and the property of the counterspecimen: good durability of the lubricating film.

7. Conclusion

- Wear resistance (often identified with hardness) and wettability by a lubricant (usually lubricating oil) come to the fore among the well known material properties which should characterize sliding pair elements.
- Surface free energy estimates based on Young's modulus, hardness and surface tension at the fusion temperature allow one to assess general strength properties. For this only the main material properties are needed.
- By calculating surface free energy dispersion component γ_S^d from the Hamaker constant one can assess the wettability of a given body and consequently, the energy of adhesion to oil.

Then one can draw conclusions about the behaviour of the two interacting elements, especially in mix friction conditions.

- By calculating dispersion component γ_S^d or Lifshitz-van der Waals component γ_S^{LW} and polar component γ_S^p or acidic-basic component γ_S^{AB} of surface free energy on the basis of the angle of wetting by calibrating liquids one can gain insight into the components resulting from interfacial interactions. Using these methods one cannot calculate the total surface free energy of solid bodies characterized by metallic and covalent bonds. Nevertheless, measurements by calibrating liquids are important for the identification of the components playing a role in interfacial interactions, i.e. dispersion component γ_S^d or Lifshitz-van der Waals component γ_S^{LW} and polar component γ_S^p or acidic-basic component γ_S^{AB}.
- The estimations and calculations of surface free energy and its components done for the combustion engine's PRC unit made it possible to well match the materials for the sliding pair elements. The goodness of the match was confirmed by the results of tribological and combustion engine tests.

References

[1] Adamson A., W., *Physical Chemistry of Surface*, Interscience Pub. Inc., New York 1960.
[2] Allen B.C., *Liquid Metals*, Marcel Dekker Inc., New York 1972.
[3] Benesch R., Janowski J., Mamro K., *Ferrous Metallurgy, Physicochemical Foundations of Processes* (in Polish), Wydawnictwo "Śląsk", Katowice, 1979.
[4] Burakowski T., Wierzchoń T., *Metal Surface Engineering*, WNT, Warsaw, 1995.
[5] Dereń J., Haber J., Pampuch R., *Chemistry of Solid Body*, PWN, Warsaw, 1977.
[6] Drzymała J., *Foundations of Mineralurgy*, Wroclaw University of Technology Press, Wroclaw, 2001.
[7] Dutkiewicz E.T., *Physicochemistry of Surfaces*, WNT, Warsaw, 1998.
[8] Fowkes F.M., *Attractive Forces at Interfaces*, Ind. Eng. Chem., 56 (12), pp. 40-52, 1964.
[9] Fowkes F.M. et al., *J. Coll. Interf. Sci.*, 1980, 78, 1, 200.
[10] Good R.J., *Intermolecular and Interatomic Forces*, in: Treatise of Adhesion and Adhesives, Ed: Patrick R.L., Vol. 1(3), New York, Marcel Dekker Inc., 1967, pp. 9-68.
[11] Gutmann V., *Donor-Acceptor Approach to Molecular Interaction*, New York, Plenum Press, 1979.
[12] Jańczuk B., Zdziennicka A., Wójcik W., *Surface Free Energy*, Wiadomości Chemiczne, 1995, 49, 5-6, pp.301-324.
[13] Jańczuk B., Zdziennicka A., Wójcik W., *Determination of Surface Free Energy of Solid Bodies from Wetting Angle*, Wiadomości Chemiczne, 1995, 49, 7-8, pp. 429-347.
[14] Kaźmierczak A., *Computer Simulation of Piston Ring–Cylinder Liner Coaction in Combustion Engine,* Proceedings of the Institution of Mechanical Engineers, Journal of Automobile Engineering – Part D, Volume 218, No. 12, 2004, Professional Engineering Publishing Limited, Northgate Avenue, Bury St Edmunds, Suffolk IP32 6BW, United Kingdom.
[15] Kaźmierczak A., *Effect of Cermetallic Coating on Tribological Processes in Ring Seal of Combustion Engine*, Wroclaw University of Technology Press, Wroclaw, 2002.
[16] Kaźmierczak A., *Friction and Wear of Piston-Ring-Cylinder Unit*, Wroclaw University of Technology Press, Wroclaw, 2005.
[17] Lennard-Jones J.E., *Proc. Roy. Soc. Ser. A.*, 1924, 196, 463.
[18] Lyklema H., *Fundamentals of Interface and Colloid Science*. Vol.1. Fundamentals, Academic Press, London, San Diego, New York, Boston, Sydney, Tokyo, Toronto, 1993.
[19] *NITROVAC Technology,* Lodz University of Technology Press, Lodz 1998.

[20] Mechanical Engineer's Guide, joint publication, WNT, Warsaw, 1985.
[21] Walkowicz J., Smolik J., Miernik K., Bujak J. *Comparative Investigation of the Wear Behaviour of TiN Monolayer Coatings, Ti(C,N) Multicomponent Coating and TiC/Ti(C,N)/TiN Multilayer Coating Deposited by the Vacuum Arc Method*, Thin Films, ed. G. Hecht, E. Richter, J Hahn, Informationsgesselschaft Verlag, Oberrursel, 1994, pp.587-590.
[22] Witek A., *Material Harder than Diamond,* Wiedza i Życie, 11, 1994.
[23] Zakrzewski M., Zawadzki J., *Strength of Materials*, PWN, Warsaw, 1983.
[24] Żenkiewicz M., *Adhesion and Modification of Surface Layer of Multimolecular Materials*, WNT, Warsaw, 2000.

Journal of POLISH CIMAC
Faculty of Ocean Engineering & Ship Technology
GDAŃSK UNIVERSITY OF TECHNOLOGY

INFLUENCE OF AN EXTERNAL NORMAL HARMONIC FORCE ON REDUCTION OF FRICTION FORCE

Robert Kostek

University of Technology and Life Sciences in Bydgoszcz
al. Prof. S. Kaliskiego 7, 85-789, Bydgoszcz
e-mail: robertkostek@o2.pl

Abstract

The paper shows; the results of studies on the influence of an external normal harmonic force upon reduction of a friction force, in the system of two bodies in a planar contact. It has been pointed out that, the main reason for the friction force reduction is due to dynamical effect; kind of stick – slip monition. Nature of the phenomenon has been described and explained in the article. The computational studies have been validated with experimental results available in literature. Moreover a nondimensional relation, between forces acting on a slider and average velocity of the slider, has been found.

Keywords: *stick-slip, friction, reduction, contact, nonlinear vibration*

1. Introduction

Interaction between the friction force and the normal forces takes place in many dynamical systems, e.g. in. vibrating plate compactors or vibrating feeders. The phenomenon was described in many publications [1-16], in context of friction reduction due to normal vibrations or forces. The reduction of the friction force, under normal vibrations and a variable normal force, is usually explained in the literature thorough:

- decreased value of friction coefficient [15];
- decreased average value of contact deflection [8, 16];
- decreased "efective" value of the reaction force [16];
- decreased average value of the real area of contact [3, 5, 7, 14]; and
- stick-slip motion caused by a variable normal reaction [4, 9, 10, 12, 13].

Although the matter has been known for a long time, there is not one widely accepted opinion for the reason of friction force reduction. The main goal of this paper is to prove that, the main reason of the friction force reduction due to an external normal harmonic force, is the stick-slip motion.

In the considered work; the friction coefficient has a constant value, contact deflection has been neglected, and the mean value of the reaction equals the earthpull (equilibrium of momentum and impulse). Moreover according to Bowden and Tabor [1]; the value of the true contact area is directly proportional to the value of the normal reaction, and of the friction force is directly proportional to value of true contact area. Therefore the factors are not considered as a reason of the friction force reduction.

2. Model

The aforementioned system of the two bodies in a planar contact, shown in Fig. 1, is investigated in the section. The system consists of a slider and a slideway. The rough surfaces undergoing friction create an elastoplastic interface. Nevertheless in this model, the contact flexibility is neglected, because the force of inertia is very slight, during vibrations excited by low frequency external force [9]. Thus the reaction force is the sum of earthpull and external force,

$$R=Q - P_a \sin(2\pi ft) , \tag{1}$$

where:
R- denotes reaction force,
Q- earthpull,
P_a- amplitude external force,
f- frequency,
t- time.
As evident from Eq. (1) the average value of reaction equals earthpull ($\overline{R} = Q$).

A constant driving force F_d is applied to the slider (Fig.1), and tends to introduce a sliding motion. While the friction force F_f acting in the contact region, tends to stop the motion. The friction force is expressed by the Coulomb's formula

$$\text{If } \dot{x}=0 \text{ then } F_f = -F_d \text{ else } F_f=-\mu R \operatorname{sgn} \dot{x} , \tag{2}$$

where:
μ- is a constant friction coefficient,
x- displacement,
F_f - friction force,
F_d - driving force.
The directly proportional relation between the reaction force and the friction force, during slip (Eq, (2)) means, that the decrease of the coeficient of friction is not considered at all. Moreover while smooth sliding takes place, the average friction force is equal to the product friction coefficient and the earthpull ($\overline{F_t} = \mu\overline{R} = \mu Q$).

The sliding motion of the slider of mass m, which is assumed to be a rigid block, is described by the ordinary differential equation:

$$\ddot{x} = m^{-1}(F_d-F_f) , \tag{3}$$

where:
m- denotes mass of the slider.

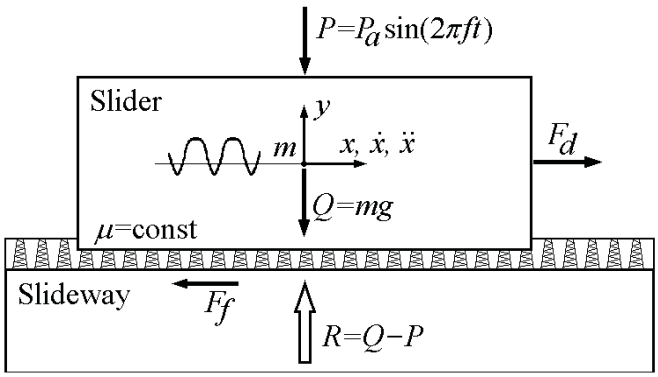

Fig. 1. Model of a simple dynamical system with external force P and Coulomb's friction

3. Investigation of friction force and sliding motion

In the case, when amplitude of external force equals zero P_a=0; then driving force must be higher or equal to friction force, to cause or maintain sliding motion in the considered system;

$$F_d \geq F_{fN} = \mu Q = \mu mg \,, \tag{4}$$

where:
F_{fN}- denotes the nominal static force in the absence of contact vibrations, and
g- is gravitation acceleration.

The sliding motion of the slider may occur at lower values of the driving force then shown previously (Eq. (4)), when the normal external force is present. The conditions for motion to occur may be written down as follows

$$F_d > \mu(Q\text{-}P_a) = F_{f\,min} \,, \tag{5}$$

where:
$F_{f\,min}$ - denotes the minimum of the friction force.
The formula delimits areas of motion and stillness (Fig. 3.). The equation of slider motion was studied in detail. Firstly the time history was simulated. Diagrams (Fig. 2.) show clearly the time histories of the motion and the mechanism of reduction friction force. The slider begins a short-time slip, at the point (*A*), in which the potential friction force μR begins to be lower than the tangential force F_d,. The reduction of the friction force is coupled with unloading of the contact by the external force. The slider accelerates to the time instance (*B*), in which the friction force F_f begins to be higher than that of the tangential force F_d. At he point (*B*) the velocity of the slider is the highest. Next the friction force F_f is higher than that tangential force F_d, in turn the velocity drops to zero at point (*C*), because the slider's kinetic energy has been dissipated. Finally is the period of stick (immobility of the slider). The period last to the time instance, when the potential friction force μR is again lower than that of the tangential force F_d. Therefore the stick-slip motion is periodical and interrupted.

In short; temporary and periodical drops of the friction force are used for slider displacement. The slider moves when conditions are the best and "waits" when conditions are not good enough to move. The periodical motion can be seen as continuos one, when frequency of the motion is high. The feature may leads sometimes to misinterpretation of the phenomena.

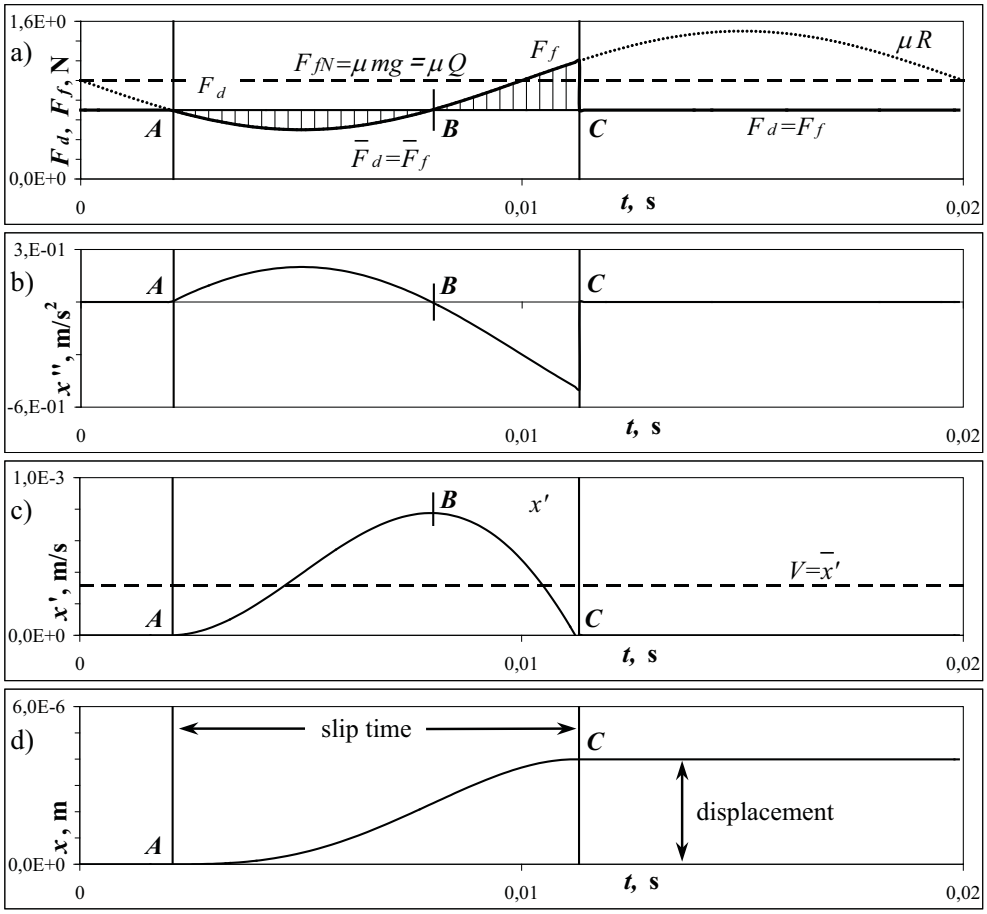

Fig. 2. Results of computer simulations illustrating time histories of forces and their influence on kinetic values $\ddot{x}, \dot{x}, x$ *characterising motion of the slider* (*adopted data:* P_a=5*N*, F_d=0,7*N*, f=50*Hz*, μ=0,1, g=10m/s^2, m=1*kg*)

In general, the occurrence of sliding motion of the slider, and its behaviour depend on: the value of the tangential force F_d (which is lower than $F_{fN}=\mu mg$); amplitude P_a of the external force (which is lower than $Q=mg$) and the frequency f of the external force. Velocity of the slider depends on time histories of the tangential force F_d and the friction force F_f, in other words on impulse of the forces (lined areas in Fig. 2a). Thus by integration of the areas velocity is calculated. Velocity of the slider is increasing, when the lined area is rising. An analysis of factors, which influence on impulse of the forces, and consequently on velocity of the slider, leads to conclusion that; a general nondimensional solution can be received (Fig. 3). Nondimensional velocity of the slider U may be written down as follows

$$U = \frac{Vf}{g\mu} \ , \tag{6}$$

where:
V [m/s] - denotes average velocity of the slider.

Influence of P_a/Q and F_d/F_{fN} , on the nondimensional velocity U of the sliding motion, has been presented on Fig. 3. In the figure, the area of variations of controllable data (F_d/F_{fN} and P_a/Q) is noticeable, in which the sliding motion does not occur (U=0). This takes place for, appropriately small amplitudes of external force and values of the tangential force. The area, in which the sliding motion occurs, is noticeable too. Nondimensional velocity U increases with the rise of the amplitude of the external force P_a and the tangential force F_d. These forces can be used to steer the slider.

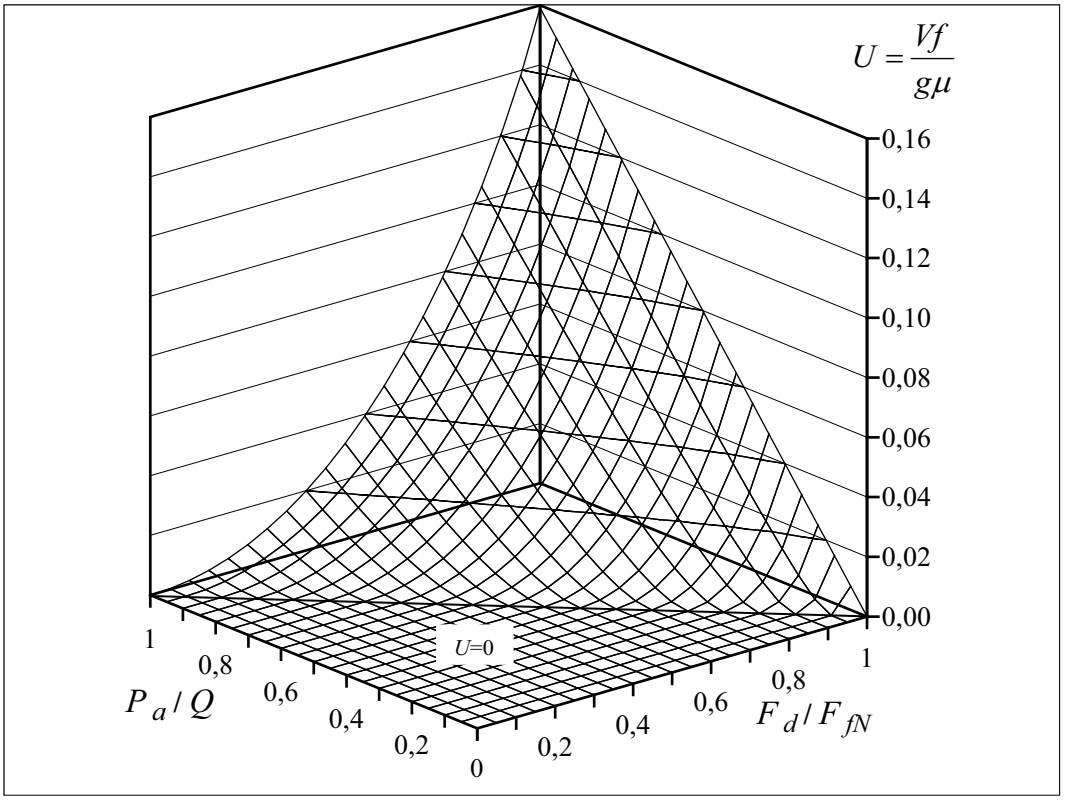

Fig. 3. Influence of P_a/Q and F_d/F_{fN} on the nondimensional velocity U of the slider

The model of the reduction friction force is verified. The results of simulation were validated with the experimental results (Fig. 4) presented by Lomakin [12]. The differences between the results are slight, which gives the opportunity to suppose, that the main reason of the friction force reduction has been presented in the article.

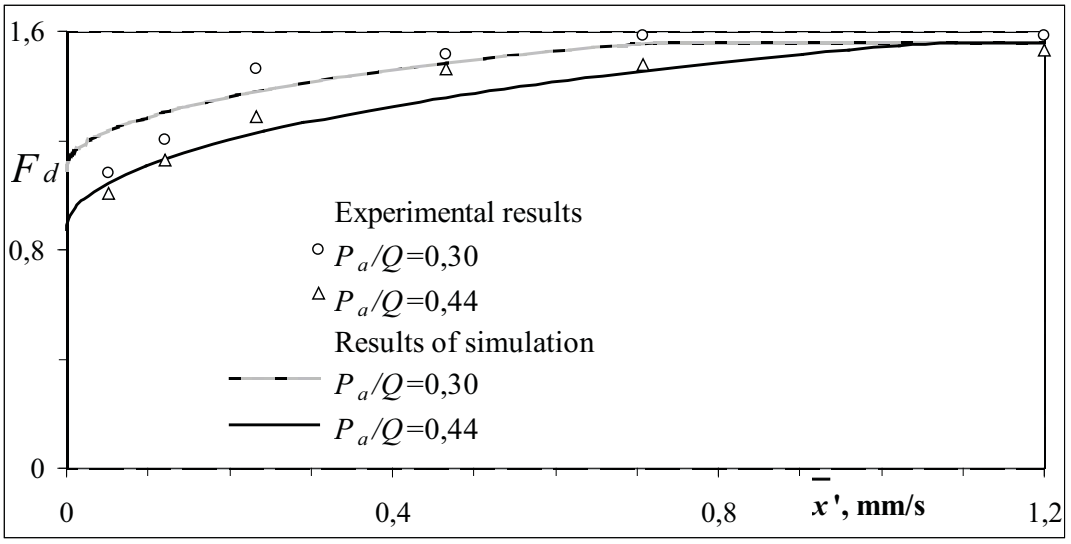

Fig. 4. Comparison of the results of simulations against the experimental results presented by Lomakin (*1955*) (*adopted data:* μ=0,156, m=1*kg*, g=10m/s^2, f=100*Hz*)

4. Conclusions

The adopted model as well as the simulations and experimental results indicate, the mechanism of the reduction of the friction force, for planar contact of solids under the normal external force. It has been shown: the influence of a normal external force on the reduction of the friction force, and that reduction of:

- mean value of the friction coefficient,
- mean value of the normal reaction,
- mean value of the real contact area,

are not necessary in order to reduce the friction force in a sliding system. The reduction can be explained, on the ground of nonlinear dynamics, as a result of stick-slip motion. Moreover the nondimensional relation, between the forces acting on the slider and the average velocity of the slider, has been found as well.

References

[1] Bowden, F. P., Tabor, D., *The friction and lubraction of solids*, Oxford University Press, 1954.

[2] Bryant, M. D., Lin, J.W., US Patent 5466979, *Methods and apparatus to reduce wear on sliding surfaces*, US Patent Issued on November 14, 1995.

[3] Chowdhury, M. A., Helali, M. M., *The effect of amplitude of vibration on the coefficient of friction for different materials*, Tribology International, Vol. 41, No. 4, pp. 307-314, 2008.

[4] Cochard, A., Bureau, L., Baumberger, T., *Stabilization of frictional sliding by normal load modulation*, ASME Journal of Applied Mechanics, Vol. 70, No. 2, pp. 220-226, 2003.

[5] Godfrey, D., *Vibration reduces metal to metal contact and causes an apparent reduction in friction*, ASME Vibration and Friction, Vol. 10, pp. 183-192, 1967.

[6] Grudziński, K., Robert, K., *Influence of normal micro-vibrations in contact on sliding motion of solid body*, Journal of Theoretical and Applied Mechanics, Vol. 43, No. 1, pp. 37-49, 2005.

[7] Hess, D.P., Soom, A., *Normal vibrations and friction under harmonic loads: Part II -Rough Planar Contacts*, Trans. ASME Journal of Tribology, Vol. 113, No. 1, pp. 87-92, 1991.
[8] Kligerman, Y., *Multiple solutions in dynamics contact problens with friction*, 2003 STLE/ASME Joint International Tribology Conference, Floryda USA, October 26-29, 2003.
[9] Kostek, R., *Investigation of the normal contact microvibrations and their influence on the friction force reduction in dynamical system*, PhD thesis, Szczecin University of Technology, 2005.
[10] Kostek, R., *Reduction of friction force due to an external normal harmonic force*, Tribologia, Vol. 218, No. 2, pp. 277-283, 2008.
[11] Lewiński, A., Pytko, S., *Izmienienija koeficjenta trenija i iznosa v uslovijach vynuzdennych kolebaniji.* Trenie i Iznos, Vol. 15, No. 2, 1994.
[12] Lomakin, G. D., *Suchoe vnešnee trenie s kolebanijami zvukovoj častoty*, Žurn. Techn. Fiziki, Tom 25, Vol. 10, pp. 1741-1749, 1955.
[13] Oden, J. T., Martins, J. A. C., *Models and computational methods for dynamic friction phenomena*, Computer Methods in Applied Mechanics and Engineering, Vol. 52, No. 1-3, pp. 527-634, 1985.
[14] Sakamoto, T., *Normal displacement and dynamic friction characteristics in a stick-slip process*, Tribology International, Vol. 20, No. 1, pp. 25-31, 1987.
[15] Shi, X., Polycarpou, A. A., A *Dynamic friction model for unlubricated rough planar surfaces*, Trans. ASME Journal of Tribology, Vol. 125, No. 4, pp. 788-796, 2003.
[16] Tolstoi, D. M., Borisova, G. A., Grigorova S. R., *Friction reduction by perpendicular oscillation*, Doklady Technical Physics, Vol. 17, No. 9, pp. 907-909, 1973.

Journal of POLISH CIMAC

Faculty of Ocean Engineering & Ship Technology
GDAŃSK UNIVERSITY OF TECHNOLOGY

THE THERMODYNAMIC AND ECONOMIC ANALYSIS OF THE SUPERCRITICAL COAL FIRED POWER PLANT WITH CCS INSTALLATION

Janusz Kotowicz, Katarzyna Janusz-Szymańska

Silesian University of Technology
ul. Konarskiego 18, 44-100 Gliwice, Poland
tel.:+48 32 237 22 04, fax.: +48 32 237 13 68
e-mail: janusz.kotowicz@polsl.pl, katarzyna.janusz@polsl.pl

Abstract

In the paper the results of the thermodynamic and economic analysis of the supercritical coal fired power plant integrated with the carbon dioxide capture installation was shown. The paper presents the algorithm for determining the power of power plant and its efficiency losses due to the membrane separation of CO_2 from the flue gases and CO_2 compression. For the purpose of separating CO_2 a membrane technology was applied. Calculations concerning the membrane separation of CO_2 were carried out with the program Aspen. For the assessment of the separation process two indices were applied: the mole fraction of CO_2 in the permeate and the recovery ratio of CO_2. The decision variables in the calculation were the pressure on the feed side and on the permeate side. The pressure on the permeate side is generated by a vacuum pump and on the feed side by a compressor. The power rating of require components determines the energy consumption of the separation and compression processes. The way of determining the minimum losses of the power rating and efficiency of the power plant in membrane separation process and compression CO_2 using calculated indices were shown. The power rating losses and efficiency of the power plant were determined for both processes. The economic analysis was calculated for power unit, taking into account investments and costs connected to the CO_2 capture installation. For the conducted analysis it is essential to determine the unit sale price of electricity as well as the cost of avoided emission CO_2.

Keywords: *supercritical power plant, capture CO_2, membrane separation*

1. Introduction

One of the priority operations in the UE is environmental protection. Poland as a members country has the task of reducing of the anthropogenic emissions of greenhouse gases, mainly CO_2 connected with the energy production from fossil fuels. The reduction of CO_2 emission prevents global climate change. Also, Improved energy efficiency, effective burning of fossil fuels and the use of alternative energy sources will help to reduce this emission. A technique that could make it possible to faster achieve large reduction of greenhouse gases emission is CO_2capture from power generation processes.

There are many possibilities of reducing the emission of CO_2 in energy processes [7]. The main methods are pre-combustion capture, post-combustion capture and oxy-combustion.

In the presented a paper use of a post-combustion process, including the membrane separation of carbon dioxide from combustion gases is described [8].

2. Thermodynamic analysis and the results of calculations

High efficiency of the electricity production has a connection to these technologies, which that influence more effective and efficient use of fuels. A modern power engineering rely on supercritical coal fired plant. Various structures and parameters with electric power of $N_{el,REF}$ = 600 MW are presented in the paper [2]. These are reference systems for the Polish power engineering after the year 2010. The model of the supercritical coal power plants integrated with CCS installation was applied for the analysis. The diagram of such an installation is presented in fig.1.

Characteristic parameters of this block are [6]:

- Temperature and pressure of live steam – 600˚C/28.5 MPa,
- Temperature of resuperheated steam – 620˚C,
- Pressure in the steam condenser – 5 kPa,
- Isentropic efficiency of all turbine stage – 0.9,
- Mechanical efficiency and efficiency of the generator – 0.99 i 0.988,
- Efficiency of the boiler – 0.95,
- Efficiency of the electricity production – 0.4878,
- Lower Heating Value – 24500 kJ/kg.

Such a systems emits 2.086 Mg/h of flue gases of the mole fraction of CO_2 amounts to 14.05%, which gases CO_2 emission equal to 121.3 kg/s [6]. Assuming that the block annual work for 8000h, the CO_2 emission would amount to 3 493 440 Mg.

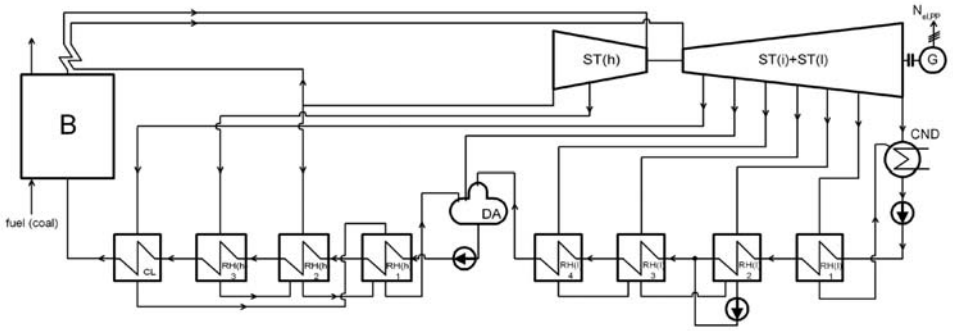

Fig.1 Reference systems of supercritical carbon blocks (B- boiler, ST – steam turbine, G – generator, CND – condenser, DA – deaerator, CL – cooling steam, RH – reheater, h, i, l – stage of turbine (high, intermediate, low)

For these reference systems of supercritical carbon blocks is characterizing by high efficiency of electricity generation, the separation of CO_2 from flue gases was applied in order to lower its emission. Diagram of the installation of membrane separation and compression of CO_2 from flue gases are presented in fig.2. This system consists of membrane module (M), flue gases compressor (C), vacuum pump (VP), CO_2 compressor (C1) and heat exchangers HE1 and HE2. The aim of membrane module is to separate CO_2 flow from the flue gases (so-called permeate). The permeate is this part of the solution flue gases which penetrates the membrane. The driving force of the process is the difference of partial pressures on both sides of the membrane.

There are two essential quantities used for the assessment of the process of separating CO_2 from flue gases: the mole fraction of CO_2 in the permeate $(Y_{CO2})_P$ (purity of permeate) and carbon dioxide recovery ratio R, determining how much of CO_2 in the flue gases leaving the boiler is contained in the permeate flow; second one is expressed by the equation:

$$R = \frac{n_{5a}\left(Y_{CO_2}\right)_P}{n_{1a}\left(X_{CO_2}\right)_{1a}}, \tag{1}$$

where:
n-flux of the flue gas, kmol/s, R-carbon dioxide recovery ratio, X,Y-mole fraction.

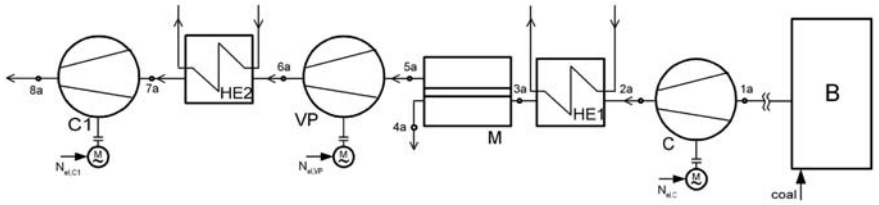

Fig.2 Diagram of the system of membrane separation and compression CO_2 from flue gases emitted by the power plant presented in Fig.1 (HE – heat exchanger, C – compressor,C1 – CO_2 compressor, VP – vacuum pump, B – boiler, M – membrane module).

Calculations concerning the membrane separation of CO_2 were carried out using Aspen software. The model of this process was developed basing on the following assumptions. The analysis was carried out in the membrane module consisting of cross-flow capillaries. The gases are considered as semi-ideals. Furthermore, constant temperature of the process at 40˚C was assumed (hence, it is necessary to use the heat exchanger HE1 which is shown in fig.2). It permitted to use the constant coefficients of permeability for the gases. It was also assumed that the flow of 900kmol/h was passing through the membrane module with a surface area of 18000 m^2. The decision variables in the calculation were the pressure of the flue gases and of the permeate [4].

For the analysis a hybrid membrane which permits the following properties i.e. the CO_2 permeability equals to 20 m^3(STP)/(m^2·h·bar) and the ideal coefficient of selectivity equals to 200 was used. The pressure of the flue gases was changed in the range 1 bar $\geq p_{2a} \geq$ 1.35 bar and the permeate pressure was changed in the range 0.005 bar $\geq p_{5a} \geq$ 0.08 bar. The pressure on the permeate side was generated by a vacuum pump and on the flue gases side by a compressor. The power rating of require components determines the energy consumption of the membrane separation process.

The power station internal load rate, including the power demand devices connected to the CO_2 separation from flue gases of reference to the power of the power plant, is mark by the symbol δ_1 and it is expressed by the equation:

$$\delta_1 = \frac{n}{\eta_{el,REF}\eta_{em}m_f \cdot LHV}\left\{\left\{T_{1a}\left(Mc_p\right)_C\left[1+\frac{\left(\frac{p_{2a}}{p_{1a}}\right)^{\frac{\kappa_C}{z_C}}-1}{\eta_{i,C}}\right]^{z_C}-1\right\}+T_{3a}\left(Mc_p\right)_{VP}X_{CO_2}\frac{R}{\left(Y_{CO_2}\right)_P}\left\{\left[1+\frac{\left(\frac{p_{6a}}{p_{5a}}\right)^{\frac{\kappa_{VP}}{z_{VP}}}-1}{\eta_{i,VP}}\right]^{z_{VP}}-1\right\}\right\}, \tag{2}$$

where:
LHV - Lower Heating Value, kJ/kg, (Mc_p) - specific molar heat capacity, kJ/kmol·K, p- pressure, bar, T - temperature, K, z - number of stages in the compressor or vacuum pump, κ - isentropic process exponent, η - efficiency, %, δ - power station internal load rate.
Index: 1a, 2a - characteristic points in the system of membrane separation (fig.2), C - compressor, VP - vacuum pump, f - fuel, el - electrical, em - electromechanical, REF - reference system

The equation (2) permits to determine what part of the power rating of the power plant is consumed during the membrane separation of CO_2 from the flue gases in relation to the assessment indices of this process e.g. carbon dioxide recovery ratio R and purity of permeate

$(Y_{CO2})_P$. The first part in the curly bracket is connected to the flue gases compression process, the second is connected to the vacuum pump.

The results of the calculations from the Aspen software are presented in figure 2. The figure presents the line of constant values of the mole fraction of CO_2 in the permeate and the line of constant values of the recovery ratio in the plane p_{2a}-p_{5a} (fig.3). This plot includes the line of constant values of the rate δ_1 which is calculated from the equation (2). For the calculation all of these isolines the algorithm of artificial networks was applied.

This figure allows to sort and to select such conditions of the process, for which value reaches δ_1 minimum and in the same time the mole fraction of CO_2 in the permeate and the carbon dioxide recovery ratio are very high.

The area in which the mole fraction of CO_2 in the permeate is greater than or equal to 0.8 and in the same time the recovery ratio is greater than or equal to 0.9 is marked in the figure.

It can be found in the literature [3,5], that for the sake of the costs of compression, transport and deposition of carbon dioxide its permeate purity $[(Y_{CO2})_P]_{limited}$ should to be contained within the range from 0.8 to 0.95, and the carbon dioxide recovery ratio (marked as $R_{limited}$) ought to be larger than 0.8 or even 0.9.

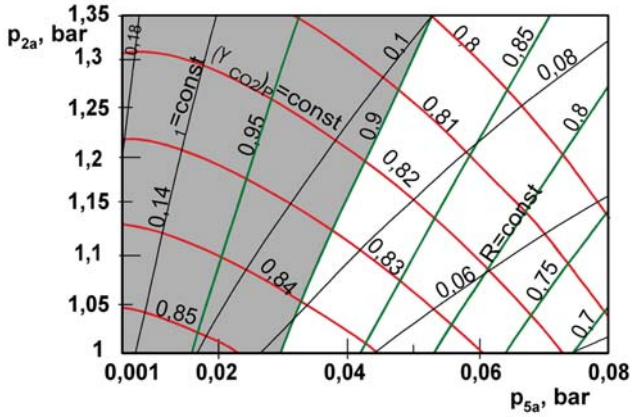

Fig.3 The line of constant values of the mole fraction CO_2 in the permeate $(Y_{CO2})_P$ = const, the recovery ratio CO_2 R = const, and the power station internal load rate δ_1 = const in the plane p_F - p_P for α^*=200 with area mark $(Y_{CO2})_P \geq 0.8$ i $R \geq 0.9$

In this area the minimum power station internal load rate δ_1 is searched for the range of value $R \geq R_{limited}$ and $(Y_{CO2})_P \geq [(Y_{CO2})_P]_{limited}$.

If assume that $(Y_{CO2})_P \geq 0.8$ and $R \geq 0.9$ and use the characteristic from fig.3 we obtain values: $(Y_{CO2})_P = 0.848$, $R = 0.9$, $p_F = 1$bar and $p_P = 0.028$bar. For such parameters the process power station internal load rate amounts to 7.51%.

It was assumed that separated carbon dioxide was subjected to atmospheric pressure and it had a high temperature. In order to transport separated CO_2, first it has to be cooled and next compressed to high pressure. Scheme of these processes is presented in fig.2. Power station internal load rate δ_2 already includes the power needed for carbon dioxide compression process.

According to the literature [4,10,12] liquefaction of CO_2 for transport needs the compression of CO_2 to pressure around 100 – 120 bar. It depends on the permeate purity. In this analysis carbon dioxide was compressed to 100 bar.

The electric power needed for the driving motor of the CO_2 compression equals to:

$$N_{elC1} = \frac{T_{7a}\left(Mc_p\right)_{C1} X_{CO_2}}{\eta_{em}} \frac{R}{\left(Y_{CO_2}\right)_P} \left\{ \left[1 + \frac{\left(\frac{p_{8a}}{p_{7a}} \right)^{\frac{\kappa_{C1}}{z_{C1}}} - 1}{\eta_{i,C1}} \right]^{z_{C1}} - 1 \right\}, \tag{3}$$

where: N - power, MW

The efficiency of electricity production in the power plant with the electric power of the motor compressors driving and vacuum pump taken into consideration cab be written as

$$\eta_{el,CCS} = \frac{N_{el,REF} - (N_{el,C} + N_{el,VP} + N_{el,C1})}{m_f \cdot LHV} = \eta_{el,REF}(1 - \delta_2), \tag{4}$$

where:

$$\delta_2 = \frac{N_{el,C} + N_{el,VP} + N_{el,C1}}{N_{el,REF}}, \tag{5}$$

and it make up power station internal load rate CCS installation.

The results of thermodynamic analysis of the influence of the CCS installation for the supercritical coal fired power plant are presented in table 1.

Tab. 1 The parameters of the devices connected to the CCS installation

Characteristic parameters	Unit	Power Plant with CO_2 capture
$N_{el,C}$	MW	0
$N_{el,VP}$	MW	45,07
$N_{el,C1}$	MW	74,07
δ_1	-	0,0751
δ_2	-	0,1981
$\eta_{el,REF}$	-	0,4878
$\eta_{el,CCS}$	-	0,3912

3. Economical analysis and the results of the calculations

In the conducted analysis of the economical effectiveness the net present value (NPV) method was used. NPV is one of the fundamental and most frequently applied economic coefficients for the assessment of the economical effectiveness of the investments. It can be described by the equation:

$$NPV = \sum_{\tau=1}^{N} \frac{CF_\tau}{(1+r)^\tau}, \tag{6}$$

The value of the discount rate was assumed at 6,2%. In order to determine the cash flow CF_τ the total investment costs (J), profits from sales (S_{el}), overall costs of production (K_{PR}), the income tax (P_d), changes of the working capital (K_{obr}), amortization charges (A), interest (F) and clearance value of the designed installation (L) $\left(L,\ L_\tau = 0\ when\ 0 \le \tau \le N-1\right)$had to be known.

Thus, the equation describing the cash flow CF_τ can be written as:

$$CF_\tau = \left[-J + S_{el} - \left(K_{PR} + P_d + K_{obr}\right) + A + F + L \right]_\tau, \tag{7}$$

The investment costs in signified analysis are given by equation:

$$J = i_N \cdot N_{el} + i_{CCS} \cdot N_{el}, \tag{8}$$

where: i_N – unit investment cost for the power installation, €/kW, i_{CCS} – unit investment costs for the CCS installation, €/kW.

The essential component of the equation (7) is the profit from sales, expressed as:

$$S_{el} = \int_0^{\tau_{el}} N_{el} \cdot C_{el} \cdot d\tau_{el} \ , \tag{9}$$

where: C_{el} – average price of electricity, € /MWh, τ_{el} – the annual time of operation, h.

Total costs of production were determined as a sum of the following costs:

$$K_{PR} = K_F + K_o + K_{ps} + K_E + K_{sr} + K_r + A_k + A + F \ , \tag{10}$$

where: K_F – cost of fuel, K_o – cost of services, K_{ps} – cost of other raw materials, K_E – other operating costs, K_{sr} – environmental costs, K_r – costs of maintenance and exploitation, A_k – excise duty, A – amortization costs, F –interest.

The economic analysis were made for the reference system and also for similar power unit, taking into account the investments and costs connected to the CO_2 capture installation. For the system with CO_2 separation previously calculated values permeate purity $(Y_{CO2})_P = 0.848$ and carbon dioxide recovery ratio R = 0.9 were assumed.

Exemplary literature data [1,4,5,9,11] for different supercritical power stations taking into account the cost for CO_2 separation were served to determine the investment costs.

For the economic analysis the investment costs were assumed at 1100 €/kW for the reference system and at 1450 €/kW for the power plant with CO_2 capture. In the calculations, operating costs of capture installation were assumed at 3 €/MWh. The annual time of operation was 8000 hours. Amortization rate was given at 6.67 %. The constant of repairs was determined at the level of 0.5% of the capital costs for the first ten years of operation and 1% for the following ten years. It has been assumed that the investment cost are spread into three years of the construction: 15% in the first year, 30% in the second year and 55% in the third year. It has been also assumed that the conduction of the power generating plant is financed in 15% by own means and in 75% by the commercial credit at the interest of 6%. The credit is assumed to be repaid in equal payments in the course of ten years. The income tax rate was assumed at 19%. Excise duty was assumed at 5 €/MWh and the average cost of fuel was 55 €/Mg. The residual clearance value of the designed system is assumed at $20\% \cdot J$, and the working capital as equal to zero.

In the economic analysis the limit sale price of electricity C^{gr} was calculated. For the reference systems without CO_2 capture it was described by the index REF and for the power plant with carbon capture installation it was described by the index CCS.

For both systems the limit sale price of electricity is a quantity determined by the condition

$$NPV(C^{gr}) = 0 \ , \tag{11}$$

An important economic rate for the power system with CO_2 capture is also the CO_2 emission avoided (E_{AV}) and its cost. The cost of CO_2 emission avoidance (C_{AV}) is calculated according the equation:

$$C_{AV} = \frac{C_{CCS}^{gr} - C_{REF}^{gr}}{E_{AV}} \ , \tag{12}$$

where:

$$E_{AV} = E_{REF} - E_{CCS} \ , \tag{13}$$

E –CO_2 emission, index: REF – reference system, CCS – plant with CO_2 capture.

The results of the economic analysis are presented in table 2. The analysis of susceptibility were also performed. The influence of the investment costs and the fuel cost were tested. The results of the susceptibility analysis are presented in figures (fig.4 i fig.5).

Tab. 2 Results of the economic analysis calculation

	Unit	**Value**
Annual operating time	h	8000
Unit sale price of electricity C_{REF}^{gr}	€/MWh	37.86

Emission CO_2 (E_{REF})	kg/MWh	726
Unit sale price of electricity after CO_2 separation C_{CCS}^{gr}	€/MWh	56.91
CO_2 emission after separation (E_{CCS})	kg/MWh	73
CO_2 emission avoided (E_{AV})	kg/MWh	653
Costs of CO_2 avoiding emission C_{AV}	€/MgCO_2	29.18

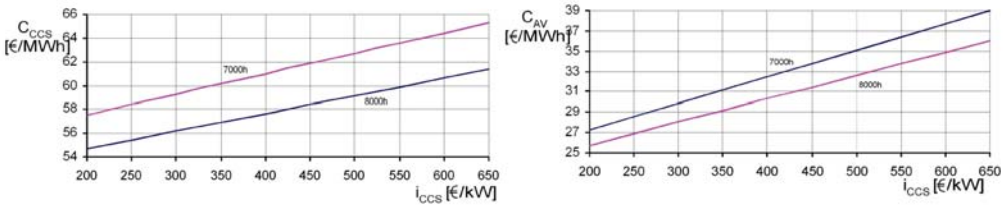

Fig.4 The influence of the investment costs of the CCS installation on the limit sale price of the electricity and on the cost of CO_2 avoided emission

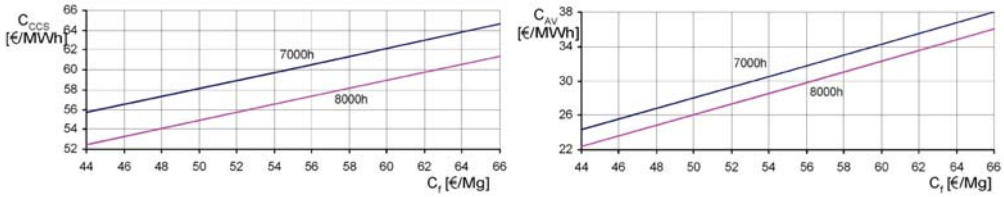

Fig.5 The influence of the fuel costs of the limit sale price of electricity and on the cost of CO_2 avoided emission for the investment costs at 1450 €/kW

The susceptibility analysis ware carried out. The analysis showed that the costs of CO_2 avoiding emissions decrease with decreasing the investment cost. The cost of fuel has an important influence on the price of electricity.

In the susceptibility analysis costs of fuel ware tested. The price of fuel was changed by 20% from considered value. A change of fuel price has an influence the change of the limit sale price of electricity by around 4 € for and above 6 € on the costs of CO_2 avoided emissions.

4. Conclusions

The paper presents the relations between the energy consumption of the membrane separation of CO_2 from the flue gases and the recovery ratio and mole fraction of CO_2 in the permeate as well as the pressure of the flue gases and the pressure of the permeate. The power rating losses and the efficiency of the power plant were determined for both processes – CO_2 separation and compression. In order to decreases power and efficiency of electricity we integrated CCS installation with supercritical coal power plant.

The power rating of installations connected to the CO_2 separation equals to 7.51% of the power station power. As a result the efficiency of the power plant decreases from 48.78% to 45.02%. Take into consideration the influence of CO_2 compression the power station internal load rate is equal to 19.81 % and the efficiency of electricity production decreases to 39.12 %.

In order to decrease heat losses the heat coming from the flue gases and the permeate cooling may be used in the reference system of the steam-water system steam turbine. It makes possible to partly eliminate the steam bleeding. Elimination of the steam bleeding causes an increase of the steam flow to the steam turbine and increases the power. The efficiency of the electricity production is growing in the reference system.

The economic analysis was calculated for the reference system and also for power unit, taking into account the investments and the costs connected to the CO_2 capture installation. In this

analysis the limit sale price of electricity and costs of CO_2 avoided emissions was calculated. This investment is profitable when the limit sale price of electricity equals to 56.91 €/MWh or purchase price of CO_2 permission exceed value of 29.18 €/MgCO_2.

In the susceptibility analysis of the investment costs, price of fuel and annual operating time was tested. The cost of electricity generation decreases with longer annual operating time and also when the investment costs decrease. When the CCS installation investment costs increase to 650 €/kW the price of electricity increase about 4,5 – 5 €. However, the costs of CO_2 avoided emissions increase about 7 – 8 €. The fuel price has an influence of about 4 € on the price of electricity and of above 6 € on costs of CO_2 avoided emissions.

Acknowledgements

The investigations presented in this paper have been carried out within the frame of the research project No. PBZ-MEiN-4/2/2006.

References

[1] Borowiecki T., Kijeński J., Machnikowski J., Ściążko M. *Czysta energia, produkty chemiczne i paliwa z węgla – ocena potencjału rozwojowego*, Wyd. Instytutu Chemicznej Przeróbki Węgla, Zabrze 2008.
[2] Chmielniak T, *Nadkrytyczne bloki węglowe*, PBZ – MEiN – 4/2/2006.
[3] Davidson J., Thambimuthu K., *Technologies for capture of carbon dioxide*, Proceedings of the Seventh Greenhouse Gas Technology Conference, Vancouver, Canada, International Energy Association (IEA), Greenhouse Gas R&D Programme, 2004.
[4] Davison J., *Perfrmance and cost of power plants with capture and storage of CO_2*, Energy 2007; 32, pp. 1163 – 1176.
[5] Kaldis S.P., Skodras G., Sakellarepoula G.P., *Energy and capital cost analysis of CO_2 capture in coal IGCC processes via gas separatin membranes*, Fuel Processing Technology 2004; 85 pp. 337 – 346.
[6] Kotowicz J., Chmielniak T., Janusz-Szymańska K., *The influence of membrane separation on the efficiency of a coal fired power plant*, Proceedings of the 21st International Conference ECOS 2008, Kraków-Gliwice 24-27 June 2008, vol.IV pp. 1739-1746.
[7] Kotowicz J., Janusz K., *Manners of the reduction of the emission CO_2 from energetic processes*, Rynek Energii 2007; 1 (68) pp. 10 – 18 (in Polish).
[8] Kotowicz J., Janusz K., *The basic of membranes gas separation*, Rynek Energii 2007; 6 (73) pp. 29 – 35 (in Polish).
[9] Romeo L.M., Abanades J.C., Escosa J.M., Pańo J., Giménez A., Sánchez-Biezma A., Ballesteros J.C., *Oxyfuel carbonation/calcination cycle for low cost CO_2 capture in existing power plants*, Energy Conversion and Management 49 (2008) pp. 2809–2814.
[10] Romeo L.M., Espatolero S., Bolea I., *Designing a supercritical steam cycle to integrate the energy requirements of CO_2 amine scrubbing*, Greenhouse Gas Control 2 (2008) pp. 563–570.
[11] Tchórz J., *Południowy Koncern Energetyczny S.A. Czyste Technologie Węglowe*, Konferencja „Czyste Technologie Węglowe CCTPROM", Pszczyna 13-15.09.2007.
[12] Zhao L., Riensche E., Menzer R., Blum L., Stolten D., *A parametric study of CO_2/N_2 gas separation membrane processes for post – combustion capture,* Journal of Membrane Science 325 (2008) pp. 284–294.

Journal of POLISH CIMAC

Faculty of Ocean Engineering & Ship Technology
GDAŃSK UNIVERSITY OF TECHNOLOGY

ASSESSMENT OF REAL ACTIVE POWER LOAD OF MARINE GENERATING SETS IN OPERATIONAL CONDITIONS OF CONTAINER VESSELS

Zbigniew Matuszak, Grzegorz Nicewicz

Maritime Academy of Szczecin
ul. Wały Chrobrego 1-2, 70-500 Szczecin, Poland
tel.: +48 91 4809414, +48 91 4809442
e-mail: zbimat@am.szczecin.pl, nicze1@wp.pl

Abstract

As far as marine generating sets driven by diesel engines are concerned, it is assumed that the optimal active power load ranges between 70 – 90% [9]. At the same time there is no unequivocal way of assuming the value of the auxiliary engine excess power factor in relation to the generator's rated active power regarded as the rated power of the set [3, 9, 10]. According to the outcome of the authors' research carried out on contemporary transport vessels, the factor ranges within 1,05 – 1,62. In operational conditions, even at low values of excess power factor, the contribution of generating set working time at load 70 – 90% appears relatively short, which has been discussed in [10]. Eventually, the process of deterioration of auxiliary engines technical condition due to their long lasting operation at low loads gets accelerated and the operation turns out economically unprofitable due to the increase in specific fuel consumption. The paper deals with broader spectrum of individual generating sets' active power load on contemporary transport vessels based on long – standing identification tests of marine electric power system loads.

Keywords: *marine generating set, auxiliary engine, active power load*

1. Introduction

Electric power system load identification tests have been carried out on various types of contemporary transport vessels, e.g. container and semi - container ships, bulk carriers and general cargo vessels. Mainly, the value of active power peak loads at fixed time intervals, allowing for setting the boundary conditions of the systems' operation, has been focused on. The tests' methodology has been discussed in [11, 12]. The obtained results enable the assessment of the generated power of the marine electric power system and individual generating sets in operational conditions. According to the literature [2, 9], considering the optimal operational conditions of auxiliary engines, the assumed active power load of generating sets driven by diesel engines should range between 70 – 90% of their rated power. The tests proves that in practice such load value of generating sets occur relatively short when taking into account their total operational time. Therefore, in order to adjust the number of power generating sets in the marine power station and their excess power factor, it appears relevant to estimate the peak load distributions of contemporary operated power generation sets. Due to the paper space limit, mainly the character of generating sets' (GS) active power load of contemporary container vessels has been focused upon. They frequently turn out to be equipped with thrusters and capable of carrying vast numbers of reefer containers, where the demanded power may be compared to the power of a single

generating set [13]. The tests outcome concerning other types of transport ships have been broadly discussed in the following works [2, 5, 6, 7].

The subject of the tests have been six container ships of various capacity: 7500 TEU, 7500 TEU, 5500 TEU, 3050 TEU, 2200 TEU and 1100 TEU equipped with certain fixed number of sockets to connect reefer containers. To ease the analysis the container ships have been marked with Roman numbers from I to VI. The marine power stations of I, II, IV and V consist of four generating sets, III contains three generating sets and a shaft generator and VI is equipped with two generating sets and a shaft generator. The vessels I, II, III, IV and V are supplied with thrusters, whereas VI is equipped with emergency electric drive.

2. Active power load of marine generating sets

For the analysis of the active power load of the marine generating sets the data on peak loads of the sets at the consecutive hours of the operation have been used. In case of IV, a 3050 TEU container vessel, the data on 24 hour peak loads have been made use of. In fig. 1 box-and-whisker plots of the obtained empirical distributions of the generating set loads have been shown; presenting the measures of location, dispersion and asymmetry of the distributions [14, 15]. The symbol of the generating set in fig. 1 consists of the ship's mark on which it was installed and its number it has been assigned on the vessel.

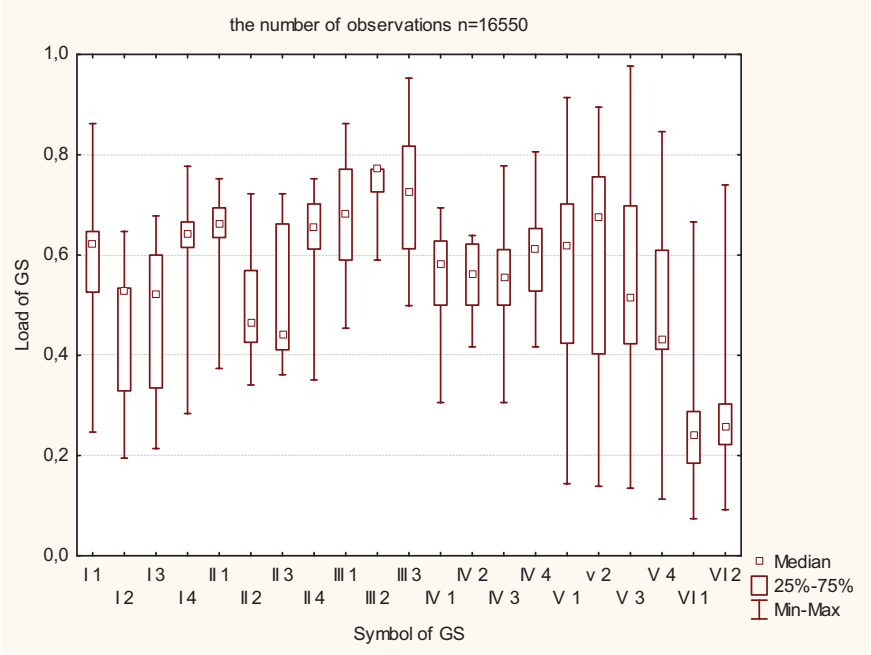

Fig. 1. Box-and-whisker plots of the generating sets' peak loads distributions from the tested container vessels

The location of the empirical distribution medians (in fig. 1) clearly shows that for over 50% of the time of operation most of the generating sets of the container vessels, the subject of the tests, (except of GS III 2 and III 3), their peak load turns out lower than 70%, which means that it is lower than the lower limit of the optimal load range. Only for 8 out of 21 analyzed generating sets the values of the recorded peak loads exceeded 80%.

Differences between peak loads distributions of particular generating sets installed on a vessel (if they are identical) come first of all from operational strategy accepted by the engine crew or ship owner technical services. Therefore, the data on peak loads in case of identical sets on

individual vessels have been aggregated for the sake of a more general approach to the analysis outcome. In this way there have been constructed box-and-whisker plots of marine generating sets' peak loads distributions, shown in fig. 2. In case of vessels equipped with not identical power generating sets, they have been marked respectively with capital letters in the alphabetical order.

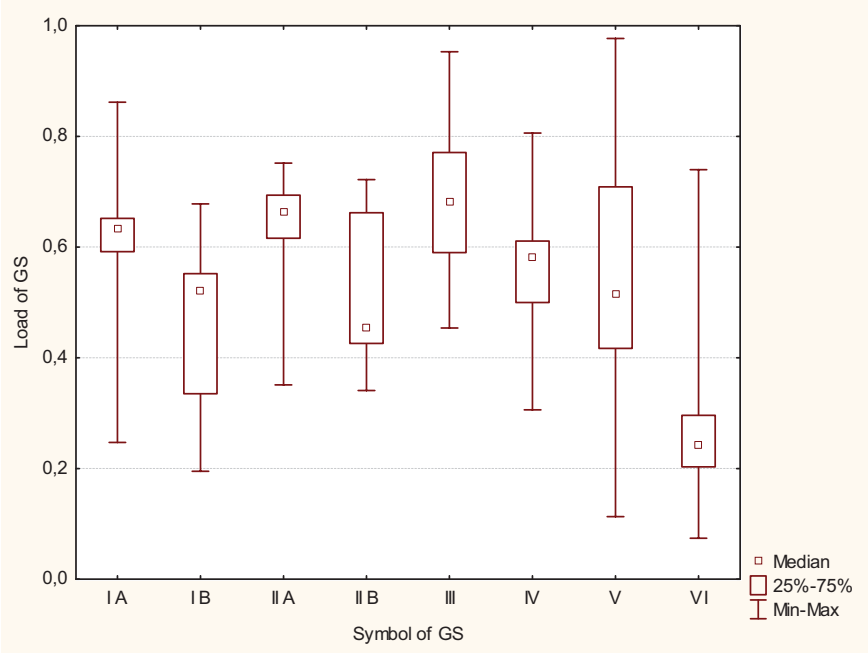

Fig. 2. Box-and-whisker plots of peak loads distributions of generating sets of the tested container ships for the aggregated data

The location of the medians of the obtained peak loads distributions for the generating sets I A, II A and III for the aggregated data (fig. 2) proves that for half of the operational time their hourly peak loads exceeded 60% of the set's rated active power. The median highest value has been recorded for generating sets installed on 5500 TEU container ship (III). As a rule, the peak loads of values higher than 70% do not occur more frequently than for 25% of the generating sets' operational time. An exception to that appear the data obtained for the generating sets of the container ship III, where the peak loads of values beyond 70% occurred for almost half of the time of operation.

3. The characteristic of the obtained empirical distributions of the generating sets' peak loads

The obtained peak loads empirical distributions of the container vessel generating sets are characterized for their asymmetry and they differ from the normal distribution, which is confirmed by the results of the statistical tests made by means of *STATISTICA 8.0* (there have been carried out the Shapiro-Wilk test if the sample number $n < 2000$, the Lilliefors and chi-square tests if the sample number $n > 2000$ as well as the normal probability plots have been computed). Some of the obtained distributions are known for their multi-modality. The example of the obtained results for the generating sets of 7500 TEU and 2200 TEU (I and V) container ships have been shown in fig. 3 and 4.

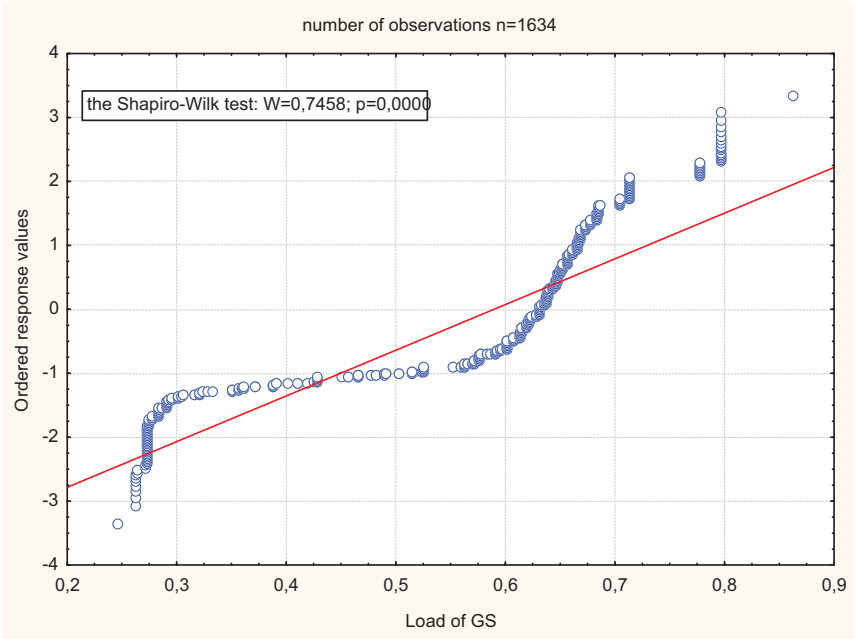

Fig. 3. Normal probability plot and the results of the Shapiro-Wilk test for the generating sets' peak loads of 7500 TEU container ship (I A)

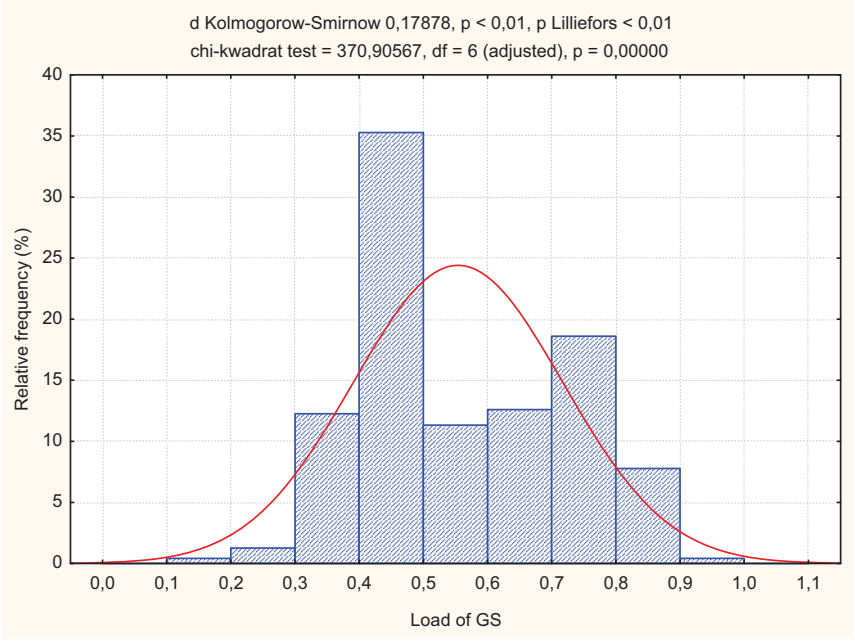

Fig. 4. Histogram of generating sets' peak loads of 2200 TEU container vessel (V) and the plotted probability density function of normal distribution (solid line) with the tests of goodness of fit results inserted

The character of the obtained empirical data on peak loads of the container vessels' generating sets does not allow for the estimation of the probability density functions of empirical distributions due to such tools like the program *STATISTICA 8.0* by means of well known functions of relatively simple theoretical distributions like normal, gamma, log-normal or exponential. The differences between the assumed models and the empirical distributions were statistically significant. The problem of estimating the probability density functions of empirical distributions of container ships' generating sets peak loads may be solved by the application of the so called distribution compositions (mixtures of distributions); however, it appears a dull, time consuming method and would go beyond the frames of the paper.

4. Final remarks

The presented analysis of the six container ships' generating sets peak loads (fig. 2) shows that only three (I A, II A, III) out of eight generating sets installed, for half of the time show hourly peak loads higher than 60%. The position of the lower quartiles (fig. 2) in case of the six types of generating sets (I A, II A, II B, III, IV, V) occurs above 40% of the sets' rated active power, thus, for 75% of the operational time the peak loads appear higher than this value. The least economic turns out the load of the generating sets of the 1100 TEU container vessel (VI).

The obtained empirical load distributions of the generating sets appear characteristic for their asymmetry and multi-modality. They considerably differ from the theoretical normal distribution. The applied test of goodness of fit for models in the form of other simple theoretical distributions like gamma, log-normal or exponential have not turned out the right ones to describe empirical distributions.

The collected statistical data on the peak loads values of the generating sets originate from container ships of various technical parameters; this refers also to the marine electric power systems and generating sets. Therefore, the hypothesis, that they belong to the same population, or in other words, that they can be treated as the realization of the same random sample, needs to be verified. Only such verification, on the basis of all the collected statistical material, enables to describe the general peak loads' value distribution of the considered container vessels' generating sets. For that purpose the Kruskal-Wallis test was applied because of the fact that the peak loads values distributions of the particular types of generating sets do not comply with the normal distribution [14, 15]. The test's detailed structure has been dealt with in [8]. The hypothesis verification has been carried out by means of the statistical package *STATISTICA 8.0*. The results have been presented in the table of the program *STATISTICA 8.0*; shown in fig. 5.

	The Kruskal-Wallis test: H (7, N=16550) = 11439,69; p =0,000	
Symbol of GS	N - total number of observation	Rank sum
I A	1634	18599489
I B	686	5942242
II A	2838	36324180
II B	908	9148490
III	1487	20356588
IV	234	2466567
V	1182	12902221
VI	7581	31219749

Fig. 5. The Kruskal-Wallis test results presented in the table of STATISTICA 8.0; N – total number of observations, 7 – number of degrees of freedom of the asymptotic distribution χ^2 of the statistic H, H – the value of the Kruskal-Wallis test statistic, p – p-value

The computed *p*-value proves that there are no bases for accepting the hypothesis of the data on peak loads values of particular types of the container ships' generating sets , in question, coming from the same general population at the assumed significance level α=0,05.

References

[1] Chybowski, L., Kijewska, M., Nicewicz, G., *Analiza obciążeń autonomicznych urządzeń prądotwórczych systemów energetycznych obiektów pływających.* II Międzynarodowa Konferencja Naukowa Systemy Wspomagania w Zarządzaniu Środowiskiem, Ekonomika i Organizacja Przedsiębiorstwa Rok LVI Nr 7 (666) Lipiec 2005, Słowacja, Zuberec 2005.

[2] Cichy, M., Kowalski, Z., Maksimow, J.I., Roszczyk, S., *Statyczne i dynamiczne własności okrętowych zespołów prądotwórczych*. Wydawnictwo Morskie, Gdańsk 1976.

[3] Figwer, J., *Zagadnienie wielkości mocy silnika napędowego w okrętowych zespołach prądotwórczych*. Budownictwo Okrętowe Nr 6, 1962.

[4] Kijewska, M., Matuszak, Z., Nicewicz, G., *Identyfikacja obciążeń systemu elektroenergetycznego siłowni okrętowych w rzeczywistych warunkach eksploatacyjnych*. SYSTEMS Journal of Transdisciplinary Systems Science Vol. 11 2006, pp. 334-340.

[5] Kijewska, M., Nicewicz, G., *Analiza rozkładu obciążeń zespołów prądotwórczych elektrowni okrętowej statku transportowego dla wybranego stanu eksploatacyjnego*. Надежность и Эффективность Технических Систем. Международный Сборник Научных Трудов, KGTU, Kaliningrad 2004, pp. 64-72.

[6] Kijewska M., Nicewicz G., *Estymacja gęstości rozkładu obciążeń zespołów prądotwórczych elektrowni okrętowej w wybranym stanie eksploatacji*. Zeszyty Naukowe Politechniki Gdańskiej nr 598 (seria: Budownictwo Okrętowe Nr LXV), Gdańsk 2004, pp. 79-87.

[7] Kijewska M., Nicewicz G., *Rozkłady empiryczne a rozkłady teoretyczne obciążeń autonomicznych zespołów prądotwórczych elektrowni okrętowych*. Надежность и Эффективность Технических Систем. Международный Сборник Научных Трудов, KGTU, Kaliningrad 2005, pp. 124-131.

[8] Kruskal W.H., Wallis W.A., *Use of Ranks in One-Criterion Variance Analysis*. Journal of the American Statistical Association, Vol. 47, No. 260. (Dec., 1952), pp. 583-621.

[9] Kuropatwiński, S., Lipski, T., Roszczyk, S., Wierzejski, M., *Elektroenergetyczne układy okrętowe*. Wydawnictwo Morskie, Gdańsk 1972.

[10] Matuszak, Z., Nicewicz, G., *Assessment of excess power factor in marine generating sets*. Journal of POLISH CIMAC – ENERGETIC ASPECTS, Vol. 3, No. 1, Gdańsk 2008, pp. 95-101.

[11] Matuszak, Z., Nicewicz, G., *Assessment of hitherto existing identification tests of marine electric power systems loads*. Polish Journal of Environmental Studies, Vol. 18, No. 2A, Olsztyn 2009, pp. 110-116.

[12] Matuszak, Z., Nicewicz, G., *Wykorzystanie szeregów czasowych do analizy obciążeń izolowanych systemów elektroenergetycznych*. Systemy Wspomagania w Zarządzaniu Środowiskiem – Monografia pod redakcją J. Kaźmierczaka, Zabrze 2008, pp. 185-191.

[13] Nicewicz G., *Obciążenie okrętowego systemu elektroenergetycznego a bezpieczeństwo statku*. Zeszyty Naukowe AMW im. Bohaterów Westerplatte Nr 168 K/1, X Konferencja Morska „Aspekty bezpieczeństwa nawodnego i podwodnego oraz lotów nad morzem", Gdynia 2007, pp. 205-215.

[14] Stanisz, A., *Przystępny kurs statystyki*. *Tom 1*. *Statystyki podstawowe*. StatSoft, Kraków 2006.

[15] StatSoft - *STATISTICA 8.0*., *Podręcznik elektroniczny STATISTICA*.

Journal of POLISH CIMAC
Faculty of Ocean Engineering & Ship Technology
GDAŃSK UNIVERSITY OF TECHNOLOGY

THE INFLUENCE OF OXYGEN DISSOLVED IN THE DIESEL FUEL ON THE COMBUSTION PROCESS AND MUTUAL CORELATION BETWEEN NITROGEN OXIDE AND EXHAUST GAS OPACITY

Jerzy Merkisz, Jarosław Markowski, Władysław Kozak, Jacek Mądry

Poznan University of Technology
ul. Piotrowo 3, 60-965 Poznań, Poland
e-mail: jaroslaw.markowski@put.poznan.pl

Abstract

The paper presents a concept of improving the injection and spraying processes with the use of the oxygen dissolved in the diesel fuel and the results of experimental investigations carried out in order to verify it.
The combustion process of the direct injection compression-ignition engine being normally performed at a high excess of combustion air factor for the whole engine operation range is affected by local deficiencies of oxygen inside the fuel sprays in a combustion chamber. This fact is one of the main reasons for forming the harmful compounds in exhaust gases such as NO_x and PM.

The aim of the presented concept is to improve the fuel spray atomization by the release of the oxygen previously dissolved in the fuel. The influence of dissolving the oxygen in the diesel fuel on the run of the combustion process and concentration toxic compounds in exhaust gas has been presented in the paper.

Keywords: *spraying processes, combustion process, emission, fuel solution*

1. Introduction

The specificity of the combustion process being realized in the direct injection compression ignition engine (CI) consist in a fact that the liquid fuel in a form of fuel sprays is supplied to the engine combustion chamber right before the piston top dead centre (TDC). Thus a complete process of preparing the mixture for being burnt, i.e. a disintegration of the fuel spray into drops, their evaporation and mixing with air needs to be performed in a very short time. For such a way of fuelling the engine some local and very significant differences of the excess air factor values λ are met (fig. 1). The values met in the combustion chamber range from the infinite high one in the area which is not covered by the fuel spray, throughout $\lambda \approx 0.8 \div 1.5$ at the edges of the fuel spray initializing the ignition to $\lambda \approx 0$ being recorded in the spray core. The local deficiencies of oxygen occur despite the high value of the global excess of air the value of which changes with the engine load and ranges from $\lambda \approx 11$ at the engine idle running to $\lambda \approx 1.4 \div 1.3$ at the engine full load, i.e. for the operating conditions corresponding to the outer engine operating characteristic.

In case of the combustion process the local deficiencies of oxygen are one of the most important reasons for forming carbon oxides, hydrocarbons, and partly of forming the particulate matter, whereas the formation of nitrogen oxides is mainly connected with the kinetics of developing the flame which generates the value of the produced heat as the heat delivery speed determines the level of temperature in a combustion chamber. All of it causes that the fuel

spraying, in addition to the air swirl, is of the decisive importance for preparing the mixture. The quality of spraying is determined by two basic physical factors: the pressure existing in the nozzle area right before the nozzle whole and the pressure in the combustion chamber where the fuel spray is directed to. An increase in the injection pressure values improves the fuel spraying and it is a current preferred tendency of the developments of the injection systems for the CI engines. The changes which are done in the Common Rail (CR) system confirm the above statement. Every next generation of this system is characterized by the injection pressure values that are higher that ones of the previously generation.

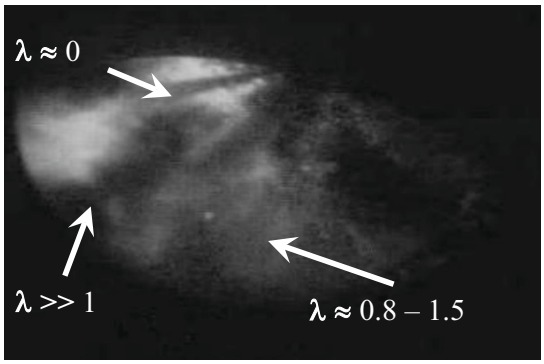

Fig. 1. The combustion process in the combustion chamber of a direct injection compression ignition engine

The improvement of the fuel spraying can be achieved not only by increasing the injection pressure but also by modifications to the mechanism causing the disintegration of the fuel spray. The velocity of the fuel outflow from the nozzle is a single physical stimulus which causes the disintegration of fuel spray in the currently used mechanism of spraying. In order to achieve the improvement of spraying it is proposed to use in the discussed mechanism an additional physical stimulus resulting from the physical properties of the gas-in liquid solution [1, 2, 5, 6]. The amount of gas that can be dissolved in a liquid significantly depends on the pressure. A spontaneous release of gas at the non-equilibrium state caused by the pressure fuel is very characteristic for such a solution. The process of releasing the gas from a liquid is of a volumetric nature, i.e. the gas is being released simultaneously from the whole liquid volume. The energetic effects which accompany that process depend on the speed of the stimulus modifications and the gas which is released always presents a tendency to break the bonds of liquid molecules. Under such conditions the state of liquid is similar to that state of boiling. The presented properties of a liquid are very desirable in the injection system of the diesel engine. Thus a concept of using the effect accompanying the process of releasing the gas from a liquid for improving the existing mechanism of fuel oil spraying has been developed.

This concept consists in adding the appropriate amount of air to the fuel, its dissolving under high pressure conditions (in a high pressure pump) and keeping it in a form of solution in a high-pressure section of the engine supply system (up to the nozzle) until the moment of injection, occurs as shown in fig. 2. In this case the assumed injection pressure determines the energetic solution level at which the equilibrium state is achieved.

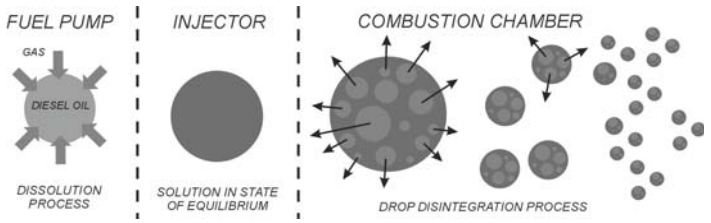

Fig. 2. The illustration of a concept of the spraying improvement by gas dissolved in fuel [1]

The use of the effect accompanying the process of releasing the air dissolved in the fuel oil occurs in the combustion chamber area when, due to a sudden pressure drop a serious disturbance of an equilibrium state occurs in a solution. The pressure drop from the injection pressure level to the pressure level existing in the surroundings of the fuel stream occurs at the moment of the injection beginning. A detailed description of this concept is presented in [1].

2. Test stand

The tests were carried out on the engine test stand equipped with the direct injection compression-ignition test engine AVL 5804. This is an one-cylinder engine equipped with a four-valve cylinder head and two camshafts. The injector is situated in the cylinder head centrally in the cylinder axis. The engine was equipped with a conceptual supply system of a Common Rail type controlled by a SesubCR system – i.e. a system specially developed for electronic controlling the Common Rail unit. The test stand was equipped with a brake provided for realization of the set value of the engine crankshaft speed regardless of the engine load. The test stand also included the lubricating oil and cooling fluid temperature stabilization systems.

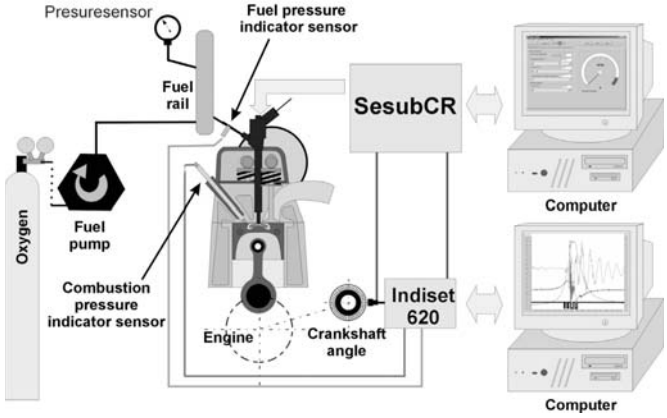

Fig. 3. The test stand

The fuel was supplied to the engine by an accumulator supply system including a supply pump with an independent drive unit. The fuel compressed in the pump was pumped (forced) to an accumulator (a container) called a pressure accumulator from which it was delivered to the BOSCH 0445 110 131 injector. Its work was controlled by the SesubCR system. The relevant injection parameters i.e. the injection commencement angle and injection duration time were set by a computer using a program for the SesubCR system. In order to perform a correct analysis of the changes in the engine operation parameters it was necessary to complete the information on the cylinder pressure characteristics, the cylinder pressure characteristics just before the injector and also on the characteristics of the pulses controlling the injector operation as a function of the crank angle. For those reasons the engine was equipped with a piezoelectric sensor of the indicated pressure situated in the engine cylinder head just before the injector directly on the injection pipe connecting the injector with the accumulator. The voltage pulses generated by those sensors, after their amplification, and the signal from pulses controlling the work of the injector as well, were sent to the Indiset 620 system provided for recording the quick changing engine processes given in the voltage form. For the comparative nature of the performed examinations it was necessary to use two supply pumps, the conventional one, which compresses the diesel oil only, and the second one which makes the gas-in-fuel dissolving possible while it is being pumped (forced) (fig. 4).

During the examinations the tonnage oxygen taken out from the high pressure oxygen cylinder with use of the pressure reducing valve was used as a gas to be dissolved in fuel. Oxygen at the pressure value of 1 bar was supplied to the forcing section area of the pump through a non-return valve during the piston moving downwards (fig. 4a). As soon as the piston reveals the lower passage the gas supplying valve closes and the diesel oil supplying to the fuel forcing section starts (fig. 4b). As soon as the piston moving upwards closes the passage supplying the fuel the compression of the oxygen and diesel oil in the forcing section starts, during which a gas-in-oil dissolving process occurs. The liquid solution obtained in this way is pumped (forced) to the fuel accumulator (fig. 4c). From the fuel accumulator it is supplied to the injector, and next to the combustion chamber of the DI engine. Considering the specificity of examinations the relevant methodology of their performing had to be developed.

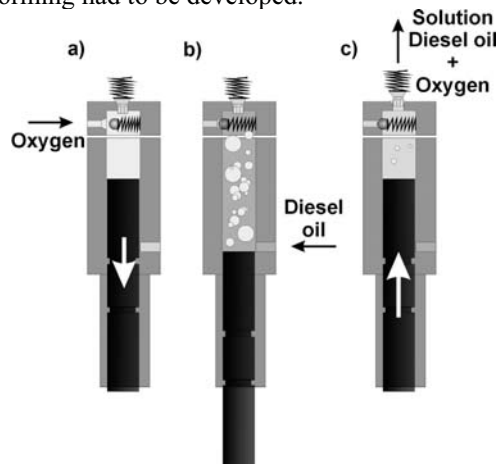

Fig. 4. The realization of the gas-in-diesel oil dissolving process

3. Examination procedure

The examination was of a comparative nature so it was carried out in two stages. In the first stage the engine was fuelled with diesel oil and the injection parameters were set as follows:
- the simulated engine speed : 2000 rpm;
- the fuel pressure in rail: 40 MPa;
- the duration time of electric pulse opening the injector: 0.55; 0.65; 0.75; 0.87; 0.98 ms.

In the second research stage the engine was fuelled with diesel oil -and-dissolved oxygen at the same settings of the above injection parameters and the oxygen pressure value in pump: 1 bar.
During the examinations some measurements of the toxic exhaust gas compounds were performed. In each of the set engine operating points the cylinder indicated pressure values, fuel in the injection pipe before the injector, and characteristics of the intensity of the injector opening current values were additionally measured. Those measurements allowed to estimate the similarity of the parameters of the fuel injection realized in each stage of the performed examinations. The obtained parameters were subject to the mutual comparative analysis.

4. Test results and discussion

The evaluation of the discussed conception will be made on the basis of the comparative analysis performed for two groups of values. The first group includes the cylinder pressure value and the rate of the cylinder pressure rise. These quantities are closely connected with the combustion process kinetics. The second group includes the basic components of exhaust gas, the emission of which is subject to the limitation. They are: nitrogen oxides NO_x, and exhaust gas smoke.

Having realized their research program the authors have gathered some very extensive comparative material which one cannot help fully presenting here. In this paper only some exemplary results are presented on a basis of which the tendencies of the influence of oxygen content in the fuel on the engine operation, that is observed in the whole research range, can be shown. These results are presented in a graphic form.

The nature of the influence of the release of oxygen dissolved in a fuel on the cylinder pressure Pc characteristic during the combustion process is shown on an example of a single point of work of the engine. This influence is presented directly on the pressure characteristic as shown in fig. 5. In this figure the characteristic of fuel pressure in the high pressure rail Pr and the characteristic of a signal t controlling the opening are additionally plotted. At introducing the fuel solution and increasing the mass of the oxygen dissolved in it a clear tendency to shorten compression-ignition delay appears. The character of changes values, as one emphasized in fig. 6, recurred for all examined engine operating conditions.

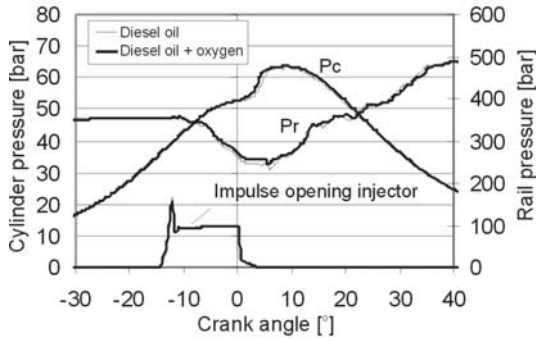

Fig. 5. Cylinder pressure of engine supply with diesel fuel and diesel fuel with dissolved oxygen; n = 2000 rpm, Pw = 35 MPa, t = 1,21 ms

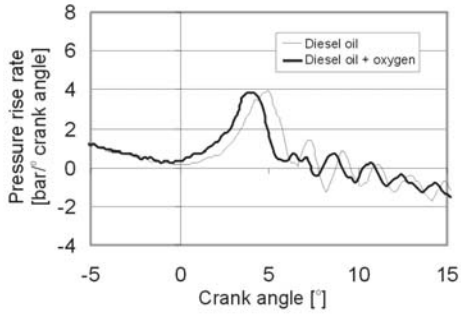

Fig. 6. Pressure rise rate as function of crank angle; n = 2000 rpm, Pw = 35 MPa, t = 1,21 ms

The discussed character of changes is closely connected with the compression-ignition delay angle. After adding the oxygen to the fuel a compression ignition delay angle is subject to a significant shortening in comparison to one noted at supplying with fuel without oxygen. This shortening depends on the amount of the oxygen dissolved in a fuel and, what should be considered as obvious, on the location of the engine operation point on the general engine characteristic. Increasing the amount of the dissolved oxygen shortens the time of the compression ignition delay.

The decrease in the pressure rise rate which is distinctly seen in the combustion chamber should be also explained by a shortened compression ignition delay angle. The tendency of such association is also unambiguous: an increase in the amount of the dissolved oxygen results in the lower rate of the pressure rise. In case of delivering the oxygen under the pressure of 1 bar the maximum rate of the pressure rise was noticeable decreased.

The results of the toxic exhaust gas compound emission measurements obtained for the individual engine operation points during the fuelling the engine with diesel oil containing the dissolved oxygen were compared with the emission values obtained for the engine fuelled with a conventional diesel oil (table 1).

The relative changes in the concentration values obtained for the individual compounds are given in figure 7. The concentration values for the individual compounds in each operating point for the engine fuelled with the conventional diesel oil were assumed as a 100% concentration value for a given compound of the exhaust gas emission. The concentration values obtained for the engine fuelled with the diesel oil and dissolved oxygen were referred to that value.

Table 1. The concentration values for the selected exhaust gas components (engine speed 2000 rpm)

Fuel	Injection time [ms]	Nitrogen oxides [ppm]	Opacity [FSN]
1	2	3	4
Diesel oil	0.55	413	2.8
	0.65	500	4.1
	0.75	516	5.5
	0.87	531	7.2
	0.98	538	9.0
Diesel oil + Oxygen	0.55	546	2.0
	0.65	561	3.2
	0.75	598	4.2
	0.87	604	5.7
	0.98	559	8.2

Comparison of the obtained results allows to evaluate the effect of the oxygen dissolved in diesel oil on the changes in concentrations of the exhaust gas components. Some changes in the concentrations of nitrogen oxides were noticed. The increase in concentration of approx. 30% occurred at low load of the engine. Next, as the engine load increased that concentration decreased and it was of 5–17 %. However, it still was higher than the concentration measured for the engine fuelled with diesel oil. The opacity in exhaust gas decreased by 5–25 %.

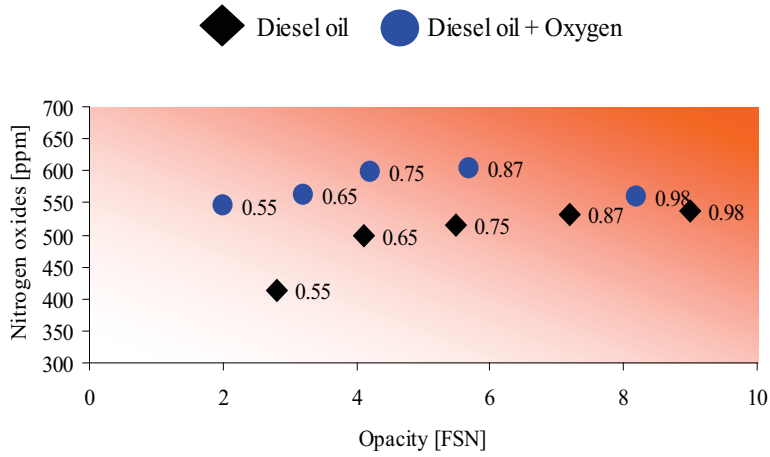

Fig. 7. Comparison of relative changes of the nitrogen oxides and opacity concentrations in exhaust gas

5. Conclusion

The observed changes in concentrations of the individual compounds in exhaust gas from the engine fuelled with diesel oil with dissolved oxygen can be undoubtedly referred to the changes occurring in the combustion process. The increase in the concentration of nitrogen oxides can prove that there is an increase in the temperature value in the flame front area and it also affects (results in) the increase in the combustion chamber temperature. This can be confirmed by the results of torque measurements the values of which increased by 5–20 % for the individual engine operating points. The obtained results show the positive changes of mutual correlation between the nitrogen oxides emission and the exhaust gas opacity especially in range of high engine load. The authors have gathered a rich experience resulting from their previous examinations carried out with the use of air and exhaust gas dissolved in diesel oil [3, 4]. Linking the present results with the previous ones they dare to say that fuelling the engine with diesel oil with dissolved air and exhaust gas gives better effects in reducing the concentrations of the toxic compounds in exhaust gas from the compression-ignition engines. Comparison of these examination results shows that the effect of releasing the gas dissolved in diesel oil, but not the oxygen concentration in the gas being dissolved, is a main factor affecting the improvement of the combustion process.

References

[1] Merkisz, J., Kozak, W., Bajerlein, M., Markowski, J., *The Influence of Exhaust Gases Dissolved in Diesel Oil on Fuel Spray Particulary Parameters,* SAE 2007-01-0488, Session: Diesel Fuel Injection and Sprays, SAE World Congress & Exhibition, 16-19.04, Detroit, Michigan, USA 2007.

[2] Kozak, W., Markowski, J., Bajerlein, M., *The application of gas dissolved In fuel with a view to improve the mechanizm of spraying*, Combustion Engines Nr 1/2005 (120).

[3] Merkisz, J., Kozak, W., Bajerlein, M., Markowski, J., *The influence of exhaust gases dissolved in diesel oil on the parameters of CI engine's performance*, 31st FISITA World Automotive Congress JSAE, 22-27.10 Yokohama, Japonia 2006.

[4] Merkisz, J., Kozak, W., Markowski, J., Bajerlein, M., *Some Possibilities of Improving The Combustion Process and Toxic Exhaust Gas Elements Emission by Dissolving The Air in The Diesel Fuel*, Thiesel 2006 – Thermo-and Fluid Dynamic Processes in Diesel Engines 13–15 September, Valencia, Spain 2006.
[5] Senda, J., Ikeda, M., Yamamoto, M., Kawaguchi, B., Fujimoto, H., *Low Emission Diesel Combustion System by Use of Reformulated Fuel with Liquefied CO_2 and n-Tridecane*, SAE Trans. Vol. 108, No. 1999-01-0798, pp.1-12.
[6] Senda, J., Ohshita, S., Yamamoto, M., Fujimoto, H.: *Low Emission Diesel Combustion System by Use of Reformulated Fuel with Liquefied CO_2 and n-Tridecane*, Proc. 6th Int. Symposium on Marine Engineering, pp.497-504, 9-11 September, Tokyo 2000.

Journal of POLISH CIMAC
Faculty of Ocean Engineering & Ship Technology
GDAŃSK UNIVERSITY OF TECHNOLOGY

THE APPLICATION OF THE ENTROPY ANALYSIS FOR THE EVALUATION OF THE PERFORMANCE OF THE PROCESSES WITHIN THE WASTE ENERGY RECOVERY SYSTEMS IN MARINE DIESEL POWER PLANTS

Ryszard Michalski
West Pomeranian University of Technology, Szczecin
41 Piastów Ave, 71-065 Szczecin, Poland
phone: +48 91 4494941
e-mail: ryszard.michalski@zut.edu.pl

Abstract

The paper presents a proposal of the application of the entropy analysis for the theoretical research of the processes occurring during the thermodynamic transformations taking place in the waste energy recovery systems in marine Diesel power plants. In view of the low exergy of waste energy carriers in these systems it becomes significant to make a proper selection of parameters in the individual points characterising the thermodynamic transformations of the working media. The method as presented herein consists an adaptation of the methods applied in the arrangements of shore power plants to the needs of the marine power plants. This article presents basic relations allowing to determine increments in entropy in the heating steam generation system, as well as the other basic elements forming the waste energy recovery systems in marine power plants. They constitute the basis to evaluate the performance of the individual processes and to disclose the places of occurrence of the major losses and to determine the manners to minimise same. The proposed method may contribute to the reduction of labour consumption of universally applied, traditional methods of searching the effective systems of waste energy recovery in marine Diesel power plants.

Keywords: *entropy analysis, waste energy recovery, marine power plants*

1. Introduction

The specific feature of the marine systems of waste energy recovery in Diesel power plants is the relatively low exergy of the energy carriers. This results in the fact that the degree of waste energy recovery is small, and the generally applied arrangements are mainly restricted to the recovery of the main engine exhaust gas heat to generate steam in the amount that satisfies wholly or partly the ship's heating needs. Only in few cases the available amount of waste energy allows additionally to generate mechanical power in gas or steam turbine on in both at the same time, which may be utilised to drive the generator or for the propeller drive [7]. However, in each case it is significant to properly select the parameter values in the individual circulation points, characterising the working media thermodynamic transformations. In order to make this choice in the appropriate manner it is necessary to conduct the relevant analyses whose results will enable the evaluation of the quality of the course of the individual processes and indicate the places of the major losses and the ways to minimise them.

The basis for the calculations of the waste energy recovery systems in marine Diesel power plants consists the mass and energy balance equation systems [9]. While designing the discussed systems enthalpy analysis has become generally applied. Exergetic analysis [6, 8, 9] can be used for the proper evaluation of, in particular the sources of waste energy, whereas for the evaluation

of the performance quality of the processes taking place during system operation entropy analysis may be considered as the appropriate one. Such analysis is presently used not only at the design stage of new systems of shore power plants, but also to conduct the heat-flow diagnostics [5] or providing the guidelines for the modernisation directions of these power plants and evaluating the effects of their modernisation [2, 4].

The entropy analysis has not been found so far so generally useful for the designing of marine power plants. Nevertheless, it should be expected that as the solutions improving widely understood effectiveness of the marine power plants are sought, its application will turn also useful in this field. Thus this article consists an attempt to present the application of the basis of entropy analysis to the evaluation of the processes occurring in the systems and the elements forming the waste energy recovery systems in marine Diesel power plants.

The inspiration to present in this article the entropy method as a supporting tool in the complex analysis of waste energy recovery in marine Diesel power plants has been provided inter alia by the studies [2, 3, 4, 5]. The general methods of entropy increment minimisation during the processes of heat exchange and in power plants have also been referred to in [1]. Its elements have also been presented earlier by the author in [6, 8].

2. Entropy Analysis of Steam and Mechanical Energy Generation System

Considering a significant similarity of marine systems of waste energy recovery, where water and steam are working media, to the shore systems of steam turbine power plant systems, the general model consisting the basis for the entropy analysis of engine exhaust gas heat recovery in marine Diesel power plants can also be presented by use of the specification contained in [3]. The figure 1 shows general diagram of the analysed part of the system.

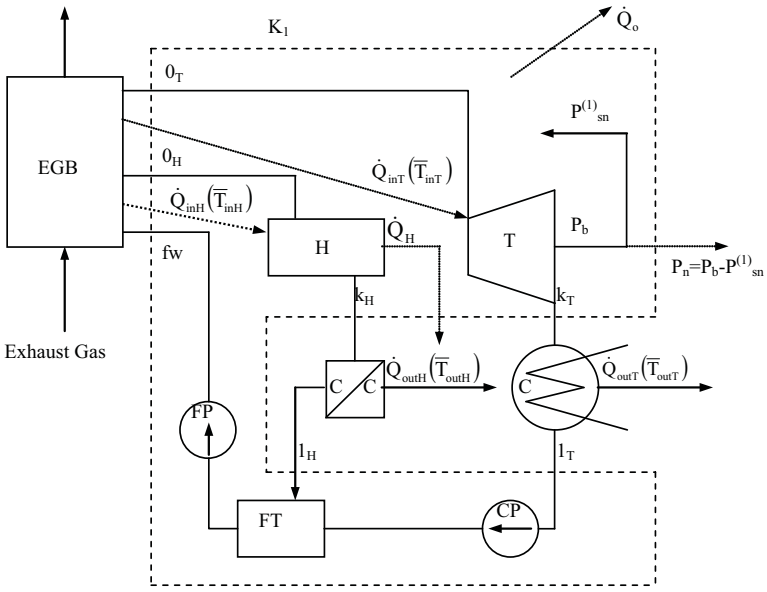

Fig 1. General diagram of the system of heat recovery of marine Diesel power plant engine exhaust gases

This part under discussion has been separated by means of cover sheet K_1, marked in the figure with the interrupted line. The diagram shows: EGB – exhaust gas boiler; H – heaters; CC – condensate cooler behind the heaters; T – waste heat turbine; C – condenser of turbine outlet steam; FT – feed tank (hotwell); CP – condensate pump; FP – feed pump.

Outside the cover sheet there are: waste heat boiler, condensate cooler and steam condenser. Processes taking place in these elements can be a subject of separate analysis which basis have been referred to in the further part of this paper.

By use of denominations applied in the figure 1 the energy balance within the cover sheet can be presented by means of the equation:

$$\dot{Q}_{inH} + \dot{Q}_{inT} - \dot{Q}_{outH} - \dot{Q}_{outT} - \dot{Q}_{o} = \dot{Q}_{H} + P^{(b)} - P_{sn}^{(1)} = \dot{Q}_{H} + P_{n} \tag{1}$$

where:

$\dot{Q}_{inH}$ - heat flux supplied to the marine heating system within cover sheet,

$\dot{Q}_{inT}$ - heat flux supplied to the turbocharger within cover sheet,

$\dot{Q}_{outH}$ - heat flux carried out of ship's heating system by the condensate cooler,

$\dot{Q}_{outT}$ - heat flux carried out from the turbine by the condenser,

$\dot{Q}_{o}$ - heat flux exchanged by the system with the environment (heat losses to the environment,

$\dot{Q}_{H}$ - usable heat flux transferred to shipboard heaters,

$P^{(b)}$ - (gross) power of generator driving turbine,

$P_{sn}^{(1)}$ - own needs of the processes taking place within cover sheet,

P_{n} - (net) power of turbocharger.

The sum of entropy generated within cover sheet can be determined as:

$$\dot{m}_{0H}\left(s_{fw} - s_{0H}\right) + \dot{m}_{0T}\left(s_{fw} - s_{0T}\right) - \dot{m}_{kH}\left(s_{1H} - s_{kH}\right) - \dot{m}_{kT}\left(s_{1T} - s_{kT}\right) + \dot{S}_{o} = \dot{S}_{gen} \tag{2}$$

where:

$\dot{m}_{0H}, \dot{m}_{kH}$ - working medium fluxes at the heater inlet/outlet, respectively,

$\dot{m}_{0T}, \dot{m}_{kT}$ - working medium fluxes at the turbine inlet/outlet, respectively,

s_{fw} - specific entropy of boiler supply water,

s_{0H}, s_{0T} - specific entropy of working medium at inlet/outlet of heaters and turbine, respectively,

s_{kH}, s_{kT} - specific entropy of working medium at the outlet of heaters and turbine,

s_{1H}, s_{1T} - specific entropy of working medium at the outlet of heating steam condensate cooler and condenser, respectively,

$\dot{S}_{o}$ - increase of entropy fluxes related with the $\dot{Q}_{o}$ loss,

$\dot{S}_{gen}$ - the sum of entropy generated in the processes taking place within cover sheet.

It should be noted that:

$$\dot{Q}_{inH} = \dot{m}_{0H}\left(h_{0H} - h_{fw}\right), \quad (3), \qquad \dot{Q}_{inT} = \dot{m}_{0T}\left(h_{0T} - h_{fw}\right), \tag{4}$$

$$\dot{Q}_{outH} = \dot{m}_{0H}\left(h_{kH} - h_{1H}\right), \quad (5), \qquad \dot{Q}_{outT} = \dot{m}_{0T}\left(h_{kT} - h_{1T}\right). \tag{6}$$

The average entropy temperatures for the heat flux flows in the individual system elements are defined as:

$$\overline{T}_{inH} = \frac{h_{0H} - h_{fw}}{s_{0H} - s_{fw}}, \quad (7) \qquad \overline{T}_{inT} = \frac{h_{0T} - h_{fw}}{s_{0T} - s_{fw}}, \quad (8)$$

$$\overline{T}_{outH} = \frac{h_{kH} - h_{1H}}{s_{kH} - s_{1H}}, \quad (9) \qquad \overline{T}_{outT} = \frac{h_{kT} - h_{1T}}{s_{kT} - s_{1T}}, \quad (10)$$

where:

h_{0H}, h_{0T} - specific enthalpy values of working media at the inlet to heaters and turbine, respectively,

h_{kH}, h_{kT} - specific enthalpy values of working media at the outlet of the heaters and turbine, respectively,

h_{1H}, h_{1T} - specific enthalpy values of working media at the outlet from heating steam condensate cooler and turbine steam condenser, respectively,

h_{fw} - specific enthalpy of boiler supply water.

By the application of the equations (2)÷(10) the sum of the generated entropy fluxes in the processes taking place within the cover sheet can be determined as:

$$\dot{S}_{gen} = -\frac{\dot{Q}_{inH}}{\overline{T}_{inH}} + \frac{\dot{Q}_{outH}}{\overline{T}_{outH}} - \frac{\dot{Q}_{inT}}{\overline{T}_{inT}} + \frac{\dot{Q}_{outT}}{\overline{T}_{outT}} + \dot{S}_o . \quad (11)$$

While eliminating by equation (1) $\dot{Q}_{outT}$ from the equation (11), the sum of entropy fluxes in the discussed processes can also be expressed by the equation:

$$\dot{S}_{gen} = -\frac{\dot{Q}_{inH}}{\overline{T}_{inH}} + \frac{\dot{Q}_{outH}}{\overline{T}_{outH}} - \frac{\dot{Q}_{inT}}{\overline{T}_{inT}} + \frac{\dot{Q}_{inH} + \dot{Q}_{inT} - \dot{Q}_o - \dot{Q}_{outH} - \dot{Q}_H - P_n}{\overline{T}_{outT}} + \dot{S}_o \quad (12)$$

From the equation (12) it results that the total entropy flux generated in the analysed system of heat recovery depends not only on the value of heat fluxes but on average entropy temperatures within the process of heat flow in the individual system elements. This property should be considered during the system designing, inter alia while adopting the adequate values of working media parameters in the individual equipment. However it should be noted that the minimising of entropy flux increments results directly in the reduction of the system operating costs, nevertheless it is related with the increase of the investment outlays. Although it is already a cliché to state that the decision-making processes while designing marine power plants should be supported by a complex multicriteria analysis, it is still worthwhile to emphasise this necessity.

By using the equation (12) the power of water heat turbocharger possible to achieve can be determined with the assumed circulation parameters:

$$P_n = \dot{Q}_{inT}\left(1 - \frac{\overline{T}_{outT}}{\overline{T}_{inT}}\right) - \dot{Q}_H - \dot{Q}_o - \overline{T}_{outT}\left(\dot{S}_{gen} - \dot{S}_o\right) - \dot{Q}_{outH}\left(1 - \frac{\overline{T}_{outT}}{\overline{T}_{outH}}\right) - \frac{\dot{Q}_{inH}\overline{T}_{outT}}{\overline{T}_{inH}} \quad (13)$$

The equation (13) allows to determine the actual achievable power output of waste heat turbocharger. Its first part shows maximum achievable value of this power output under assumption that the entire heat flux would be used for the production of mechanical energy and

that no heat losses to the environment occur, whereas the processes taking place are not accompanied by entropy increase. By use of the above models it is relatively simple to determine the optimum parameters of working media in the individual points of transformations.

3. Entropic Analysis of Selected Equipment of Steam and Mechanical Energy Generation System

While analysing the processes taking place in marine waste heat boilers there should be distinguished three functional types of heat exchange section. These are, in case of the most complex and extended system, supply water exhaust gas heater, separating sections (high and low-pressure) and steam heater. The processes of heat exchange between heating exhaust gases and the media receiving heat are accompanied by working media entropy increase. It originates both from the heat flow process itself as well as from the pressure losses due to friction. The latter however are much smaller in comparison with the former ones. Thus they will be omitted here.

The entropy increase in waste heat boiler is equal to the sum of entropy increments of all bodies participating in the transformation:

$$\sum \Delta S = \Delta S_{hm} + \Delta S_{eg} \tag{14}$$

where:

ΔS_{hm} - entropy increase of the heated medium (water and steam),
ΔS_{eg} - exhaust gas entropy increase.

The increase of exhaust gas entropy flux is calculated under assumption of its constant specific heat capacity:

$$\Delta \dot{S}_{eg} = \int_{T_0}^{T_1} \frac{d\dot{Q}}{T} = \dot{m}_{eg} c_{peg} \int_{T_0}^{T_1} \frac{dT}{T} = \dot{m}_{eg} c_{peg} \ln \frac{T_1}{T_0}, \tag{15}$$

where:

T_0, T_1 - exhaust gas temperature in the beginning and end of the process,
c_{peg} - average specific heat capacity of exhaust gases,
$\dot{m}_{eg}$ - exhaust gas mass flux.

The increase of entropy flux of water (steam-water mixture or overheated steam) should be calculated as the difference of specific entropy values at the outlet and inlet from the section under consideration “i” of the waste heat boiler:

$$\Delta \dot{S}_{wi} = \dot{m}_{wi} \left(s_{1wi} - s_{0wi} \right), \tag{16}$$

where:

$\dot{m}_w$ - water mass flux,
s_{1wi}, s_{0wi} - specific entropy value of the working medium at the outlet and inlet of the section under consideration.

The study [9] presents the results of exergetic analysis of the processes occurring in the marine waste heat boiler. Its completion required the determination of entropy increments in its individual

sections. By use of the results of this analysis it can be stated that the biggest losses do take place in the evaporating section. These are related inter alia with the water properties, and more specifically with the relatively large value of evaporation specific enthalpy with the moderate pressure values of steam. Its reduction takes place along with the increase of stem in boiler, however, it leads to the reduction of the degree of the heat utilisation of the engine exhaust gases. Therefore it is of major importance while designing marine engine exhaust gas heat recovery systems to adopt the appropriate steam pressure.

By use of denominations in figure 2, the increase of entropy flux in steam separator can be determined as [9]:

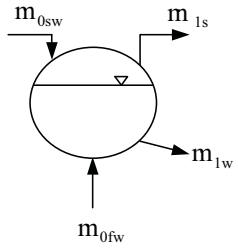

Fig 2. General diagram of steam separator

$$\Delta\dot{S} = \dot{m}_{1s}\left[x_1 s_{1s} + (1 - x_1)s_{1w}\right] + \dot{m}_{1w}s_{1w} - \dot{m}_{0fw}s_{0fw} - \dot{m}_{0sw}\left[\frac{s_{0s}}{k_c} + s_{0w}\left(1 - \frac{1}{k_c}\right)\right], \qquad (17)$$

where:

$\dot{m}_{1s}, \dot{m}_{1w}$ - steam and water mass fluxes at the separator outlet,

$\dot{m}_{0fw}, \dot{m}_{0sw}$ - mass fluxes of feed water and steam-water mixture at the separator inlet,

s_{1s}, s_{1w} - specific entropy of steam and water at the separator outlet,

s_{0s}, s_{0w}, s_{0fw} - specific entropy of steam, boiling water and feed water at separator inlet,

x_1 - steam dryness degree at separator outlet,

k_c - number of circulations in boiler.

The adoption of the appropriate value of the number of circulations in boiler should be particularly emphasised. Adoption of too big value of this parameter results in the straight manner in the increase of the losses. On the other hand, too small value may lead to intensive sedimentation of boiler scale in boiler evaporating section.

The entropy increments in the surface heat exchangers can be calculated in the similar mode as in case of waste heat boiler. The simple method is reading of the relevant entropy values from the available tables or charts. It is also possible to assume constant specific heat capacity of a medium and calculating the entropy increase as:

$$\Delta\dot{S} = \dot{m}c_p \ln\frac{T_1}{T_0}, \qquad (18)$$

where:

$\dot{m}$ - medium mass flux,

c_p - medium specific heat capacity of medium,

T_1, T_0 - medium temperature at the exchanger outlet and inlet, respectively.

Mixing-type heater, summing T-pipe and hotwell are the elements where, similar as in steam separator, the entropy increments are chiefly caused by the process of mixing of working media. Entropy increase in these elements can be determined on the basis of the readings taken from the appropriate entropy tables or charts of the individual media "i" at the inlet and outlet of the recovery system element under consideration. The entropy increase flux is determined by:

$$\Delta\dot{S} = s_1 \sum_1^n \dot{m}_{0i} - \sum_1^n \dot{m}_{0i} s_{0i}\,, \tag{19}$$

where:

$\dot{m}_{0i}$ - mass flux of i-medium at the inlet,

s_{0i} - specific entropy of i-medium at the inlet,

s_1 - specific entropy of the mixture at the outlet,

n - number of media fluxes at the inlet.

The increase of entropy flux in throttle valve can be determined as:

$$\Delta\dot{S} = \dot{m}(s_1 - s_0), \tag{20}$$

where:

$\dot{m}$ - medium mass flux,

s_1, s_0 - medium specific entropy values at the outlet and inlet.

In the effect of friction in the steam turbine the expansion process is not isentropic. In the result the actual expansion work is less than isentropic expansion work and the process itself is a source of irrecoverable exergy losses.

The entropy value can be taken from the diagram of i-s for steam or calculate them basing on the appropriate relations as functions of eg pressure and temperature of steam in the relevant points of process taking place in the turbine.

The liquid specific entropy increase in pump can be expressed by formula [9]:

$$\Delta s = v(p_1 - p_0)\frac{1}{\overline{T}}\left(\frac{1}{\eta_i} - 1\right), \tag{21}$$

where:

v - liquid specific volume,

p_1, p_0 - pressure at delivery and suction side,

$\overline{T}$ - averaged liquid temperature,

η_i - pump internal efficiency.

Conclusions

Although the enthalpy method allows to determine the effectiveness of energy transformation in the designed installation, it does not allow to determine clearly the places where energy losses occur or size of these losses.

The restriction of energy losses is of particular importance while designing the waste energy recovery systems in view of small exergy of this energy sources.

The entropy method allows to determine the energy losses in the individual processes and locations of the performance of the thermodynamic transformations which in consequence allows to take actions aiming at their reduction.

The entropy method can consist the supplement to enthalpy method which is generally applied in designing marine power plants, including the designing of waste energy recovery in marine Diesel power plants.

While designing the systems of recovery of waste energy in marine Diesel power plants it should be taken into consideration that the reduction of losses is accompanied in general by the increase of investment outlays related with the execution of energy-saving arrangement. Thus it is important to conduct a complex, multicriteria evaluation of the solutions possible to implement, including not only thermodynamic and technical aspects but also inter alia ecological and widely understood economic aspects.

References

[1] Bejan, A., *Fundamentals of exergy analysis, entropy generation minimization, and the generation of flow architecture*, International Journal of Energy Research, Volume 26, Issue 7, pp.0 - 43, May 2002.

[2] Chmielniak, T., Efektywność termodynamiczna modernizacji turbin parowych, [*The Thermodynamic Effectiveness of Steam Turbine Modernisation*] II Materiały III Konferencji Problemy Badawcze Energetyki Cieplnej, Wyd. Politechniki Warszawskiej, Prace Naukowe, Konferencje z.15, pp.79 - 86, Warszawa 1997.

[3] Chmielniak, T., Technologie energetyczne [*Power Engeneering Technologies*] WNT, Warszawa 2008.

[4] Chmielniak, T., Kosman ,G., Kosman, W., Modernizacja elektrociepłowni przy dużym zużyciu elementów, kotłów i turbin parowych, [*The Modernisation of Heat and Power Generating Plants with Large Consumption of Elements, Boilers ad Steam Turbines*] http://www.itc.polsl.pl/centrum/kogen/materialy/art3.pdf, pp.51 - 69.

[5] Chmielniak, T., Łukowicz, H., Analiza entropowa siłowni parowej, wyniki obliczeń, [*The Entroy Analysis of Steam Power Plant, results of calculations*] Konferencja Problemy Badawcze Energetyki Cieplnej, Prace Naukowe PW, Mechanika z.181, pp.23 - 27, Warszawa 1998.

[6] Michalski, R., Przykład zastosowania analizy egzergetycznej do badania procesów utylizacji ciepła odpadowego w siłowniach motorowych, [*An Example of of the Aplication of the Exergetic Analysis for the Investigation of Waste Energy Recovery Sysytems in Marine Diesel Power Plants*] XX Sympozjum Siłowni Okrętowych, AMW w Gdyni, pp. 119 - 126, Gdynia 1998.

[7] Michalski, R.: Siłownie okrętowe, [*Marine Power Plants*] Wyd. Politechniki Szczecińskiej, Szczecin 1997.

[8] Michalski, R., Zeńczak, W., Ocena egzergetyczna procesów zachodzących w elementach układów utylizacji ciepła odpadowego, [*The Exergetic Evaluation of the Processes Taking Place in the Elements of Waste Heat Recovery Systems*] XII Międzynarodowe Sympozjum Siłowni Okrętowych, WSM w Szczecinie, pp. 211 - 223, Szczecin 1990.

[9] Szargut, J., Petela, R., Egzergia, [*Exergy*], WNT, Warszawa 1965.

The study financed from the means for the education within 2009 – 2012 as own research project No N N509 404536

Journal of POLISH CIMAC
Faculty of Ocean Engineering & Ship Technology
GDAŃSK UNIVERSITY OF TECHNOLOGY

THE MONITORING OF SHIP PROPULSION BY TORQUE AND ROTATIONAL SPEED MEASUREMENTS ON THE PROPELLER SHAFT

Leszek Morawski

Gdynia Maritime University
ul. Morska 83, 81-225 Gdynia, Poland
e-mail: lmoraw@am.gdynia.pl

Zbigniew Szuca

e-mail: zszuca@interia.pl

Abstract

In paper device for measuring of torque and rotational speed at the ship main drive propeller shaft transferred will be described.. This device connected to the power plant monitoring systemt. It may be used for continuous control of operating costs of the ship and for the choosing of safe and best engine operational parameters. It is possible to observe the actual point of engine's operational state marked against the mechanical characteristic chart. The limited, safe area of acceptable working points is displayed on the diagram as well. The presented torque meter has possibility to measure instantaneous fluctuations of the torque and engine rotational speed as a function of the shaft rotation angle. This is a piece of important diagnostic information for fast preliminary assessment of the load on a particular cylinder and of the quality of engine work.

Keywords: *ship's propulsion unit, main engine, torque measurement, torque meter*

1. Introduction

Safe and efficient operation of ship propulsion system requires accurate data on current load of the main propulsion engine. A device providing those data is a torque meter. Its basic function is continuous assessment of load of the main propulsion engine, and signaling when permissible parameters have been exceeded. The torque meter can be used also to economisation of ship's motion bases on selecting an optimal relation between the cost of consumed fuel and the obtained transporting result. Its measure can be the speed reached by the ship, for instance. Evaluating instantaneous fuel consumption requires accurate data on current load of the main propulsion engine.

Torque meters employed in practice on watercraft are used for measuring:

a) shear stresses – strain gauge torque meters;
b) shaft torsion angle - string torque meters and torque meters with toothed rings.

In described below a torque meter is applied photo optic method for measure a torsion angle of propeller shaft.

2. Characteristic of torque meter

The principle of operation of torque meters bases on photo-optical measurement of a torsion angle of the propeller shaft section. Two rings with machined teeth (usually 2.2÷2.4 teeth for 1 cm

diameter of shaft) are fixed on the shaft at a distance of abt. 400 mm. They are designed in such a way that their teeth are in the same plane, and are covered by one measuring head.

The average torque and power values, measured and calculated for the period of 4 to 240 sec (adjustment selected by operator), are displayed as percents of nominal parameters, with 0.1% resolution. At the same time the rotational speed is determined at the 0.1 rev/min resolution.

Fig. 1 shows a schematic block diagram of the entire configuration of the mentioned torque meter. The configuration includes the following basic components:

- photo optical measuring head – signals source;
- microprocessors main module – one-chip micro-computer;
- Programmable Logic Controller – basic signals acquisition, arithmetical calculations, communication with outer units, archive measured and calculated output data, tooth rings technical condition self test;
- Operating Panel (LCD colour touch panel) – displaying current results of the engine's load measurements (rotation speed, torque, power), data archived in memory, efficiency indexes; used by operator for communication and giving commands;
- LED display – displaying current results of the „rotational speed-torque-power" measurements on the navigating bridge.

The device has a modular structure. Its basic component is a programmable PLC controller that executes controlling and calculating functions for measurement and calculation data, as well as storing of part of them. By using proper interfaces, the controller communicates with an „intelligent" module used for preliminary processing of measurement signals, and with other terminals. It is connected with the operator's console, displays, PC computer and the system that monitors operation of the marine power plant.

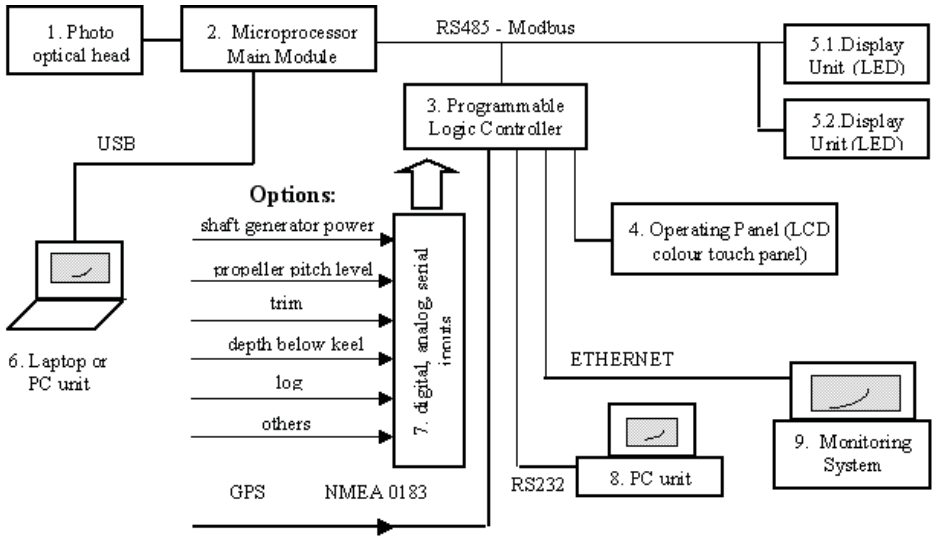

Fig. 1. Schematic block diagram of the entire configuration of torque meter

The module used for preliminary processing of measurement signals from a photo-optical head (laser measurement head) was designed using a fast micro-processor system that processes signals in a real time of an order of several milliseconds. The optional components of torque meter are:

- PC or Laptop unit equipped with special software for observe torque and shaft speed fluctuations which can help in diagnosing the engine. If PLC damage the measured torque, revolutions and engine power are show on PC/Laptop screen;
- analog and digital serial data inputs for acquisition additional data;

- PC unit for archiving the measured and calculated data and visualisation of actual point of engine's operation state, diagrams and trends (in case of lack of Monitoring System);
- Monitoring System – as above and communication with the owner's technical department.

In the presented torque meter, new technical solutions were applied that base on experience gained during design, production and use of previous versions of the device. So far, several dozens of torque meters have been produced and installed on merchant and training vessel, as well as in university laboratories. The novelty of the present design is the use of a programmable logic controller PLC along with own codes allowing easy integration of the torque meter with any computer system, or a special system for monitoring operation of marine power plant devices.

3. The torque meter as a device for efficient exploitation of ship propulsion system

The torque, power and rotational speed of propeller shaft are the parameters that carries important information about technical condition of the engine, and are sensitive to they changes. Therefore they can be considered as a diagnostic parameters, especially torque and rotational speed of shaft.

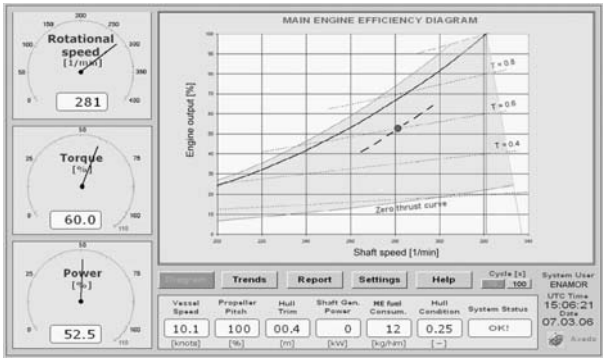

Fig. 2. The main engine efficiency diagram in power plant monitoring system on the training ship m/s "Horyzont II". Marked point of actual working state of main engine

The knowledge about the torque (or power output) and rotational speed unmistakably identifies a point in the propulsion engine operation area. On the Fig. 2 is presented the exemplary diagram with the actual point of engine's operational state marked against the mechanical characteristic chart. This example of efficiency engine diagram is taken from the monitoring system, which together with torque meter are installed on the training ship m/s "Horyzont II".

The area of safe and acceptable working points is displayed on this diagram. This field is marked darker colour. The borders of safe and acceptable area of engine working mark: power characteristic for nominal or exploitation fuel supply set, propeller characteristic in captive test of ship, control characteristics for minimal and maximal rotational speed and characteristic of minimal torque (in that case zero thrust curve) [5]. The nominal propeller characteristic is marked as a fat line. The dashed lines are the lines of solid torque. The power and torque actual values are expressed as percents of nominal parameters, with 0.1% resolution.

Along with the fuel consumption basing upon the engine characteristic, stored in the device's memory, it is possible to calculate theoretical fuel consumption in each measuring cycle. The volume of this fuel consumption is also summed up in a "Last 24hours fuel consumption" counter. The result showed by the counter represents sum of power produced by the propulsion engine. Pulses delivered from GPS satellite navigation system or from a log, allow assessing a valuable, from the point of view of fuel economization, factor referred to as "normalized fuel consumption per 1 nautical mile". This factor immediately responses to any change in parameters of ship's

motion, as well as and to changes in trim, wind direction with respect to ship's course, propeller pitch (if CPP applicable), etc.

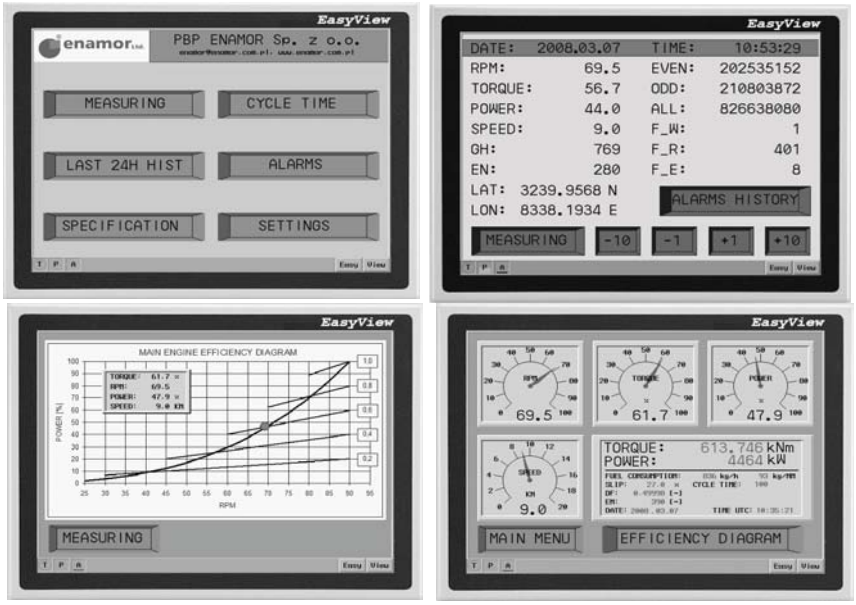

Fig. 3. The examples of the diagrams on the LCD operating panel

Mentioned above exploitation parameters are displayed not only on the efficiency diagram but also on the LCD handy operating panel (Fig.3). It is possible through the operating touch panel to put to the torque meter necessary parameters of engine, propeller shaft, number of teeth on ring and threshold values of signalling alarms. Reading the current measurements other exploitation and diagnostic parameters and their history, trends from the last 24 hours it is possible also.

The torque meter has a memory for automatic storing and reading the results of measurements and calculations covering several hundreds of consecutive measurement cycles. This function is of essential applicability on ships on which a computer system for data storing has not been installed.

Storing and analysing data from long time intervals, together with other parameters normally recorded during marine power plant operation, brings information of great value. Observation of trends in those data allows preparing long-term reports, as well as assessing changes in technical condition of propulsion system components and the risk of their possible failure. Their correlation with fuel consumption at given changes of operating conditions, like state of the sea, wind direction and force, draught and trim, propeller pitch, etc., help to make a sensible decision on the main engine operation. The analysis of costs resulting from changes in technical condition of the propulsion system facilitates making important decisions on repair, cleaning of underwater hull parts without docking, or modifying its components. In case of malfunction or worsened technical condition of any component of the propulsion system, it is possible to gain information of the possible location of its origin. As a result, all this simplifies and shortens servicing and diagnostic actions during ship operation. These characteristics of the torque meter allow considering it a valuable diagnostic tool.

Essentially helpful is the torque meter in propulsion systems equipped with the controllable pitch propeller, as this provides opportunities for evaluating the most favourable parameters of engine operation for a given propeller pitch. A new design of the torque meter makes it possible to take into account additional engine load caused by the operation of a shaft generator. In this case, along with operating parameters of the main engine, the engine-propeller co-operation point is

evaluated as well.

The torque meter is equipped with procedures that detect and signal failures, or dirt on the photo-optical head and toothed rings.

Optional codes are being prepared for a PC computer that will allow evaluating time-histories of shaft torque and angular velocity in a single turn (for a slow and medium rotational speed engines). This is a piece of important diagnostic information for fast preliminary assessment of the load on a particular cylinder and of the quality of engine work [1]. On the basis of these data one can conclude about the power transmitted by particular cylinders to the propeller shaft. Also, a "piston-cylinder" system can be identified which reveals visible differences from standard performance [2], [6].

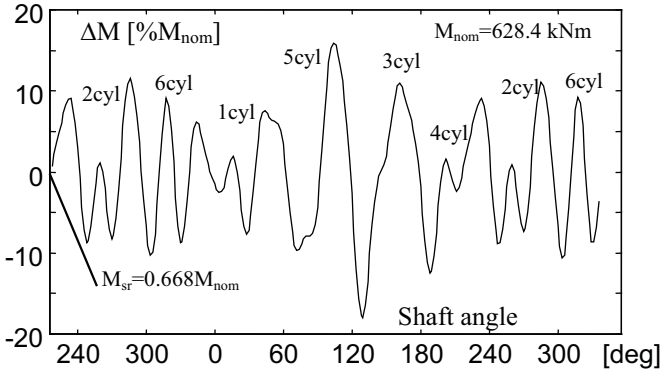

Fig. 4. Instantaneous torque fluctuation curve, reconstructed from the frequency spectrum. (the bulk carrier m/s "Powstaniec Listopadowy")

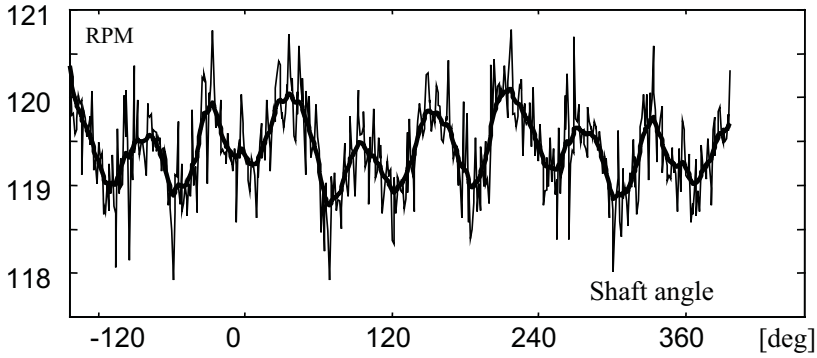

Fig. 5. Propeller shaft rotational speed computed and filtered at RPM=118.8 rev/min, torque $M_{śr}$=66.8%$M_{nom.}$, (the bulk carrier m/s "Powstaniec Listopadowy")

It should be stressed here that the number of points corresponding to one shaft revolution in which the torque is measured is equal to a double number of teeth in one ring, while for the rotational speed the number of points is four times bigger than the number of teeth. The torque and speed rotations fluctuation curves computed from the measured data are significantly deformed. It is affected by deformations caused by, among other things, an inaccuracy in manufacturing and installing the toothed discs on the shaft, resonances of free torsion vibrations of the shaft, vibrations of the shaft deflection, propeller load fluctuations and etc.

The deformations of measurements of low-frequency can be eliminated using a method of spectral analysis which was presented in [3] and [4]. A high-frequency deformation was eliminated using a forward-backward type filter. As example, on the Fig. 4 and 5 are presented

reconstructed and filtered time-histories of torque and rotation speed fluctuations in consecutive shaft revolutions. The presented measurements was made on the bulk carrier m/s "Powstaniec Listopadowy" (33767DWT, L=185m, main engine SULZER 6RL66, 8160 kW, 124 rpm).

5. Conclusion

Concluding, it should be stressed that described the torque meter can bring measurable profits resulted from safe and efficient exploitation of ship propulsion system. This opinion is backed up by the following arguments:

- continuous torque control helps operate the propulsion system without the effect of increased current repair cost;
- current control of mutual relation between real and calculated fuel consumption, the latter being indicated by the torque meter, allows evaluating changes in internal efficiency of the engine, thus avoiding the effect of increased repair costs and fuel investments;
- the knowledge of calculated fuel consumption used for covering 1 nautical mile make possible to select the most profitable parameters of the propulsion system (most significant – controllable pitch propeller), for instance with respect to the fuel consumption.
  More important: immediate feedback of any action taken to improve vessel operation – this is a potential source of fuel economisation;
- the combined knowledge of the torque and ship's speed allows controlling changes in technical condition of hull and screw surfaces. This, in turn, allows making decisions on possible cleaning of those surfaces;
- the information of shaft torque and rotational speed fluctuation in a single turn makes a form of preliminary diagnostic of the propulsion engine operation;
- storing results of measurements and calculations, along with other parameters kept in the device's memory, allows the ship owner to evaluate, and possibly correct, the way in which the vessel is operated.

References

[1] Fehrenbach H.,.Quante F., *Diagnosis of Combustion Engines by the Analysis of the Crankshaft's Rotational Speed*, VDI-Berichte, no 644, pp. 72-80, 1987.

[2] Morawski L., Szuca Z., *The new device for measuring torque and rotational speed on the propeller shaft of ship with possibilities of diagnostics and estimation of ship propulsion system state, Report of Project KBN Nr 6T12 2003C/06267* (in polish), Gdynia Maritime University, PBP ENAMOR Ltd, 2006.

[3] Morawski L., Sikora M., *The microprocessor device measuring torque and rotational speed on the propeller shaft of ship applied for monitoring of the ship propulsion system*, (in polish), Pomiary Automatyka Kontrola, nr 7, pp272-277, SIGMA Warszawa 1998.

[4] Morawski L., Szuca Z., *The application of the photo optic torque meter to estimation of torque and rotational speed fluctuations on the propeller shaft of a ship,* Journal of Polish Cimac, Vol.2, No.1, 2007.

[5] Włodarski K, Witkowski K., *The combustion engines of ship,* (in polish), Gdynia Maritime University, Gdynia 2006.

[6] Morawski L., *Measurements of instantaneous fluctuations of torque and rotational speed on the propeller shaft for diagnosis of ship propulsion system,* (in polish), Automatyka i Informatyka Technologie Informacyjne Diagnostyka, PWNT Gdańsk 2007.

Journal of POLISH CIMAC
Faculty of Ocean Engineering & Ship Technology
GDAŃSK UNIVERSITY OF TECHNOLOGY

INFLUENCE OF OPERATIONAL EXTERNAL LOADS ON PARAMETERS OF THE SURFACE GEOMETRIC STRUCTURE

Janusz Musiał

University of Technology and Life Sciences
Prof. S. Kaliski Av. 7, 85-789 Bydgoszcz, Poland
tel.: (++48 52) 340-86-56,
e-mail: jamusual@utp.edu.pl

Abstract

In this paper, a proposal of a new method for assessment of changes occurring in geometric structure of elements of turning bearing surfaces has been presented. The bearing curve parameter value changes serve as the measurement of the observed changes in the function of stress amplitude, for different use times. The research was carried out within BS 06 on the subject „Selected problems of a product manufacture and life engineering". The results of the performed empirical tests reveal that description by means of the proposed method of changes occurring in the structure of the tested surfaces, throughout the wear process, is possible.

Keywords: *surface geometric structure, bearing curve*

1. Introduction

The surface layer of the machine elements is a factor which largely determines their properties and combination of surface layers of two cooperating elements determines properties of the kinematic pair formed by these elements. One of the quantities characteristic for the surface layer is the surface of geometric structure which determines the process of wear.

Extending knowledge on profiling the surface geometric structure (SGP), elaboration and application of new ways for its assessment (qualitative and quantitative) has been made possible, also thanks to the precise and computer aided measuring equipment. New programming possibilities of the surface analysis in a spatial system (3D) which , in combination with improved precision of measuring tools, allows for observation and measurement of SGP elements in a nanometric scale as well as for its description by means of numerous parameters, not only areal, but also volumetric, spatial, hybrid and functional ones, and with the use of characteristics in the form of curves. The most popular example is the Abbot-Firestone's chart, called a bearing curve. The parameters of the curve served for the evaluation of the investigated surface changes.

2. Object and method of investigations

An oblique ball bearing was accepted for the investigations. This type of bearing was selected due to its structural form and the resultant kinematics of its elements, big intensity of phenomena accompanying transformation of the surface geometric structure which improves the observation conditions.

For the investigations, stress values σ_ψ = 200MPa, 621MPa, 887MPa, 1381MPa, 1520MPa were accepted. Such values demonstrate changes on the whole perimeter of the ring.

The tests results were registered for three time values τ:

- at the beginning of the investigations (beginning of period I), for τ_1=0 s,
- in the period of a fixed intensity of changes (more or less in the middle of period II), $\tau_2=2{,}1\cdot10^5$ s,
- at the end of the bearing life (period III), $\tau_3=3{,}9\cdot10^5$ s.

Measuring points with the above coordinates were accepted on the basis of results of overall research on oblique turning bearings, contained in works[7].

In figure 1, a typical wear process has been presented. Three periods can be easily seen in them.

I – fast increase in wear intensity,
II – fixed level or slight wear changes ,
III – repeated fast increase in wear intensity.

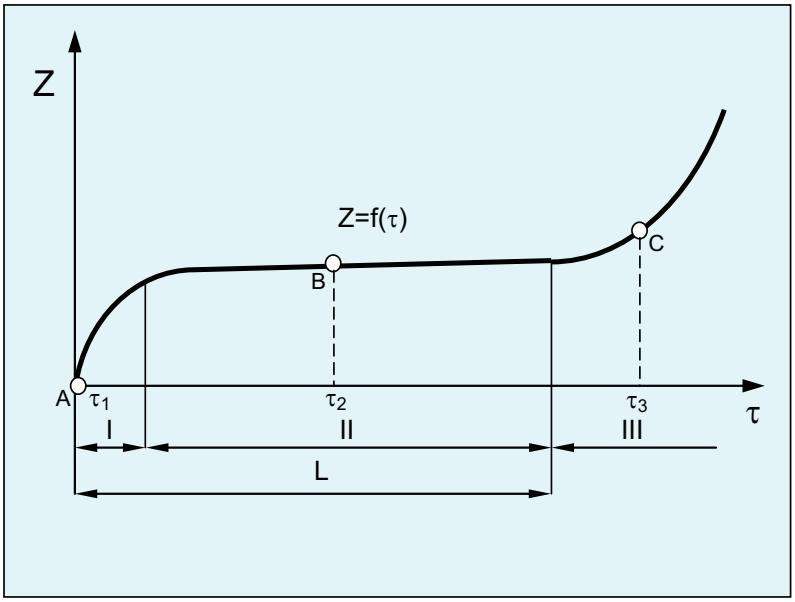

Fig 1. Graphic record of a typical wear process

According to a traditional approach it is accepted that the life is a sum of period I and II. On the basis of investigations [7], it was found that with the life criterion in the form of the motion resistance level, a part of period III can also be considered as the period determining the usability boundary, that is the bearing life. Therefore, in this period the third point was also accepted, in which changes were registered. Coordinates of measuring points: A,B,C , used for measurements and observations, are marked in Figure 1.

Parameters of the bearing curve were accepted as parameters defining properties of the examined surfaces. The curve called Abbot –Firestone's chart describes the material distribution in the profile. Since the bearing curve provides information on the profile course, in a precise form, it is possible to read from it the profile properties, significant for surface function [4]. Parameters characterizing the bearing curve of roughness profile are:[3,6]:

- Sk – height of the core roughness, μm,
- Spk – reduced height of roughness profile elevation, μm,

- Svk – reduced depth of roughness profile hollow, μm,
- Sr1 – bearing share of peaks ,%,
- Sr2 – bearing share of hollows, %,
- A – the core area,
- A1 – area of elevations filled with the material,
- A2 – area of hollows free from the material

Graphic interpretation of these parameters are presented in figure 2.

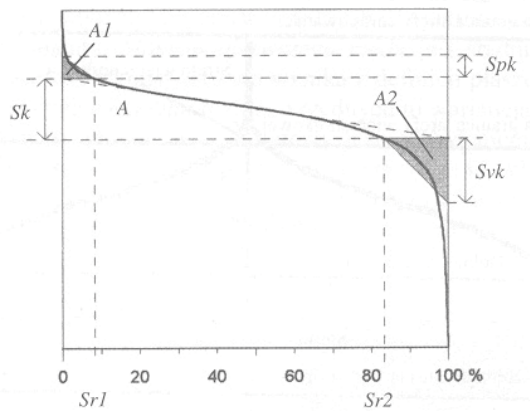

Fig.2. Characteristics of bearing curve [5]

Parameter Spk can serve as a measurement of effective roughness depth. The value of parameter Spk reflects the surface abrasion resistance – the smaller it is the bigger the resistance is. Parameter Svk is a measurement of the cooperating surfaces capability to maintain the fluid, therefore, the aim of finish machining is to obtain its possibly high value.

3. Investigation results

Commonly used amplitude parameters do not fully define properties of the examined surfaces, so for this purpose the surface characteristics in the form of bearing curves, were used to extend the evaluation.

In Tables 1, 2 and 3, determined values of the bearing curve parameters are compared for three times, in which the effects of changes in SGP were observed, depending on the stress amplitude.

Tab. 1. Parameters characteristic for bearing curves for τ_1=0 s

Stresses / Parameters	σ, MPa				
	200	621	887	1381	1520
Sk, *μm*	2.26				
Spk, *μm*	1.05				
Svk, *μm*	1.38				
Sr1, *%*	9.30				
Sr2, *%*	88.80				

In the first transformation period (from τ_1 to τ_2), parameters Sk, Spk decreased by about 40%, whereas, parameter Svk underwent minor changes – it decreased in the range from 11.6% to 24.6%. This proves that in result of the balls rolling over the path there occurred lowering of peaks in the direction to the roughness core. Further operation – until τ_3 time, caused significant changes (increase) of parameters: Spk and Svk by 10 times, and Sk even by 20 times. The cause of such a situation is an increase in the wear process intensity reflected in the form of all kinds of damages to the surface (craters, cracks, grooves, etc.).

Tab. 2. Characteristic parameters of bearing curves for $\tau_2=2{,}1\cdot 10^5$ s

Stresses / Parameters	σ, MPa				
	200	621	887	1381	1520
Sk, *μm*	0.23	1.26	1.27	1.31	1.34
Spk, *μm*	0.28	0.58	0.58	0.58	0.60
Svk, *μm*	0.10	1.04	1.09	1.14	1.22
Sr1, *%*	9.80	9.30	9.20	9.10	8.90
Sr2, *%*	88.90	90.00	89.50	88.70	88.20

Comparing parameters of the bearing curve in the function of stresses, presented in Table2 and Figure 3, it was found that along with the stresses increase, values of all parameters increased, as well. For minor changes $\sigma_\psi \langle 200;621\rangle$, the increase was a few times higher, and then slight. The only parameters whose value in the whole stress changeability range σ changed to a small degree, were material shares – Srl and Sr2. A slight increase in the value of parameter Sr1 along with time proves grinding in of the observed surfaces of working bearings under the influence of turning elements rolling on them, whereas slight changes of Sr2 parameters met the expectations as the action of external loads at the micro-unevenness base should be insignificant.

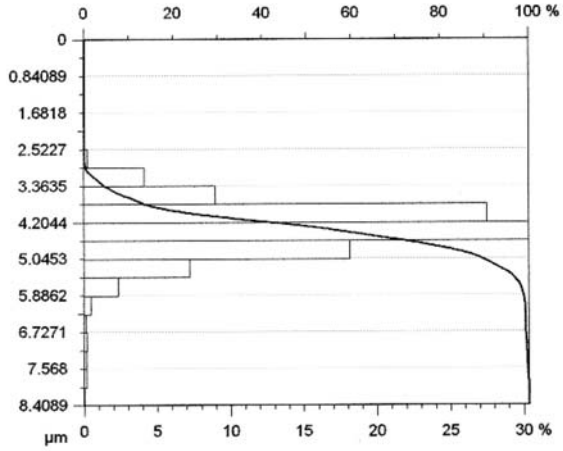

Fig. 3. Chart of bearing curve for time τ_2 (621 MPa)

In Table 3 and Figure 4, there have been presented dependencies of parameters accepted for the surface geometric structure on stresses, for the third period of use.

The character of changes is similar as for time τ_2 for the smallest stresses, a large rise of the examined parameters values was found.

Tab. 3. Characteristic parameters of bearing curves for $\tau_3=3,9\cdot 10^5$ s

Stresses / Parameters	σ, MPa				
	200	621	887	1381	1520
Sk, *μm*	0.29	19.30	22.40	25.78	28.80
Spk, *μm*	0.13	5.70	5.90	6.41	6.50
Svk, *μm*	0.28	10.70	10.94	11.15	11.30
Sr1, *%*	9.60	9.60	9.60	9.80	9.80
Sr2, *%*	88.00	90.20	89.40	88.90	89.00

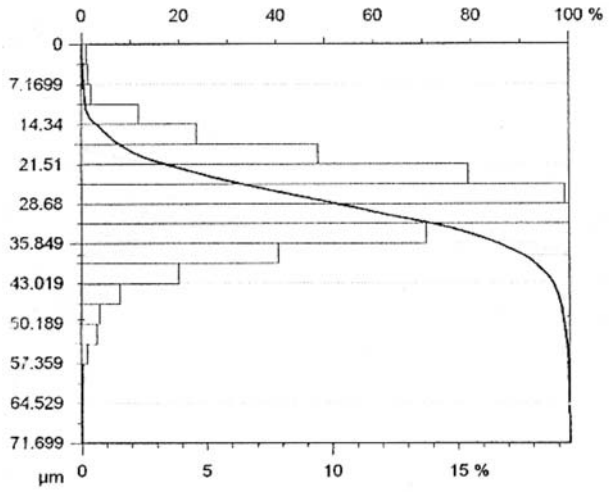

Fig. 4. Chart of bearing curve for time τ_3 (621 MPa)

On the basis of the results contained in tables 1,2,3 it can be found that the paths of turning bearings in period II are characterized by the best features of bearing surfaces. A big difference between values Sr1 and Sr2 and a small value of Sk prove that the roughness profile is of the plateau surface type character. Surface of this type is featured by high bearing capacity, small friction and abrasion resistance, that is features highly desired for working surfaces of turning bearings. These observations are confirmed by the expected stabilized intensity of the surface wear process in this period.

4. Summary

Dependencies of parameters describing SGP, that is, characteristics of the bearing curves and stresses in the points of turning elements contact with the turning path, on the internal elements, produced by the bearing external loads, facilitate the choice of the surface layer properties, for which it will be characterized by the expected usability features. As these characteristics depend on the kind of finish machining and its parameters, being familiar with these dependencies should make easier its choice, which is of great importance for the final effect of machining.

References

[1] Musiał, J., *Badania wpływu wybranych obciążeń zewnętrznych na zmiany geometrii powierzchni roboczych łożysk tocznych,* praca doktorska, Akademia Techniczno-Rolnicza, Bydgoszcz 2003.

[2] Musiał, J., *Wybrane zagadnienia tribologicznych badań łożysk tocznych*, Materiały Konferencji „Problemy naukowe młodych w obszarze budowy i eksploatacji maszyn", s. 93÷101, Bydgoszcz 1998.

[3] Nowicki, B., *Zaawansowane metody opisu i pomiarów struktury geometrycznej powierzchni,* s. 36÷41, Mechanik nr 1/2007.

[4] Nyc, R., *Ocena zużycia współpracujących powierzchni elementów maszyn na podstawie krzywych nośności,* s.349÷355, Tribologia nr 3/2001.

[5] Oczoś, E.K., Liubimov, V., *Struktura geometryczna powierzchni,* Oficyna Wydawnicza Politechniki Rzeszowskiej, Rzeszów 2003.

[6] Piekoszewski, W., Szczerek, M., Wiśniewski, M., *Charakterystyki tribologiczne chropowatości powierzchni elementów maszyn*, Zagadnienia Eksploatacji Maszyn, s. 43÷69, z 3(123)/2000.

[7] Styp-Rekowski, M., *Znaczenie cech konstrukcyjnych dla trwałości skośnych łożysk kulkowych,* Wydawnictwo Uczelniane ATR, seria Rozprawy, nr 103, Bydgoszcz 2001.

Journal of POLISH CIMAC
Faculty of Ocean Engineering & Ship Technology
GDAŃSK UNIVERSITY OF TECHNOLOGY

RELATION BETWEEN THE NUMBER OF REEFER CONTAINERS AND THE LOAD OF THE MARINE ELECTRIC POWER SYSTEMS

Grzegorz Nicewicz

Maritime Academy of Szczecin
ul. Wały Chrobrego 1-2, 70-500 Szczecin, Poland
tel.: +48 91 4809442
e-mail: nicze1@wp.pl

Abstract

Rapid development of unit cargo transport caused the contemporary container vessels to be adjusted to carrying a considerable number of reefer containers. They need to be plugged in to the marine electric power system right after being loaded providing they contain any cargo. They are assumed to be unplugged for no longer than twelve hours without any damage to the cargo. At present container vessels are equipped with even a few hundred of sockets for plugging in reefer containers. In case of loading the maximum number of reefer containers, they become the most powerful energy receiver on board the ship. The regulations of the classification institutions [4] define the marine electric power to be consumed by the reefer containers. The paper has been an attempt of estimation of a real value of power consumed by reefer containers illustrated by a container vessel 2200 TEU adjusted to carrying 350 reefer containers and a comparison of the achieved results with the directives of the selected classification institutions [4]. Moreover, a critical approach to the shipyard offices' methods of establishing the number of reefer containers to be plugged in for the needs of ship owning companies ordering new vessels has been presented.

Keywords: *marine electric power system, marine generating set, reefer containers*

1. Introduction

Within the identification tests concerning real loads of transport vessels' electric power systems in operating conditions, that have been carried out by the author of the paper for years, observations were led on various types of vessels including container ships. The adequate operational data related to the highest demand for the electric power at fixed time intervals were collected by an observer, the engine crew member making use of the measuring instruments, the standard power plant equipment. The tests' methodology and, partially, their results have been broadly discussed in the following works [5, 6, 7, 8, 10, 11, 12, 18]. The paper has been focused on the results concerning the relation between the number of the carried reefer containers and the load of the marine electric power system of the container vessels.

Six various types of container vessels owned by foreign ship owning companies were the subject of the tests. What seems interesting, the number of their carried reefer containers appeared considerably smaller than the possible maximum number assumed by the ship manufacturers. The analysis of documents [13, 14, 15, 16, 17] of one of the companies showed that such a situation has been maintained for several years. At the same time, when viewing the regulations of the international classification institutions [4], or the container ships energy balance [1], reefer containers with their maximum number assumed by the shipyard designing office appear the most

powerful receiver of electric power on board the ship. Thus, the aim was to estimate the relationship between the number of the carried reefer containers and the load of the marine electric power systems.

Because of the paper space limits there have been presented results achieved on a 2200 TEU container vessel built in Taiwan in 2003. The observations were carried out during a typical operational voyage from Europe to West Africa lasting for approximately a little more than thirty days. The number of the carried reefer containers usually appears considerably smaller than the possible maximum number of reefer containers to be loaded on board a ship (350 FEU). Power supply is provided by the marine power station consisting of four identical generating sets of rated active power 1200 KW each. The peak load recorded at the consecutive hours of the voyage was considered the measure of the active power of the marine electric power system (MEPS). The automatic measuring instruments of the power plant enabled the reading of the active power produced by the generating sets with the accuracy of 0,01 kW. When carrying the analyses the achieved values got rounded to 1 kW.

2. Results of the field tests

Due to the record of the peak loads of the 2200 TEU container vessel's electric power system, performed at the consecutive hours of the voyage, the scatter plot of peak loads of the marine electric power system depending upon the number of reefer containers was created by means of STATISTICA 8.0 with the correlation between the variables determined. The scatter plot [19, 20] with the correlation line (full line) and the limits of 95% of confidence interval have been presented in fig. 1.

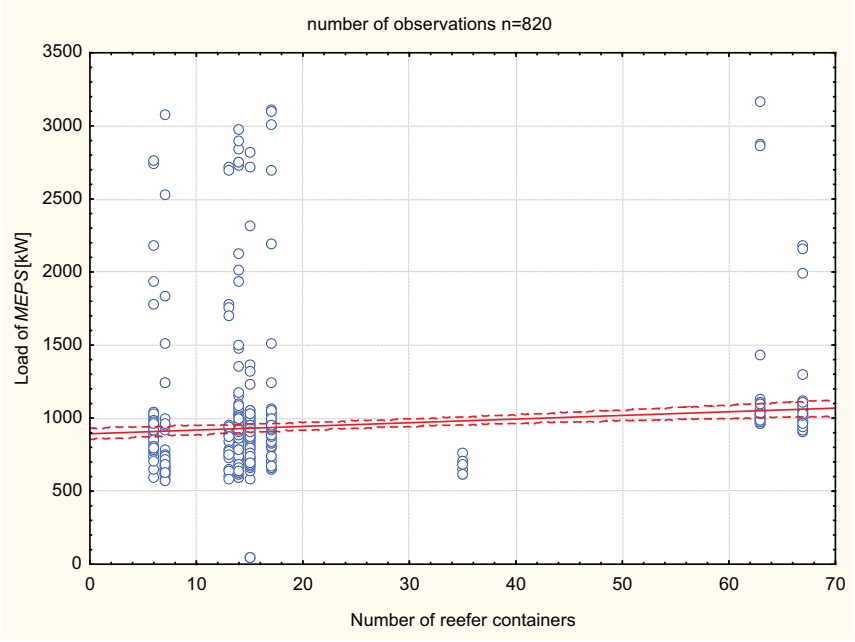

Fig. 1. The scatter plot between load of the container ship's electric power system (MEPS) and the number of carried reefer containers

Correlation between the active power load of the marine electric power system (N_{MEPS} [kW]) and the number of carried reefer containers ($k \leq 350$) has been presented by means of the formula:

$$N_{MEPS} = 893{,}004 + 2{,}5111k \text{ [kW]} \quad (1)$$

with the 95% confidence interval assumed.

In the process of testing there occurred a controlled black-out (break in the continuity of electric power supply) caused by the damage of the vessel sea water system and for a few hours power was provided by the emergency generating set. Thus, the data on peak load during the emergency generating set supply was rejected. In this way modified plot has been shown in fig. 2.

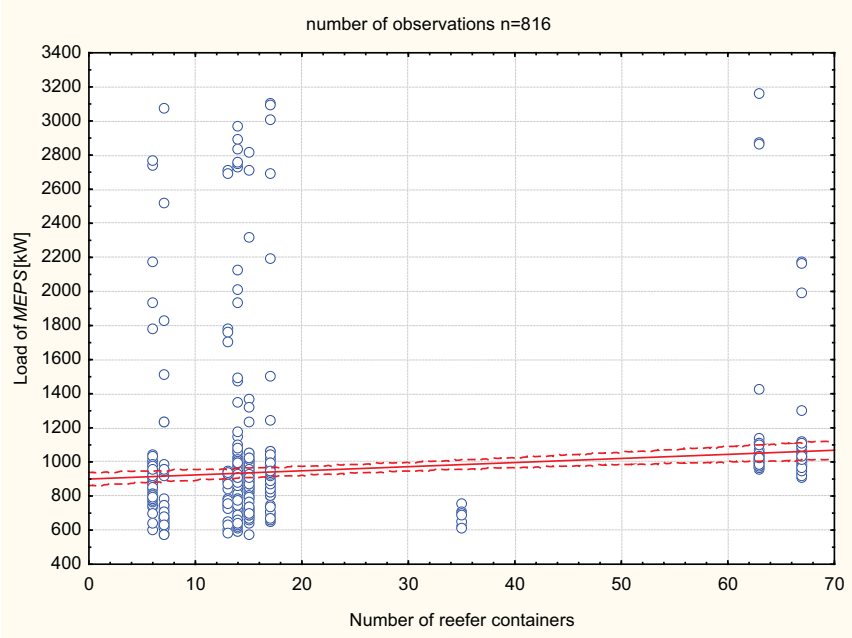

Fig. 2. The scatter plot between the load of the marine electric power system (MEPS) and the number of carried reefer containers without the data on peak load of the emergency generating set

The correlation between the active power load of the marine electric power system (N_{MEPS} [kW]) and the number of carried reefer containers ($k \leq 350$) is then presented as a formula:

$$N_{MEPS} = 899{,}8145 + 2{,}4158k \text{ [kW]} \quad (2)$$

at the 95% confidence interval assumed.

The rejection of the data on the peak load of the emergency generating set had negligible influence upon the scatter plot modification (fig. 1 and 2) as well as the function of linear correlation between the MEPS load and the number of reefer containers on board the ship – there is only few percent difference.

According to the data provided by the ship manufacturer [1] (classification supervision of the vessel during the process of her construction and operation was carried out by Bureau Veritas), it was calculated that the power demand for a single reefer container was 6,5257 kW. Thus, for the basic operational state, which is a sea voyage, the marine electric power system load (with the linear dependence upon the number of reefer containers) is defined by the formula:

$$N_{MEPS} = 767 + 6{,}5257k \text{ [kW]} \quad (3)$$

where $k \leq 350$.

The power demand of a single reefer container, achieved on the basis of the field data, appears 2,7 times lower than the values assumed by the manufacturer. However, it should be kept in mind that during the tests the number of reefer containers on board the ship did not exceed 70, which makes only 20% of their maximum number.

3. Regulations of classification institutions concerning the reefer containers power consumption

On the basis of the analyses presented in the previous chapter it seems to be worth referring to the regulations of selected classification institutions dealing with the ways of defining the reefer containers power demand. Classification Societies possess their own directives for estimation of the reefer containers power demand. The principles of determining the reefer containers power consumption have been presented in fig. 3 on the basis of Germanischer Lloyd regulations [4]. In case of the lack of field data it is recommended that the following principles are applied when balancing the power demand [4]:

- for a single 20' container – 8,6 kW;
- for a single 40' container – 12,6 kW.

The level of the assumed coincidence factor is 0,9 [4].

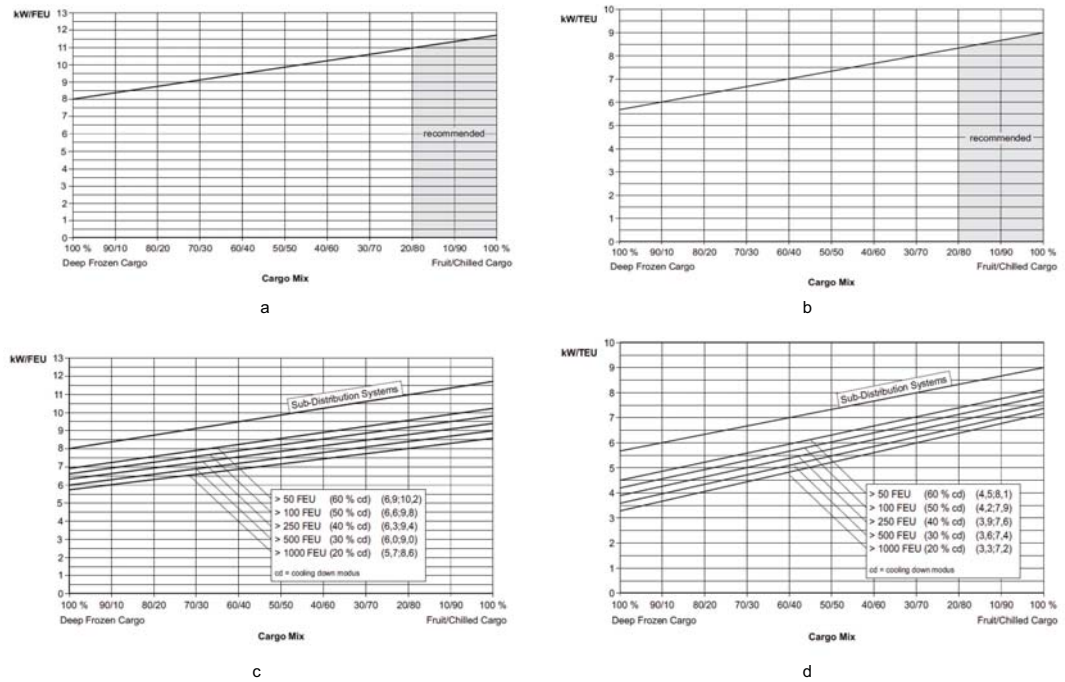

Fig. 3. GL directives for defining the power demand of the cargo hold ventilation system and reefer containers: a) and c) in case of 40' reefer containers; b) and d) in case of 20'reefer containers, according to [4]

The above presented GL regulations appear even more protective than the ones applied during the construction of the vessel, the subject of the analyses presented in the paper. Such approach of the classification institutions may cause a considerable overestimation of the reefer containers power demand and lead to long lasting operation of generating sets at low load, especially in case of a number of carried containers smaller than the one recommended by the ship manufacturer for power balancing. This may endanger the shipping company to considerable financial losses due to the deterioration of the technical condition of auxiliary engines fed mostly with residual fuels [2, 3, 9, 10].

4. Final remarks

During the process of 2200 TEU container vessel construction, when balancing the electric power demand, the shipyard designing office assumed that at the total number of 350 reefer containers to be loaded, the load per one container equaled 6,5257 kW, that is almost three times higher than the result obtained due to the calculations carried out by the author on the basis of the field data. This low value estimated by the author may result from the relatively small number of reefer containers carried at the time of tests. It should be noted that not all ship owners of container vessels transport vast numbers of reefer containers, what is proved by the data collected on the six container ships, the subject of tests. Thus, the shipyard designing departments should make use of such documents as [13, 14, 15, 16, 17] possessed by the ship owner technical services while designing the number of socket connections for reefer containers to be plugged in and estimating their power demand. This type of exaggerated equivocation of classification companies and ship manufacturers may lead to considerable overestimating concerning the assessment of electric power demand and adjustment of the number of power generating sets, which puts the shipping companies at risk of financial losses. In case of 1100 TEU container vessels, the subject of the tests, the ship owner technical services decided to have the residual fuel oil for auxiliary engines to be changed for the distilled fuel due to the low loads of generating sets. This way of long lasting (several years) operation has significantly increased its costs. Moreover, a part of power plant fuel system turned out useless (e.g. residual fuel oil heating system). At the same time the auxiliary engines operation at low loads caused accelerated deterioration of their technical condition, especially the fuel injection equipment. In order to avoid this type of mistakes, it seems necessary to make use of field data at the stage of designing vessels. The knowledge of real electric power demand, or the data on the number of carried reefer containers allows for adjusting the product – a newly constructed vessel – to the requirements of a recipient (a shipping company).

References

[1] China Shipbuilding Corporation, *Electric Load Analysis – 2200 TEU Container Vessel, HNO. 777*. Taiwan 2002.

[2] Cichy, M., Kowalski, Z., Maksimow, J.I., Roszczyk, S., *Statyczne i dynamiczne własności okrętowych zespołów prądotwórczych*. Wydawnictwo Morskie, Gdańsk 1976.

[3] Figwer, J., *Zagadnienie wielkości mocy silnika napędowego w okrętowych zespołach prądotwórczych*. Budownictwo Okrętowe Nr 6, 1962.

[4] Germanischer Lloyd, *Rules for Classification and Construction,* Volume I *Ship Technology,* Part 1 *Seagoing Ships,* Chapter 3 *Electrical Installations*, Edition 2009.

[5] Kijewska, M., Matuszak, Z., Nicewicz, G., *Identyfikacja obciążeń systemu elektroenergetycznego siłowni okrętowych w rzeczywistych warunkach eksploatacyjnych*. SYSTEMS Journal of Transdisciplinary Systems Science Vol. 11 2006, pp. 334-340.

[6] Kijewska, M., Nicewicz, G., *Analiza rozkładu obciążeń zespołów prądotwórczych elektrowni okrętowej statku transportowego dla wybranego stanu eksploatacyjnego*. Надежность и Эффективность Технических Систем. Международный Сборник Научных Трудов, KGTU, Kaliningrad 2004, pp. 64-72.

[7] Kijewska M., Nicewicz G., *Estymacja gęstości rozkładu obciążeń zespołów prądotwórczych elektrowni okrętowej w wybranym stanie eksploatacji*. Zeszyty Naukowe Politechniki Gdańskiej nr 598 (seria: Budownictwo Okrętowe Nr LXV), Gdańsk 2004, pp. 79-87.

[8] Kijewska M., Nicewicz G., *Rozkłady empiryczne a rozkłady teoretyczne obciążeń autonomicznych zespołów prądotwórczych elektrowni okrętowych*. Надежность и Эффективность Технических Систем. Международный Сборник Научных Трудов, KGTU, Kaliningrad 2005, pp. 124-131.

[9] Kuropatwiński, S., Lipski, T., Roszczyk, S., Wierzejski, M., *Elektroenergetyczne układy okrętowe*. Wydawnictwo Morskie, Gdańsk 1972.
[10] Matuszak, Z., Nicewicz, G., *Assessment of excess power factor in marine generating sets*. Journal of POLISH CIMAC – ENERGETIC ASPECTS, Vol. 3, No. 1, Gdańsk 2008, pp. 95-101.
[11] Matuszak, Z., Nicewicz, G., *Assessment of hitherto existing identification tests of marine electric power systems loads*. Polish Journal of Environmental Studies, Vol. 18, No. 2A, Olsztyn 2009, 110-116.
[12] Matuszak, Z., Nicewicz, G., *Wykorzystanie szeregów czasowych do analizy obciążeń izolowanych systemów elektroenergetycznych*. Systemy Wspomagania w Zarządzaniu Środowiskiem – Monografia pod redakcją J. Kaźmierczaka, Zabrze 2008, pp. 185-191.
[13] MIDOCEAN Ship's Office, *Machinery abstracts, m/v Suzanne Delmas, Voyage 875, 879,* 2002.
[14] MIDOCEAN Ship's Office, *Machinery abstracts, m/v Suzanne Delmas, Voyage E17, EFE315, EFE 316, 323, 2003*.
[15] MIDOCEAN Ship's Office, *Machinery abstracts, m/v Mol Horizon, Voyage 419, 423, 427, 431, 435,* 2004.
[16] MIDOCEAN Ship's Office, *Machinery abstracts, m/v Mol Horizon, Voyage 503, 506, 509, 512, 515, 518,* 2005.
[17] MIDOCEAN Ship's Office, *Machinery abstracts, m/v Mol Rainbow, Voyage 611, 616, 621, 626, 631, 636, 641,* 2006.
[18] Nicewicz G., *Obciążenie okrętowego systemu elektroenergetycznego a bezpieczeństwo statku*. Zeszyty Naukowe AMW im. Bohaterów Westerplatte Nr 168 K/1, X Konferencja Morska „Aspekty bezpieczeństwa nawodnego i podwodnego oraz lotów nad morzem", Gdynia 2007, pp. 205-215.
[19] Stanisz, A., *Przystępny kurs statystyki*. *Tom 1*. *Statystyki podstawowe*. StatSoft, Kraków 2006.
[20] StatSoft - *STATISTICA 8.0*., *Podręcznik elektroniczny STATISTICA*.

Journal of POLISH CIMAC
Faculty of Ocean Engineering & Ship Technology
GDAŃSK UNIVERSITY OF TECHNOLOGY

IMPULSE ACTION OF UNDERWATER SHOCK WAVE AS A CAUSE OF DISABLING THE SHIP POWER PLANT

Zbigniew Powierża, Beata Wojciechowska

Gdynia Maritime University
Faculty of Marine Engineering
ul. Morska 83-87, 81-225 Gdynia, Poland
tel.: +48 58 6901 331, fax.: +48 58 6901 399
email: bearud@am.gdynia.pl

Abstract

This paper presents action of shock wave resulting from an underwater non-contact explosion, exerted on ship hull plating. The impulse load was considered in the range of wave regular reflection and refraction at the boundary of two media: water and steel. In most cases the impulse action leads to failures or damages of elements of ship power plant as well as shipboard equipment, however without endangering ship's floatability. Typical kinds of failures which recurred on ships of various tonnage, are presented, a.o., on the example of ships sailing in Red Sea waters during Iraq-Iran war.

Keywords*: explosion, pressure, shock wave, destruction*

1. Introductory remarks

Underwater non-contact explosion does not cause usually ship's sinking but only complete loss of its maneouvrability due to many failures in the ship's power plant and shipboard equipment. And, ship's hull plating which takes up the first impulse of load may sustain local plastic deformations; the loss of ship's maneouvrability does not constitute itself a danger in the case of ships not engaged in warfare as it took place e.g. during Iraq-Iran war where a dozen or so ships flying various flags sustained failures. A good example describing consequences of explosion is a general cargo ship, m/s „Józef Wybicki"[1]. In the case of ships taking part in warfare (e.g. convoys to Murmansk) such situation became extremely dangerous and usually led to ship's loss.

On all the ships such failures due to impact load were similar. The most endangered were elements made of fragile materials, e.g.: cracks in shaftline casings, lugs of foundations of combustion engines and electric motors, tearing off electric driving motors of compressors, pumps and hoisting winches (fig. 1, 2, 3).

Another type of failures are plastic deformations of screw joints, bending deformations of main engine crankshafts and propeller shaft segments. Radiocommunication and navigation equipment sustains failures of another type [1, 5].

This way, i.e. as a result of non-contact explosion of mines, 17 ships in total have been damaged during one month in Red Sea waters.

Depending on magnitude of experienced impulse load the ships had to be subjected to various repairs: beginning from minute repairs performed by crew personnel itself to serious repairs

in shipyards, lasting many months.

Fig. 1. A crack in upper casing of shaftline bearing

Fig. 2. Foundation bolts torn off the seating of main engine's turbocharger

Fig. 3. Electric driving motor torn off the hoisting winch body

2. Reflection and refraction of two-dimensional acoustic wave

Value of impulse load resulting from shock wave action to ship's hull plating decides on acceleration to which ship equipment elements are subjected.

In [2] is presented the load resulting from shock wave reflection from non-deformable plane, both in the regular and irregular range.

In this paper the load applied to a flat wall is considered in regular range, with taking into account wave refraction at its passing into the other medium.

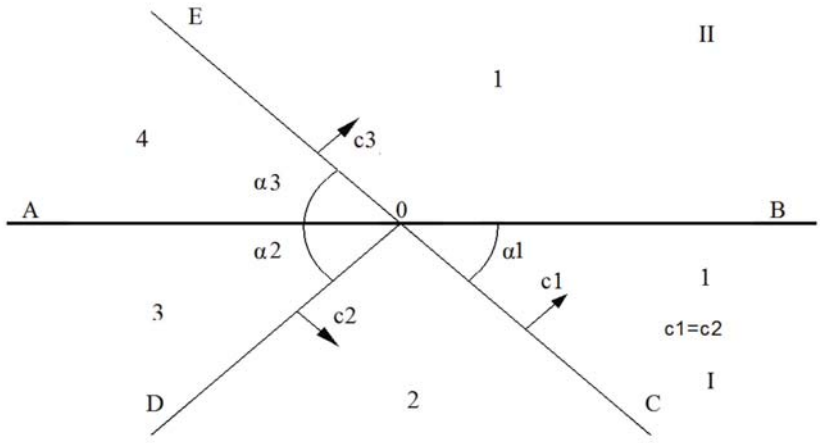

Fig. 4. Acoustic wave reflection from and refraction at a flat wall

Fronts of incident wave and reflected one propagate in the medium I (water). The refracted wave penetrates the medium II (steel). In the zone 1 limited by the front of the waves OC and OE the both media, I and II, are undisturbed. In the zone 2 between the incident wave and reflected one, OC and OD, the medium is disturbed at the parameters of the incident wave. In the zone 3 between the dividing boundary AB and the reflected wave front OD, the medium I is disturbed by the reflected wave parameters. In the zone contained between the refracted wave front OE and the dividing boundary AB, the medium II is disturbed by the refracted wave parameters (fig. 4).

Where:
AB – boundary between two media: I and II,
OC – incident wave front,
OD – reflected wave front,
OE – refracted wave front,
α_1 – incidence angle,
α_2 – reflection angle,
α_3 – refraction angle,
c_1, c_2, c_3 – wave propagation velociti*es* in the media: I and II, respectively,
ρ_1, ρ_2 – density of the media: I and II,
p_1, p_2, p_3 – pressure of incident, reflected and refracted wave, respectively.

By making use of: the regular reflection condition, the crossing point of wave fronts on the boundary of media, Snellius principle, as well as the continuity conditions [4] it yields:

from the reflection condition: $\alpha_1 = \alpha_2$ i $c_1 = c_3$

and, from the Snellius principle:

$$\frac{c_1}{\sin\alpha_1} = \frac{c_3}{\sin\alpha_3} \Rightarrow \frac{\sin\alpha_1}{\sin\alpha_3} = \frac{c_1}{c_3} \tag{1}$$

From the continuity condition of velocity of normal displacements and pressures on the dividing boundary of the media it results that:

$$\begin{aligned} c_1\cos\alpha_1 - c_2\cos\alpha_2 &= c_3\cos\alpha_3 \\ p_1 + p_2 &= p_3 \end{aligned} \tag{2}$$

The formulas for pressure of reflected wave and refracted one have the form:

$$\frac{p_2}{p_1} = \frac{\rho_2 c_3\cos\alpha_1 - \rho_1 c_1\sqrt{1-\frac{c_3^2}{c_1^2}\sin^2\alpha_1}}{\rho_2 c_3\cos\alpha_1 + \rho_1 c_1\sqrt{1-\frac{c_3^2}{c_1^2}\sin^2\alpha_1}} \tag{3}$$

$$\frac{p_3}{p_1} = \frac{2\rho_2 c_3\cos\alpha_1}{\rho_2 c_3\cos\alpha_1 + \rho_1 c_1\sqrt{1-\frac{c_3^2}{c_1^2}\sin^2\alpha_1}} \tag{4}$$

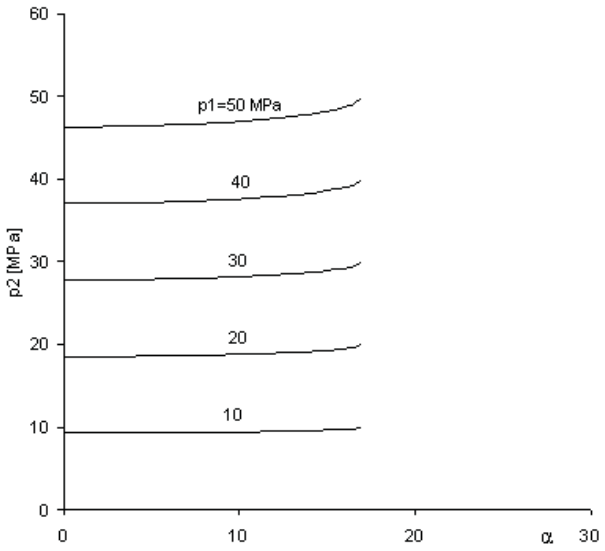

Fig. 5. The pressure p_2 on the reflected wave front in function of the incidence angle α_1 and the shock wave pressure p_1

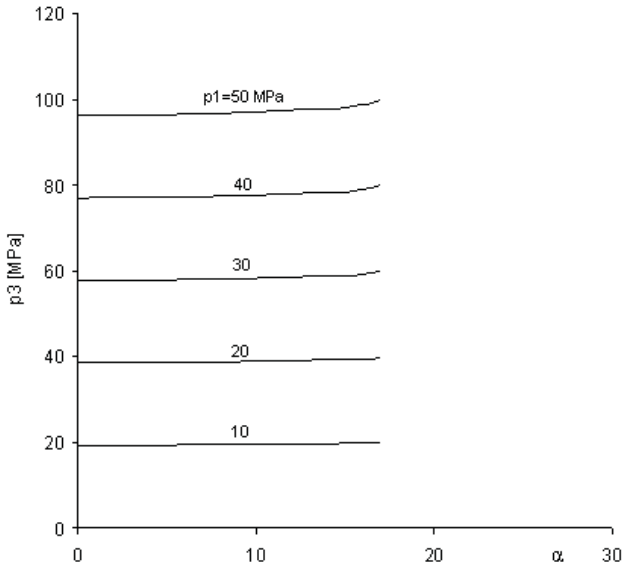

Fig.6. The pressure p_3 on the refracted wave front in function of the incident angle α_1 and the shock wave pressure p_1

The shock wave pressure at cross-section of a perfectly stiff wall was considered in [2]. Formulating the equation of mass conservation, equation of momentum, and equation of the state Teta, one has calculated the pressure acting on ship's hull plating (i.e. the pressure due to reflected wave), hence also the impact load.

The pressure p_2 applied to the wall in function of the incidence angle α_1 and the shock wave pressure p_1 is presented in fig. 7:

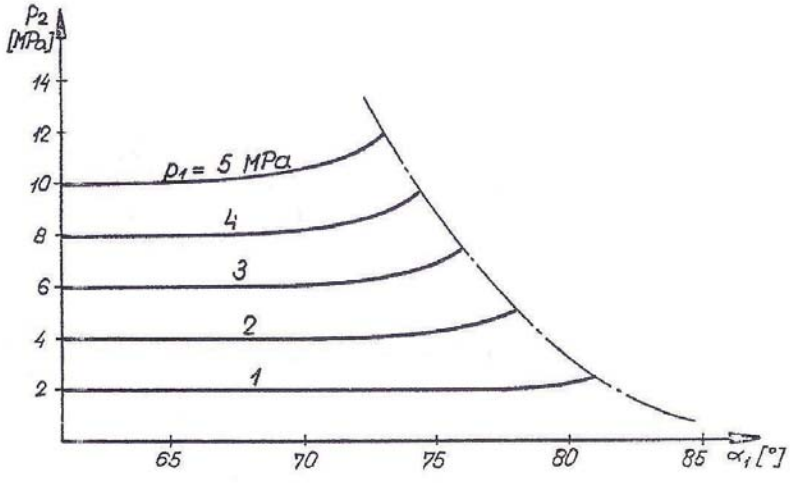

Fig. 7. The pressure p_2 applied to the wall in function of the incidence angle α_1 and the shock wave pressure p_1

3. Remarks and conclusions

As results from the above given formulas, the ratio of the reflected wave pressure and the refracted wave pressure to the incident wave pressure depends on the acoustic wave resistance of the media and the incidence angle α_1. In the case when the medium II is more stiff than the medium I, i.e. $c_2 > c_1$, real values of reflection coefficient are obtained at the angle values $\alpha_1 \le \alpha_{kr} = arc\sin\frac{c_1}{c_3}$. In the considered case: $c_1 \approx 1500\frac{m}{s}$ (water), $c_3 \approx 5000\frac{m}{s}$ (steel), $\alpha_{kr} = arc\sin 0{,}3 = 17°30'$. At a high value of wall stiffness the pressure p_3 (fig. 6) and pressure p_2 (fig. 5) differs only a little to each other in this range, hence the assumption on perfectly stiff wall results in loads greater than real ones.

As a result of explosion a part energy is transferred into stiff hull structure and propagated inside the ship through particular structural elements which serve as a kind of waveguides. Difraction, refraction and interference of waves takes place. In consequence apart from damages of elements made of fragile materials, also failures of joints of steel elements occur.

References

[1] Dobrociński, S., Powierża, Z., *The consequences of underwater explosion on the general cargo vessel ms „ Józef Wybicki"*, Journal of Kones, Powertrain and Transport Vol. 14, No. 1, Warszawa '2007.

[2] Powierża, Z., *Wytrzymałość ogólna kadłuba okrętu przy niekontaktowych wybuchach podwodnych*, Zeszyty Naukowe AMW No 108A, Gdynia 1991.

[3] Włodarczyk, E., *Skośna regularna refrakcja płaskich fal akustycznych i uderzeniowych ośrodku wielofazowym*, Biuletyn WAT No 12, Warszawa 1973.

[4] Włodarczyk, E., *Fale uderzeniowe w ośrodkach ciągłych*, WAT, Warszawa 1977.

[5] Klatka, N., *Analiza strat statków w latach 1981 – 1984 w wyniku działania broni rakietowej i min*, Technika i Uzbrojenie No 6, 1986.

Journal of POLISH CIMAC
Faculty of Ocean Engineering & Ship Technology
GDAŃSK UNIVERSITY OF TECHNOLOGY

SYSTEMIC STRUCTURE OF THE KNOWLEDGE ON TECHNICAL OBJECT MAINTENANCE

Leszek Powierża
Warsaw University of Technology
ul. Łukasiewicza 17, 09-400 Płock, Poland
tel.: +48 24 3675995, fax.: +48 243675995
inzsyst@pw.plock.pl

Abstract

Against the background of mentioned semantic, methodical and essentials flaws and errors in articulation and generating of the maintenance and operating knowledge, transferred in education, scientific and popularizing literature as well as in realization of the maintenance activities, a proposal concerning systemic configuration of this knowledge was presented in this paper. Taking into account that the semantic aspects of essence articulation in presented proposal make the substance of these considerations, the names of scientific disciplines and the terms of specific notions are given in Polish language.

Keywords: *action, exploitation, knowledge, maintenance, methodology, operation, system, science, theory*

1. Introduction

For effective realization of activities ensuring the technical systems to be set in motion – including the main systems of ship driver – apart from material, energy and time resources, the adequate knowledge on operating and maintenance is necessary. However, the effectiveness of such activities depends not only on essential correctness of this knowledge but also on its practical usability. First of all the knowledge ought to be configured and drafted correctly and clearly, in essence, methodology and semantics.

From the systematic view point the operation and maintenance knowledge is a market product and the demand for it depends not only on its essential correctness but also on its semantic and methodological "wrapping". Systemic configuration of the maintenance and operation knowledge increases the communicativeness of its articulation and perception.

2. Problem

Within the limits of this pronouncement it is possible only to relate to some subjectively selected principal questions.

Quite large group of flaws to be noticed in texts fixing the knowledge – not only on the operation and maintenance includes the semantic – methodological flaws which consist in occurring inadequacy of the terms and ideas a well as some methodological deficiencies. As an example may be mistaking the notions such as "thesis" and "hypothesis" or using "thesis in situations where it should not be used. It deals also with the following relations: *działanie – funkcjonowanie, działanie – proces, zależność – związek, równanie – teoria, wielkość – wartość, liczba – cyfra, wyznaczanie – określanie, pojęcie – termin, masa – materia* (action – functioning,

action – process, relationship – connection, equation – theory, magnitude – value, number – figure, determining – qualifying, notion – term, mass – matter).

To frequent cases belongs also unperceiving the defferences between a physical quantity and its symbol and – consequently – mistaking "equation" as symbolic structure with the relationship between physical quantities, or the errors consisted in personification of the things though attributing them the causative power.

3. Basic notions

Postulated usability of systemic formulation ought to be revealed beginning from the remembrance of necessary basic notions, starting with the key notion of "system" important for further considerations. In accordance with Wintgen`s [6] set theory we assume that system (S) is a functional whole, or the set of determined elements (E), provided to of determined relations (R), what may be written as:

$$S = < E, R >$$

Consequently, it may be assumed that generator of subject knowledge – in this case the knowledge on maintenance and operation – is adequate subjective "scientific discipline", treated according to Greniewski [1] definition, as "relatively individual informatic system" (fig.1).

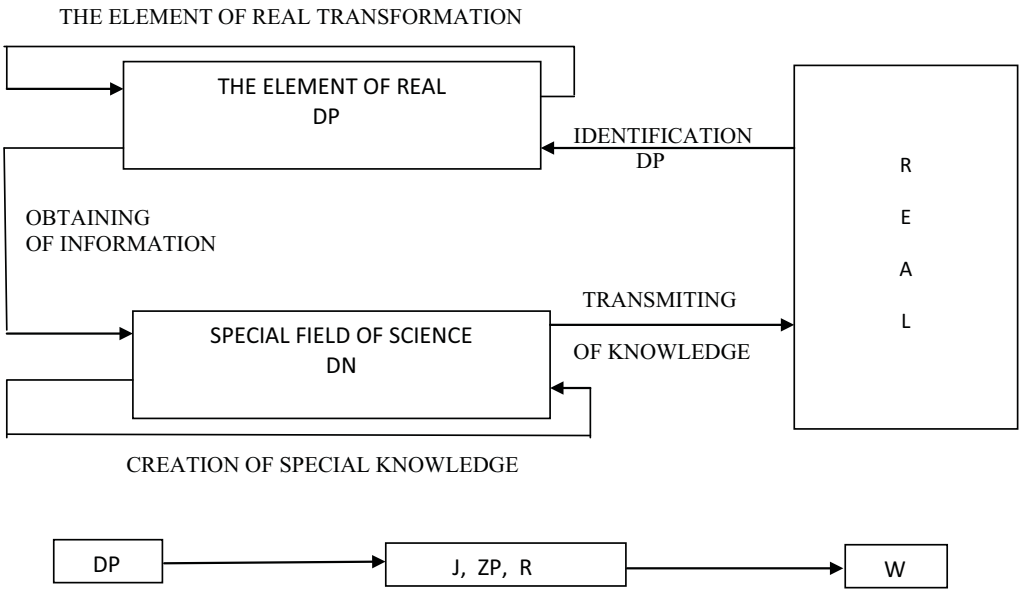

Fig. 1. Model of special field of science as a systems

$$DN = < DP, J, ZP, R; W >$$

where: DN – scientific discipline,
DP – subjective domain, J – language, ZP – laws, R – rules, W – knowledge.

During gaining applicable knowledge numerous circumstances may occur which threaten its credibility, quality and finally – its practicability. The reason of such a situation consists in

ambiguous identifications included into given system of elements.

From the systemic view point the language of scientific discipline creates a set of elementary systems TPD (fig. 2) called the Ogden – Richards triangle [6]

$$J = < T, P, D : RI >$$

where: J – language, T, P, D – term, notion, designation, RI – relations among: T, P, D.

The source of many diversities in meaning at interpretation of the maintenance and operations knowledge is lighting the univocal character requirements of relations occuring among the TPD system elements, i.e. among the term, notion and designation.

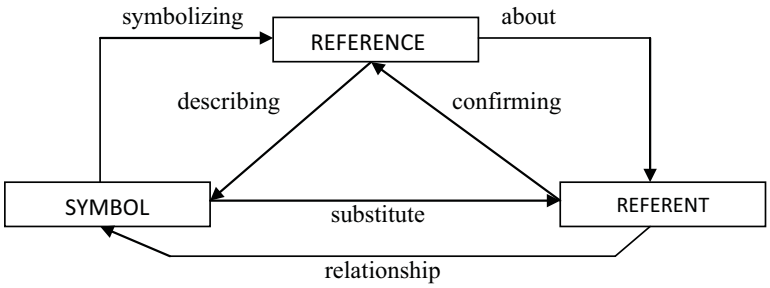

Fig. 2. TPD System [5]

Resigning the wider descripion of mentioned flaws, it is still necessery on selected exaples, to explain - as: *hipoteza, teza, teoria, równanie, zależność, związek korelacyjny, czy współwystępowanie (hyphotesis, thesis, theory, equation, dependence, correlation or joint appearance).*

Thus, *„udowodnienie hipotezy" (proof of a hyphothesis)* – as often may be read – is an methodological error; the hyphothesis is not a theorem, but only an assumption, the rightness of which may be doubtful and its configuration would be needful.

A mistake is also to make use of the "theasis" in empirical sciences as it a theorem which needs to be confirmed, what is possible in the formal sciences only. Commonly used term "równanie teoretyczne" (theoretical equation) is also a redundancy what may be easily proved on the basis of systemic formulation. Both, the "theory" and "equation" are the systems. Equation, as an element of the theory, is used to its formal articulation.

The "theory" is an abstract structure (R) created to describing the relations appearing among concrete and abstract objects of reality; it forms a functional whole or the system (TE) of the laws (P), rules (Z), theorems (T) and hypotheses (H):

$$TE = < P, Z, T, H; R >$$

Whereas the "equation" is an abstract structure being a notion of relations among the symbols which, together with the relations, create a functional while, i.e the "system".

The fault is also to misinterpret the "eqation" – a formal structure built of the symbols, and the "dependence" on "correlation connections". "Dependence is such an eqation where concrete physical magnitudes are the symbols and it expresses the causative – "correlation connection" means their coexistence described by an eqation in which concrete physical magnitudes are the symbols. An example of wrong interpreting the terms of "process" and "activity" (działanie) are controversions around the definition of "maintenance and operation" (eksploatacja). "Activity is

a sequence of elementary changes in objective state of reality fragment caused by human influence, whereas the "process" is a sequence of elementary changes in objective state of reality fragment affected by the impact of various factors, where the human participation is not necessary. Thus, the "activity" (działanie) consists in creating the process in most possible and expected way. In accordance with Polish language convention the name`s ending for "activities" is "- anie", while for the "process" – cja"[5].

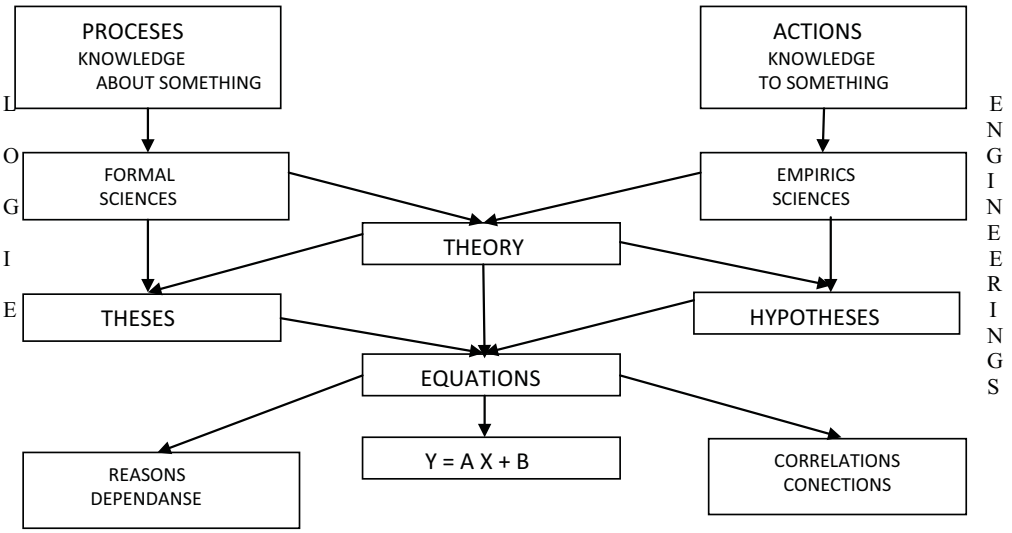

Fig. 3. The structural model of science

In the case of systems such as objectively oriented scientific disciplines, their functions – in general formulation (fig. 3) – may consist in shaping and configuration of knowledge:

- about something, i.e. on the processes, phenomena and relations, or on informatively available, existing concrete and abstract objects of the reality;
- to something, i.e. to realize activities consisted in creating the new existences, not appearing in such a shape.

Sciences of the first group, conventionally and according to custom, are determined as the basic sciences, sciences of the second group – as the applied ones. The objective sphere, not fully covering the essential division, is division into "formal" (formalne) and "empirial" sciences, based on methodological premises. In semantic convention, the names of basic disciplines – sciences on the processes, phenomena and relations, have in Polish language the ending "- logia". Thus, they may be conventionally named "- logie", as opposed to appleied disciplines, supplying the kowedge necessary for activities, which may be called as "techniques" (techniki) or "engineerings" (inżynierie). From methodological view point both mentioned groups are distinguished in this, that "- logies" generate knowedge on the basic of information, whereas the "techniques" (engineerings) – on the basic of knowledge generated by "logies". Techniques (engineerings), generating the knowledge objectively directed, are functioning as the tools useable in practical activities. What are them the sources of interesting us "maintenance and operation" knowledge?

4. The maintenance and operation knowledge

The starting point to articulate the range of knowledge useful for keeping the systems moving

is an identification of this action during exiting of the system (fig. 5) as a phase of resource circulation process (fig. 4).

Fig. 4. Real circulation of the resources

Perceiving the difference between process and activity, and using terminology in convention of the Polish language, the process of exhausting usable resources contained in the object will be named – "eksploatacja" (exploitation) while the activity consisted in extraction of these resources – "eksploataowanie" (exploiting).

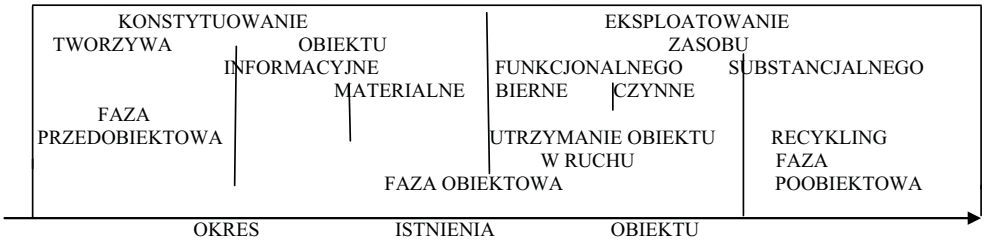

Fig. 5. Phases of the objects` life

Fig. 5 shows that the process of object exploitation proceeds since the moment of its arising until the management of substantial resources contained in it (object and postobject phases), being in continuous relations with its infrastructure (fig. 6).

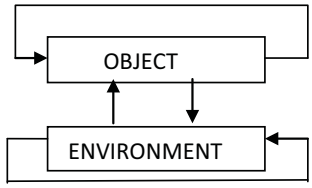

Fig. 6. Object and environment

After decomposition of object infrastructure into: technological infrastructure (everything connected with realization of functions attributed to the object), exploitation (maintenance and operation) structure ensuring realization of these functions by the object, as well the environmented structure (reminder of ecological and sozological environment), the maintenance and operation (exploitation) situation of the object , in most generalized formulation, will be look on the fig. 7.

During whole exploitation period the object may find itself in the state of passive (fig. 8a) or active exploitation.

At the state of active exploitation, when the object is being exploited it may be in the conditioning (fig. 8b) or functional (fig. 7) stage.

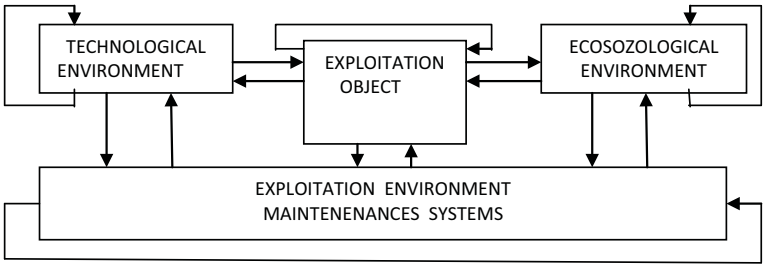

Fig.7. General configuration of object exploitation. Object in of functional exploitation state [3]

When the object is not subjected to the effect of technological and exploitation infrastructures, being affected by the environmental infrastructure only, then it is in the state of passive exploitation (fig. 8a).

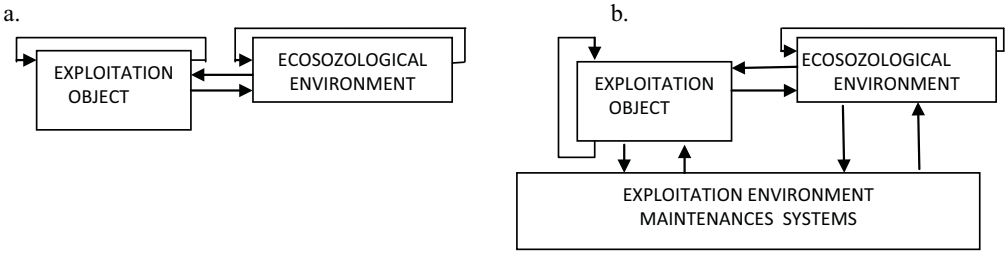

Fig. 8. Exploitation configurations of the object: a – passive exploitation, b – active exploitation, configuration of conditioning (treatment) exploitation

Diversity of the phenomena processes and activities taking place during exploitation, as resulted from a number of various relations among the object elements and its infrastructure, generates demand for the knowledge necessary to realize exploitation activities, i.e. to keep the technical systems in motion. This knowledge is being obtained from many different scientific disciplines including these phenomena, processes and activities as the subject of scientific cognition.

According to earlier identification of scientific disciplines, the science on exploitation as a process of exhausting the resources of used object, will be called “exploitology”
(eksploatologia). Exploitology supplies the knowledge on exploitation process, through the compilation of knowledge acquired in many specialistic scientific disciplines engaged in cognition of the phenomena affecting the course of process.

The course of exploitation process is affected, apart from the environmental process, also by

exploitation activities or exploiting and therefore, getting out the useful resources contained in the object. The science supplying knowledge on exploiting will be named "exploitation engineering". The knowledge on exploiting is formed on the basis of knowledge taken from other, kindred branches of engineering, as well as from the knowledge on "exploitology" and "exploitics", engaged in exploitation techniques and implements.

The whole of knowledge on exploitation, i.e. exploitation process and accompanied connected process, as well as on exploiting and participating in it activities, may be named "exploitation cognitivistics" (kognitiwistyka eksploatacyjna) which may be treated as some scientific "metadiscipline" fed by many subject – directed disciplines [3].

Specification of these disciplines, presented in fig. 9, may be treated as an identification of the state of exploitation knowledge sources, necessary to designing, generating and exploiting the technical objects, as well as to keeping them in motion.

Procesy	Narzędzia	Działania
LOGIE	TECHNIKI	INŻYNIERIE
EKOLOGIA KWALITOLOGIA MATERIAŁOLOGIA METODOLOGIA METROLOGIA PSYCHOLOGIA PRAKSEOLOGIA REOLOGIA SOCJOLOGIA SOZOLOGIA SYSTEMOLOGIA TECHNOLOGIA TRIBOLOGIA	CYBERNETYKA EKONOMIKA ERGONOMIKA INFORMATYKA MATEMATYKA MECHATRONIKA MECHANIKA METRONIKA PROBABILISTYKA STATYSTYKA TRIBONIKA	INŻYNIERIA EKONOMICZNA INŻYNIERIA ERGONOMICZNA INŻYNIERIA INFORMATYCZNA INŻYNIERIA JAKOŚCI INŻYNIERIA LOGISTYCZNA INŻYNIERIA MATEMATYCZNA INŻYNIERIA MECHANICZNA INŻYNIERIA MECHATRONICZNA INŻYNIERIA METROLOGICZNA INZYNIERIA NIEZAWODNOŚCI INŻYNIERIA PRAKSEOLOGICZNA INŻYNIERIA REOLOGICZNA INŻYNIERIA SYSTEMÓW INŻYNIERIA SOZOLOGICZNA INŻYNIERIA TRIBOLOGICZNA INŻYNIERIA WIEDZY
EKSPLOATOLOGIA	**EKSPLOATYKA**	**INŻYNIERIA EKSPLOATACJI**
K O G N I T Y W I S T Y K A E K S P L O A T A C Y J N A		

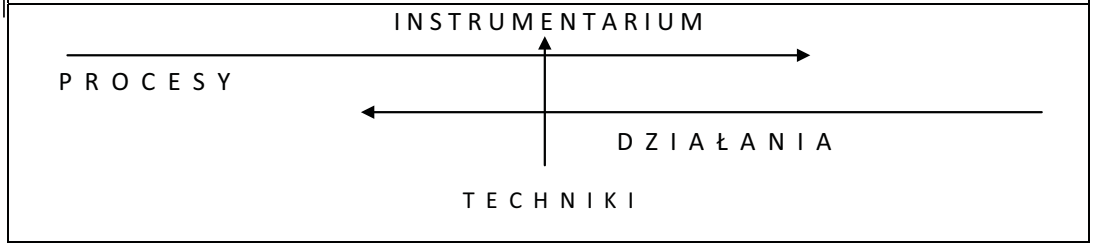

Fig. 9. Model of exploitation knowledge resources

In particular it deal with the combustion engines, as well as the machines and devices necessary to keep these engines in motion within the technological structure such as a ship, and also within environmental structure where the ship occurs.

Structural model of exploitation as a process, considering the activities and exploitation states, may be presented in form as given in fig. 10.

There are presented in the model (fig. 10) the states and activities occurring in objective stage of exploitation, thus refered to that, what in exploiting means keeping the system in motion. The feedbecks in particular stages of exploitation were neglected in the figure. It was also necessary to resign the description of post – object exploiting stage, or the recycling phase, including management of usable object resource which left in substancial form after using up the resources for functioning.

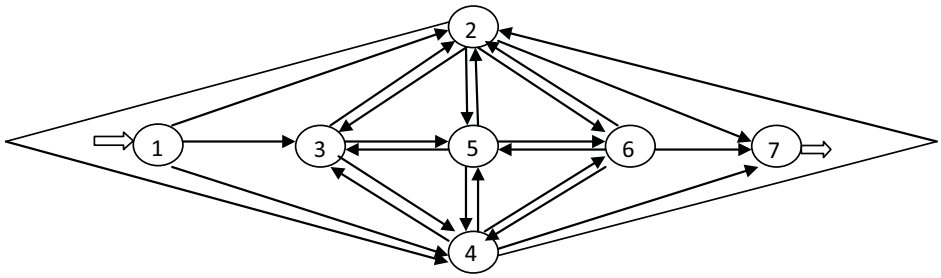

Fig. 10. Model of objects exploiting. 1 – classification, 2 – operators service, 3 – supplying service, 4 – awaiting, 5 – treatment service, 6 – storage, 7 – removal (liquidation)[4]

5. Termination

Presented systemic identification of wide spectrum of the scientific disciplines as the knowledge source, showed very strong objective differentiation and wide thematic extension of exploitation knowledge [2]. This multiweft specificity inclines to assumption that the exploitation knowledge is generated in the sphere of some "meta – science", which may be defined as "exploitation cognitivistics" (kognitywistyka eksploatacyjna).

It is rather difficult to expect that on the basis of knowledge from one discipline will be possible to realize the tasks defined in subject matter of this conference: they include designing, production and exploitation with the aspect of keeping in motion the ship driving systems, considering the safety, diagnostics, ecological abilities, energy consumption, functionality, logistics as well as the reliability, serviceability, optimiziation, rationality, controllability and usability.

References

[1] Greniewski H. *Cybernetyka niematematyczna*, PWN, Warszawa 1969
[2] Lewitowicz J.,*Podstawy eksploatacji statków powietrznych*, ITWL, W-wa 2007
[3] Powierża L. *Eksploatacja, eksploatyka, eksploatologia – czyli kognitywistyka eksploatacyjna*, Zagadnienia Eksploatacji Maszyn, z. 2 (126), 2001, s. 235 – 244
[4] Powierża L. *Systemowe podstawy eksploatacji*, Materiały Międzynarodowej Konferencji EXPLO- DIESEL'03, Gdańsk – Lund, 2003, s. 501 – 510
[5] Powierża L. *Semantyczne aspekty terminologii*, Inżynieria Systemów Bioagrotechnicznych, z. 2-3 (11 – 12), 2003, s. 99 – 106
[6] Wintgen G. *System cybernetyczny w świetle teorii mnogości*, Problemy Organizacji, z.2, 1972

Journal of POLISH CIMAC
Faculty of Ocean Engineering & Ship Technology
GDAŃSK UNIVERSITY OF TECHNOLOGY

IDENTIFICATION OF SHIPS PROPULSION ENGINE OPERATION BY MEANS OF DIMENSIONAL ANALYSIS

Jan Rosłanowski

Gdynia Maritime Academy
Faculty of Marine Engineering
81-87 Morska str.
81-225 Gdynia Poland
e-mail: rosa@am.gdynia.pl

Abstract

The following article presents the metod of determining the ship´s propulsion engine operation basing on the engines work parameters by means of dimensional analysis .The ships propulsion engine activity, as noticed by J. Girtler in his works [4,5], can be used for its diagnostics. of ship propulsion. Diagnostics engines increases safety of ships movement and at the same time protects the sea environment from pollution in case of its sinking. According to Girtler engine operation can be considered as, a new physical quantity of dimension Joul multiplied by second $[J \cdot s]$. *This quantity can be determined on the basis of algebraical diagram of dimensional analysis constructed by S. Drobot. This diagram allows to control the correctness of conclusion rules, in respect of mathematics, used in numerical functions of ship propulsion engine operation.*

Keywords: *ship propulsion engine operation dimensional analysis, diagnostics of ship engine*

1. Introduction

The Basic operating problem of ship propulsion systems is diagnostics of ship propulsion engines. Loss of operational capability of ship propulsion engine endangers the ships movement and in case of ship´s sinking may cause dangerous pollution of sea environment. Diagnostics of ship propulsion engines, as noticed by J. Girtler in the works [1,2,3], can be carried out by means of engine operation. Engines operation is interpreted as energy transmission in form of work or heat to the surroundings and expressed by the product of Joul and second [1,2].

Identification of engine operation by means of dimensional analysis in aspect of its usability to diagnostics has been carried out in the present article. The engine operation has been treated according to J. Girtler Works [1,2,3] as a new physical quantity to be used in diagnostics of ship propulsion engines.

2. Forms of dimensional functions of ship propulsion engine performance

Engine operation as dimensional quantity together with other quantities of his type characterizing the movement of ship propulsion system belongs to dimensional space elements. Products of dimensional space elements create abelian group together with involution of real exponent. It allows to describe dimensional space by means of positive real numbers. These

numbers create the underspace of dimensional space. It means that both dimensional and nondimensional quantities belong to dimensional space. Out of dimensional space elements we can select, a determined by space dimension, amount of dimensionally independent quantities called the space base [4,5,6].

Elements of the same dimensional space can be arguments of the function defined as not an ordinary function and called a dimensional one. A dimensional function must equally well describe engines operation in each configuration of units and automatically fulfill the condition of invariance. Apart from this condition it must fulfill the condition of dimensional homogeneity. If in dimensionally invariant and homogeneous function there are independent and dependent arguments so an the basis of Buckingham theorem we can express the last by means of numerical function. Such information can be obtained only by means of experiment.

Analysis of ship engine activity in conditions of its operating creates great difficulties as it requires the knowledge of defining functions and also the knowledge of dynamic features of ship propulsion system.

The activity of ship propulsion engine in the course of its operation is defined by the following parameters:

-the effective Power of the engine **N,**
- torque of the engine **M,**
- rotational speed of the engine **n**,
- fuel volume consumed by the engine $\dot{V}$
- supercharging air compression **p**,
- time of engine activity **t**.

The function form of ship engine propulsion operation **D** can be determined on the basis of functional dependence among the above mentioned parameters. They have adequate dimensions in an accepted system of measure units. Besides on the basis of measurement we can attribute to them defined numerical values. Taking into account the above mentioned premises quantities we can write the following dimensional functions of ship propulsion engine operation **D** as below:

$$D = \Phi\left(M, n, \dot{v}, p, t \right) \tag{1}$$

$$D = \Phi\left(N, n, \dot{v}, t \right) \tag{2}$$

where:

Φ - symbol of dimensional function,

M – torque of the engine in $\left[\frac{kg \cdot m^2}{s^2}\right]$,

n – rotational speed of the engine in $\left[\frac{1}{s}\right]$,

$\dot{v}$ - fuel volume consumed by the engine in $\left[\frac{m^3}{s}\right]$,

N – effective power of the ship propulsion engine in $\left[\frac{kg \cdot m^2}{s^3}\right]$,

p – supercharging air pressure in $\left[\frac{kg}{m \cdot s^2}\right]$,

t- time of engine activity in $[s]$,

D – activity of ship propulsion engine in $\left[\frac{kg \cdot m^2}{s}\right]$.

Functions of ship propulsion engine operation (1) and (2) are described in dimensional space of the third grade, which means that among function arguments there are three dimensionally independent argument creating so called dimensional base. All possibilities of their choice in given functions (1) and (2) are presented in tables 1 and 2. Forms of numerical function of ship propulsion engine operation can be determined on the basis of measurements carried out in the course of its operation.

Tab. 1. Choice possibilities of arguments dimensionally independent, so called dimensional bases, in function of ship propulsion engine operation $D = \Phi\left(M, n, \dot{v}, p, t\right)$

Ordinal number	Form of dimensional function	Dimensional base	comments
1	$D = f\left(\phi_v, \phi_t\right) \cdot \frac{M}{n}$ $\phi_v = \frac{\dot{v} \cdot p}{M \cdot n}, \cdots\cdots \phi_t = n \cdot t$	M,n,p	
2	$D = f\left(\phi_p, \phi_t\right) \cdot \frac{M}{n}$ $\phi_p = \frac{p \cdot n \cdot \dot{v}}{M}, \cdots\cdots \phi_t = n \cdot t$	$M,n,\dot{v}$	
3	$D = f\left(\phi_M, \phi_t\right) \cdot \frac{\dot{v} \cdot p}{n^2}$ $\phi_M = \frac{M \cdot n}{\dot{v} \cdot p}, \cdots\cdots \phi_t = n \cdot t$	$n,\dot{v},p$	
4	$D = f\left(\phi_M, \phi_n\right) \cdot \dot{v} \cdot p \cdot t^2$ $\phi_M = \frac{M}{\dot{v} \cdot p \cdot t}, \cdots\cdots \phi_n = n \cdot t$	$\dot{v},p,t$	
5	$D = f\left(\phi_n, \phi_t\right) \cdot \frac{M^2}{\dot{v} \cdot p}$ $\phi_n = \frac{n \cdot M}{\dot{v} \cdot p}, \cdots\cdots \phi_t = \frac{\dot{v} \cdot p \cdot t}{M}$	$\dot{v}, p, M$	
6	$D = f\left(\phi_n, \phi_{\dot{v}}\right) \cdot M \cdot t$ $\phi_n = n \cdot t, \cdots\cdots \phi_{\dot{v}} = \frac{p \cdot t \cdot \dot{v}}{M}$	p,t,M	
7	$D = f\left(\phi_n, \phi_p\right) \cdot M \cdot t$ $\phi_n = n \cdot t, \cdots \phi_p = \frac{p \cdot t \cdot \dot{v}}{M}$	$M,t,\dot{v}$	

Tab. 2. Choice possibilities of arguments dimensionally independent so called dimensional bases in function of ship propulsion engine operation $D = \Phi\left(N, n, \dot{v}, t\right)$

Ordinal number	The form of dimensional function	Dimensional base	comments
1	$D = f(\phi_t) \cdot \frac{N}{n^2}$ $\phi_t = n \cdot t$	$N, n, \dot{v}$	
2	$D = f(\phi_n) \cdot N \cdot t^2$ $\phi_n = n \cdot t$	$N, \dot{v}, t$	

3. Determination of numerical function form of ship propulsion engine activity on the basis of dimensional argument measurements

To measure work parameters of propulsion engine of general cargo vessel with displacement of 5500 DWT all devices and measurement apparatus installed as ships standard equipment have been used. All measurements the results used in this work were taken during normal 17 days long voyage. Those measurements were taken at the time of engines steady work (excluding maneouevres) four times, a day at 8,11,14 and 20 o′clock of ship′s time. The general cargo vessel was propelled by 5RD68 engine made by H. Cegielski – Sulzer. The measurement results concerning the arguments of dimensional function of ship propulsion engine performance in the course of its operation in nondimensional form have been presented in drawing 1. Dependence of variable dependent on independent ones allows, in the domain of real numbers, to determine the numerical form of operational function by means of multiple regression and define its constant coefficients.

Drawing 1 presents measurement caordinates of numerical function of ship propulsion engine activity with sharply outlined linear dependence. These coordinates have been fitted to multiple regression which helped to obtain the equation of the following form:

$$\frac{D}{M \cdot t} \cdot 10^6 = 10^{-6} \cdot \frac{p \cdot \dot{v} \cdot t}{M} + 6{,}27 \cdot 10^6 n \cdot t - 0{,}001 \tag{3}$$

or

$$D = 10^{-12}\, p \cdot \dot{v} \cdot t^2 + 6{,}27 n \cdot t^2 \cdot M - 10^{-9} \cdot M \cdot t \tag{3a}$$

where:-
symbols like in formula (1).

Correlation coefficient of the above fitting to the straight line amounts to:

$r = 0{,}99999572 \Rightarrow r^2 = 0{,}99999144$ and after correction $r^2 = 0{,}99999092$

which gives a standard estimation error equal to 0,00952.
Calculations that fit the straight line to measurement data included in table 4 were carried out by means of the programme STATISTICA

Tab. 3. Parameters measurements results of ship propulsion engine opetration which are arguments of dimensional function of its operation

Number	time of operation $t \cdot 10^6$ $[s]$	rotational speed $n\left[\frac{1}{s}\right]$	torque $M\left[\frac{kg \cdot m^2}{s^2}\right]$	fuel volume consump. $\dot{v}\left[\frac{m^3}{s}\right]$	effective power $N \cdot 10^6$ $\left[\frac{kg \cdot m^2}{s^3}\right]$	engine operation $D \cdot 10^{12}$ $\left[\frac{kg \cdot m^2}{s}\right]$	Super charging air compres. p $\left[\frac{kg}{s^2 \cdot m}\right]$
1	0	2,0833	22094	0,0209	2,8471	0	39226,8
2	0,0648	2,0900	22511	0,0194	2,9104	1240,65	41188,14
3	0,1512	2,0733	22094	0,0215	2,8339	6576,57	41188,14
4	0,1620	2,0650	22511	0,0224	2,8751	7661,34	43149,48
5	0,1728	2,0733	22511	0,0229	2,8868	8751,93	41188,14
6	0,1944	2,0833	22094	0,0224	2,8471	10923,92	41188,14
7	0,2376	2,0633	22094	0,0215	2,8199	16161,78	41188,14
8	0,2484	1,9900	21052	0,0192	2,5919	16241,63	34323,45
9	0,2592	1,9867	21052	0,0194	2,5875	17655,32	35304,12
10	0,2808	2,0567	22084	0,0231	2,8111	22502,09	41188,14
11	0,3240	2,0633	22094	0,0203	2,8199	30068,14	39226,80
12	0,3348	2,0633	22094	0,0203	2,8199	32106,10	39226,80
13	0,3456	2,0633	22094	0,0202	2,8199	34210,87	38246,14
14	0,3672	2,0683	22094	0,0203	2,8265	38714,45	39226,80
15	0,4104	2,1017	22719	0,0222	2,9538	50530,61	41188,14
16	0,4320	2,1200	22511	0,0208	2,9523	55960,04	43149,48
17	0,4536	2,1217	23136	0,0215	3,0361	63459,73	41188,14
18	0,4968	2,1067	22511	0,0213	2,9332	73542,86	41188,14
19	0,5076	2,1017	22511	0,0214	2,9266	76592,92	41188,14
20	0,5184	2,0967	22511	0,0212	2,9192	79696,81	41188,14
21	0,5400	2,1083	22302	0,0228	2,9089	86147,68	42168,81
22	0,5616	2,0667	22511	0,0244	2,8780	92194,77	42168,81
23	0,5616	2,0950	22511	0,0219	2,9170	93457,23	41188,14
24	0,5832	2,1200	22302	0,0238	2,9251	101040,29	47072,16
25	0,5832	2,1233	22928	0,0227	3,0111	104038,10	46091,49
26	0,6264	2,1283	22928	0,0227	3,0185	120304,64	45110,82
27	0,6372	2,1317	22928	0,0226	3,0229	124102,79	45110,82
28	0,6480	2,1300	22928	0,0222	3,0207	128847,40	45110,82
29	0,6696	2,1317	23343	0,0223	3,0413	140182,41	45110,82
30	0,7128	2,1283	23553	0,0221	3,1001	160027,39	45110,82
31	0,7236	2,1267	23553	0,0232	3,0979	164789,47	47072,16
32	0,7344	3,1733	24595	0,0247	3,3053	181138,80	52956,18
33	0,7560	2,0917	22928	0,0229	2,9663	172222,16	46091,49
34	0,8208	2,0967	23344	0,0219	3,0273	207188,73	43149,48
35	0,8424	2,1283	22928	0,0224	3,0185	217578,31	44130,15
36	0,9288	2,1300	23553	0,0222	3,1023	271925,61	45110,82

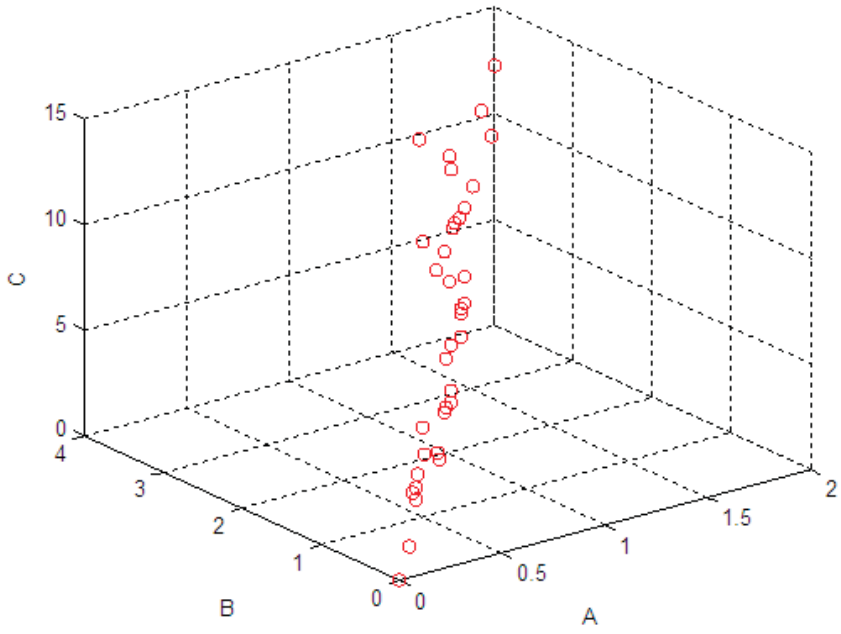

Fig. 1. Measurement coordinates of numerical function of ship propulsion engine activity in an established dimensional base p,t,M of the form C=f (A, B). (table1- position 6). Explanations: $C = \frac{D}{M \cdot t} \cdot 10^6$ *-nondimensional index of engine operation,* $A = n \cdot t \cdot 10^6$ *- similarity invariant of engine rotational speed,* $B = \frac{p \cdot v \cdot t}{M}$ *-similarity invariant of fuel volume consumed by the engine, the rest of symbols like in formula (1)*

In dimensional function of ship propulsion engine defined by the formula (2) one can select four different dimensional bases , but only two are correct, in respect of dimensional structure. Structures of numerical functions obtained from formula (2), were given in table 2, position 2, similarity invariable of numerical function concerning engine operation is independent of its rotational speed as shown in drawing 2. On the other hand its value depends on engine work parameters in established conditions.

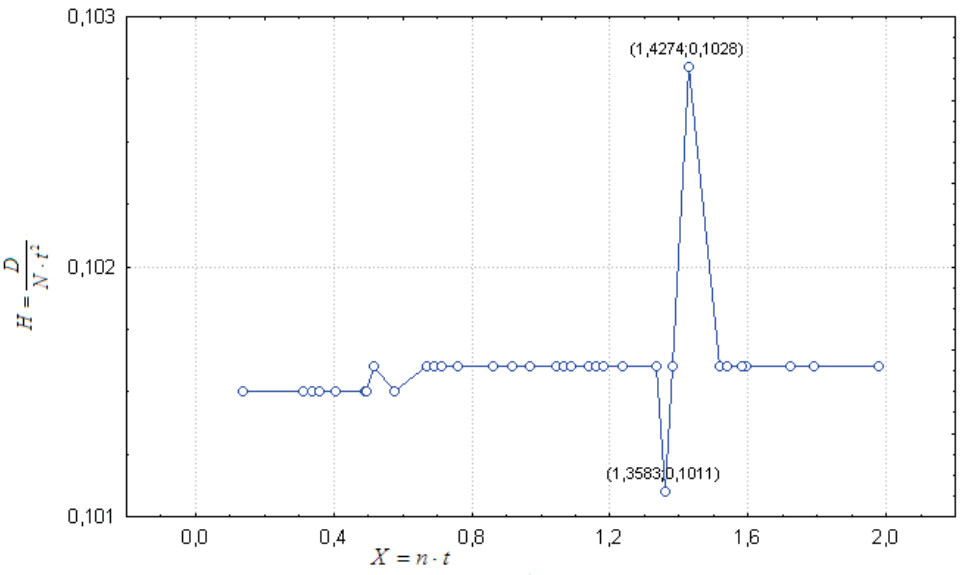

Fig. 2. Probability invariant measurements of numerical function concerning ship engine operation in an established dimensional base $_{N,\dot{v},t}$ *of the form* $H = f(X)$ *(look table 2 position 2). Explanations:* $_{H=\frac{D}{N \cdot t^2}}$ *- nondimensional index of ship engine operation,* $_{X=n \cdot t}$ *- similarity invariant of engine rotational speed, the rest of symbols like in formula (2)*

Peak occurence taking place in similarity invariant in numerical function of engine operation shown in drawing, is caused by the average of propulsion engine. After twelve days of the ship′s voyage broke the liner of engine cylinder head on third unit. First it caused, a decrease of operation value brought about by a faulty action of the third system and next an increase of operation value as a result of augmentem work of the remaining systems. Numerical structure given in table 2 position 2 on the basis of invariant changes of the engine operation similarity (numerical function dependent variable) can be recorded in the following way, drawing 2.

$$\left\{\begin{array}{l} \dfrac{D}{N \cdot t^2} = 0{,}1015 \Rightarrow 0 \le n \cdot t \le 0{,}5775 \cdot 10^6 \\ \dfrac{D}{N \cdot t^2} = 0{,}1016 \Rightarrow 0{,}5775 \cdot 10^6 \le n \cdot t \end{array}\right\} \tag{4}$$

or

$$\left\{\begin{array}{l} D = 0{,}1015 \cdot N \cdot t^2 \Rightarrow 0 \le n \cdot t \le 0{,}5775 \cdot 10^6 \\ D = 0{,}1016 \cdot N \cdot t^2 \Rightarrow 0{,}5775 \cdot 10^6 \le n \cdot t \end{array}\right\} \tag{4a}$$

where:
symbols like in formula (2).

4. Conclusions

Two different forms of numerical functions concerning propulsion engine operation (1) and (2) are possible to obtain, by means of algebraic diagram of dimensional analysis given by S. Drobot. Different numerical structures are given in tables 1 and 2.

These structures allow us to define superficially, dependence among dimensional quantities describing ship operation. Obtained on their basis numerical functions estimators of engine operation are their models can be defined accuratelly according to the established coefficients determined on the basis of engine work parameters.

Formulas (3) and (4) which define the ship engine operation can be treated only as correct proposals is respect of dimensional aspect. Forms (1) and (2) of dimensional function of engine operation differ one from another due to number of explanatory variables.

Reducing one explanatory variable [function form (2)] make it possibile to obtain numerical function structure of one variable. In case of five explanatory variables (form 1) one can obtain numerical function structures of two variables.

The best numerical function model of ship propulsion engine is the one of a simple form and easy to interpret physically. Numerical function models of operation distinquish themselves by the fact that they take into account the essential quantities which describe the work of an engine depending on the time of its operation. So they are of dynamic character and due to this can be used for diagnostic and prognostic purpose.

The form of numerical function models of ship propulsion engine operation can be defined on the basis of engine operation parameters. They can be true only for the engine at which the measurements were carried out.

5. References

[1] Girtler, J., *Energy-based aspekt of machine diagnostic*, Diagnostyka 1 (45), pp. 149-155, 2008.

[2] Girtler, J., *Work of a compression-ignition engine as the index of its reliability and safety*, II International Scientifically-Technical Conference Expo-DIESEL & GAS TURBINE"01 Coference Proceedings, pp.79-86, Gdańsk- Międzyzdroje-Copenhagen, 2001.

[3] Girtler, J., *Identyfication metod of technical state of othe objects on the Grodnu of estimation of their work*, Diagnostyka 2 (46), pp. 126-132, 2008.

[4] Drobot, S., *On the foundation of dimensional analysis*. Dissertation Mathematic, vol. XIV, 1954.

[5] Rosłanowski, J., *Modelling of ship movement by means of dimensional founction*, Transport No 3 (23), pp.443-448, Radom University of Technology, 2005.

[6] Rosłanowski, J., *The methodology of energetical process model construction in ship propulsion systems by means of dimensional analysis defining their dynamical features*, International Conference Technical economic and environmental aspects of combined cycle power plants, pp. 59-66, Gdańsk University of Technology, 2004.

Journal of POLISH CIMAC

Faculty of Ocean Engineering & Ship Technology
GDAŃSK UNIVERSITY OF TECHNOLOGY

ON MAKING OPERATIONAL DECISIONS WITH TAKING INTO ACCOUNT VALUE OF OPERATION APPLIED TO SHIP MAIN PROPULSION ENGINE AS AN EXAMPLE

Jacek Rudnicki

Gdansk University of Technology
Faculty of Ocean Engineering & Ship Technology
Department of Ship Power Plants
tel. (+48 58) 347-29-73
e-mail: jacekrud@pg.gda.pl

Abstract

Objectivity and rationality in making decision, assumed optimal in given conditions, forces to apply an evaluating (quantitative) approach to the problem, hence to search for such their parameters (indices) which, in a given decision situation, can be deemed most adequate.

And, to precisely determine the task it is necessary to specify also its duration time, apart from conditions in which it will be realized.. When considering propulsion engine, i.e. the main element of ship propulsion system, especially important becomes not only the problem which amount of energy could be at one's disposal but also within which time interval it could be delivered. Therefore apart from applying the commonly used reliability indices, it seems sensible to consider the operation in such evaluating approach as it could be determined by energy and time simultaneously. The presented method may be deemed a valuable supplement to the ways have been applied so far of description of reliability features of the driving system, considered crucial for ship power plant and ship itself.

Keywords*: operation, ship power plant, Poisson process, Markov process*

1. Introduction

As described elsewhere [4, 5], in operational practice of ship devices (like in the case of other complex functional systems of mechanical devices) working life of the same elements installed in different power plants is not an adequate criterion for unambiguous determination of an operation strategy because it is not an unambiguous measure of their wear and tear.

In decision making situation, reality of operation can be better represented by introduction of at least one random variable as a model parameter though it leads solely to more or less probable conclusions , that results from the fact that to particular values of decision variables not only one value of criterion function but many values occurring with different probabilities, are attributed. To the most often applied probabilistic decision models belong those in which the expected value of consequence of taking the decision is selected to aid in choosing optimum value of decision variable [10]. Hence in choosing an optimum value of a decision variable one should be aided by the expected value of criterion function [4].

In such situation it is easier - from formal point of view - to present decision-making procedure in one of the structural forms most commonly met, namely : decision tree or decision table. In general case the decision tree takes the form shown in Fig.1.

For the below presented tree, the criterion function is constituted by maximization of the expected value of the consequence $c(d_j, s_i)$, which , for particular decision tree nodes which symbolize the fact of taking a given decision d_j , can be determined as follows [8, 9]:

$$E(c/d_j) = \sum_{i=1}^{k} \left[p(s_i)/d_j \cdot c(d_j, s_i) \right] \qquad i = 1,2,...,k \qquad j = 1,2,...,n \tag{1}$$

And, it should be observed that the decision situation is deterministic as it consists in choosing only one decision out of n possible ones, in spite of that occurrence probabilities of the state s_i (i = 1,2, …, k) under assumption of taking the decision d_j (i = 1,2, …, n) appear.

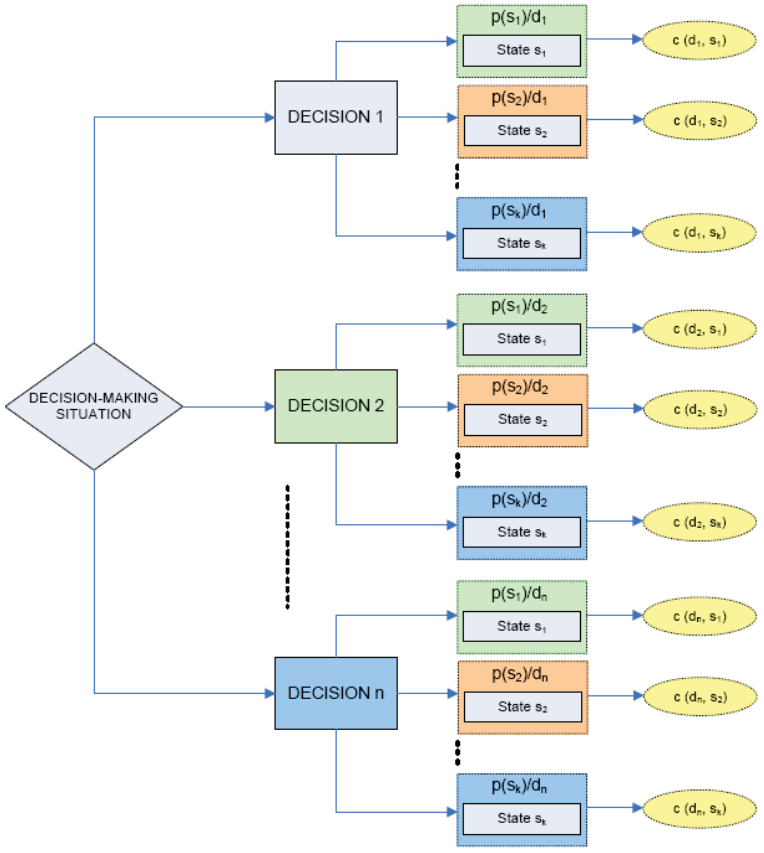

Fig.1. General case of decision tree. n – number of considered decisions; $p(s_i)/d_j$ – conditional probability of occurrence of the state s_i in the case of taking the decision d_j,; $c(d_j, s_i)$ – consequence of occurrence of the state s_i in the case of taking the decision d_j

Application of the decision procedure shown in Fig. 1. requires, apart from determination of a repertoire of possible decisions, to know how to determine values of the conditional probabilities $p(s_i)/d_j$.

In practice, predictions concerning tasks to be realized are usually based on the wide-understood notion of service reliability of an object or system. And, when considering the notion of service reliability of power devices (e.g. ship diesel engines) attention should be paid to that from the

user's point of view the most important problem is quality of execution of a given task (in extreme case – its not fulfillment). This way the notion of reliability is inseparably associated with unambiguous determination of the task in question.

Moreover to precisely determine a task , apart from assuming conditions in which it will be performed, it is necessary to specify is duration time. The problem is especially important in such domains as sea shipping where specificity of tasks is as a rule associated with necessity of the functioning of crucial mechanisms and devices (e.g. installed on ships) for long periods.

Therefore it is especially important not only which quantity of energy would be available during operation of a given power device but also for which duration time it could be delivered.

The presented approach is made realizable by considering engine's operation (further referred only to ship main propulsion engine) in such evaluating way as to make simultaneous determining it by energy and time possible.

In this case the operation (D) within the time interval [0, t] can be interpreted as a physical quantity determined by the product of the time-variable energy E = f(t) and time t , which can be generally expressed by the following relation [7]:

$$D = \int_0^t E(\tau)\mathrm{d}\tau = 2\pi \int_0^t M_0\, n\, t\mathrm{d}t \tag{2}$$

2. Estimation of occurrence probability values of ship motion limitations resulting from the lowering of total efficiency of ship main propulsion engine

One of the possible ways of estimation of occurrence probability values of limitations in ship motion with a given speed is the above mentioned quantitative evaluation of operation. The way is as much versatile that it is possible to apply it in the case when results of operational investigations are lacking, and adopted assumptions and model parameters are determined exclusively on the basis of engine's technical and operational documentation and determined task realization conditions.

In the case of ship main engine, with a view of taking into account the so-called design sea margin as well as service power margin [10] for the engine operating under partial loads , the process of the decreasing of available power output (hence also of the possible operation D_M) will be realized in two phases:

- In the first phase only an increase of hourly fuel oil consumption will take place (at a relatively constant value of developed engine torque), hence operational cost will also increase;
- in the second phase a limitation of effective power developed by the engine will appear due to design limitations and lack of possible increasing fuel charge.

If partial engine load is assumed constant the phenomenon can be interpreted as follows:

- In the first phase the time-variable drop of total engine efficiency results first of all in increasing its hourly fuel oil consumption (increase of specific fuel oil consumption). It can be described as a series of the recordable events F consisting in increasing the fuel charge $g_p^{i\%}$ by the increment Δg_p at a relatively constant value of the torque M_o (appropriate to a given engine load state) . This way an increase of engine's operational cost is generated, however without any limitations imposed on ship motion parameters, in principle;
- Gradual degradation processes during further engine operation result in that the recordable events U which consist in decreasing the engine torque M_o at the constant fuel consumption g_p (i.e. $g_p = G_{p\ max}$), to occur. Further long-lasting operation of the engine results in significant worsening its characteristics which impose serious limitations on ship motion with a given speed or course. In heavy weather conditions such situation will obviously lead to producing a hazard to ship safety.

In the context of the above mentioned quality of task realization to know the following data becomes important in making decisions with the use of a probabilistic decision process :

a) expected value of increased cost of task realization, resulting from increased fuel oil consumption,
b) value of occurrence probability of such number of F events which cause the fuel oil charge $g_p^{i\%}$ to increase up to the value $G_{p\,max}$, and ship motion limitations to occur subsequently.

In the considered case of ship main diesel engine the problem defined in a) can be solved by making use of the assumption that the number of repetitions $N_{\Delta gp}$ of the event F within the time interval (0, t) is a random variable of non-negative integer values.

The dependence of the random variable on time constitutes the stochastic process $\{N(t) : t \geq 0\}$.

3. An example of application of stochastic process theory to estimation of value of the probabilities $p(s_i)/d_j$

Under assumptions on stationarity [3, 11], lack of consequences and flow singularity, the Poisson's homogeneous process can be applied to the process of increasing the fuel charge $g_p^{i\%}$ as a result of decreasing the engine's total efficiency η_e (in steady load conditions of the engine), and the random variable $N_{\Delta gp}$ is characterized by the distribution [1]:

$$P(N_{\Delta gp} = k) = \frac{(\lambda_f \cdot t)^k}{k!} \exp(-\lambda_f t); \quad k = 1,2,...,n \tag{3}$$

where:

λ_f - a constant interpreted as occurrence intensity of the event F (increasing $g_p^{i\%}$ by the value Δg_p).

Main particulars of the engine, on which the carried out calculations are based, deal with 9RT-flex60C-B Wartsila engine (according to [12]); hence for the selected contract parameters : the contract power output N_x = 80% N_{R1} = 17370 kW, engine speed n_x = 90% n_{R1} = 102,6 rpm it can be assumed that the state of engine operation under 85% load is typical one as in this point of engine's working area specific fuel oil consumption value reaches its minimum. Hence the parameters of the typical state of operation are determined as follows:

- n = 97,2 rpm,
- N_e = 14 764,5 kW,
- g_e = 169,4 $\frac{g}{kWh}$.

Taking into account the above mentioned , one can determine value of the fuel charge $g_p^{85\%}$ as follows:

$$g_p^{85\%} = \frac{N_e \cdot g_e}{n \cdot i} = \frac{14764{,}5kW \cdot \frac{168{,}2}{3600}\frac{g}{kW \cdot s}}{\frac{97{,}2}{60}\frac{1}{s} \cdot 9} = 47{,}3g \tag{4}$$

$G_{pmax} = g_p^{110\%}$ can be simultaneously assumed as precise data concerning parameters of injection apparatuses are lacking, and:

$$g_p^{110\%} = \frac{19107kW \cdot \frac{170{,}8}{3600}\frac{g}{kW \cdot s}}{\frac{105{,}9}{60}\frac{1}{s} \cdot 9} = 57{,}1g \tag{5}$$

therefore:

$$\Delta G_{pmax} = g_p^{110\%} - g_p^{85\%} = 9{,}8g \approx 10g \tag{6}$$

Next, value of T_{Gpmax} at which value of G_{pmax} resulting from degradation processes is reached, should be estimated. In the case of lacking appropriate results of operational investigations the only one, practically useful way of its determination is to analyze engine's technical and maintenance documentation on the basis of which the most unreliable engine's elements and systems can be selected in line with indications of engine's manufacturer.

In the considered example such analysis revealed that the most unreliable functional subsystem of the engine is its fuel system (which complies with many results of other independent research [6]) . Therefore when analyzing the service time-scale of the above mentioned system as well as other maintenance operations, to assume T_{Gpmax} = 1000 h has been deemed justified.

If accuracy class of the applied flowmeters is assumed equal to 0,5 and value of recorded fuel flow rates is also assumed, then in the considered case the value of Δ_{gp} can be determined on the level of Δ_{gp} = 0,004 kg/s. Therefore on the basis of the above mentioned assumptions it can be stated that during the time T_{Gpmax} the following number of F events which would result in imposing limitations in realizing the assumed ship sailing speeds:

$$N'_{\Delta g_p} = k' = \frac{G_{p\max} - g_p^{x\%}}{\Delta g_p} = \frac{10}{4} = 2{,}5 \approx 3 \tag{7}$$

Hence the determined value of λ_f amounts to:

$$\lambda_f = \frac{N'_{\Delta g_p}}{T_{\Delta G_{p\max}}} = \frac{3}{1000} \cdot \frac{1}{h} \tag{8}$$

Finally, for the considered example the occurrence probability of k' number of F events amounts to:

$$P\left(N_{\Delta gp} = k'\right) = \frac{\left(\lambda_f \cdot t\right)^k}{k!} \exp\left(-\lambda_f t\right) = \frac{\left(3 \cdot 10^{-3} \cdot t\right)^3}{3!} \cdot \exp\left(-3 \cdot 10^{-3} \cdot t\right) \tag{9}$$

and, the function $P\left(N_{\Delta gp} = k'\right) = f(t)$ is presented in Fig.2.

Moreover , to make the figure more clear, the occurrence probability of a lower number (k = 2) as well as higher ones (k = 4 and 5) of F events is also shown in it. Interpretation of the probabilities presented in function of time confirms expectations as it can be observed that occurrence probability of a lower number k of F events decreases along with time in favour of their greater values. In decision-making process such analysis of the probabilities in question makes it possible to estimate expected consequence values and to select a task realization variant. The assumptions concerning T_{Gpmax} as well as Δg_p may be deemed somewhat doubtful , however in any instant their determined values can be replaced by different, more realistic ones, but the procedure itself does not undergo any modifications.

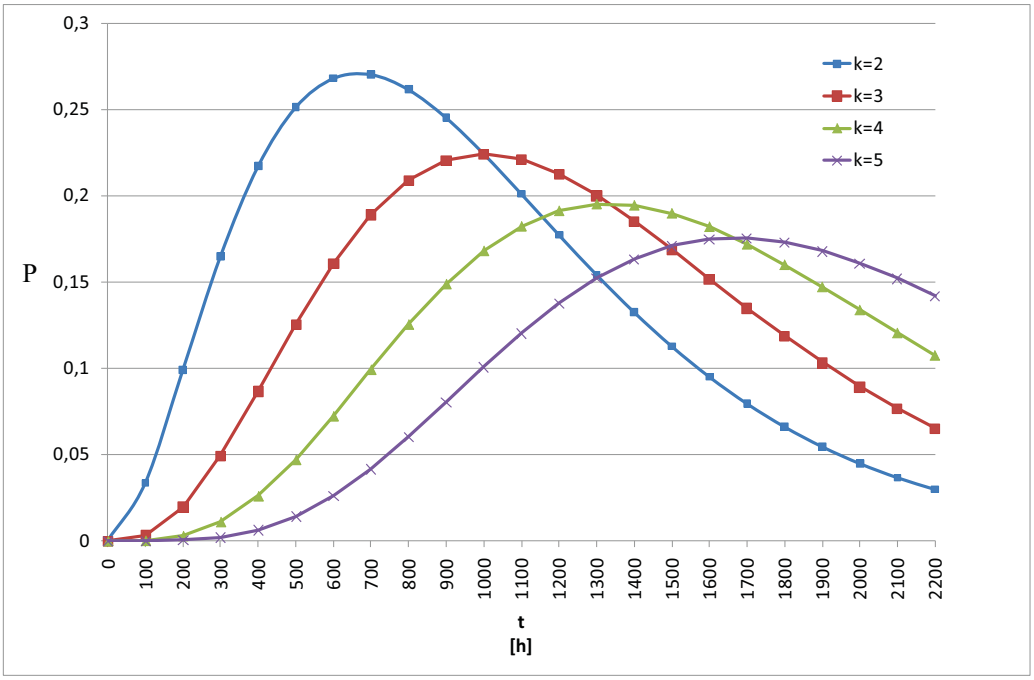

Fig. 2. $P\left(N_{\Delta gp} = k\right) = f(t)$

In the next phase the above presented problem was solved by using a model in the form of the Markov process {X'(t) ; t ≥ 0}. The state transition graph of the considered process with taking into account the values obtained from the relation (8) is presented in Fig. (3)

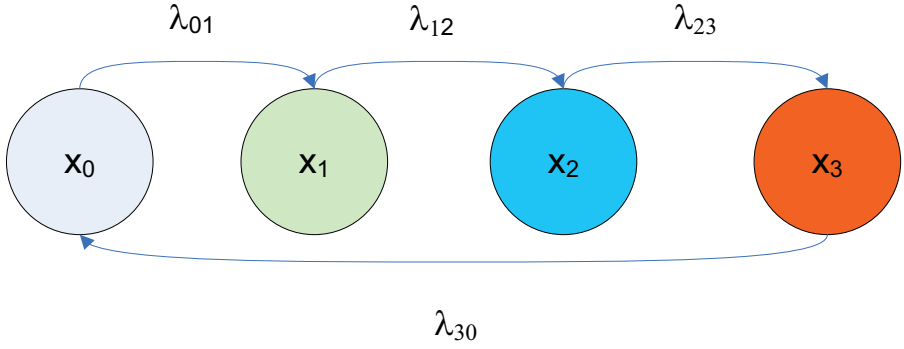

Fig. 3. State transition graph of the process {X'(t) ; t ≥ 0}

and the initial distribution of the proces:

$$p_0 = P\{X(0) = x_0\} = 1,$$
$$p_i = P\{X(0) = x_i\} = 0 \quad \text{dla } i = 1,2,3. \tag{10}$$

Therefore the set of Kolmogorov – Smirnov equations takes the form:

$$\left.\begin{aligned}
\frac{dP_0(t)}{dt} &= -\lambda_{01}\cdot P_0(t) + \lambda_{30}\cdot P_3(t)\\
\frac{dP_1(t)}{dt} &= -\lambda_{12}\cdot P_1(t) + \lambda_{01}\cdot P_0(t)\\
\frac{dP_2(t)}{dt} &= -\lambda_{23}\cdot P_2(t) + \lambda_{12}\cdot P_1(t)\\
\frac{dP_3(t)}{dt} &= -\lambda_{30}\cdot P_3(t) + \lambda_{23}\cdot P_2(t)\\
P_0(t) + P_1(t) + P_2(t) + P_3(t) &= 1
\end{aligned}\right\} \qquad (11)$$

The set can be transformed by applying Laplace transform [2] as well as the assumed initial distribution of the process to the set of linear equations in the domain of transforms having the following form:

$$\left.\begin{aligned}
s\cdot P_0^*(s) - 1 &= -\lambda_{01}\cdot P_0^*(s) + \lambda_{30}\cdot P_3^*(s)\\
s\cdot P_1^*(s) &= -\lambda_{12}\cdot P_1^*(s) + \lambda_{01}\cdot P_0^*(s)\\
s\cdot P_2^*(s) &= -\lambda_{23}\cdot P_2^*(s) + \lambda_{12}\cdot P_1^*(s)\\
s\cdot P_3^*(s) &= -\lambda_{30}\cdot P_3^*(t) + \lambda_{23}\cdot P_2^*(s)\\
P_0(t) + P_1(t) + P_2(t) + P_3(t) &= 1
\end{aligned}\right\} \qquad (12)$$

Attempting to solving the above mentioned set one should determine the transition intensity λ_{ij}. To estimate values of the parameters is possible provided expected values of the random variables T_{ij} are known. In practice the mean time of remaining the process in the state x_i provided the next will be the state x_j , can be considered to be the estimator $E(T_{ij})$. In such case the searched for value λ is expressed as follows:

$$\lambda_{ij} = \frac{1}{E(T_{ij})} \cong \frac{1}{\bar{x}_{ij}} \lambda_{ij} = \frac{1}{E(T_{ij})} \qquad (13)$$

In the case in question, as 3 transitions of the process, which result from the lowering of total engine efficiency by the same value, are considered, it is justified to assume the following assumptions associated with determining λ_{ij} values :

- in the most common case of lacking results of operational investigations it is possible to assume that in a rational system of operation to distinguish duration time of any of the states except the state x_k , i.e. in this case - x_3 , is unjustified (as there is no reason to claim that any of the states should last for a longer or shorter time),
- it can be therefore assumed that $E(T_{01}) \approx E(T_{12}) \approx E(T_{23})$, hence $\lambda_{01} \approx \lambda_{12} \approx \lambda_{23} = \lambda$,
- the mean duration times of the distinguished states x_0, x_1 and x_2 should be then assumed the same, it is therefore justified to assume its value equal to:

$$\bar{x} = \frac{T_{G_{p\max}}}{k'} \qquad (14)$$

On substitution of the data for the considered case the value : $\lambda \approx 0{,}003$ was obtained. By taking into account the above specified assumptions and the notation : $\lambda_{30} = \mu$, the set of equations (12) can be presented in the following form:

$$\left.\begin{aligned} s\cdot P_0^*(s)-1 &= -\lambda\cdot P_0^*(s)+\mu\cdot P_3^*(s)\\ s\cdot P_1^*(s) &= -\lambda\cdot P_1^*(s)+\lambda\cdot P_0^*(s)\\ s\cdot P_2^*(s) &= -\lambda\cdot P_2^*(s)+\lambda\cdot P_1^*(s)\\ s\cdot P_3^*(s) &= -\lambda\cdot P_3^*(t)+\lambda\cdot P_2^*(s)\\ P_0(t)+P_1(t)+P_2(t)+P_3(t) &= 1 \end{aligned}\right\} \qquad (15)$$

The solving of the above mentioned set of equations in the domain of transforms and the subsequent executing of inverse Laplace transform makes it possible to find the searched for distribution $P_3(t)$ graphically presented in Fig. 4.

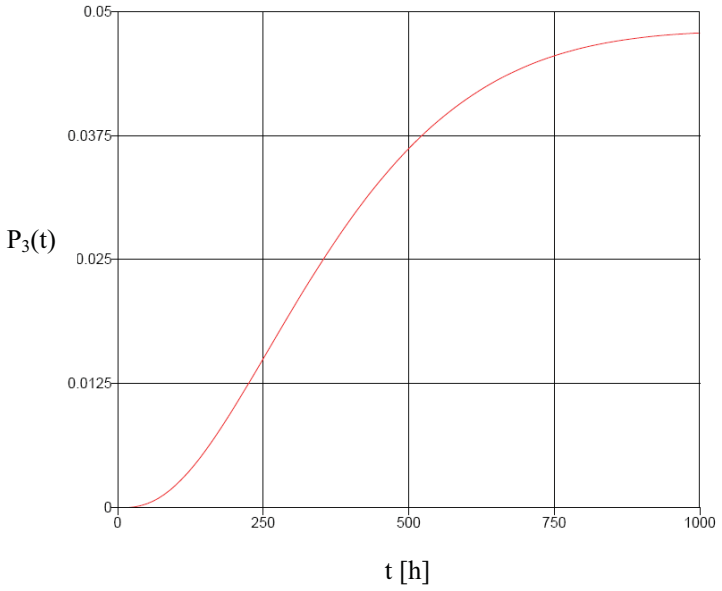

Fig.4. The probability distribution $P_3(t)$

4. Summary

The presented method may be deemed a valuable supplement to the ways have been applied so far of description of reliability features of the driving system, considered crucial for ship power plant and ship itself . Its basic advantage consists in connecting energy assessment with duration of time in which a task is realized. The time is very important in the case of sea shipping tasks usually long lasting.

Making use of it one is able to determine, for a given instant , useful work (useful energy) which can be produced by the whole driving system, as well as to determine value of occurrence probability of such number of F events which would cause additional limitations to form during realization of a task (due to not possible propelling the ship with a given speed) or to make its realization impossible at all. Value of the probability can be hence taken as that of reliability index and implemented in making operational decisions. Its additional advantage is versatility which makes it possible to apply it to reliability analysis of every ship power device or subsystem including those not being machines, e.g. heat exchangers.

References

[1] Benjamin J.R., Cornell C.A., *Rachunek prawdopodobieństwa, statystyka matematyczna i teoria decyzji dla inżynierów,* WNT, Warszawa 1977.

[2] Bobrowski D., Ratajczak Z., *Przekształcenie Laplace'a i jego zastosowanie,* Wydawnictwo Politechniki Poznańskiej, Poznań 1985.

[3] Gichman I.I, Skorochod A.W., *Wstęp do teorii procesów stochastycznych,* PWN, Warszawa 1968.

[4] Girtler J., *Sterowanie procesem eksploatacji okrętowych silników spalinowych na podstawie diagnostycznego modelu decyzyjnego,* Zeszyty Naukowe AMW, nr 100A, Gdynia 1989.

[5] Girtler J., Kuszmider S., Plewiński L., *Wybrane zagadnienia eksploatacji statków morskich w aspekcie bezpieczeństwa żeglugi,* WSM, Szczecin 2003.

[6] Rudnicki J., *Model niezawodnościowo – funkcjonalny okrętowego, tłokowego silnika spalinowego*, Rozprawa doktorska (11.03.2000), Politechnika Szczecińska, Wydział Techniki Morskiej, Szczecin 2000.

[7] Rudnicki J., *Działanie systemu energetycznego w ujęciu wartościującym z uwzględnieniem jego struktury niezawodnościowej oraz stopnia zużycia potencjału użytkowego,* Praca wykonana w ramach projektu finansowanego przez MNiSW Nr N509 045 31/3500, Projekt badawczy pt. „*Kształtowanie bezpieczeństwa działania systemów energetycznych środków transportowych na przykładzie systemów okrętowych*", Gdańsk, 2008.

[8] Rudnicki J., *Przydatność wybranych modeli matematycznych procesu eksploatacji w aspekcie ich zastosowania podczas podejmowania decyzji eksploatacyjnych*. Praca wykonana w ramach projektu finansowanego przez MNiSW Nr N509 045 31/3500. Projekt badawczy pt. „*Kształtowanie bezpieczeństwa działania systemów energetycznych środków transportowych na przykładzie systemów okrętowych*". Gdańsk, 2008.

[9] Sadowski W, *Teoria podejmowania decyzji,* Państwowe Wydawnictwo ekonomiczne, Warszawa 1976.

[10] Urbański P, *Podstawy napędu statków,* Wyd. Fundacji Rozwoju Akademii Morskiej, Gdynia 2005.

[11] Wentzell A.D, *Wykłady z teorii procesów stochastycznych,* PWN, Warszawa 1980.

[12] General Technical Data. WinGTD ver. 2.8. Wärtsilä Switzerland Ltd 2004.

Journal of POLISH CIMAC

Faculty of Ocean Engineering & Ship Technology
GDAŃSK UNIVERSITY OF TECHNOLOGY

NEW ECOFUEL FOR DIESEL ENGINES

Lech J. Sitnik

Politechnika Wrocławska
ul. Ign. Łukasiewicza 7/9, 50-371 Wrocław,
tel. +48713477918,
e-mail: Lech.sitnik@pwr.wroc.pl

Abstract

The World is strongly dependent on crude oil for its transport needs. In order to diminish this dependence, we need to introduce clean, CO_2-efficient, secure and affordable transportation fuels. The current production of liquid biofuels in the EU25 is less than 1% of the market. Recent assessments have concluded that the 2010 targets, 18 Mtoe used in the transport sector, are unlikely to be achieved. There can be three basic possibilities of accomplishing this target: i) the use of alcohols (first of all ethanol) and their mixing with petrol; ii) the use of fatty acids esters (methyl or ethyl) of vegetable oils and their mixing with diesel fuel, iii) the use of synthetic hydrocarbons of the synthetic gas coming from biomass resources and eventually their mixing with other "classical" hydrocarbons.

This paper presents a new way of utilizing alcohols as fuels for a diesel engine. It is proposed to use heavy alcohols as a mix with vegetable oils and conventional diesel fuel. It is presented another way to use alcohols. Namely the use of heavy alcohols as a solvent for vegetable oil (called the biomix or BM) and after the obtainment of the density which would be similar to diesel fuel, mixing the biomix with diesel fuel to obtain biomixdiesel (BMD). This solution will be shown for example with butanol as heavy alcohol, rape oil as vegetable oil and conventional diesel fuel. The investigations are carried out with a simple diesel engine on the engine test bed. Main parameters of engine (power output, torque, specific fuel consumption) and the main exhaust gas components (in this case CO, NO_x, PM) were investigated. There were better results achieved than one expected. Contrary to existing experiences, the maximum of power output and the torque of engine is higher in the whole range of the rotatory speed of the engine crankshaft when the engine biomixdiesel (BMD) is reinforced. The addition of the biomix component to fuel influences the specific fuel consumption. Generally with the larger part of the biomix component the specific fuel consumption grows. Because the power of engine also grows up one should expect that in exploitation the specific fuel consumption should not increase. It is very important that this fuel could be used to reinforce old, existing now and the future diesel engines.

It's worth paying attention that the presented solution in which a virgin vegetable oil (contrary to today's situation in which as a fuel ingredient we have only fatty esters) is an ingredient for fuel.

The production of butanol is known (from biomass and in other way with electrolysis of ethanol). The possibility to get butanol from ethanol gives a very good perspective for the use of ethanol from today's overproduction and moreover without the essential change of infrastructure.

All this leads to the conclusion that fulfilling the expected requirements of European Union regarding the biofuels is fully possible.The introduction of new fuel needs carrying out of a lot of complicated investigations, but chosen direction may be interesting.

Keywords: *diesel engine, butanol, biofuel, ecofuel*

Introduction

The World is strongly dependent on crude oil for its transport needs. In order to diminish this dependence, we need to introduce clean, CO_2-efficient, secure and affordable transporta-

tion fuels. The current production of liquid biofuels in the EU25 is less than 1% of the market. Recent assessments have concluded that the 2010 targets, 18 Mtonnes used in the transport sector, are unlikely to be achieved.

There can be three basic possibilities of accomplishing this target: i) use of alcohols (first of all ethanol) and their mixing with petrol; ii) the use of fatty acids esters (methyl or ethyl) of vegetable oils and their mixing with diesel fuel, iii) the use of synthetic hydrocarbons of the synthetic gas coming from biomass resources and eventually their mixing with other "classical" hydrocarbons.

It is known that today in EU we have an overproduction of ethanol. Together we have an overproduction of petrol. We need more and more fuels for diesel engines. Also in the nearest future, thanks to increasing of engine efficiency, the situation will be not change.

This paper presents a novel way of using alcohols as fuels for a diesel engine. Namely it shows the use of heavy alcohols as a solvent for vegetable oil (this mixture is called the biomix or BM) and after the obtainment the density by biomix which would be similar to the density of diesel fuel, mixing the biomix (BM) with diesel fuel (D) to obtain biomixdiesel (BMD).

This solution will be shown for example with butanol as heavy alcohol, rape oil as vegetable oil and conventional diesel fuel.

Investigations

The technology of butanol production is known. There are three separated ways to use.

- Directly
  - Conventional
    Traditionally, the production of fermentation products such as Bioethanol has relied on feedstock's that are rich in either sugars (cane or beet) or starch which is easily broken down into sugars (wheat, corn or rice). The future is in new plants the working with another art of microorganisms like thermophiles.
  - TMO technology process
    TMO's technology platform is based on a select group of ***t**hermophilic **m**icro-**o**rganisms* (*Thermophiles*). The optimal feedstock for bioconversions would be waste biomass (e.g. straw, wood chips and paper pulp effluent) and crops specially grown for their high biomass production rate (kenaf, miscanthus and short rotation woody crops). Such sources can be described as "cellulosic biomass" for their high cellulose and hemicellulose content.
- Indirectly – from ethanol
  Electrolysis. The electrolysis is an old process, but with develops a fuel cell and new art of solar cell the electrolysis process may by develop to the new process of butanol production from ethanol. The elektrolyse is going from chemical eqation;

$$2C_2H_5OH + 2C_2H_5OH \rightarrow 2C_4H_9OH + 2H_2 + O_2$$

The properties of butanol and its comparison to the light alcohols and conventional engine fuels are as following.

Tab.1. The properties of different fluids

Fuel	Energy density	Heat of vaporization	Kinematic viscosity at 20°C
Diesel	38.6 MJ/l	0,47 MJ/kg	>3 cSt
Gasoline	32.0 MJ/l	0.36 MJ/kg	0.4–0.8 cSt
Butanol	29.2 MJ/l	0.43 MJ/kg	3.64 cSt
Ethanol	19.6 MJ/l	0.92 MJ/kg	1.52 cSt
Methanol	16.0 MJ/l	1.20 MJ/kg	0.64 cSt

It is interesting that the butanol is similar in the energetically properties to the petrol. The solvent properties of butanol for solving heavy hydrocarbons (such diesel fuels) are very good. The mix is homogenous (both fluids don't separate after several months). This is in contrary to the ethanol, which doesn't solve the diesel fuel. It is important that the butanol practically doesn't solve water (contrary to the ethanol which solves water in any proportion).

There were prepared three mixtures for investigation.

In the first step the rape oil (vegetable oil) is mixed with butanol from which we have the mixture, the density of which would be similar to the density of diesel fuel. This mixture is called as a BM (Bio Mix). In the second step this fuel (BM) was mixed with conventional diesel fuel (EN 590) to obtain biomixdiesel (BMD). These fluids were mixed in the following proportions.

- biomix (BM) 10 % v/v, diesel fuel (D) 90 % v/v, called as 10BMD,
- biomix (BM) 20 % v/v, diesel fuel (D) 80 % v/v, called as 20BMD,
- biomix (BM) 50 % v/v, diesel fuel (D) 50 % v/v, called as 50BMD.

All above mixtures are very homogeneous. It is impossible to see any phases (contrary to, for example, the mix of rape methyl ester with conventional diesel fuel).

The engine investigations are carried out with a simple diesel engine on the engine test bed.

Main parameters of engine (power output, torque, specific fuel consumption) and the main exhaust gas component (in this case CO, NO_x, PM) will be evaluated.

The investigation results are given in the following figures.

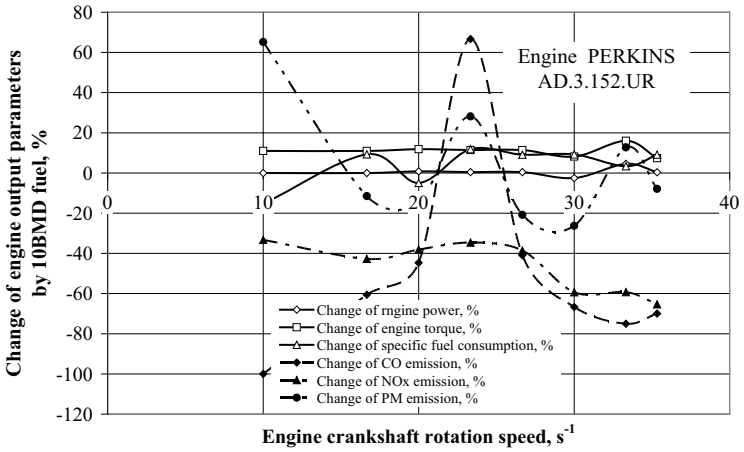

Fig. 1. The change of engine output parameters as a dependant factor of crankshaft rotation speed of the PERKINS AD.3.152.UR engine supplied with 10BMD.

The additive of 10% „bio" phase to the mineral diesel fuel leads to the remarkable increase of engine torque by unchangeable specific fuel consumption. Consequently the emission of NO_x decreases by 30% to 60%. At the same time emissions of CO and PM decrease, too.

Likewise the parameters change by supplying the engine with 20BMD.

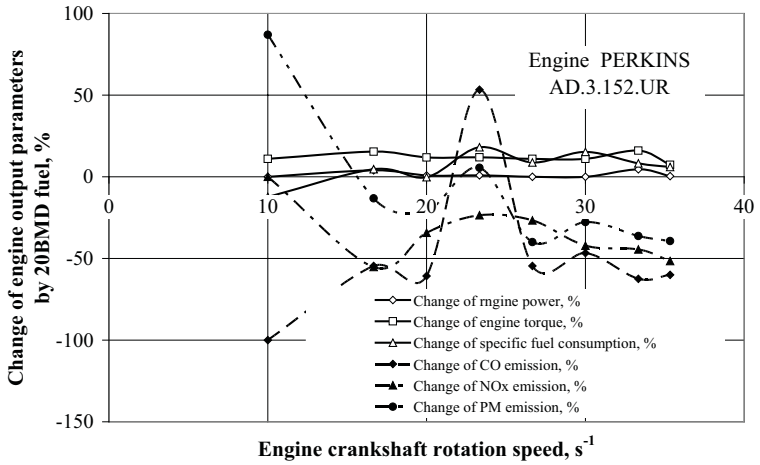

Fig. 2. *The change of engine output parameters as a dependant factor of crankshaft rotation speed of the PERKINS AD.3.152.UR engine supplied with 20BMD.*

Undoubtedly the biggest changes of engine parameters occur with supplying the engine with 50BMD. In this case the maximum of engine power and engine torque increases with the simultaneous increase of specific fuel consumption. Fuel consumption increases only with the higher engine crankshaft speed. The fuel consumption increases by the percentage as the engine torque, but increasing of torque was registered with all engine crankshaft rotation speeds. All the emissions of toxic parts of engine exhaust gases were decreased considerably.

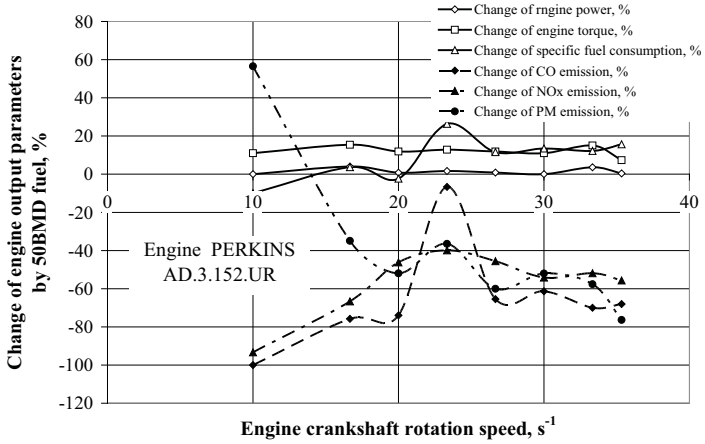

Fig. 3. *The change of engine output parameters as a dependant factor of crankshaft rotation speed of the PERKINS AD.3.152.UR engine supplied with 50BMD.*

The above results were obtained without any change of engine control parameters (the engine control parameters were the same as with supplying the engine with conventional diesel fuel), so without any optimization of control parameters. It appears that after optimization of engine control parameters; the results will be much better.

Conclusions

There have been given the first results of investigations of application of heavy alcohols as an ingredient of diesel fuel. In this case there have been presented the first results of investiga-

tions of the mixture of butanol (as heavy alcohol), rape oil (as vegetable oil) and conventional diesel fuel. This mixture was called the biomixdiesel (BMD).

There were better results achieved than one expected. Contrary to existing experiences, the maximum of power output and the torque of engine is higher in the whole range of the rotatory speed of the engine crankshaft when the engine biomixdiesel (BMD) is reinforced. The addition of the component biomix to fuel influences the specific fuel consumption. Generally with the larger part of the biomix component the specific fuel consumption grows. Because the power of engine also grows up one should expect that in exploitation the specific fuel consumption should not increase. It is very important that this fuel could be used to reinforce old, existing now and the future diesel engines.

The production of butanol is known (from biomass and in another way from electrolysis of ethanol). The possibility to get butanol from ethanol gives a very good perspective for the use of ethanol from today's overproduction and moreover without the essential change of infrastructure.

There has also been presented another way to use alcohols (and vegetable oils – without transestrification) as diesel engine fuel.

All this leads to the conclusion that the use of ethanol overproduction and European production of vegetable oils will contribute to fulfilling of the expected requirements of European Union regarding the biofuels.

It is very important that this fuel could be used to reinforce old, existing now and the future diesel engines.

The future works should refer to, first of all, the better adjusting of the engine to fuel (especially engine control parameters) and also fuel to the engine for specific exploitation needs.

Literature

[1] *Biofuels in the European Union. A vision for 2030 and beyond. Final report of the Biofuels Research Advisory Council*. European Commission. Directorate-General for Research Sustainable Energy Systems, 2006. ISBN 92-79-01748-9.

[2] Appendix C: *Biofuels and bio-based chemicals (background)*, http://www.dni.gov/nic/PDF_GIF_confreports/disruptivetech/appendix_C.pdf.

[3] http://en.wikipedia.org/wiki/Butanol.

[4] http://en.wikipedia.org/wiki/Biobutanol.

Journal of POLISH CIMAC
Faculty of Ocean Engineering & Ship Technology
GDAŃSK UNIVERSITY OF TECHNOLOGY

THE RESEARCH OF THE INFLUENCE OF THE CYLIDRICAL HEATING SURFACE LOCATION ON THE LOCAL HEAT TRANSFER COEFFICIENTS IN FLUIDISED BED OF THE MARINE FLUIDISED BED BOILER

Wojciech Zeńczak

West Pomeranian University of Technology in Szczecin
41 Piastów Ave, PL 71-065 Szczecin, Poland
tel.: +48 91 4494431, fax: +48 91 449 4737
e-mail: wojciech.zenczak@zut.edu.pl

Abstract

The article presents the results of the experimental research of the heating cylindrical surface location influence on the local heat transfer coefficients in the bubbling fluidised bed in the physical model of the marine fluidised bed boiler. A particular feature of this boiler model is positioning it in a kind of cradle simulating ship's motion on sinusoidal type regular wave. The heating surface is located in the traditional ship's centre line or in her midship section. The testing has been conducted in the conditions where the fluidising column remained motionless while being at the same time deflected from the vertical by a constant angle and in the conditions of continuous oscillating movement. In the effect there has been obtained the distribution of the heat transfer local coefficient values in the fluidised bed in three points located at the diameter of the column at a certain distance from the separating grid with various locations of the heating surface. The research has indicated that column oscillations contribute to the increase of the bubbling fluidised bed local heat transfer coefficients, at the parallel positioning towards ship's centre line. The further results of research may provide the grounds to formulate guidelines for designing the shipboard fluidised bed boilers.

Keywords: *heat exchange, fluidised bed boiler, design, ship*

1. Introduction

While designing the marine steam boilers, certain rules due to ship's rolling motion on waves should be observed in order to make the boiler operation safer and the risk if its damage gets less. In case of water-tube boilers with natural circulation such rule is for instance positioning of boiler drums in such a manner that their axis of symmetry is parallel to ship's centre line. On the other hand, their positioning with the axis in perpendicular to ship's centre line would cause excessive fluctuations of water level while rolling thus threatening the proper and safe boiler operation.

Whereas in case of forced circulation boiler heating surfaces, e.g. evaporator or superheater consisting of pipe bunches, their location towards the ship's centre line becomes less significant. There are arrangements encountered involving pipe positioning both rectangular and in parallel to this line. The ship's side rolling has no such significant impact in this case onto the pump-forced working medium flow. Also in connection with exhaust gas flow in view of its strong turbulent motion and its minor inertia, the ship's rolling motion practically does not affect the performance of the said heat exchangers.

On the other hand the situation changes completely if we consider the heating surface immersed in the bubbling fluidised bed formed by grains of fuel and inert material suspended in the stream of flowing air. Such is the case with fluidised bed boilers. Under the influence of ship's rolling such bubbling bed behaves similar to liquids. Also the movement of grains in the bed itself changes which influences the local coefficients of heat transfer in the bed [5]. In this situation it is interesting to investigate the influence of the positioning of heating surface on the values of the local coefficients of heat transfer within the bed.

2. The Course of the Research

In order to find the answer to the question asked in the introduction several experiments have been conducted on the test stand specified in detail in [2]. The same method of determination of the local coefficients of heat transfer has been applied as referred to in the studies [5, 2]. The equivalent to a pipe in boiler bunch is here a cylindrical heating element (copper pipe) with electric spiral placed inside. The scope of research has required conducting of series of measurements for two various pipe positions, i.e. while the pipe axis is situated in parallel to midship section, and then when the pipe axis is situated in parallel to ship's centre line. In the present construction of the stand the pipe can only be positioned in such a manner that its axis remains perpendicular to the column axis. This restriction results from the circular column cross-section. In the future it is planned to apply new version of the stand with the column of square cross-section which will allow to locate the pipe along the side walls of the column. The diagram of both positions of the pipe, distribution of thermocouples and the directions of movement of fluidising column are shown in Fig. 1, and the Fig. 2 demonstrates the view of a stand part.

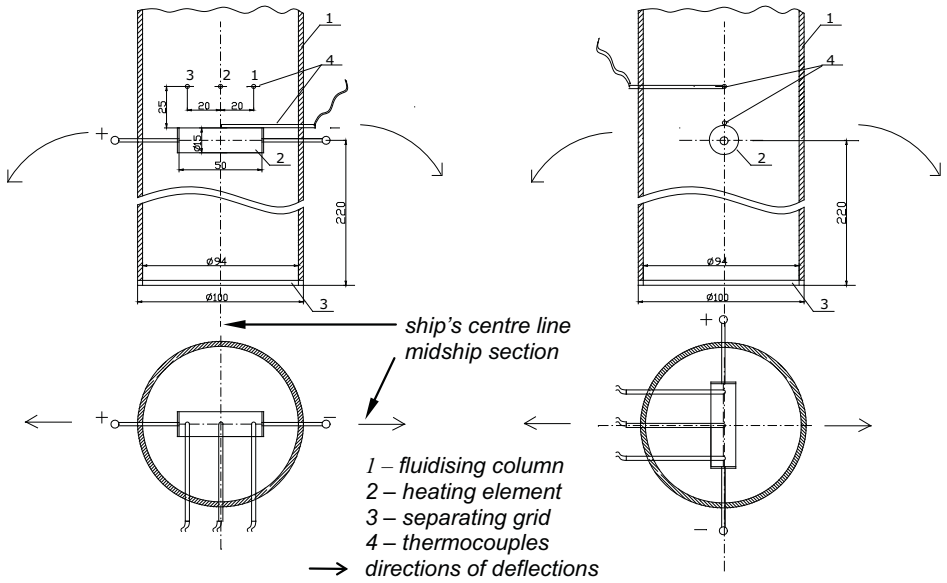

Fig. 1. Diagrams of the positioning of heating element and distribution of thermocouples

3. The Results of the Research and their Analysis

At the stand in question there have been previously tested the local heat transfer coefficients in the bed involving one permanent positioning of heating pipe, i.e. in parallel to midship section, whereas the bed height in rest condition and number of fluidisations have been changed. The

influence of column deflection from vertical has been also investigated with regards to the values of the local heat transfer coefficients. A major conclusion from this investigation has been the statement that the column deflection from vertical results in reduction of mean values of heat transfer coefficients, while the reduction tended to grow at the side towards which the deflection occurred. The results of these investigations have been presented inter alia in [5].

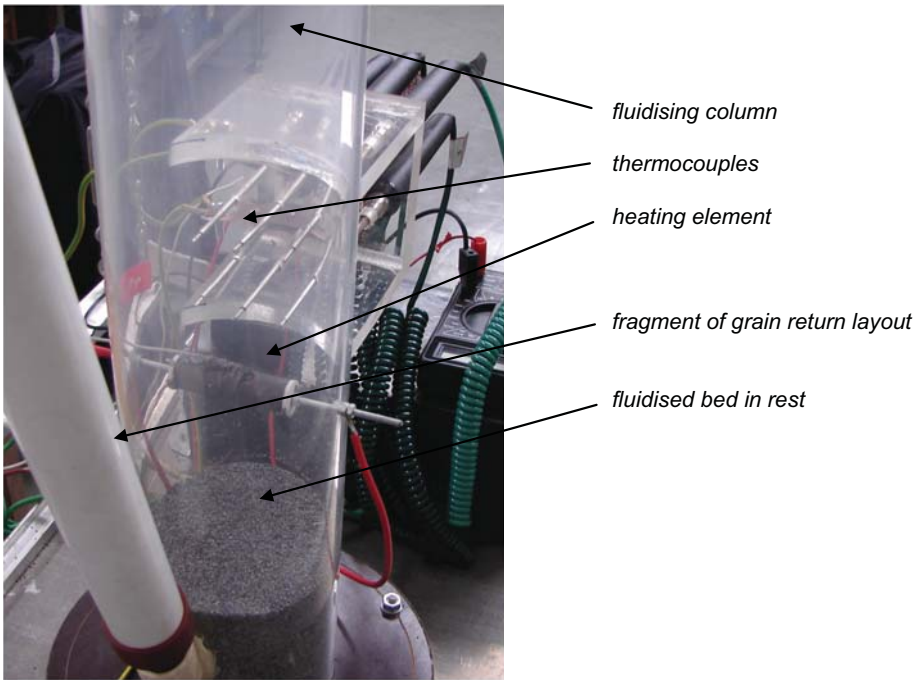

Fig. 2. View of the stand

The first test upon the change of heater positioning to that in parallel to ship's centre line has been the checking of the influence of the number of fluidisations on the values of heat transfer coefficients in the bubbling fluidised bed. The examinations have been conducted for the permanent bed height in rest, i.e. 0.12 m. The bed material, similar like in the former testing, have been the poppy seeds. The heater power has been kept at the constant level of 45 W. According to the suppositions, in view of full symmetry of the system, in the column vertical position, the nature of the changes of heat transfer coefficients has remained the same as in the positioning referred to above – heater parallel to midship section. As the fluidising air velocities grow, also the heat transfer coefficients grow as well. Their distribution along the radius R of the column for the velocities 2.6 m/s and 4.5 m/s at the distance of 0.245 m over the separating grid in points separated by the value r from the column axis is presented in Fig. 3.

As can be observed from the course of the curves, the values of the local coefficients of heat transfer are somewhat smaller closer to the walls on account of the circulation occurring inside the bed caused by well entry loss.

The subsequent measurement series have been conducted for the column inclined by permanent angle of 22 ° to the left, and then inclined permanently by the angle of 28 ° to the right. The investigation has been conducted for the fluidising air velocity of 4.5 m/s. The results are presented in Fig. 4. They indicate the symmetry of the distribution of the coefficient value of heat transfer regardless from the direction of column inclination (V – vertical, L – left, R – right). Thus in this case the characteristic reduction of coefficient values at the inclination direction does not occur. On the other hand there can be noticed general reduction of all coefficient values at the

column inclination. The bigger decrease of the values can be observed at a bigger inclination , in this case for the inclination towards the right (alpha 4.5-R). But a slight reduction of the coefficient values in each case at the right side of the column results from the constant difference in the indications by thermocouples 1 and 3 (Fig. 1).

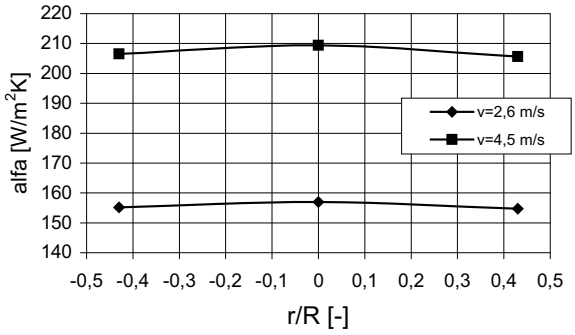

Fig. 3. The values of the local coefficients of heat transfer along the line at a distance of 0.245 m over the separating grid with the column in vertical position

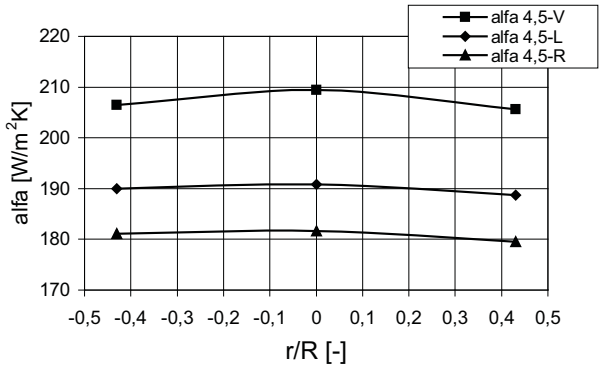

Fig. 4. The values of the local coefficients of heat transfer along the line at a distance of 0.245 m over the separating grid with the column vertical position (V), inclinations to the right (R) and to the left (L)

Fig. 5 presents the diagrams showing the distribution of the values of the local heat transfer coefficients for the same fluidising air velocity of 2.4 m/s with two different heater positions, i.e. in parallel to ship's centre line (alfa 2,4–R longitudinally) and rectangular to it (alfa 2,4-R transversely) in another manner, in parallel to midship section, with column permanently inclined to the right. To make the comparison better there is also presented a diagram showing the distribution of the values of local heat transfer coefficients with the column positioned vertically (alfa 2,4 V). As already mentioned with the vertical column positioning the heater orientation is of no consequence.

The same measurements have been repeated for the column inclined to the left with the same fluidising air velocity, i.e. 2.4 m/s. Fig. 6 presents the results in the form of diagrams. The line marked as "alfa2,4–L longitudinally" shows the distribution of the values of heat transfer

coefficients with heater positioned in parallel to ship's centre line, whereas the line marked as " alfa2,4 – L transversely" with the positioning rectangular to this centre line. Similar as in Fig. 5 also here a diagram is presented to show the distribution of the local values of heat transfer coefficients with column vertical positioning (alfa 2.4 V).

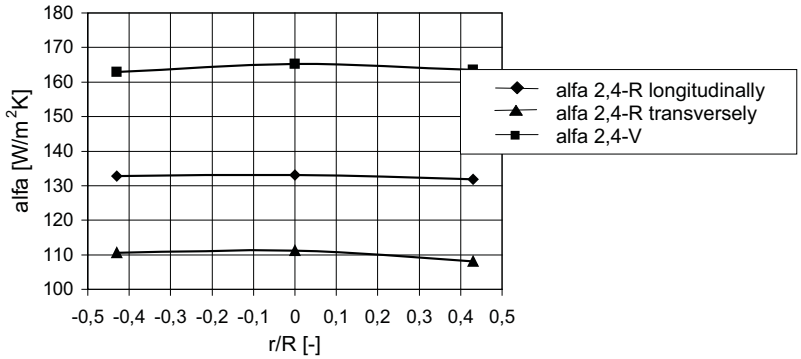

Fig. 5. The values of the local coefficients of heat transfer along the line at a distance of 0.245 m over the separating grid with the column vertical position (V) and column permanently inclined to the right (R) and heater transverse and longitudinal positioning in relation midship section

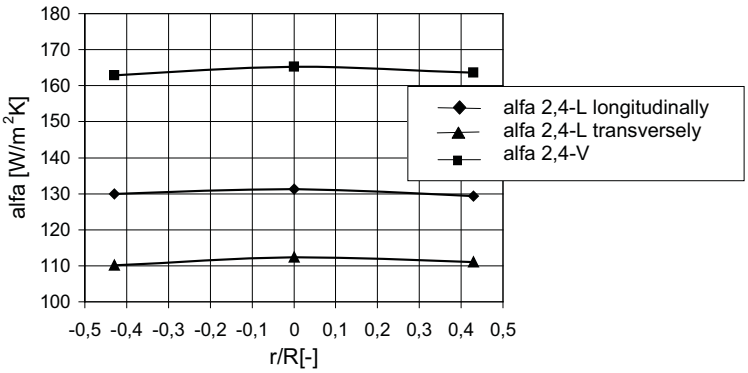

Fig. 6. The values of the local coefficients of heat transfer along the line at a distance of 0.245 m over the separating grid with the column vertical position (V) and column permanently inclined to the left (L) and heater positioned longitudinally or transversely in relation to ship's centre line

As visible in figures 5 and 6, in case the heater is positioned transversely to the ship's centre line, there can be observed previously mentioned typical reduction of the value of the local heat transfer coefficient at the side to which the inclination has occurred. However, the most meaningful conclusion is that with the heater positioned transversely the mean values of the local heat transfer coefficient, regardless of the column inclination direction, along through the line of the heater are less than the values of the coefficients along the heater while it is positioned longitudinally to ship's centre line.

In the maritime practice the conditions when a vessel sails with a permanent major list to one side are quite rare. More complex ship's movements on the waves are however general. In many shipbuilding issues, however, it is sufficient to take into account only so called simple rolling, i.e. of one degree of freedom, occurring only in ship's centre line or midship section. Such approach is most frequently related to ship's rolling movements which on the their intensity due to direct

relation with the stability safety and also the effectiveness of the performance of some systems and operations are of special significance [3]. Simple rolling without being combined with any other movements is however a little too far fetched approximation of actual conditions, but still acceptable in the research of the behaviour of the fluidised bed in these conditions which is proven also in other research studies, e.g. [4].

The stand where the aforesaid testing has been made allows to conduct the examination of the average values of the local coefficients of heat transfer during the constant oscillating movement approximating just the ship's rolling on a regular wave of sinusoidal type. It is also assumed that the vessel is on even keel.

The examinations have been conducted for the transverse and longitudinal heater positioning with constant oscillating movement of 28 s period and inclinations of 22 ° to each side. The figure 7 shows the results in the form of diagrams. The line marked as "alfa L–R longitudinally" shows the distribution of the values of heat transfer with heater positioned in parallel to ship's centre line during pendular motion, whereas the line marked as "alfa L–R transversely" with its positioning rectangular to this line also during pendular motion.

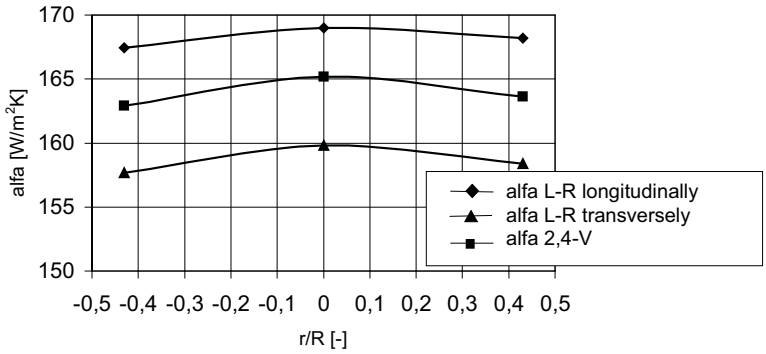

Fig. 7. The values of the local heat transfer coefficients along the line at a distance of 0.245 m over the separating grid with the column positioned vertically (V) and during column pendular movements with transverse or longitudinal heater positioning in relation to ship's centre line

For the sake of comparison also diagram is presented that shows the distribution of the values of the local heat transfer coefficients with permanent motionless vertical column positioning and air velocity of 2.4 m/s (alfa 2,4–V). During the column oscillating motion the fluidising air velocity has changed by itself within 2.4 up to 3.2 m/s. The velocity fluctuations are caused by the varying resistance characteristics of the fluidised bed during inclinations. The fluidised bed location out of parallel in relation to the separating grid during inclinations causes the drop in flow resistance and faster transfer into fluidised state, as well as increase in air velocity. These issues have been discussed more in detail in the study [1].

As can be observed from the courses in the diagrams the smallest average values of the local heat transfer coefficients along the line at a distance of 0.245 m above the separating grid occur during oscillation with the transverse heater positioning towards ship's centre line. They are however bigger than with the constant list to port or starboard, in such heater positioning with the fluidising air velocity of 2.4 m/s (figures 5 and 6). The biggest values of the local heat transfer coefficients are reached with the longitudinal heater positioning and during column oscillation (alfa L–R longitudinally). Therefore the conclusion can be drawn that the column oscillations contribute to the increase of the local heat transfer coefficients, with parallel heater positioning in relation to ship's centre line, in comparison to the values of the coefficients obtained in motionless

column positioned vertically (alfa 2.4-V). Another reason of such result are the local changes in the material concentration within heater area.

4. Conclusions

On the basis of the presented research results it can be concluded that the manner of heater positioning in relation to ship's centre line does influence the average values of the local coefficients of heat transfer with permanent list or in continuous oscillating movement. In the examined positions the arrangement with the heater in ship's centre line has proven better.

On the basis of the results obtained, however, it cannot be unambiguously stated that in the construction of marine fluidised bed boilers – on account of heat exchange conditions – there should be preferred the longitudinal positioning of the pipes of heat exchangers immersed in bed in relation to ship's centre line. It is necessary to complete the examination of the heat transfer coefficients with the heater also positioned in parallel planes to ship's centre line and the examined midship section with the application of fluidising column of square cross-section.

The conclusions from the above investigations, conducted with the use of certain simplifications, give the grounds to continue experimenting with the application of more advanced simulators of ship's full movement on irregular wave. It also seems worthwhile to extend the scope of research by the inclusion of circulating fluidised bed.

References

[1] Adamkiewicz, A., Zeńczak, W., *Model Testing of Fluidised Bed Boiler for Sea-Going Ships*, Marine Technology Transactions, Vol.17 , Gdańsk 2006, pp.23-35.

[2] Adamkiewicz, A., Zeńczak, W., *Koncepcja badań modelowych kotłów fluidalnych w aspekcie możliwości ich zastosowania na statkach morskich*, Systems, 2006, Vol.11, Special Issue 1/1 ss. 112-119, Wrocław 2006.

[3] Dudziak, J., *Teoria okrętu*, Wydawnictwo Morskie, Gdańsk 1988.

[4] Ikeda, S., Ito, S., Someya, T., *An Experimental Marine Fluidised –Bed Boiler Plant*, Marine Engineers Rev, 1983,10, pp 15-17.

[5] Zeńczak, W., *Investigation of Fluidised Bed of the Physical Model of the Marine Fluidised Bed Boiler*, Journal of POLISH CIMAC, Vol.3, No.1,pp 183-190, Gdańsk ,2008.

The study financed from the means for the education within 2009 – 2012 as own research project No N N509 404536

Journal of POLISH CIMAC
Faculty of Ocean Engineering & Ship Technology
GDAŃSK UNIVERSITY OF TECHNOLOGY

MULTIDIMENSIONAL CONDITION MONITORING OF CRITICAL MACHINES

Bogdan ŻÓŁTOWSKI

UTP, Faculty of Mechanical Engineering
Bydgoszcz, Poland
bogzol@utp.edu.pl

Leonel Francisco CASTAÑEDA HEREDIA

Universidad EAFIT
Departamento de Ingeniería Mecánica
Medellín, Colombia
lcasta@eafit.edu.co

Abstract

Technical systems are more complex every day as their electronics and mechanics. Technological advances tend to be autonomous in its performance and perform an auto-diagnosis that allows determining an abnormality existence in a component or subsystem and deciding if the system has to be stopped or not. The conventional maintenance does not allow an integrated diagnosis analysis of a system. Among the factors that generated condition can be found a lack of communication between units: bad information management, ignoring relevant information, a lack of a clear monitoring policy and variables tendency.

Keywords: *diagnostics, monitoring, system of exploitation, reliability, damages*

1. Introduction

The energy processors theory is based on a main energy flow analysis, where a system balance arises between input energy N_i, dissipated energy N_d and useful energy N_u.

Through a residual process series as vibration, noise and heat the input energy is dissipated in one of these phenomena, that reflect the technical system wear (accumulated dissipated energy), therefore the dissipated energy study through the system provides inference about the artefacts wear and therefore is a interest determining the system technical condition. Figure 1, shows the methodology followed by the mini-central technical diagnosis. This process involved the next diagnosis stages:

- Register and acquisition of residual energy (reception and selection points of vibration signals and operation variables).
- Signal processing.
- Statehood monitoring of Francis turbine.
- Multidimensional Monitoring Condition.

- Maintenance ratios establishment.

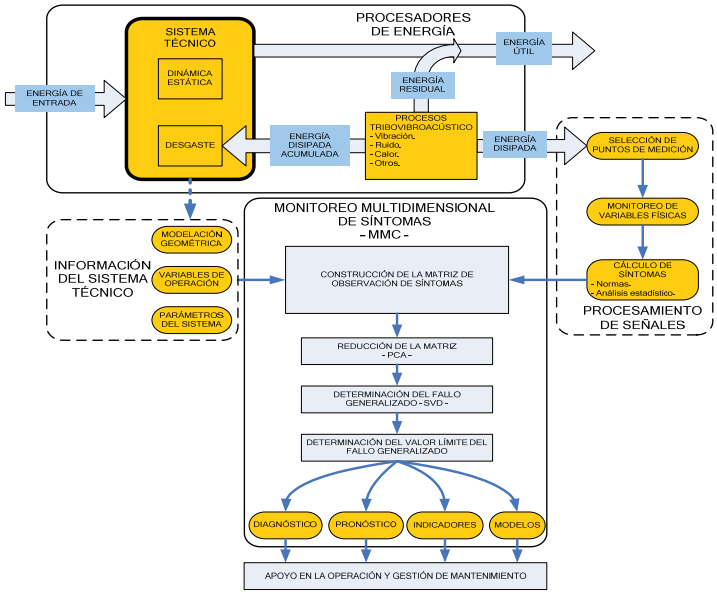

Fig.1. Technical diagnosis methodology for a Francis turbine in slow time

2. Study Case

As study case for presented methodology is La Herradura's Mini-central Hydroelectric property of Empresas Públicas de Medellín, which is located in the municipality of Frontino, near of Medellín, Antioquia. The mini-central has two Francis type turbines of horizontal axis, each one with a rated power of 10.4MW and a $5m^3/s$ flow, with a rotation speed of 900rpm and a design net jump of 230.6r.p.m. Fig.2 shows up a general scheme of parts forming the turbine.

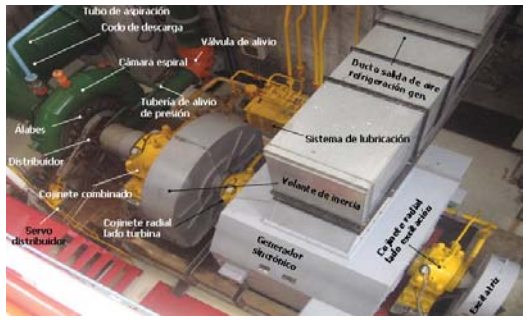

Fig.2. Francis turbine

The Mini-central has two systems able to obtain information of Mini-central technical condition, the first one is the vibration monitoring system and the second one is the Mini-central monitoring and control system.

The permanent vibration monitoring system for the generator is based on an instrument with the serial number "VDR-24" (Vibro Diagnostics Recorder – 24 channels), in the VDM data module and in the "ATLANT" diagnosis program. The vibrations measurement chain is showed on Fig.3.

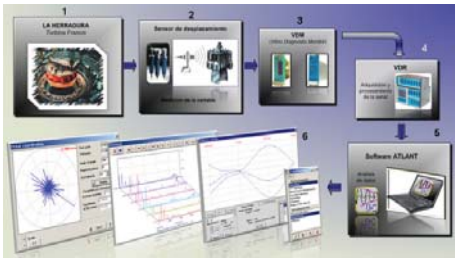

Fig.3. Measurement chain, vibration analysis system [1) La Herradura's Mini-central. 2) Sensors – Variable Measurement. 3) VDM – Data Module. 4) VDR – Processing and signal acquisition.. 5) ATLANT Software. 6) ATLANT signal and analysis transformation]

Through this system the r.m.s signals vibration value is monitored (speed and displacement) in points (1-8) presented on Fig.4.

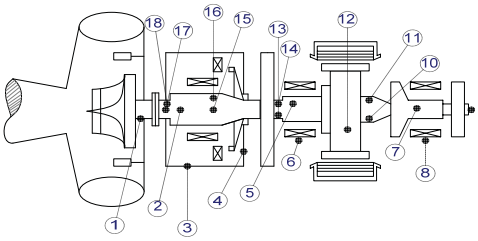

Fig.4. Acquisition point scheme of variables related to vibration (1-8 points)

The system used to central monitoring and control from operation station is the V7 Monitor Pro from Schneider Electric (Fig.5), this allows the data acquisition, monitoring and real time control and has a setting Server-Client and an unlimited number of TAG's (variables).

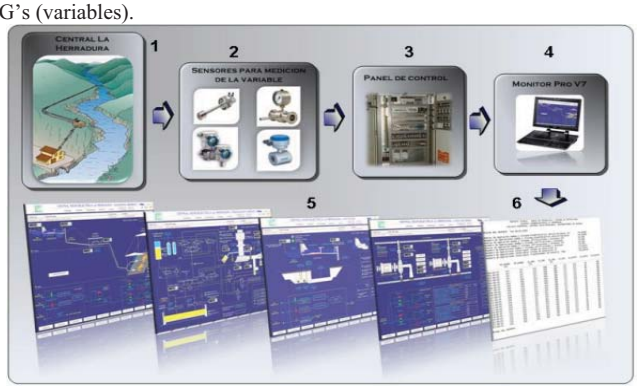

Fig.5. Measurement chain, monitoring and control system

[1) La Herradura Mini-central. 2) Variables measurement sensors (Pressure, temperature, current, voltage). 3) Control panel. 4) V7 Monitor Pro Software. 5) General deployments of generation and monitoring units. 6) Historical board and reports]

3. Measurement points selection

Based on measurement points algorithm the mechanical vibration signal is analyzed, received from the three hydro-dynamical bearings based on independence criterion and information quantity. Fort the first case the information independence will be given by inverse area under the curve of coherence $\gamma_{xy}^2(f)$ between two signals measured at the same place, for the current study the signals are taken from vertical and horizaontal speed in every bearing therefore, there will be a greater information independence when the maximum area, according to the next expression [5]:

$$AC_{xy} = \frac{1}{\int_0^F \gamma_{xy}^2(f)dF} \tag{1}$$

To determine the information quantity the coherence values are taken between signals depending on certain frequencies (system characteristic frequencies) and a criterion under the following expression [5]:

$$In_{xy}(\theta_i) = \sum_{x=1}^{l} Log\left(\frac{1}{1-\gamma_{xy}^2(f_x, \Delta f_x, \theta_i)}\right) \tag{2}$$

AC_{xy} and In_{xy} values are registered in a data base, given the data volume to analyze, an optimization problem is set out, which aims to determine the generation bearing in which the independence and information quantity are the highest. According to Fig.6, the reception points of diagnosis signal are located almost at the same distance from the optimal point. This means that has reliable information for the technical diagnosis of the generation unit.

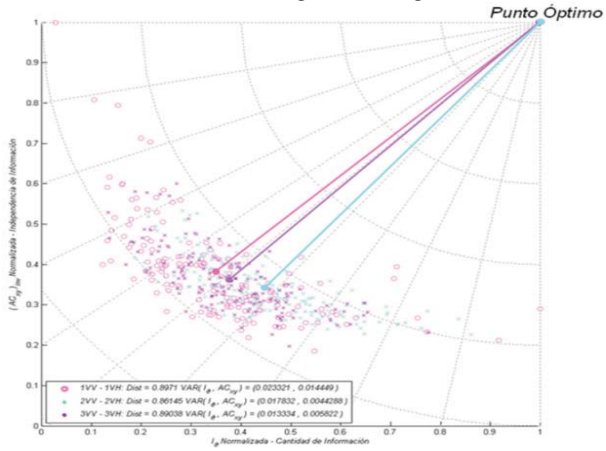

Fig.6. Reception point analysis from diagnosis signal

4. Symptoms Calculation

During the diagnosis model implementation, a series of new symptoms were calculated to make a registered signals by the vibration monitoring system, Fig. 7 shows an example of the spectrum amplitude *(225Hz):2VV* symptom: this refers to the vibration speed amplitude of impeller blades frequency flow (225Hz), in vertical direction of 2 bearing. A data tendency was observed during monitoring time, which indicates the evidence of a system abnormality, thus the evidence the real system statehood condition, allows detecting, locating and evaluating failures in the system. On [6] is showed the symptom definition and some examples are suggested.

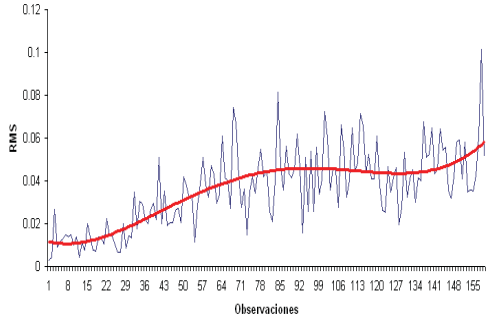

Fig.7. Vibration speed frequency from impeller blades flow (225Hz), in a vertical direction of 2 bearing

5. Observation Matrix Elaboration

To elaborate the symptom matrix 25 generation and control variables were considered, corresponding to specific average values registered during the monitoring day. This selection was made along with the systems operators, seeking to include the variables that in a certain case can provide abnormality evidence in the system. Regarding to vibration monitoring signals, 210 symptoms were calculated each monitoring day, also based on operators experience and appropriate literature. Among them highlights scalar estimators as: average, RMS value, peak value, peak to peak value, shape factor, standard deviation, bias, among others. In this way a new observation matrix of symptoms will contain 235 variables and 157 observations. The symptoms observation matrix from a system is represented as follows [7]:

$$O_{pr} = \{S_{ij}\} = \overbrace{\begin{bmatrix} S_{1,1} & S_{1,2} & \cdots & S_{1,j} & \cdots & S_{1,r} \\ S_{2,1} & S_{2,2} & \cdots & S_{2,j} & \cdots & S_{2,r} \\ \vdots & \vdots & \ddots & \vdots & & \vdots \\ S_{i,1} & S_{i,2} & \cdots & S_{i,j} & \cdots & S_{i,r} \\ \vdots & \vdots & & \vdots & \ddots & \vdots \\ S_{p,1} & S_{p,2} & \cdots & S_{p,j} & \cdots & S_{p,r} \end{bmatrix}}^{\text{Síntomas Varaibles}} \begin{matrix} \rightarrow \theta_1 \\ \rightarrow \theta_2 \\ \vdots \\ \rightarrow \theta_i \\ \vdots \\ \rightarrow \theta_p \end{matrix} \left.\begin{matrix} \\ \\ \\ \\ \\ \\ \end{matrix}\right\} \begin{matrix} \text{Observaciones} \\ \text{Mediciones} \end{matrix} \tag{3}$$

Where columns $j = 1,2,\cdots,r$ are different measured symptoms and rows $i = 1,2,\cdots,p$ are observations or measurements made for every symptom in different life cycle times of technical system.

6. Limit value establishment for estimators

Symptoms limit value of diagnosis systems were calculated according to the following relation: [5]:

$$S_{\lim} = \overline{S} + \sigma_P \sqrt{\frac{G}{2A}} \tag{4}$$

Where: $\overline{S}$ is the symptom average value during machine operation time θ and the symptom standard deviation σ_P, A - is the tolerable level of unnecessary established repairs and G is the machine availability.

Fig.8 shows the relation between the manufacture established limit and the previous calculated method. The set limit observed can be found way above from normal data behavior therefore do not show variable changes evidence. On the other hand, the calculated limit can identify subtle variable changes being in an historical behavior range.

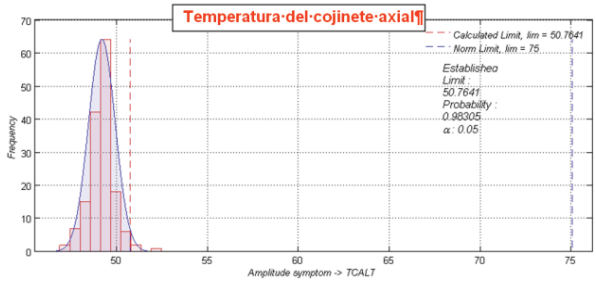

Fig.8. New limit calculation

7. Singular Value Decomposition

Following the proposed methodology, symptoms observation matrix, its dimensions are reduced through PCA. Then the Singular Vale Decomposition (SVD) is applied with the purpose of extracting different failure modes that evolve in a system, assessing the wear advance used en new indexes and ratios. The SVD an application for sizing the symptoms observation matrix can be expressed as follows [8]:

$$O_{pr} = U_{pp} * \sum_{pr} * V_{rr}^{T} \tag{5}$$

U_{pp}: dimension orthogonal matrix. p, are the left singular vectors. V_{rr}: is an r dimension orthogonal matrix of right singular vectors. $\sum_{pr}$: is a diagonal matrix of singular values.

The failures profiles are determined using singular values and vectors σ_t, u_t, v_t found with SVD, obtaining a conditon evolution interpretation of technical system. These failures are given by [9]:

$$SD_t = O_{pr} \times v_t = \sigma_t \cdot u_t \tag{6}$$

Where SD_t is the left singular vector amplified by a respective singular value σ_t. Hence this value leads as bug and information about intensity of failures due to the inclusion of σ_t [9].

The total generalized failure profile $P(\theta)$ or $SumSD$, which represents the general evolution of condition of technical system is determined through [10,11]:

$$P(\theta) = SumSD = \sum_{i=1}^{z} \left| SD_i(\theta) \right| \tag{7}$$

8. Implementation Methodology

During the implementation methodology at La Herradura's Mini-central an evolving failure on Francis turbine was detected, which is showed on Fig.9.

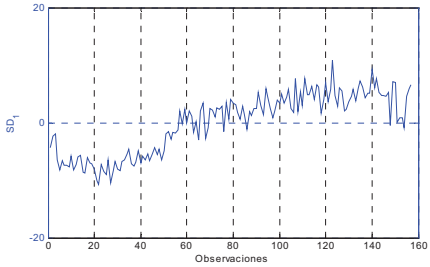

Fig.9. First Francis turbine failure evolution

The technical diagnosis showed up that the evolution profile of machine was strongly correlated with variables that describe the technical condition of first Francis turbine bearing. The temperature, the relative axis displacement with respect to combined bearing and the 225 Hz spectral component are part of diagnosis parameters that dominate in this first evaluation unit. A continuous component increase was observed during the machine operation time. This occurs as a consequence of interaction between impeller blades and distributor moving blades, a pulse is generated due to the frequency flow pressure of impeller blades (225 Hz, this pulse is labirynths transported from turbine seals causing an axis push in axial sense, generating a vibration at the same frequency level. With the turbine seals wearing increase, the pulse effect increases, hence, the axial push increases generating vibrations increase.

On Fig.10 the diagnosis parameters tendencies are showed for Francis turbine operating time related to identify failure.

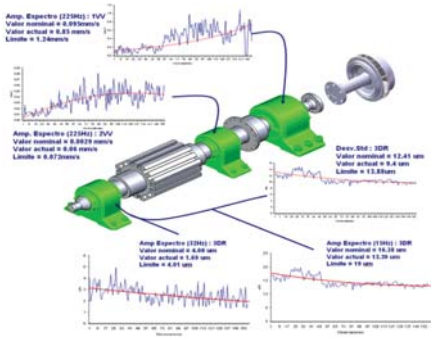

Fig.10. Vibrations evolution related to failure profile

The probabilistic decision model (Fig.11) and reliability symptoms function (Fig.12) of Francis turbine were determined with important information in any strategy of critical operating systems maintenance. These machine's behavior patterns allow making correct decisions just in time and reducing risk. It is important to remember the implemented methodology during this project, which is based on real data of Francis turbine condition during utility time.

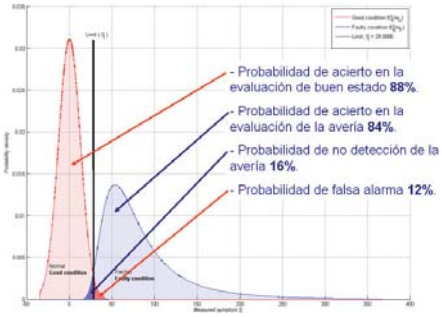

Fig.11. Probabilistic diagnosis model

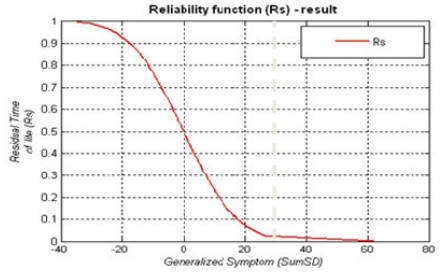

Fig.12. Reliability symptoms function of Francis turbine

9. Conclusions

Techniques and algorithms used in different branches of science can be applied to technical condition monitoring, as the case of main components analysis and the singular values decomposition.

The multidimensional symptoms monitoring allows identifying changes in the system technical condition and establish possible causes from that condition.

This kind of monitoring in the specific analyzed case generate a maintenance decision-making support, which impacts in cost reduction related to maintenance and optimal personal use besides, it generates an increase in the system's availability and reliability.

The study was made in real exploitation conditions, considering dynamic variables of generators with the purpose of obtaining information about the general technical condition of system.

Bibliography

[1] ŻÓŁTOWSKI B., CASTAÑEDA L., BETANCUR G.*: Monitoreo multidimensional de la interfase vía-vehículo de un sistema ferroviario*. En: Congreso Internacional de Mantenimiento (9: 22-23, Marzo: Bogotá). Memorias. Bogotá D.C.: ACIEM, 2007. 10p.

[2] ŻÓŁTOWSKI B., CASTAÑEDA L., BETANCUR G.: *Monitoreo multidimensional de la condición (MMC) basado en la descomposición en valores singulares (SVD) Caso de estudio: sistema ferroviario*. En: Revista Universidad EAFIT. Julio - Agosto - Septiembre, 2007, vol. 43, no. 147, p. 81-94. ISSN 0120-341X.

[3] ŻÓŁTOWSKI B., CASTAÑEDA L.: *Wielokryterialny system oceny bezpieczenstwa i komfortu jazdy wagonów pociagu*. In: DIAGNOSTYKA. Augustówka, 2008, nr. 2 (46), p. 45-50. ISNN 641-6414.

[4] OCAMPO J.E. *et al*.: *Diagnóstico Técnico de una turbina hidráulica tipo Francis bajo una aproximación holística*. En: Congreso Internacional de Mantenimiento (10: 9-11, Abril: Bogotá). Memorias. Bogotá D.C.: ACIEM, 2008.

[5] ŻÓŁTOWSKI B.: *Podstawy diagnostyki maszyn*. Bydgoszcz, ATR, 1996. 467 p. ISBN 83-900853-9-9. [6] NATKE H. G., CEMPEL C.: *Model-aided diagnosis of mechanical systems. Fundamentals, Detection, Localization, and Assessment*. New York: Springer-Verlag, 1997. 248 p. ISBN 3540610650.
[7] NATKE H. G., CEMPEL C.: *Symptom observation matrix for monitoring and diagnosis*. In: Journal of sound and vibration. Germany University of Hanover, 2001. 597 - 661, 603, 609 - 613 p.
[8] BONGERS D. R.: *Development of classification scheme for fault detection in long wall systems*. Brisbane, Australia, 2004.
[9] CEMPEL C.: *Innovative Developments in Systems Condition Monitoring*. Key Engineering Materials, vol 167-168, Poznan, Poland. 1999, p 172-188.
[10] CEMPEL C.: *Multi - fault condition monitoring of mechanical system in operation*. XVII IMEKO, Dubrovnik, Croatia. 2003. 1-4 p.
[11] CEMPEL C., TABASZEWSKI M.*: Multidimensional vibration condition monitoring of non-stationary mechanical systems in operation*. Twelfth International Congress on Sound ans Vibration ICSV 12, Lisbon, 2005.

Journal of POLISH CIMAC

Faculty of Ocean Engineering & Ship Technology
GDAŃSK UNIVERSITY OF TECHNOLOGY

MULTIDIMENSIONAL MONITORING OF CONDITION – MMC - BASED ON THE SINGLE VALUE DECOMPOSITION – SVD - CASE STUDY: RAILWAY SYSTEM

Bogdan Żółtowski WIM, UTP, **Leonel F. Castañeda Heredia** EAFIT University
German R. Betancur Giraldo EAFIT University

Abstract

The multidimensional monitoring of symptoms applied to railway systems allow to detect and locate the sections of the track (straight and curved) that generate the decrement of the safety and comfort of the passengers. It also evaluates the technical state of the rail-vehicle interface. In addition, it allows observing, evaluating, and controlling the reliability and availability of the system. The objective of the study is to propose an alternative to evaluate the condition of the technical state of railway systems from a dynamical point of view which guarantees safety and comfort of the passengers. One looks for diminishing operative costs of maintenance, improving the use of equipment for maintenance tasks of the track, vehicle and auxiliary equipment, optimizing the time of the maintenance personal, the maintenance frequencies (corrective, preventive, etc.). It also aims to identify the variables related to maintenance actions that have a high influence on the technical state of the system. This paper presents the results obtained when applying a modeling of this type to a railway system, being centered mainly in the application of SVD theory to the technical diagnosis of systems.

Keywords: *multidimensional monitoring of condition (MMC), Singular Value Decomposition (SVD), railway technical diagnosis*

1. Introduction

Technical systems are becoming more complex when talking about their mechanics and electronics. Technologic advances tend to be more auto-sufficient, and able to auto-diagnose themselves, which allows to determine if any anomaly is present in any subsystem or component, to finally decide whether the system must or must not be stopped.

The conventional maintenance with some factors, such as the lack of communication between dependencies, a not proper management of information, not having a clear monitoring policy or variables trends among other, do not allow the performance of an integrated diagnosis of the system.

Due to the previous factors, it is necessary to implement new methodologies of technical diagnostics, in order to satisfy all of the company's needs for obtaining results, an integrated diagnosis

through computing simulation, tools, analysis methods, and information evaluation from the machine's technical state.

The multidimensional monitoring of symptoms – MMC – has been developed as an alternative that fits the new technology demands; it assures obtaining performance indicators such as the reliability before any damage within the system, giving as a result less critical failures, unexpected pauses of production, dead times, maintenance costs, and the mistreatment of human resources, among others.

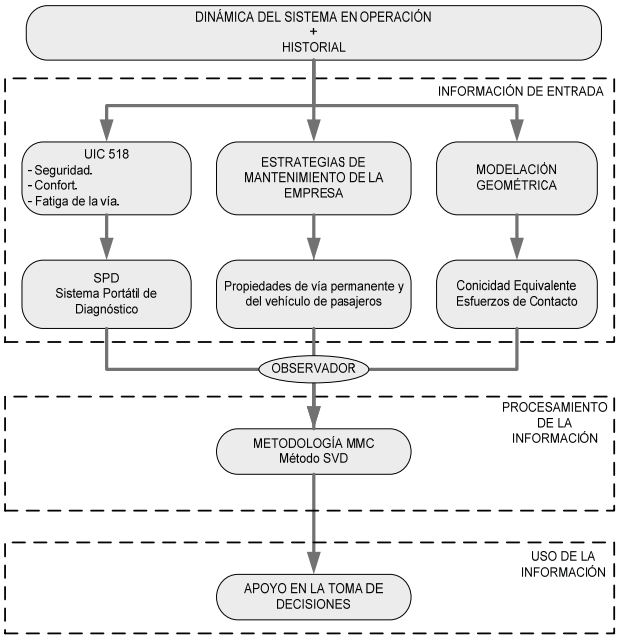

Fig. 1. Diagnosis Model with a holistic approximation for the railways systems

The holistic approximation presented in the previous figure, obtains information about the dynamic system operation, and the maintaining activity history through:

- The portable diagnose system (PDS) which registers acceleration and force signals in order to evaluate the security, comfort, and railways fatigue according to the International Law UIC518[1].
- The managing strategies of the company, taking into account the permanent way and vehicle variables.
- A geometric modeling of the wheel-rail interface, through which it is possible to obtain the equivalent iconicity and the contact efforts, which are the factors describing the relation mentioned above.

[1] UIC518, Tests and approval of rail vehicles from the point of view of their dynamic behavior, safety, railway wear and quality of the travel (comfort)

- The holistic approximation, based on the application of MMC methodology which is based on the singular values decomposition method (SVD) as well. SVD determines the general failure of the system, which is the indicator of the integral technical state of the system. Its evaluation allows the improvement of the actual management actions and the rise in the availability, reliability, and maintainability indicators of the technical system.

2. Multidimensional monitoring of condition

Figure 2 shows the implemented methodology for this study case, 4 main groups are warned; in the first one, the energy processors theory is reflected, where through the exit energy study, the technical state of the system and its deterioration can be inferred. First, signal processing (second group) must be done due to the fact that phenomena like vibration, noise and heat can be measured by data acquisition equipment, and instrumentation (symptom monitoring).

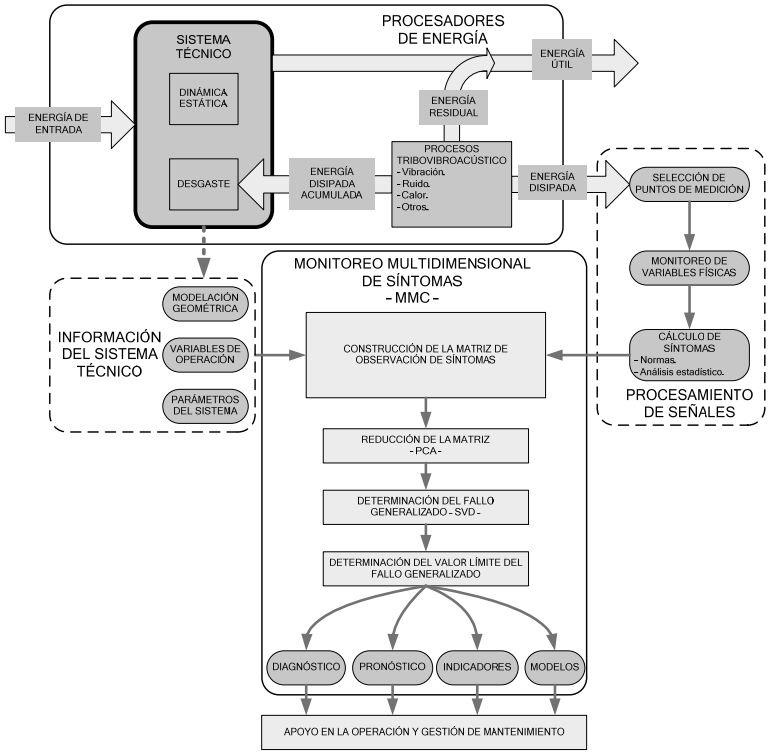

Fig. 2. Methodology for holistic approximation

At this point, it is important to establish what kind of measuring points of the physical variables are appropriate in order to obtain relevant information, that is why a selection of measuring points will be performed to establish the point generating a larger amount of information, and a smaller amount of useless information about the technical state of the system.

Once the measuring points are established, the monitoring of the physical variables can be made, assuring relevant information about the system.

Acquired signals are then transformed into a symptom series. The calculation parameters of these symptoms might be obtained by any norm alignment, or by a temporal series statistic analysis, in which basic statistic scalars can be calculated, among many others, as the half, standard deviation, bias, form factor, clearance factor. Way more complex analysis like the spectral, the envolvent, the cepstral, frequence time, ciclostationarie and superior order statistic analysis might also be developed in order to obtain symptoms which reflect the measuring signal. For the present study, the signal processing is being done through SPD.

A third group within the methodology is composed of the technical system's proper information, like system operation variables, system parameters, and a technical system geometric modelation. Among those sources of information, a series of periodically measured variables can be found

To perform a multidimensional monitoring is necessary as the first step to determine the symptom observation matrix which is composed of the symptoms in its columns and the measures of those symptoms in its rows. This matrix contains information about the system's technical state and the proposed methodology seeks to extract the relevant information.

The observation matrix is reduced through a Principal Component Analysis PCA which, along with a series of reduction criteria, allows identifying the symptoms containing relevant information about the system's technical state.

Based on the reduced matrix (space of reduced symptoms), and by using the Singular Value Decompositions SVD, the general failure that presents the evolution of the system's technical state is determined. It is a variable which consolidates the information about the system's technical state, contained in principle in the symptom observation matrix.

Once the general failure and its limit value have been determined (through statistical methods), it is possible to perform an integral diagnosis of the system by estimating the conditions under which the general failure exceeds its limit value. Forecasting tasks can be made, beginning with the general failure, in order to predict the future technical state of the system. It is also possible to create indicators of the system's technical state from the general failure, such as the functions of risk and reliability which support the system diagnosis. And finally, it is possible to establish general models (through multiple linear regression) which describe the behavior of the general failure in order to enter current, future, real or assumed values to the model and so determine their influence over the general failure.

3. SVD General Theory

The symptoms observation matrix defined by $O_{pr} \in \Re^{r \times p}$ is an array of symptoms at certain moments of the life of the technical device θ. It can be said that the symptoms observation matrix is a discrete way of observing symptoms (Cempel, 2000, p.2).

The aim of obtaining a symptoms observation matrix O_{pr} is to obtain all the information related to the condition of state of the technical system and to distinguish different forms of failure that evolve during its operation (Cempel, 2000, p.2). The symptoms observation matrix of a system is represented as follows (Natke-Cempel, 2001, p.599):

$$O_{pr} = \{S_{ij}\} = \overbrace{\begin{bmatrix} S_{1,1} & S_{1,2} & \cdots & S_{1,j} & \cdots & S_{1,r} \\ S_{2,1} & S_{2,2} & \cdots & S_{2,j} & \cdots & S_{2,r} \\ \vdots & \vdots & \ddots & \vdots & & \vdots \\ S_{i,1} & S_{i,2} & \cdots & S_{i,j} & \cdots & S_{i,r} \\ \vdots & \vdots & & \vdots & \ddots & \vdots \\ S_{p,1} & S_{p,2} & \cdots & S_{p,j} & \cdots & S_{p,r} \end{bmatrix}}^{\begin{matrix} Variable \\ Symptoms \end{matrix}} \begin{matrix} \rightarrow \theta_1 \\ \rightarrow \theta_2 \\ \vdots \\ \rightarrow \theta_i \\ \vdots \\ \rightarrow \theta_p \end{matrix} \left.\begin{matrix} \\ \\ \\ \\ \\ \\ \end{matrix}\right\} \begin{matrix} Observations & i = 1,2,\cdots,p \\ Measurements & j = 1,2,\cdots,r \end{matrix}$$

Where columns $j = 1,2,\cdots,r$ are the measured symptoms and rows $i = 1,2,\cdots,p$ are the measurements made to each symptom at certain moments of the technical system's life.
In some cases the information of several columns can be redundant and varies among symptoms contained in the matrix O_{pr}. This can be avoided by removing the correspondent (redundant) columns using tools such as the PCA.

The Singular Value Decomposition SVD is used in order to obtain different modes of failure which evolve in a system, evaluating the wear progress through indexes and indicators.

The application of the SVD to dimension the symptoms observation matrix is expressed as follows (Bongers, 2004, p.42), (Cempel, 2000, p.4), (Cempel, 2004, p.2), (Cempel, 1999, p.179), (Cempel, 2003, p.1293), (Cempel, 2003, p.2), (Cempel, 2000, p.5), (Cempel-Tabaszewski, 2006. p.3), (Cempel-Tabaszewski, 2003. p.216), (Cempel-Tabaszewski, 2005. p.3), (Wall-Rechtsteiner-Rocha, 2003, p.2):

$$O_{pr} = U_{pp} * \sum_{pr} * V_{rr}^{T} \tag{1}$$

U_{pp}: is an orthogonal matrix of dimension p of the left singular vectors

V_{rr}: is an orthogonal matrix of dimension r of the right singular vectors

$\sum_{pr}$: is a diagonal matrix of the singular values:

$$\sum_{pr} = diag(\sigma_1, \sigma_2, \cdots, \sigma_i) \tag{2}$$

The singular values σ_t are expressed by numbers and u_t, v_t are the singular (orthogonal) vectors representing the columns of their corresponding matrices $\sum_{pr}, U_{pp}, V_{rr}$. At the same time, these vectors are creating independent sub-matrices $(O_{pr})_t$ which totally describe the modifications of the operational system, that is its evolution, wear or its failure modes at time $t = 1,2,\cdots,z$ (Cempel, 2003, p.1293).

The singular values different from zero $\sigma_t > 0$ indicate failure or damage. These values are used to detect changes in the system and to evaluate their intensities. Failure intensities are organized by their magnitudes, as shown in the main diagonal of the singular values of O_{pr} (Natke-Cempel, 2001, p.610).

General failures are determined by using the singular values and vectors σ_t, u_t, v_t found through the SVD, obtaining an interpretation of the evolution of the state condition of the technical system. These technical failures are given by (Cempel, 2000, p.4), (Cempel, 2004, p.2), (Cempel, 1999, p.179), (Cempel, 2003, p.1293), (Cempel, 2003, p.2), (Cempel, 2000, p.5), (Cempel-Tabaszewski, 2006. p.3), (Cempel-Tabaszewski, 2003. p.216), (Cempel-Tabaszewski, 2005. p.3), (Wall-rechtsteiner-Rocha, 2003, p.2):

$$SD_t = O_{pr} \times v_t = \sigma_t \cdot u_t \tag{3}$$

where SD_t is the left singular value amplified by the corresponding singular value σ_t. Hence, this value has independent information in the form of failure as well as information in the intensity of these failures because of the inclusion of σ_t.

Therefore, for a lifetime θ of the system, quantities $SD_t(\theta)$ and $\sigma_t(\theta)$ are independent from one another and act as indexes of the system changes during the operation.

From the viewpoint of energy equivalence of a norm, the following can be said: $\sigma_t(\theta)$ can be treated as an index of the wear progress (intensity), while the $SD_t(\theta)$ is the momentary form during the evolution of the condition of state of the system (Cempel, 2003, p.1294).

One of the indexes which can be obtained through the SVD is the profile of total general failure $P(\theta)$ or $SumSD$ which represents the evolution of the general state of the technical system and is estimated as (Cempel, 2003, p.1296), (Cempel-Tabaszewski, 2005. p.4):

$$P(\theta) = SumSD = \sum_{i=1}^{z} |SD_i(\theta)| \tag{4}$$

The profile of total general failure $SumSD$, will be used to describe the technical state of the system under research and from now on will be called general failure.

Through the general failure, it is possible to perform diagnostic and forecast tasks, as well as determine some additional indicators of the condition of the technical system, and define state models.

4. Implementation of the multidimensional condition monitoring

We implement multidimensional monitoring of symptoms in a railway system type metro and present the information sources of the system's technical state as well as the conditions considered for the implementation and the results obtained through a computational tool based on the proposed methodology.

4.1 Description of the experiment

The analysis focuses on a commercial railway and it is developed for a sample of approximately 16 straight sections and 37 curved sections, as well as a representative sample of passenger vehicles (17 out of a 42 cars fleet).

The related symptoms are the estimators considered by the UIC518 standard for the evaluation of security, comfort and wear of the railroad; the geometric properties of rail and vehicles as well as estimators related to the wheel-rail interface. Two groups of matrices are formed:

$$O_{pr} = O_{16x32} = \begin{bmatrix} Estimadores & Estimadores & Estimadores \\ rueda-riel & UIC & vía \\ \{Z_{i,j}\} & \{W_{i,k}\} & \{Y_{i,l}\} \end{bmatrix} \quad \begin{matrix} i \approx 1,2,\cdots,16 \\ j = 1,2,\cdots,5 \\ k = 2,3,4,8,9,10,13,\cdots,18 \\ l = 1,3,4,\cdots,15 \end{matrix}$$

The first group is made of the estimators calculated from the UIC518 standard $W_{i,k}$, the properties of the railroad $Y_{i,l}$, and the estimators related to the wheel-rail interface $Z_{i,j}$ (for the lot of 31 estimators). There is a sample of straight sections i as observations of these symptoms. So we have 17 matrices of this type, one for each passenger vehicle analyzed.

The second group is similar to the first one, but here a sample of curved sections i is considered for a total of 35 estimators. 17 matrices of this type are obtained as well.

$$O_{pr} = O_{37x35} = \begin{bmatrix} Estimadores & Estimadores & Estimadores \\ rueda-riel & UIC & vía \\ \{Z_{i,j}\} & \{W_{i,k}\} & \{Y_{i,l}\} \end{bmatrix} \quad \begin{array}{l} i \approx 1,2,\cdots,37 \\ j = 1,2,\cdots,5 \\ k = 1,4,6,8,9,10,11,13,\cdots,20 \\ l = 1,2,\cdots,15 \end{array}$$

To contract the matrices mentioned before, we used information obtained from maintenance employees of the company, as well as from experimental measurements performed in normal operation conditions of the system.

4.2 Experiment Results

Each of the formed matrices is implemented into the multidimensional monitoring of condition MMC. As the first step, they are transformed considering the mean value and the standard deviation of each of the estimators; then, they are implemented into the dimensionality reduction module through the analysis in main components. Once the estimators providing little information about the technical state have been established, they are removed from the original matrix (with no transformations).

The reduced matrix is again transformed, but this time with respect to the initial value of each estimator. It is included in the singular value decomposition module SVD through which the general failure is determined. This is an indicator of the general state of the technical system whose limit value is calculated by the Neyman-Pearson method, considering the availability of $G = 0.9$ and the level of unnecessary repairs of $A = 0.1$

Once the general failure and its correspondent limit value have been calculated for each group of matrices, diagnosis is performed, the indicators of state are generated and its general models are proposed. We now present the obtained results for each group of matrices formed.

Figure 3 shows the general failure obtained from an observation matrix where symptoms are the variables measured on the railroad, the estimators obtained after applying the SPD and the ones calculated for the wheel-rail interface. The observation of these symptoms was made in vehicle 05 running through different curved sections of the railroad.

Axis x represents the observations obtained from the general failure (curved sections) while axis y represents the amplitude of the failure. The diagnosis is, hence, developed when determining the railroad section in which the general failure exceeds its limit value; section where the company should consider performing maintenance.

Figure 4 shows the co-variances (axis y) between the general failure and the symptoms considered at the analysis (axis x). Symptoms having a high relative covariance when compared to other symptoms are assumed to be responsible for the exceeded value of the general failure (with respect to its limit value). Therefore, once we identify the road section in which the general failure exceeds its limit value, we find through covariances the symptom generating this condition and, in this way, maintenance actions can be focused on particular road sections and on possible phenomena happening in these sections.

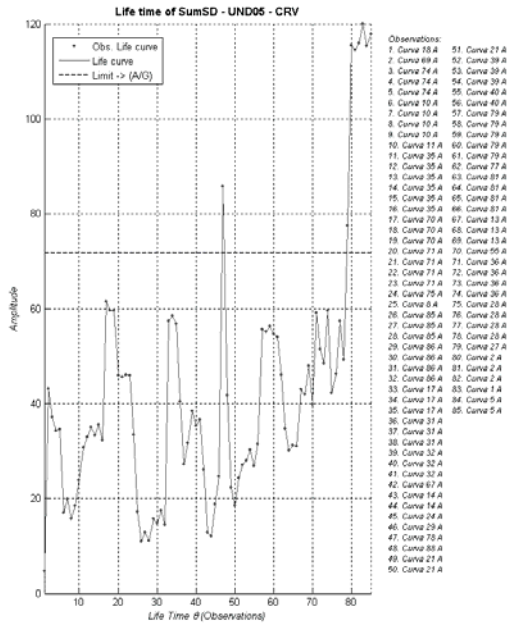

Fig. 3. Profile of the general failure

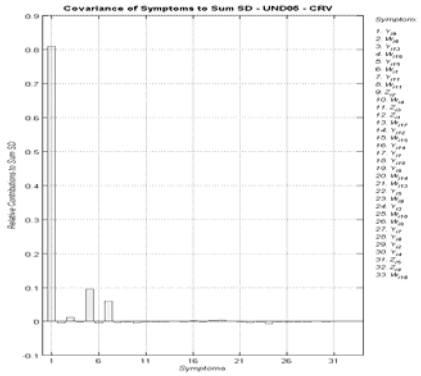

Fig. 4. Covariance of symptoms with the general failure

4.3 Results for UIC estimators, railroad properties and estimators of the wheel-rail interface for straight sections.

The procedure described before is applied to the 17 matrices in which the evolution of symptoms is given by the straight sections of the railroad. In 64.7% of the cases (analyzed units), the variable representing a greater importance is the railroad corrugation, 11.8% is due to the rail corrugation and its alignment, 11.8% is due to the alignments only, a 5.9% is due to the equivalent conicity and 5.9%

to the lateral forces.
In 76.5% of the cases, the system's reliability is reduced in the straight section ENV-86. In 70.6% of the cases, reliability is reduced in the straight section 77-81. This happens because the general failure exceeds its limit value.

4.4 Results for UIC estimators, railroad properties and estimators of the wheel-rail interface for curved sections.

In 41.2% of the cases (analyzed vehicles) the most relevant variable was the railroad corrugation, 17.6% is due to the railroad corrugation and the horizontal alignment, 23.5% due to the lateral forces and 17.6% due to the quasi-static lateral accelerations. In 76.5% of the cases, the system's reliability decreases in curve 2 and in 70.6% of the cases, reliability decreases in curve 5.

4.5 Models of state for the general failure

Once the general failure and its relationship with the measured symptoms has been determined, an analysis of multiple regression is developed considering the matrix formed by the estimators of the UIC518 standard, the geometric properties of the railroad and the estimators related to the wheel-road interface, for straight and curved sections.

The general failure found after the application of the SVD is considered as a dependent variable. The most representative symptoms in each case (symptoms having a great participation on the general failure) are considered as independent variables.

Particular models for each of the 17 analyzed vehicles are determined, and then each of these models is applied to real data from the other 16 vehicles in order to obtain a general model adaptable to most of the cases.

We now present the general model obtained for the general failure *SumSD* from the straight sections of the railroad:

$$\begin{aligned} SumSD = {} & 18.74 + 24.80Y_{i,9} + 14.28Y_{i,15} - 11.36Y_{i,14} - 7.91Y_{i,10} - 5.02W_{i,18} \\ & - 4.62Y_{i,8} + 3.09W_{i,2} + 3.00Y_{i,13} + 2.49Y_{i,12} - 1.26W_{17} - 0.97Y_{i,3} - 0.44Z_{i,1} - 0.20Y_{i,11} \end{aligned} \quad (5)$$

This model adapts with an acceptable global significance to 7 of the 17 vehicles under research (the level of significance is assumed $\alpha = 0.05$). Figure 5 shows the three best adaptations of the general model.

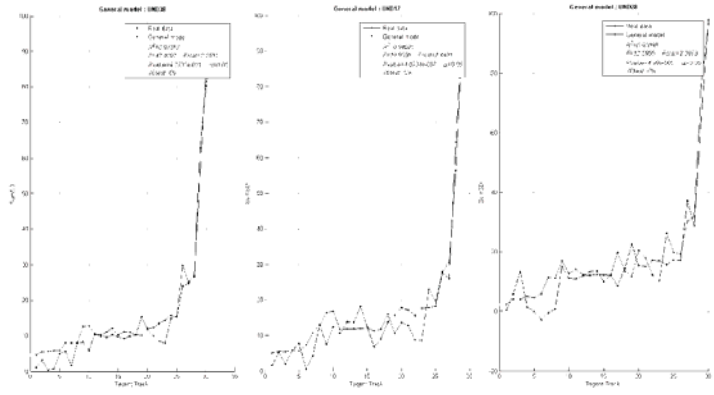

Fig. 5. Representation of the three best adaptations of the general model obtained for straight sections of the railroad

The following is the general model obtained for the general failure *SumSD* from the curved sections of the railroad:

$$SumSD = 44.13 + 27.07Y_{i,9} + 8.00Y_{i,15} + 7.78Y_{i,11} + 4.30Z_{i,2} + 1.80W_{i,11} + 1.38Z_{i,1} + 0.32W_{i,4} - 0.31W_{i,1} - 0.13W_{i,6} + 0.06W_{i,18} \quad (6)$$

This model adapts with an acceptable global significance to 8 of the 17 vehicles under research (the level of significance is assumed $\alpha = 0.05$). Figure 6 shows the three best adaptations of the general model.

By determining these models we tend to establish the condition of the general failure of the system for current conditions of the geometric parameters of the rail-vehicle interface. This allows to make a rapid diagnosis of the system in order to identify the necessary actions of maintenance.

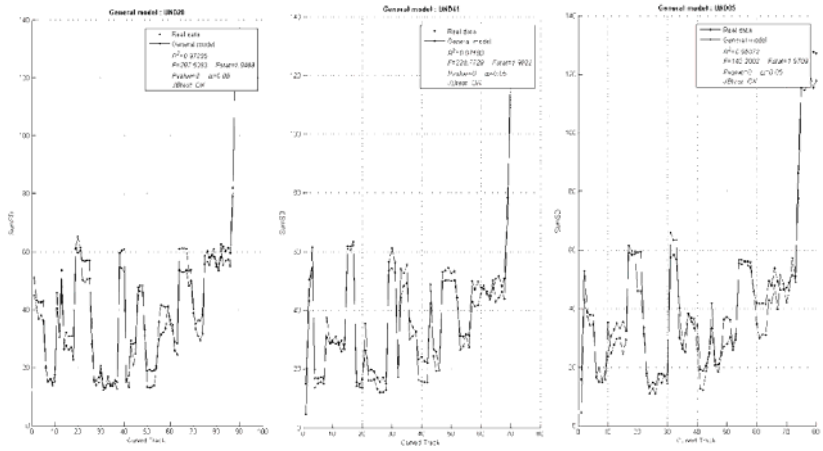

Fig. 6. A representation of the three best adaptations of the general model obtained for curved sections of the railroad

5. Conclusions

The multidimensional monitoring of symptoms helps us identify the railroad sections and vehicles needing a detailed revision by the personnel of railroad maintenance and movilization. It also gives us clues about what happens in the road sections under research. Hence, this type of monitoring in this specific case becomes a tool that supports maintenance decisions which translate into a reduction in maintenance-related costs, an optimal use of the maintenance personnel, and it additionally increases the availability and reliability of the system.

The research was performed under normal conditions of operation considering dynamic variables of the vehicles, estimators related with the wheel-rail interface, and with parameters commonly used by the personnel of maintenance and movilization in order to obtain information about the general technical state of the system.

Rails corrugation is the main factor affecting the reliability of the system in straight and curved sections since it influences the general failure, which lets us infer about the general technical state of the system. It is also known that the railroad corrugation produces vibrations on the suspended masses of the vehicle and such vibrations are transmitted to the passengers, causing discomfort.

Other influencing factors are the lateral forces measured in the axes' extrems. These forces affect the stability and security of the vehicle when it travels through curved sections, as well as the railroad alignments and the quasi-static lateral accelerations measured in the vehicle's box (which measures the influence over the passengers' comfort).

Road sections generating a loss of reliability on the system are: straight section ENV-86, straight section 77-81, straight section 85-87, curve 2, curve 5, curve 4 and curve 1. Therefore, we could suggest a change in the maintenance routines in order to give priority to these road sections.

Two general models for the evaluation of the general failure in straight and curved sections were established. This was made in order to quantify the general failure in current conditions of the rail and the vehicle, supporting the maintenance activities.

References

[1] BONGERS Daniel R., *Development of a classification scheme for fault detection in long wall systems*. Brisbane, Australia : University of Queensland. 2004. Major thesis submitted for the degree of doctor of philosophy. Department of mechanical engineering.

[2] CEMPEL C., *Fault oriented decomposition of symptom observation matrix for systems condition monitoring*. Hannover, Aleman: Hannover University, 2000. 2- 16 p.

[3] CEMPEL C., *Implementing multidimensional inference capability in vibration condition monitoring*. Surveillance 5 CETIM. Senlis 11-13 October 2004.

[4] CEMPEL C., *Innovative Developments in Systems Condition Monitoring*. Key Engineering Materials, vol 167-168, Poznan, Poland. Poznan University of Technology. 1999, p 172-188.

[5] CEMPEL C., *Multi dimensional condition monitoring of mechanical systems in operation*. Mechanical systems and signals processing, Poznan, Poland: Poznan University of technology. 2003. 1294 - 1301 p.

[6] CEMPEL C., Multi *fault condition monitoring of mechanical system in operation*. XVII IMEKO world congress. Dubrovnik, Croatia. 2003. 1-4 p.

[7] CEMPEL C., *Signals, symptoms, faults. Condition oriented multi dimensional monitoring of systems in operation*. Poznan, Poland: Poznan University of technology. 2000. 7 - 11 p.

[8] CEMPEL C., TABASZEWSKI M., *Averaging the symptoms in multidimensional condition monitoring for machines in non-stationary operation*. Thirteenth International Congress on Sound and Vibration ICSV13, Vienna, Austria, July 2-6, 2006.

[9] CEMPEL C., TABASZEWSKI M., *Extraction methods of multi-fault information in machine condition monitoring*. Key engineering materials, vol. 245 - 246. Poznan, Poland, 2003. 215 - 221 p.

[10] CEMPEL C., TABASZEWSKI M., *Multidimensional vibration condition monitoring of non-stationary mechanical systems in operation*. Twelfth International Congress on Sound and Vibration ICSV 12, Lisbon, 11-14 july 2005.

[11] CEMPEL C., TOMASZEWSKI Franciszek, *Diagnostyka maszyn : zasady ogólne – przyklady zastosowań*. Radom, 1992. ISBN 83-85064-81-8.

[12] NATKE H., G., CEMPEL C., *The symptom observation matrix for monitoring and diagnostics*. In: Journal of Sound and Vibration. London. 2001. 597 – 620 p.

[13] WALL M. E., RECHTSTEINER A., ROCHA Luis M., *Singular value decomposition and principal component analysis*. In: A practical approach to micro array data analysis. Eds. D.P. Berrar, W. Dubitzky, M. Granzow. Kluwer : Norwel, MA, 2003. p 91-109. LANL LA-UR-02-4001.